Project Report

Chemical & Isotopic Characterization of Deep Aquifers of Middle Ganga Basin

Under

PURPOSE DRIVEN STUDY (PDS)

Submitted to

NATIONAL HYDROLOGY PROJECT (NHP)

PI: Dr. Sudhir Kumar, Sc. 'G' & Director (Rtd), NIH

Co-PI: Dr. M Someshwar Rao, Sc. 'F', H. I. Division

NATIONAL INSTITUTE OF HYDROLOGY

ROORKEE (UTTARAKHAND) 247 667, INDIA

2024

Purpose Driven Studies (PDS)

1.1 Project Title: *Chemical & Isotopic Characterization of Deep Aquifers of Middle Ganga Basin*

1.2 Lead Research Organization

Name of the organization: National Institute of Hydrology, Roorkee
Head of the organization: Director, National Institute of Hydrology
Address: National Institute of Hydrology, Jalvigyan Bhawan, Roorkee-247667
Telephone: Tel: 01332 272106 FAX: 01332 273976

1.3 Principal Investigator (PI) from Lead Organization

Name & Designation	: Dr. Sudhir Kumar, Sc. G (Project Coordinator)
Date of Birth	: 5th November, 1963
Address	: National Institute of Hydrology, Roorkee
Telephone	: 01332-249308, 275969, **FAX:** 01332 272123;
Mobile	: 9897-024025
E-mail	: skumar.nihr@gov.in; sudhir.nih@gmail.com

1.4 Co-PIs from Lead Organization

Name & Designation : Dr M Someshwar Rao, Sc. E

Date of Birth	: 1st June, 1965
Address	: National Institute of Hydrology, Roorkee
Telephone	: 01332 249225, **FAX:** 01332 272123
Mobile	: 9719537302
E-mail	: somesh.nihr@gov.in; 65somesh@gmail.com

1.5 Partner Organization (if any)

Name of the organization: CGWB, Lucknow
Head of the organization : Chairman, CGWB

1.6 Total Cost of Project (Rs.): Rs 55.40 lakhs

a) Lead Organization: 55.40 lakhs

b) Partner Organization: NIL

1.7 Duration: 2018 – 2024

CONTENTS

List of Tables

List of Figures

1. INTRODUCTION

Water is an essential resource that is crucial for sustaining life and plays a vital role in various aspects of human activities. It is vital for drinking, culinary purposes, irrigation, construction, and industrial processes. The significance of water stems from the fact that it constitutes approximately 60% of an individual's body mass and is essential for regulating body temperature and facilitating physiological functions. Adequate hydration, achieved through both liquid intake and water-rich foods, is necessary to replenish the fluid lost through respiration, perspiration, and digestion. Insufficient availability of water can lead to extensive famine conditions, particularly affecting agricultural output.

The world's population is projected to reach 8 billion on 15 November 2022, and India is projected to surpass China as the world's most populous country in 2023 (UN 2022). In the industrial sector, water serves multiple purposes and is indispensable for various operations. Industries such as thermoelectric power generation, manufacturing plants, ore refining units, and hydroelectric facilities heavily rely on water. Water acts as a solvent, cooling agent, and chemical reagent in these processes. According to the United States Geological Survey (USGS), water is integral to product creation, processing, cleansing, dilution, cooling, and transportation in industrial contexts. Critical industries like smelting, petroleum refining, food and paper manufacturing, and chemical production heavily depend on water.

Agriculture plays a fundamental role in India, providing subsistence for a significant portion of the population. About 45.8% labor forces are engaged in agricultural pursuits (PLFS, 2022-23), highlighting the substantial water utilization in irrigation and the nation's dependability both for productivity and employment of water resources. Groundwater withdrawal for irrigation purposes has increased in India, particularly in the state of Uttar Pradesh (UP). UP is the 4th largest state in terms of geographical area in the Indian sub-continent, and the 5th highest population density state (excluding Union Territories) in the country (Census, 2011). As per agro-productivity data of the economic survey for the year 2022-23, UP is the largest producer of wheat and sugarcane, 2nd largest producer of rice, and the 3rd largest producer of tur in the country. Considering uses of groundwater in all the sectors (irrigation, domestic and industrial), the stage of groundwater extraction (percentage of groundwater extraction with respect to annual extractable groundwater) of the state is 70.18%. However, if the unreported or underreported data pertaining to these sectors are considered then the stage of groundwater extraction is likely to reach to 85.24%. 70% administrative blocks of the state are witnessing groundwater devline. This is despite the fact that the major rivers of Himlayan origin such as Ganges, Yamuna, Ghaghara Gomti, Rapti, Gandak, Son, Sarda etc, flows through the state; the huge network of canal originating from these rivers caters the irrigation needs, and that the Central Ganga Plain is known for having the richest groundwater repository in the World (Sinha, 2021).

Table 1.1: Some salient features of the state Uttar Pardesh, India

Parameters	Details	Significance	References
Geographical Area	2,43,286 km^2	4th Largest state in India	https://up.gov.in/en
Population **Population density**	20.0 crores (2011) 23.89 (1st July, 2024) 829 per km^2 (2011)	The most populated state in India	Report of the Technical Group on Population Projections, July 2020; Nat. Comm. On Population, MoH&FW, GoI
Agrculture Cultivated area Gross Cropped area Production	 1,65,730 km^2 2,54,140 km^2 1st in Wheat and Sugarcane 2nd in Rice & Tur	**Land use** Net sown area: 69% Cropping area: Wheat: 48% Rice: 25% Sugarcane:10.74% Vegetables:6.79%	State Environment Plan for Uttar Pradesh, 2023, UPPCB
Water Resources Average rainfall Monsoon Non-monsoon WR from annual precipitation Total SW resource* Utilizable SW** Extractable GW resource	 Total: 872.5mm 771.2 mm 101.3 mm 228.28 BCM 161.64 BCM 118.47 BCM 65.25 BCM	**Utilizable WR** SW resource:118.47 Exploitable GW: Actual water utilized for irrigation SW: 43.8 BCM GW: 48.5 BCM Enhancement through the on going SW development projects: 27.8 BCM 43.2 BCM is non-utilizable water resource.	Uttar Pradesh State Water Policy, 2020 https://idup.gov.in/en/page/state-water-policy Dynamic Ground Water Resources of Uttar Pradesh (As on March, 2022) * Annual natural flow through rivers after considering ET losses **As per present strategy and technology Abbreviations: SW: Surface water GW: Groundwater WR: Water Resource

When rainwater or surface water infiltrates the ground, it undergoes a natural filtration process as it percolates through soil and rock layers. Soil particles act as a physical filter, capturing larger particles and sediment in the water. Bacteria and microorganisms contribute to the degradation and removal of organic pollutants. Clay and organic matter attract and retain dissolved ions, heavy metals, and certain organic compounds through adsorption. Ion exchange occurs when ions in the water are exchanged with ions on soil particles, causing changes in the water's hydrochemical characteristics. Various geochemical reactions, such as dissolution, ionic

exchange, reverse-ion exchange, and degassing, take place during infiltration, altering the chemical characteristics of the groundwater. For example, certain minerals release cations and ions into groundwater, while salt deposits or saline formations can increase sodium and chloride ion concentrations.

However, it's important to note that the natural filtration process is not foolproof and may not remove all contaminants. Some substances, including certain pesticides, volatile organic compounds (VOCs), persistent pollutants, and others, can bypass or resist filtration and enter the groundwater (Carlos et al., 2007, Karunanidhi et al., 2021). Additionally, excessive contamination or pollution in surface water can overwhelm the soil's filtration capacity, compromising groundwater quality. Therefore, it is crucial to assess and monitor the chemical quality of water to ensure its suitability for drinking and irrigation purposes.

Groundwater quality is influenced by various anthropogenic and natural factors as water travels from its recharge area to the point of observation. Analyzing the hydrochemical characteristics of groundwater and studying its spatial and temporal variations helps evaluate the hydrochemical processes that have shaped groundwater quality over time (Benhamiche et al., 2016; Passarella and Caputo, 2006). Groundwater quality is essential for agriculture and human health. Elevated salt levels in irrigation water can degrade soil fertility and agricultural productivity, while consuming contaminated groundwater can have serious health effects. Human activities and natural processes both impact groundwater quality. Spatial variations in hydrochemical facies indicate changing hydrochemical processes along the groundwater flow path, while seasonal variations reflect changes in the chemical composition of groundwater (Sarkar et al., 2017; Yuan et al., 2022).

To protect groundwater quality and ensure sustainable water resources, decision-makers need comprehensive databases and trend analyses. These tools aid in developing management and mitigation strategies, raising awareness about contamination risks, promoting safe practices, and implementing preventive measures. Comprehensive monitoring and assessment are crucial for safeguarding water resources and striking a balance between human needs and environmental integrity.

The past-literature offers numerous reviewes on groundwater chemistry and analysis tools for a comprehensive understanding of groundwater chemistry (Freeze and Cherry, 1979; Hem, 1985; Hewitt, 1992; Mazor, 2003; Apeelo and Postma, 2005; Machiwal et al.,2018; Fraser 2021). These tools aid in identifying contamination sources, supporting decision-making for sustainable groundwater management, and facilitating vulnerability assessments. Hydrochemical analysis plays a key role in understanding hydrogeochemical processes, water quality evolution, and the characterization of water sources. It provides vital information on the composition of groundwater, including major and trace elements, isotopes, and various physical and chemical parameters. By analyzing these data, researchers can unravel the interactions between water and rock formations, identify geochemical reactions, and assess the influence of natural and human factors on groundwater quality. Hydrochemical analysis is also useful in identifying recharge areas, detecting contaminant pathways, and aiding in the formulation of effective plans for protecting water resources from contamination and ensuring their long-term viability.

Another important aspect of groundwater research pertains to the impact of climate change on groundwater resources. Specifically, changes in rainfall patterns and temperature extremes have significant implications. Alterations in rainfall patterns, such as heightened intensity and frequency of extreme rainfall events, can result in rapid runoff and diminished infiltration, thereby restricting groundwater recharge. Conversely, prolonged dry periods can reduce groundwater recharge, exacerbating water scarcity issues during droughts.

Temperature shifts also play a role in influencing groundwater dynamics. They affect evapotranspiration rates and groundwater evaporation. Higher temperatures can accelerate evaporation rates, leading to increased water loss from aquifers. Moreover, temperature variations can modify the timing and magnitude of snowmelt, thereby affecting the recharge rates of groundwater systems reliant on snowmelt. Consequently, it is crucial for research efforts to explore the correlation between groundwater level trends and climate parameters, in order to comprehensively understand the impact of climate change on groundwater resources. Such research can aid in formulating adaptive strategies and policies for sustainable groundwater management in response to the impacts of climate change.

Research Objectives: The objective of this study is to conduct a comprehensive investigation of the hydrological aspects in the Upper-Middle Gangetic Basin. The study focuses on water quality assessment, groundwater interaction between shallow and deep aquifers, and the impact of climate change on groundwater resources. By utilizing primary data through sample analysis and archival data, the study assesses these hydrological aspects to develop groundwater augmentation strategies for sustainable groundwater management in the Upper-Middle Ganga Basin.

The specific objectives of the study can be delineated as follows:

Thematic Mapping: To prepare various thematic maps that provide insights into the spatial variation of hydrogeological characteristics in the study area. These maps will aid in understanding the distribution and nature of the hydrological features.

Groundwater Recharge Potential Assessment: To evaluate the spatial variation of groundwater recharge potential and identify suitable sites for implementing artificial recharge measures. This assessment will facilitate the development of strategies for augmenting groundwater resources.

Climate Change Analysis: To analyze climate change parameters, including rainfall patterns, drought occurrences, and temperature variations, and assess their influence on groundwater resources. This analysis will contribute to understanding the impact of climate change on the hydrological dynamics of the study area.

Groundwater Quality and Hydrogeochemistry Analysis: To examine the groundwater quality and hydrogeochemical characteristics, including the interaction between shallow and deep aquifers. This analysis will involve the use of water quality parameters, fingerprint diagrams, ionic ratio biplots, and stable isotopic characterization.

Assessment of Drinking Water Quality: To assess the spatial variation of groundwater quality specifically for drinking water requirements. This assessment will involve the utilization

of Water Quality Index (WQI) and Heavy Metal Pollution Index (HPI). The findings will be crucial for ensuring the availability of safe drinking water and implementing measures to mitigate pollution.

By achieving these specific objectives, this study aims to provide a comprehensive understanding of the hydrological dynamics in the Upper-Middle Gangetic Basin. The insights gained will contribute to the formulation of effective strategies for sustainable groundwater management and facilitate informed decision-making processes.

2. STUDY AREA

1.1. Ganga Basin: The Ganga River, also known as the Ganges, is broadly divided into three units: the upper Ganga stretch, the middle Ganga stretch, and the lower Ganga stretch. The upper Ganga stretch covers the river section from Gomukh to Haridwar, spanning approximately 294 km. The middle Ganga stretch extends from Haridwar to Varanasi, covering approximately 1082 km. Lastly, the lower Ganga stretch stretches from Varanasi to its delta in Gangasagar, covering around 1134 km (Chakraborti et al., 2003; Dutta et al., 2020). From a hydrological perspective, the Government of India (MoWR, 2014) divides the Ganga River into three stretches. The Upper Ganga stretch encompasses the origin of the Ganga River up to the Narora Barrage in Bulandshahar district, Uttar Pradesh. The Middle Ganga stretch extends from the Narora Barrage to Ballia district in Uttar Pradesh. Finally, the lower Ganga reach includes the stretch from Ballia up to the coastline, including the deltaic region and Sundarbans.

The Ganga Basin is a sub-basin of the composite Ganga-Brahmaputra-Meghna basin. The catchment area of the Ganga sub-basin lying in India covers nearly 26.2% of the total geographical area of the country (CWC, 2009). Approximately 40% of India's population lives in the Ganga river basin. The Ganga Basin can be broadly classified into three physiographic units: the Upper Ganga Basin, Ganga Plains, and the deltaic region. The Upper Ganga Basin is situated at an elevation ranging from about 7500 m to 100 m above mean sea level (Bharati and Jaykody, 2010). The Ganga Plains span an elevation range of 30-100 m above mean sea level, while the deltaic region is located within 0-30 m above mean sea level (Jha and Bairagya, 2011). The plains of the Ganga Basin are further divided into three physiographic zones: the Upper Ganga Plains, Middle Ganga Plains, and Lower Ganga Plains. The upper Ganga plain is bounded by the Shiwalik Hills in the north, the Peninsular Plateau in the south, the river Yamuna in the west, and the 100-meter contour line in the east. The Middle Ganga Plain is bounded by the 100-meter contours in the west, the 75-meter contour in the east, and the 30-meter contour line in the southeast. The Lower Ganga Plains encompass areas from the foothills of the Himalayas in the north, extending from West Bengal to the Ganges Delta in the south, including the Ganga Sagar area.

The riverbank sustains a variety of festivals, including the most famous festival 'Kumbha Mela.' Recognizing the significance, importance, and value of the river, the Government of India changed its ministry's name from the Ministry of Water Resources to the Ministry of Water Resources, River Development, and Ganga Rejuvenation. They have initiated programs like the National Mission on Clean Ganga and Namami Gange. Additionally, the government established the National Ganga River Basin Authority

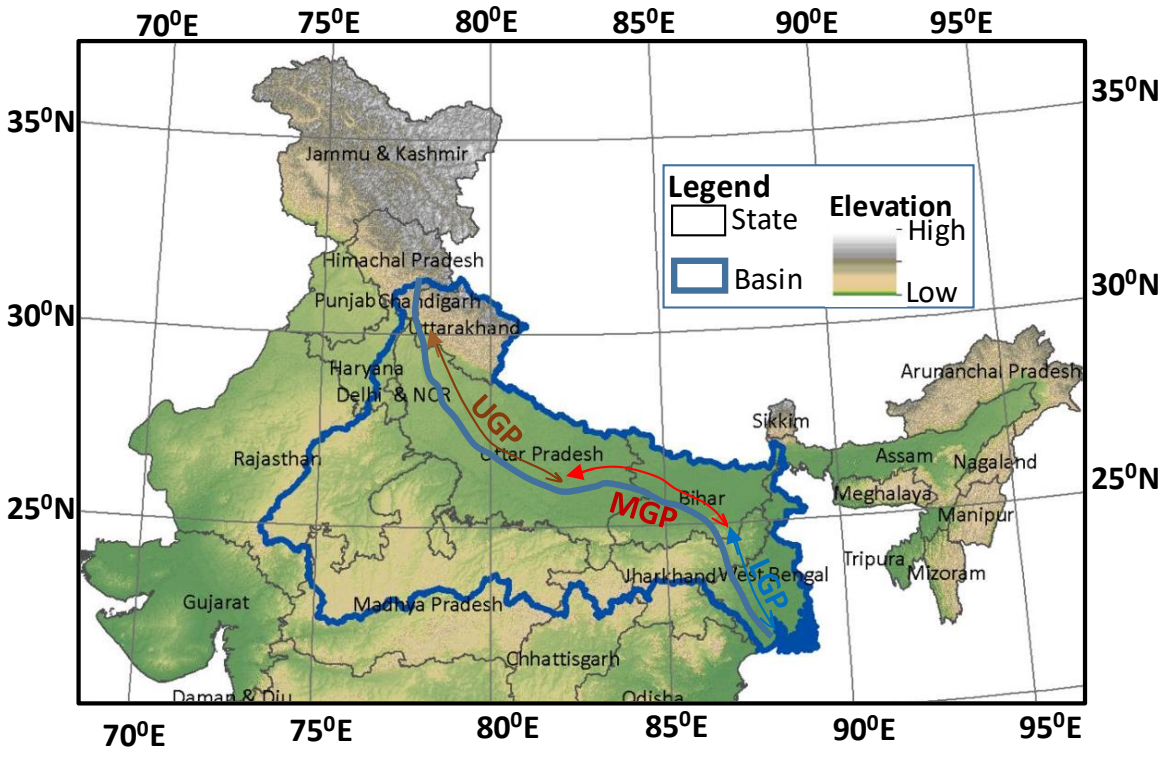

Fig 2.1. Ganga Basin (source:www.india-wris.nrsc.gov.in)
UGP:Upper Ganga Plain, MGP:Middle Ganga Plain, LGP: Lower Ganga Plain.
Note: UGP does not cover hilly parts of Uttarakhand region (Source:Dutta et al., 2020)

1.2. Study Area: The study area of this research focuses on the middle Ganga basin, which extends from the foothill region of the Siwalik hills (~500m above mean sea level) in the north to 30m above mean sea level in the plains in the southeast, primarily falling within the state of Uttar Pradesh. The study area is bounded between latitudes 29.742°N and 25.036°N and longitudes 78.37°E and 82.904°E, covering an area of 95,900 km². The study area is bordered by the Ganga River to the south and the Sharda and Ghaghara rivers to the north. It encompasses 27 districts in Uttar Pradesh, with a total population exceeding 91.1 million. The terrain is predominantly gently sloping, with a northwest to southeast slope direction, except for the northern boundary districts, which border the Shiwalik foothills which is a piedmont region, and has a moderately undulating terrain.

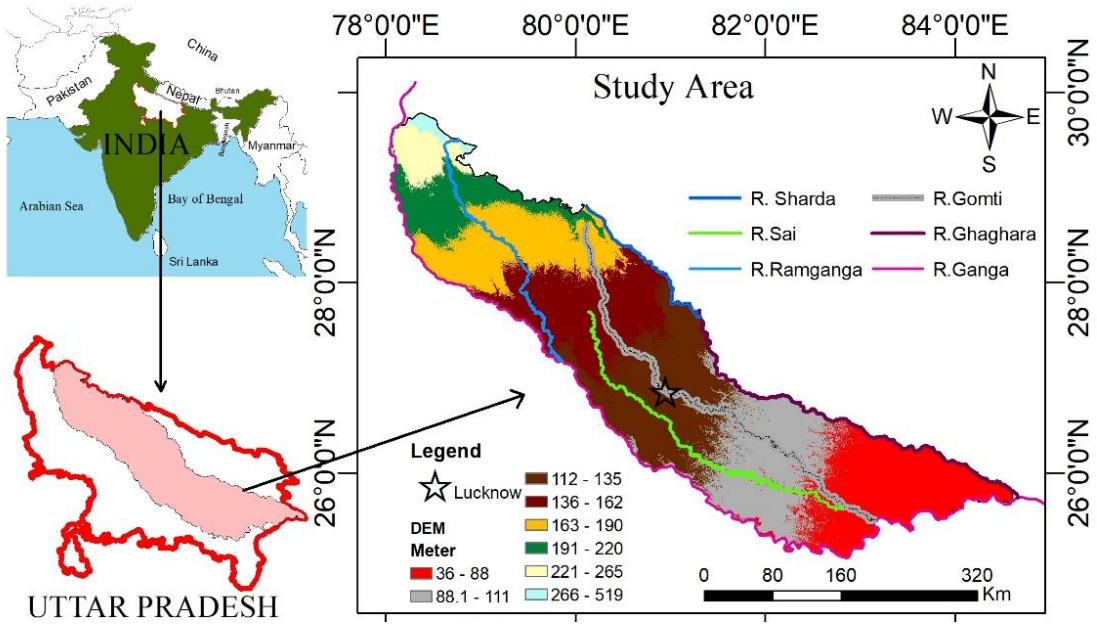

Fig. 2.2. Study Area. In the left hand side shown the study area (area filled in pink) in the state of Uttar Pradesh (red contour). In the shown the DEM overlaid with main rivers in the study area.

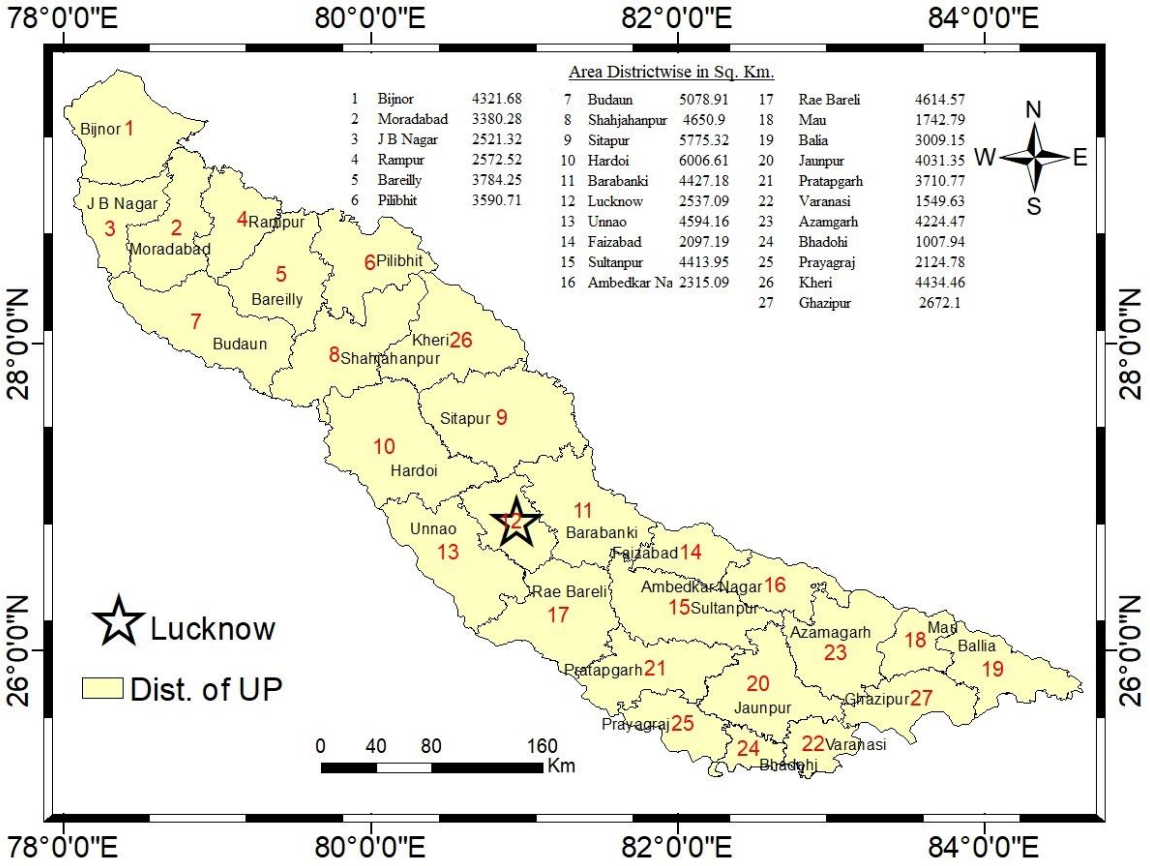

Fig 2.3: Adminsitrative districts (of Uttar Pradesh) falling in the study area

1.3. Climate: The region experiences a humid subtropical climate with dry winters. Rainfall patterns vary, with the northern part near the hills receiving high rainfall (>1400 mm) and the southwestern part receiving less than 600 mm annually. The mean annual rainfall (1991 to 2020) is 867.5 mm, with nearly 88% received during the monsoon season from June to October. The region also experiences winter rainfall from western disturbances, beneficial for Rabi crops, and occasional spring and summer rainfall.

1.4. Topography: The land cover in the study area includes thick forests in the foothill region, grasslands, sandbars, floodplains, and various alluvial plains. Soils range from sandy to clayey, with aquifer depths varying across different zones. The central part hosts active floodplains and terraced alluvium deposits, while the lower part consists of sandy to loamy soils, with swampy and marshy low-lying areas. The middle and lower zones of the study area are crisscrossed by a dense canal network, extensively contributing to irrigation water supply.

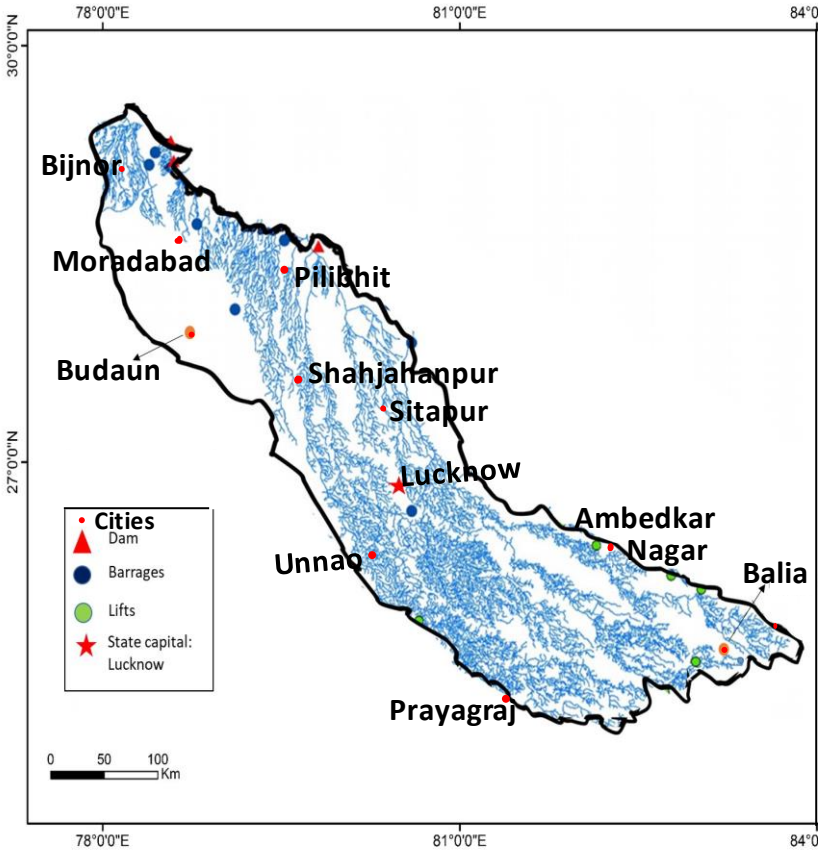

Fig 2.4. Canal network, dams, barrages and major cities in the study area

Fig 2.5. Distribution of major industries in the study area

1.5. Hydrological Issues in the Sudy Area: A fundamental hydrological challenge faced by any region is ensuring the provision of sustainable freshwater resources to meet the needs of a growing population, as well as supplying water of suitable quality for various vital sectors including agriculture, power generation, industries, and other essential services. These challenges are particularly pronounced in the study area, the upper-middle Ganga plains, due to its heterogeneous demographic, agricultural, and industrial landscape.

The population in the study area is steadily increasing, and the region is characterized by intensive agricultural activities alongside a concentration of various industries. Unfortunately, improper disposal of wastewater has resulted in many tributaries of the Ganga becoming conduits for sewage and industrial effluents, leading to contamination of surface water sources and nearby dumping sites, thereby posing a significant risk to groundwater quality. The extent of infiltration of contaminants into the groundwater remains uncertain.

Moreover, the dual impacts of climate change and evolving land use patterns are emerging as crucial factors influencing groundwater sustainability, impacting both the region's economic development and ecosystem health. Addressing these multifaceted challenges forms a central focus of the present project, which aims to systematically assess and mitigate the complex interactions between human activities, environmental dynamics, and groundwater resources in the upper-middle Ganga plains.

1.6. Objectives

The combined impacts of increasing population, urbanization, increased water use with prosperity, land-use change, inexpensive drilling and pumping technology, industrialization, expansion of irrigated agriculture, institutional changes, stricter water quality standards, and perhaps the early influence of climate variability, have led to widespread, often unmanaged, use of groundwater [Gorelick, S., M. et. al. 2015]. In order to solve the groundwater problems in the study area, the following objectives have been ascertained in the current study:

a) ***The trend analysis and the forecasting of the rainfall and the temperature using ARIMA model***: The rainfall and the temperature are variable through space and time. This can affect the quantity of the water reaching to the aquifers. A proper forecast of the climate variables will help to know the future groundwater deficit.

b) ***Groundwater modelling and groundwater flow analysis***: The groundwater fluctuation depends upon factors like rainfall amount, water extraction rate, and water movement under the ground. All the factors must be properly studied to understand the groundwater system.

c)Making a Groundwater Recharge Potential Zone (GWRPZ) and recharge sites in the study area: The recharge potential of the area varies from place to place due to many factors which affect the infiltration of the water into the soil. After taking those factors into consideration the study area can be divided into many zones, each zone of different groundwater recharge capacity.

d)Groundwater vulnerbility to quality: Contaminations due to trace metals and other ions are the major issue in the populus areas in Middle Ganga Basin. Areas under high contamination through drinking possesing health risk are needed to be identified. The grade of irrigation water available to irrigators has a significant impact on crops as well as yields as majority (more than 80% of the study area is under agriculture). Therefore, it is a need to better understand irrigation water quality.

e) Shallow-Deep groundwater interaction zones- Zones where shallow-deep groundwater intermixing are needed to be identified for early management of contamination reaching deep aquifers directly.

f) Groundwater management plan for conservation of groundwater: A) Supply side measures aimed at increasing extraction of ground water depending on its availability and B) Demand side measures aimed at controlling, protecting and conserving available resources.

3. LITERATURE REVIEW

Groundwater plays a pivotal role globally, especially in agriculture accounting for 43 percent of total water usage (Rodella et al., 2023), is facing alarming depletion rates; mainly due to overdrafting and mismanagement (Margat and Van der Gun 2013). Infact, the data depicts that over half of the world's major aquifers depleting faster than they can naturally recharge, posing a threat to global food and water security (Benavides et al., 2023). Figure 1 provides an illustration of trends in agricultural withdrawals and areas equipped for irrigation in countries with the highest agricultural withdrawals, highlighting the magnitude of this issue. In addition to the agriculture water deand, profound impacts are also due to increasing urbanization, population density, and industrialization. These factors directly or indirectly are depleting the fresh water resources as the intensification of these these parameters is resulting in the loss of vegetation, expansion of impermeable surfaces like pavements, increased extraction of groundwater, and contamination from waste discharge (Li et al., 2019; Liu et al., 2020); Alley et al., 2017). Further, growing population is resulting in rising food demand thereby increasing the irrigation water demand (USGS, 2020). These factors are not only depleting the aquifers but also contaminates them with heavy metals, pesticides, and chemicals, posing significant challenges for sustainable water management practices.

India, with its growing population and substantial agricultural demands, heavily relies on groundwater, surpassing even the combined usage of the United States and China (MoWR, 2022). The increase in the withdrawal is estimated to be between 122 to 199 billion m^3 from 2002 to 2016, accounting for approximately 30% of the total annual groundwater recharge (Mishra et al., 2018; MoWR, 2023). In the northwest Indian states (Rajasthan, Punjab, and Haryana), the groundwater is depleting at a rate of 4.0 ± 1.0 cm yr^{-1} (Panda et al., 2021). This depletion poses a threat to food security, and also resulting in the reduced discharge in the river flows (Mukharjee et al., 218) which is becoming a threat to the aquatic species. Hence, an urgent attention is necessary to implement strategic plans for sustainable groundwater utilization (Rodella et al., 2023).

Uttar Pradesh, the largest state in terms of population in India, despite being located in the Gangetic basin, is experiencing a notable decline in groundwater levels. The decline was up to 3m in 2009-2010 (Panda et al., 2021). The declining, particularly in its western and central regions (CGWB, 2022). Approximately 46% of monitored groundwater observation wells in the state show declining levels, with significant depletions observed in areas such as Budaun and Gautam Budh Nagar (CGWB, 2022). For example, data from August indicates considerable fluctuations in groundwater levels, with maximum depletions of 12m and 14m observed in Budaun and Gautam Budh Nagar, respectively (CGWB, 2022). This localized scenario highlights the urgency of implementing region-specific management strategies to mitigate groundwater depletion risks and ensure sustainable water resource management. Conservation efforts, efficient utilization practices, and suitable recharge measures are imperative to address the challenges posed by declining groundwater levels in Uttar Pradesh.

The groundwater recharge is directly related to the rainfall amount; and therefore directly links with the seasonal changes in the rainfall pattern, and the decadal scale rainfall pattern, i.e.,

impact of climate change (Fistikoglu et al., 2016, Gunduz et al., 2011, Hussin et al.,2020, Fallahi et al., 2023).

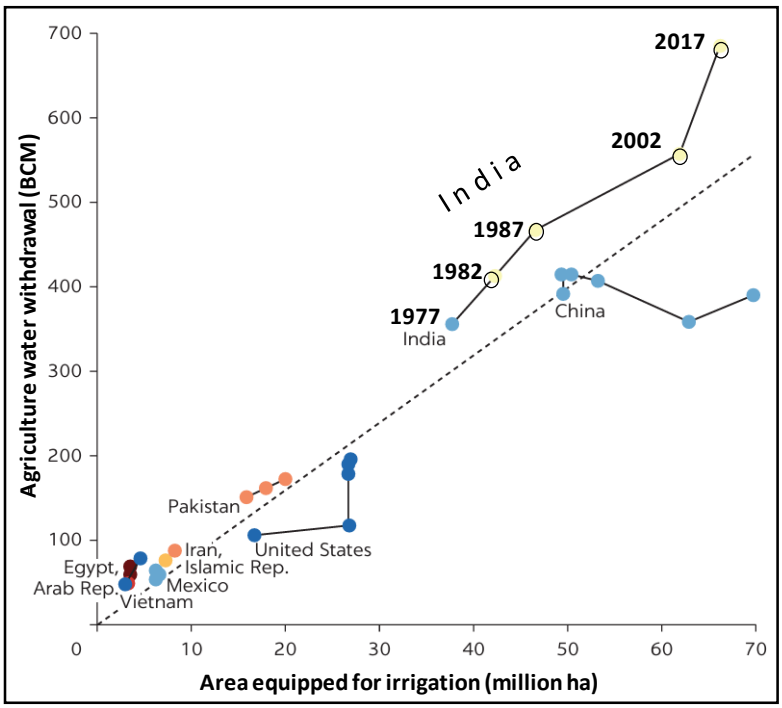

Fig.3.1 Countries with the largest agricultural water withdrawals (Fig.source: Reproduced from Susanne & Tréguer, 2018)

Trends in the time series of rainfall, temperature etc., are usually done using statistical tests such as, Mann-Kendall's test and Sen's test etc, whereas, statistical analysis of draught and wet peroids are usually done using indices such as Rainfall Anomally Index, Standard Anonaly Index (SAI), departure from normal etc (Jiqin et al., 2023; Zaveri et al., 2020).

Artificial recharge serves as a crucial strategy in mitigating groundwater depletion. However, effectively implementing this method necessitates the meticulous mapping of zones potential for groundwater recharge. These zones are the areas that favor high infiltration. The map for groundwater recharge potential zones (GWRPZ) provide a comprehensive assessment of landscape for groundwater recharge mapping. Since, recharge depends upon various factors like,

slope, lineament, land-use, drainage density, geomporphology, soil type etc., the map for groundwater potential rechargeable zones is prepared by integrating the thematic maps based on these parameters by assigned weights to each parameter and then adding these by Analytic Hierarchy Process (AHP). For large study areas GWRPZ are conveniently mapped using remote sensing (RS) –GIS technique (Bonacci et al., 2018; Li et al., 2019; Dar et al., 2021; Zwedie et al., 2024).

Quality of groundwater is determined by measuring and analysing water quality parameters viz., major ions, heavy metals, microbiological parameters, EC, pH, temperature etc. Groundwater acquires its hydrochemical characteristics through chemical interactions with geological formations and sources of contamination along its flow path. These interactions involve processes such as dissolution, precipitation, and chemical equilibria. As a result, the concentration of water quality parameters changes smoothly along the groundwater flow path, reflecting the cumulative effects of these interactions. Analyzing correlations between chemical parameters provides valuable insights into the overall hydrogeological setting and water quality dynamics.

The Pearson correlation matrix (or simply the Correlation Matrix) is the coefficient of linear relationship between two variables. Positive values indicate a positive linear correlation, meaning that as one variable increases, the other tends to increase as well. Negative values indicate a negative linear correlation, indicating that as one variable increases, the other tends to decrease. The magnitude of the correlation coefficient indicates the strength of the relationship, with values closer to 1 or -1 indicating a stronger correlation, and values closer to 0 indicating a weaker correlation or no correlation. The magnitude of the values reflects the strength of correlation, indicating the likelihood that the observed correlation is not due to random chance but rather represents a genuine relationship between the variables.

Principal Component Analysis (PCA) is a powerful tool for simplifying data and identifying key factors that influence water quality. By recognizing patterns and relationships among inter-correlated variables, PCA helps to reduce the dataset into components that describe the chemical parameters of groundwater. Eigenvalues, which represent significance, guide the selection of principal components (PCs) where values greater than 1 are considered significant. Typically, these significant PCs explain more than 85% of the variance in the groundwater dataset, which is crucial for understanding groundwater geochemistry.

3.1 Groundwater chemistry and quality: Groundwater chemistry is largely a function of mineral composition, the formation through which it flows due to rock–water interaction. Evaporation and concentration, dilution due to precipitation also can change the chemical composition of groundwater but rock–water interaction is the major process because solid phases (inorganic and organic matter) are the primary sources and sinks of dissolved constituents of groundwater. During groundwater movement along its path from recharge to discharge areas, a variety of chemical reactions with solid phases take place. These chemical reactions vary spatially and temporally, depending on the chemical nature of the initial water, geological formations and residence time. The resulting concentrations of major ions of groundwater can be used to identify the intensity of rock–water interaction and chemical reactions.

Hence, knowledge on rock–water interaction that control groundwater chemical evolution will lead to improved understanding of hydrogeochemical characteristics of an aquifer. This would contribute in the effective management and utilization of groundwater resources.

To understand the same, major cations and anions were evaluated. These variables were further analyzed for vulnerability in qualitative aspect for drinking and irrigation purposes using physical parameters, major ions and trace metals. These are discussed below –

3.2. Water Quality Parameters

3.2.1 Physical Parameters (pH, EC and Total Hardness)

i) pH: The pH of water is an important indicator of the acidic-basic interaction of the components of water and a number of minerals (Dev and Bali, 2019). The water is thus slightly acidic in many cases and the shift towards the alkaline side may be due to the geological formation of the area which composed mainly of CaCO3. Low pH levels, high carbon dioxide content, and low mineral content are the characteristics of corrosive water (Saha et al, 2019). It is observed in several studies that pH increases with increasing groundwater age due to hydrolysis of silicate minerals, which are abundant in the bedrock and glacial materials under the water body. Because these reactions do not rapidly reach equilibrium, the pH is generally greater in older groundwater (Kai et al., 2021).

ii) Electrical Conductivity(EC): The electrical conductivity (EC) that results in increase in the groundwater salinization can be due to various reasons such as; due to groundwater mineralization with increasing age of groundwater, dissolved minerals of saline soils, seawater intrusion, pollution, evaporation enrichment of salts, etc. (Kaushal et al., 2021).

iii) Total Hardness(TH): Calcium and magnesium are the major constituents responsible for water hardness results in dissolution of carbonate minerals such as calcite and dolomite. "Hardness" is a term relating to the concentrations of certain metallic ions in water, particularly magnesium and calcium and is usually expressed as an equivalent concentration of dissolved calcite ($CaCO_3$). In hard water, the metallic ions of concern may react with soap to produce an insoluble residue. These metallic ions may also react with negatively charged ions to produce a solid precipitate when the water is hard. Total hardness is a measure of the capacity of water to the concentration of calcium and magnesium (usually expressed as the equivalent of $CaCO_3$ concentration). Abundance of carbonate hardness may be attributed due to dissolution of aragonite bearing minerals due to pedological differentiation in sedimentary cycle of depositional environment (Roopvathi et al., 2016).

Hardness is an important factor in determining the suitability of water samples for domestic, and irrigation purposes as it is involved in making the water. The water hardness is classified as, soft, hard, moderately hard and very hard. For the maximum permitted limit of total hardness for drinking is specifies as 500 mg/l. However, for irrigational purposes, more than 1000 mg/l of hardness is also accepted (Prasanth et al., 2012, Vetrimurugan, et al., 2013).

3.2.2 Major cations (Na, K, Ca, and Mg)

i) Calcium(Ca^{2+}) and magnesium(Mg^{2+}): Calcium is sometimes referred to as lime. It is essential component for the preservation of the human skeleton and teeth. It also assists the functions of nerves and muscles. The use of more than 2.5 grams of calcium per day without a medical necessity can lead to development of kidney stones, bone calcification, sclerosis of kidneys and blood vessels. Extremely high dose causes kidney stones and increase the risk of prostate cancer. High calcium diets may have a deleterious effect upon bone mineralization because of their hypomagnesic (magnesium depleting) effect and can interfere with the absorption of phosphorus, which like calcium is important for the bones. Mg deficiency in drinking water can produce calcification disorders and neuropathologies including traumatic brain injury, headache, suicidal ideation, anxiety, irritability, insomnia, short-term memory loss and general depression (Rapant S., 2017).

Magnesium Hazard (MH) index evaluates the potential impact of magnesium content on water quality, particularly in terms of soil dispersion. High levels of magnesium in water can have a negative impact on crop yields as it can increase soil alkalinity, making the soil unsuitable for plant growth. It is recommended that irrigation water has a magnesium-to-calcium ratio of more than 1 and an exchangeable magnesium percentage in soils exceeding 25% can lead to soil issues (Chakraborty et al., 2022).

ii) Sodium(Na^{+}) and Potassium(K^{+}): Weathering of Na–K bearing minerals, like halite and plagioclase, cation-exchange process and industrial or agricultural activities may be responsible for the dominance of Na–K in ground water in the study area. Exchange of Na and K by Ca and Mg, adsorbed on the surface of the clay minerals can cause their (Na, K) higher concentration [29]. The natural sources of potassium in water are the minerals of local igneous rocks such as feldspars (orthoclase and microcline), mica and sedimentary rocks as well as silicate and clay minerals. Water with a Na level above 200 mg/l presents a serious health risk for people with heart conditions, nephropathy and circulatory problems (Thompson et al., 2022). Water with high sodium content is not suitable for agriculture, as it tends to deteriorate the soil for crops. Sodium associates with chloride and sulphate making the water unpalatable (Guy, 2017). Sodium and potassium concentrations are also influenced by the cation exchange mechanism. Groundwater salinity and its sodium content directly influence crop productivity. The decomposition of granitic terrain containing feldspar may be another reason for increased concentration of both the ions.

3.2.3 Major anions (Alkalinity (Carbonate and Bicarbonate), Cl, SO_4, NO_3, F)

i) Alkalinity (Carbonate and bicarbonate): In the range of normal ground water chemistry, alkalinity primarily results from the HCO_3^- content of the water. Although the alikalinity can have inorganic and organic origin, but at high pH values carbonate mainly contribute to alkalinity (Michałowski, 2012). Most of the data sets resulted pH values lower than 8. This

indicates that observed in groundwater of study area may be affected from HCO_3^- was found at slightly higher levels in the post monsoon period indicating that some contributions might have come from the carbonate weathering process due to heavy downpour in the catchment. The dissolution of gases and minerals, particularly CO_2 and CO_3 compounds in the atmosphere and in the unsaturated zone during precipitation and infiltration, would impart the observed HCO_3^- water type. Further, feldspar is among the major minerals present in the region and kaolinization of K-feldspar and consequent production of bicarbonate ions can also be explained by this factor. The geo-chemical reaction may be expressed as (Singh et al. 2021):

$$2\text{K-Feldspar} + 2CO_2 + 11H_2O \rightarrow \text{Kaolinite} + 2K^+ + 2HCO_3^- + 2H_2SiO_4$$

ii) **Chloride:** Rain water usually comes with the chloride concentration in the range from a few ppm to few tens of ppm (Tiwari et al., 2006; Naik et al, 2016). In the unsaturated zone, Cl^- remains as a conservative ion it hardly sorbs to soils or plants and does not undergo any chemical reactions. The presence of high chloride in the soil solution reduces the ability of the plants to take up water and this leads to reduction in the growth rate. High chloride content reduces pH (alkalinity), increases salinity, increases corrosive character, reduces plant growth and deterioriates potable quality of water.

iii) **Sulphate:** Sulphates are found in small quantities in groundwater, mostly coming from anthropogenic additions in the form of sulphate fertilizers (Pawar and Shaikh, 1995) and also from domestic and industrial wastes. Sulfate enters into groundwater through incorporation of sulpher in surface water through oxidation of sulfide minerals during chemical weathering, atmospheric deposition from acid rain, human and animal waste, farming, and industrial processing and manufacturing. Sulfates are corrosive to metallic materials due to conversion from sulfates to sulphides by anaerobic reducing bacteria.

iv) **Fluoride:** While on a local scale anthropogenic activities, such as the application of phosphate containing fertilizers or aluminium smelting, may introduce considerable amounts of fluoride into the environment, its concentration in the groundwaters is mainly governed by geogenic processes. Possible sources of fluoride (F^-) are weathering and leaching of F^- bearing minerals under the alkaline environment. Various minerals, e.g., fluorite, biotites, topaz, and their corresponding host rocks such as granite, basalt, syenite, and shale, contain fluoride that can be released into groundwater (Amini et al. 2008). The concentration of fluoride increases with the increase in the depth of the groundwater (Wen et al. 2013). High fluoride concentrations can be built up in groundwaters, which have long residence times in the host aquifers. Groundwater flow is slow and reaction times between water and rocks are therefore enhanced which leads to the release of fluoride.

v) **Nitrate:** Application of fertilizers after exceeding plant uptake and removed after harvesting brings with it a large N-export into rivers and ponds causing eutrophication of freshwater reservoirs, as well as damaging groundwater reservoirs. The proximity of pit latrines area and the individual setting (e.g. depth) are the most important factors affecting nitrate concentrations (Kringel et al. 2016). Nitrate concentration in ground water exceeding an arbitrary threshold of 3 mg/l may be indicative of contamination of natural groundwater as a result of human activities. Elevated concentration of nitrate in groundwater leads to human and environmental health risks. Excessive consumption of nitrate in drinking water has been associated with the risk of methemoglobinemia or 'blue baby syndrome' in humans, stomach cancer. Besides, denitrification processes contribute to the emission of greenhouse gases due to production of N_2O (Zapata et al. 2014). The nitrate concentrations in groundwater have decreased due to common understanding that the total N applied as manure and synthetic fertiliser by far exceeded plant demand. This stimulated farmer to reduce chemical fertiliser inputs requirements. So in this way the concentration of nitrate has decreased gradually now a day (Grinsven et al. 2016). The high nitrate content observed in the surface water bodies is most likely related to the leaching of nitrate salts that are retained in the agricultural lands by the first rains that occurs it is washed away to the surface water bodies (Sena et al. 2012). Agriculture is the main source of nitrate. Nitrate from diffuse sources is typically delivered to streams via subsurface pathways, with links between increasing nitrate concentrations and groundwater contributions (Mockler et al. 2017).

3.2.4 Trace metals (As, Cu, Cr, Mn, Pb, Fe, Zen)

i) **Arsenic (As):** Dissolved arsenic concentrations are high where sulfate is essentially absent from the groundwater and low in areas that contain high concentrations of sulfate. The release of arsenic requires reducing conditions that solubilize the Fe oxide phases onto which the arsenic is sorbed. It is therefore not a surprise that arsenic concentrations are inversely correlated to concentrations of sulphate (Lawson et al. 2013). According to different authors high concentrations of As, together with Fe and Mn, can be found in alluvial aquifers that contain natural organic matter buried in sediments (i.e., peat) due to a reductive dissolution mobilization mechanism, which considers manganese and iron oxides as As carriers (sources) and degraded organic matter as the redox driver of the release. In particular, As contamination may not be fully developed until the Fe oxides approach complete reduction because As can be readsorbed to residual Fe oxides that are not yet reduced. Prolonged period of iron reduction leads to release of As (III) in the form of ferrihydrite transformation to magnetite (Kocar et al. 2006). It has been found that As is derived from microbially reductive dissolution of Asrich Fe-oxyhydroxides. When the redox environment of groundwater changes from oxidizing to reducing conditions, reduction of Fe(III) leads to the dissolution of Fe (hydr)oxides and the release of adsorbed As. Microbial reduction of As(V) to As(III) also increases the mobility of As because As(V) adsorbs to minerals more strongly than As(III) under neutral conditions (Tong et al. 2014). In some of the studies it has been found that As concentration decreases with

the increase in depth (Rotiroti et al. 2014). Thus groundwater is much better for human consumption and other household purpose than surface water.

ii) **Cadmium (Cd):** Cadmium is the most harmful of all the heavy metals found in groundwater, this is because Cd can cause the impairing of DNA/RNA and ribosomes (Gerhard et al. 1998). Cadmium (Cd) is one type of harmful heavy metal for human blood vessels and may accumulate in vital organs, especially in liver and kidney. In low concentration, Cd effects on disturbances in emphysema, lung and renal tubular chronic disease. Cadmium usually mixes with other heavy metals such as Zn and Sn. This heavy metal causes lethal for aquatic biota such as Crustacean (Effendi et al. 2016).

iii) **Chromium (Cr):** Chromium has genotoxic potential, can alter the human immune system and induce throat cancer; nasal lesions and perforation of the septum and skin; kidney and liver disorders. Several studies have shown that exposure to chromium can result in DNA damage (Morais et al. 2016). In drinking water, the level of chromium is generally low, but contaminated well water may contain the dangerous hexavalent chromium. In the present work, only total Cr was determined and Cr (III)/Cr (VI) speciation was not attempted. In groundwater, chromium occurs predominantly as Cr (III) and Cr (VI). The relative distribution of the species depends on the aquifer redox conditions. The two species differ in their toxicity towards organisms and their behavior in the aquatic environment; Cr (III) is essential micronutrient, whereas Cr (VI) is a suspected carcinogen; Cr (III) is almost immobile, whereas Cr (VI) is highly soluble and mobile Under the alkaline pH and the high buffering capacity of these samples, Cr (VI) was highly soluble (Kumar and Riyazuddin, 2009).

iv) **Copper (Cu):** Unlike the other metals studied, Cu^{2+} is essential for plants' metabolic activities, so the metals may have been used up by aquatic and terrestrial plants in the river and soils, thereby reducing the levels that ultimately get to the groundwater (Etchie et al. 2012). The source of copper may be due to the intrusion of industrial and domestic wastes. Corrosion of brass and copper pipes also contributes to copper level in water. The alkaline pH of the medium can also be the cause of low level of copper, as heavy metals are precipitated as their salts at high pH and are deposited as sediments (Jameel et al. 2012).

v) **Iron (Fe):** Iron is a natural constituent present in most groundwaters. Iron bearing minerals such as pyroxenes, amphiboles, biotite, and magnetite are commonly present in hardrock. In sedimentary rocks, pyrite, marcasite, siderite, and ferric oxyhydroxides are the common iron bearing minerals. In addition, iron is present in organic wastes and plant debris in the soils. The activities in the biosphere may have a strong influence on the occurrence of iron in groundwater. At pH values (6–10) encountered in groundwater, Fe (III) is almost insoluble; however, complexation of Fe (III) may increase its solubility (Kumar et al. 2009). Iron is the most commonly available metal on planet earth. The high concentration of iron is a matter of concern as large amount of ground water is abstracted by drilling tube wells, etc. both in rural and urban

areas for drinking and irrigation purposes. Also the presence of iron is responsible for the brownish – red colour of the water when allowed to stay for some time. Other sources of iron in drinking water are iron pipes, cookware, etc. It affects organs like the liver, cardiovascular system and kidneys (Jameel et al. 2012). Iron is essential to almost all living things, from microorganisms to humans. Its concentration in aquatic environment is greatly affected by its speciation. Iron (II) is more soluble than iron (III) in water. Modern oxygenated seawater contains approximately 1-3 ppb of iron. Rivers contain approximately 0.5-1 ppm of iron (Firdaus et al. 2014). Ingestion of Fe in large quantities results in a condition known as 'haemochromatosis', which results in tissue damage causing due to high iron concentration (Tiwari et al. 2015).

vi) **Lead (Pb):** Lead contamination of the ground water may be the result of entry from industrial effluents, old plumbing, household sewages, agricultural run-off containing phosphatic fertilizers and human and animal excreta. In addition to the symptoms found in acute lead exposure, symptoms of chronic lead exposure could be allergies, arthritis, hyperactivity, mood swings, nausea, numbness, lack of concentration, seizures and weight loss (Jameel et al. 2012). Lead accumulated in bones dissolves over time and may lead to inflammation in kidneys and abnormalities in brain and nervous system functions, and that IQ levels of children decrease due to the increase of lead in blood (Kahvecioglu et al. 2003,).

vii) **Manganese (Mn):** Exposure to elevated Mn in drinking water is associated with neurotoxic effects in children and diminished intellectual function. Mn oxides, found in soils and sediments, are highly reactive and strong scavengers of heavy metals and trace elements, including As. The presence of manganese oxides decreases As availability and As mobilization both by the oxidation of arsenite and sorption of arsenate. This behaviour is consistent with the observed negative correlation between As and Mn. Mn is very harmful for children and new born babies as this may affect the intellectual development of the baby (Diwakar et al. 2015).

viii) **Zinc (Zn):** Zn is an essential element for physiological processes in both plant and animals, the WHO has not given any guideline value for Zn but even then a very high concentration of Zn in water may cause harmful health effects. Zinc and its salts are used to manufacture goods and are added to agricultural fertilizers in the study area. Zinc contamination generally enters water through two pathways: identifiable point sources such as industrial effluents and diffuse sources such as agricultural runoff (Zhang et al. 2015). Zinc (Zn) is a quite important material for enzyme and protein production. The high value of Zn is possibly caused by industrial activities and mining wastewater input. Zinc tends to be found in only trace amounts of unpolluted surface water. Nevertheless, it is often found in domestic supplies as a result of iron piping corrosion, tanks and disinfection of brass fittings (Effendi et al. 2016).

3.2.5 Water Quality Diagrams

The US Salinity diagram is a tool used to assess irrigation water quality based on salinity (EC) and sodium absorption ratio (SAR) levels. The diagram divides water quality into 16 zones

based on increasing sodium hazard (S1 to S4) and salinity levels (C1 to C4). This categorization is essential for assessing irrigation water suitability for different crops and soils. By identifying specific subzones within the diagram, agricultural practitioners can make informed decisions to optimize crop selection and irrigation practices, thus maximizing agricultural productivity and sustainability.

There are also other methods commonly used for evaluating irrigation water quality, such as %Na, permeability index, Kelly's Index (KI), and Magnesium Hazard (MH). The Percent Sodium (%) relative to other cations in water if high indicates sodium hazard. Typically, a SAR value below 2.0 is considered very safe for plants especially if the sodium concentration is also below 50 mg/L (Rosu et al., 2014). High sodium content can cause soil structure problems like clay dispersion, which can lead to reduced water infiltration and increased soil erosion (Hailu et al., 2021). Additionally, high sodium levels can increase soil salinity over time, further affecting plant growth.

The permeability index in relation to irrigation water indicates how easily water can move through soil. High permeability means water flows easily through the soil, while low permeability implies water movement is restricted. When considering irrigation, high permeability soils may allow water to drain too quickly (Lu et al., 2024), potentially leading to water wastage and inadequate moisture for plants. On the other hand, low permeability soils might retain water excessively, causing waterlogging issues.

Kelly's Index (KI) is a measure used in agriculture to assess the suitability of irrigation water for crop production based on its sodium content relative to calcium and magnesium. A KI value higher than 1 indicates that the water has a high sodium content relative to calcium and magnesium, which can lead to soil degradation and reduced crop yield. A KI value lower than 1 suggests a low sodium content relative to calcium and magnesium, indicating safer irrigation water for agricultural purposes (Chakraborty et al., 2022).

The development of the Water Quality Index (WQI) has been a significant advancement in environmental science and water resource management. Originating with Horton's (1965) and Liebman (1969), the WQI provides a comprehensive assessment of water quality by transforming complex water quality data into a single numerical score. This index plays a crucial role in monitoring surface and groundwater pollution. The importance of the WQI lies in its ability to simplify vast amounts of water quality data into a user-friendly format that is easily used for comparison of water quality across different locations and time periods. WQI serves as a valuable tool for regulatory agencies, environmental organizations, and water utilities in setting water quality standards, designing monitoring programs, and allocating resources for pollution prevention and remediation efforts (Soltan, 1999; Stigter, 2006)

Industrialization has resulted in widespread pollution of surface water and groundwater worldwide, primarily due to the contamination of heavy metals. These heavy metals, known for their high density and toxicity, pose significant health risks even at low concentrations. They

originate from various sources such as industrial effluents, landfill leachate, and mining activities. Monitoring the concentration of heavy metals, especially in groundwater sources used for drinking water, is crucial for mitigating waterborne diseases and safeguarding public health.
Certain heavy metals, though essential for bodily functions, can be harmful when present in excessive amounts. Arsenic, for example, is a major concern in many parts of Asia and is primarily of geogenic origin.

Industrial practices such as combustion, extraction, and processing contribute to heavy metal pollution. Industries like tanneries are significant sources of chromium contamination. Inadequate waste management practices, including improper handling of landfills and municipal wastewater, exacerbate the pollution of groundwater and soil, particularly in developing countries. Various indices, such as the Heavy metals pollution index (HPI), Heavy metal evaluation index (HEI), and Hazard index (HI), are used to assess heavy metal contamination, reflecting their combined impact on groundwater quality (Elumalai at al., 2017; Sharma et al., 2022). These indices are crucial for estimating the potential health risks associated with prolonged exposure. Heavy metal toxicity can lead to severe health consequences, including disorders of the nervous system, kidney and liver damage, cardiovascular disease, reproductive abnormalities, and cancer.

Furthermore, stable isotopes of water serve as fingerprints of recharge sources (Joshi et al., 2018), aiding in identifying leaky overlying aquifers and confirming the source of contamination by comparing water quality parameters in the overlying and deep aquifers (Alley et al., 2017; USGS, 2020). These isotopic studies provide valuable insights into the movement and behavior of groundwater and can inform management strategies.

Our study employed a wide range of techniques, including GIS-based Groundwater Recharge Potential Index (GWRPI), Water Quality Index (WQI), %Na, Principal Component Analysis (PCA), correlation matrix, Gibbs plot, Piper Diagram, US Salinity Diagram, Sodium Adsorption Ratio (SAR), Kelly's Index (KI), Heavy Pollution Index (HPI), Heavy Extent Index (HEI), Heavy Index (HI), stable isotope characterization, and more, to assess groundwater quality and address the pressing need for sustainable groundwater management strategies. We specifically focused on regions experiencing significant depletion rates and contamination threats.

To examine the climate data, we utilized statistical tests such as Mann-Kendall's test, Sen's test, and IMD's percent departure from normal. These tests allowed us to analyze and understand the trends and patterns in rainfall, an essential component of the water resource assessment in our study area. Isotopic data is used as a tracer for groundwater dynamics.

By employing a multidimensional analysis approach, our present project comprehensively assessed the water resources, including both rainfall and groundwater dynamics, in the study area. This holistic approach enabled us to gain valuable insights and develop a comprehensive understanding of the water resource situation.

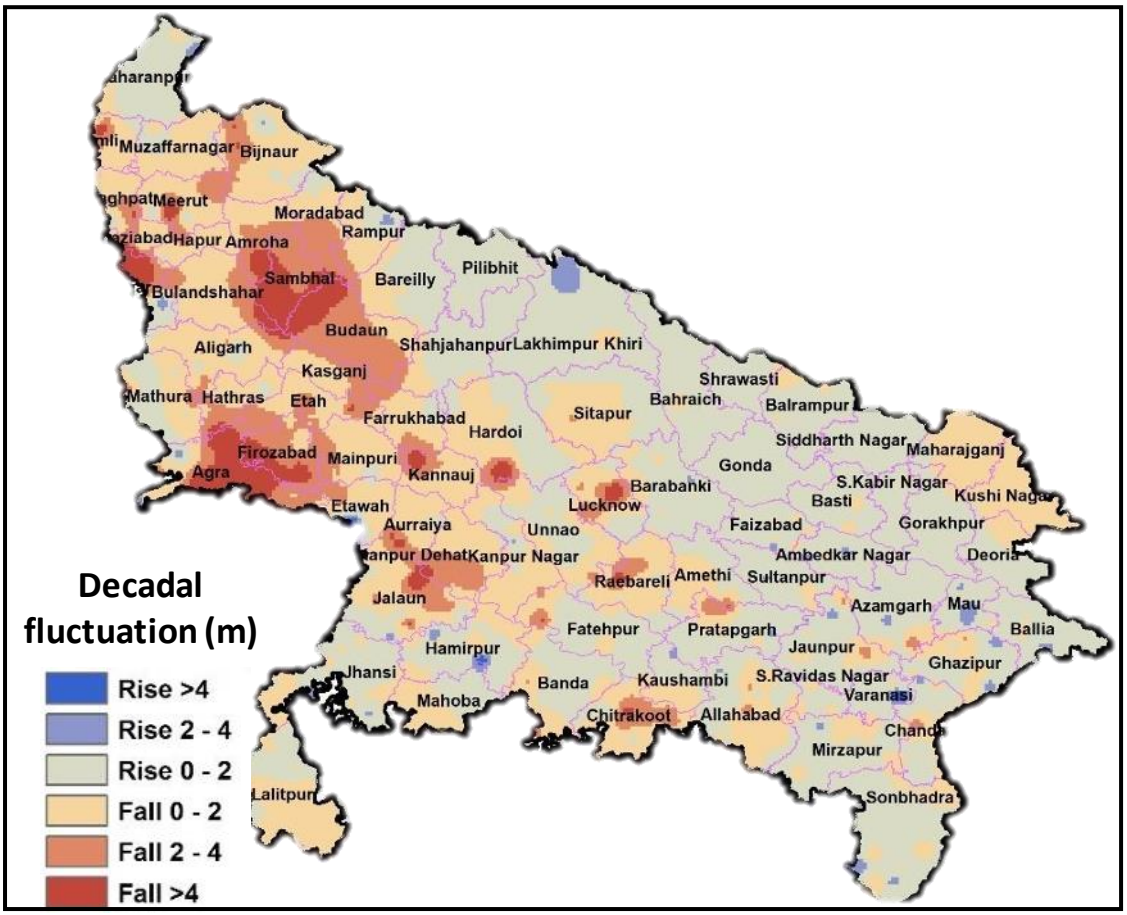

Fig.3.2. Decadal ground water level (GWL) fluctuation (Calculated as GWL for May(2012-2021)$_{mean}$- GWL for May 2022)

4. MATERIALS AND METHODS

4.1. Data source

In the current study, various types of data have been used for analysis and interpretation. This data was obtained from many sources. This section covers the account of the source of the data used in this study. For each variable/ physical quantity, the data source has been discussed separately.

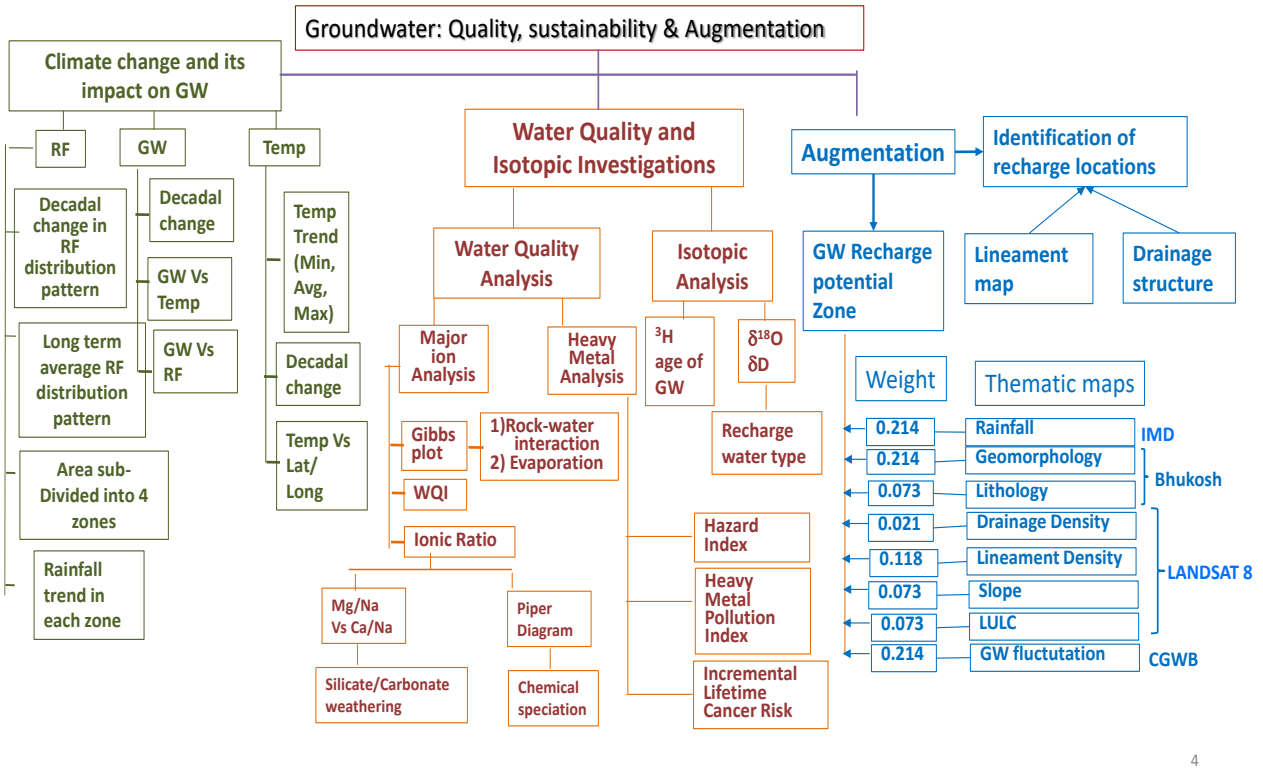

Fig. 4.1.: Flowchart showing methodological approach and the work elements

4.2. Digital Elevation Model (DEM)

The digital elevation model was prepared with the help of Google Earth Pro and ArcMap 10.x. The Google Earth shows images captured using Landsat satellites whose spatial resolution is 30 m. This DEM can be used to obtain slope and contour of the study area. It can also help in the drainage analysis of the study area. A path is drawn in Google Earth and saved in .kml format. The .kml file is uploaded on GPS Visualizer website (https://www.gpsvisualizer.com). In the GPS Visualizer the file is converted from .kml format to .gpx format. The file of newer format (.gpx) is imported into the ArcMap 10.x. The "GPX to Features" tool is utilized to convert the imported file into Features. Now, very small points are visible in the map at a small distance making the appearance linear or continuous. In the attribute table, the elevation of all the points is written. The interpolation technique is used to calculate the value of elevation at the unknown points. After the interpolation is finished, the Digital Elevation Model is prepared, and is converted into the raster file.

4.3. Lithological, geomorphological and lineament map

Recharge to groundwater depends upon surface and near-surface features viz., gemoprhology, lineament density, and lithological data specifies. The data for preparing the thematic maps related to these features are obtained from Bhukosh (https://bhukosh.gsi.gov.in/Bhukosh/Public).

4.4. Rainfall and temperature data

The rainfall and temperature data for the 52 desired gridded coordinate points from 1991 to 2020 were acquired from Indian Meteorological Department (IMD), Pune, Government of India (Nandi et al., 2024), in netCDF format (.nc) using the "imdlib" file library. Among the 52 selected points, only 4 fall outside the study area, while the rest uniformly cover the entire study area. GRIB (GRIdded Binary or General Regularly-distributed Information in Binary form) is a concise data format widely used in meteorology for storing historical and forecast weather data. GRIB files comprise self-contained records of 2D data. Each GRIB record consists of two components: the header describing the record and the actual binary data. GRIB-1 data are typically converted to integers using scale and offset, followed by bit-packing, while GRIB-2 also supports compression. Using Python (3.6), the data in .nc format were converted to .csv. Daily data for the entire 1991-2020 period for all locations were consolidated into a single file. Monthly and annual rainfall averages were computed by averaging daily data for the respective month and year. Similarly, monthly and annual temperature averages were derived from the temperature time series. Two types of temperature data were considered: minimum and maximum temperature data. The average of these temperatures yields the average temperature.

4.5 Generating Raster image

In the present study, for generating raster images, Inverse Distance Weighted (IDW) interpolation method is used. In IDW technique, the magnitude of the unknown values decreases as the distance from the known value increase. The IDW is a deterministic type of interpolation. The unknown values are calculated by the weighted average of the known values. In the IDW method, value of the variable u at an unknown unknown point x is calculated as follows: -

$$u(x) = \frac{\sum_{i=1}^{N} w_i(x) u_i}{\sum_{i=1}^{N} w_i(x)}, \text{ if } d(x, x_i) \neq 0, \text{ for all } i, \text{ or}$$

$$u_i, \text{ if } d(x, x_i) = 0, \text{ for all } i,$$

Where $w_i = \frac{1}{d(x, x_i)^p}$,

x denotes an interpolated (arbitrary) point,

$\mathbf{x}_i$ is an interpolating (known) point,

d is a given distance (metric operator) from the known point x_i to the unknown point x,

N is the total number of known points used in interpolation and

p is a positive real number, called the power parameter.

4.6. Analytic Hierarchy Process

The Analytic Hierarchy Process (AHP) was developed by Thomas L. Saaty in the 1970s, and revised and refined over time (Ho, 2008; Dai et al, 2001; Alonso et al.2006; González-Prida et al., 2014; Donegan et al. 1992; Chorol & Gupta 2023). AHP is a decision-making technique used for situations

with multiple criteria. It breaks down complex problems into a hierarchical structure, allowing decision-makers to prioritize variables and make informed choices based on judgments and expert opinions.

Multi-Criteria Decision Analysis (MCDA) is a method used for decision-making with multiple criteria, aiming to reduce biases and improve group decision-making. It involves ranking or choosing alternatives based on explicit weights and trade-offs between criteria. MCDA consists of four components: alternatives, criteria, weights, and decision-makers' preferences. It accommodates different numbers of alternatives and criteria and offers methods for determining the weights. Multiple types of MCDA techniques exist, each with its own utility based on specific conditions.

To map the Groundwater Recharge Potential (GWRP) Zones using the Analytic Hierarchy Process (AHP), the following steps are undertaken. Firstly, factors influencing GWRP are identified. Then, pairwise comparisons are conducted to ascertain the relative significance of these factors. Thirdly, alternatives within each factor are compared in pairs, generating a pairwise comparison matrix. Subsequently, criteria weight factors are computed using a normalized weight method. A matrix, n x m, is then constructed utilizing these weight factors, delineating 'n' factors and 'm' alternatives. Finally, the global score of each alternative can be determined employing the following formula: -

$$G_a = \sum_{c=0}^{n} w_c \star S_{a,c}$$

where a is the alternative,
c is the factor,
w is alternative weight,
S is the alternative score, and
G is the global score of the alternative.
The major advantage of using the AHP over other techniques is that it uses pairwise comparisons rather than a numerical value. The decision making by using AHP is good if the consistency measured is less than 10%. The Consistency Index (CI) gives a measure of consistency which is calculated by using the following formula: -

$$CI = \frac{\lambda_{max} - n}{n - 1}$$

where λ_{max} is the largest Eigen value of the matrix.

4.7. Regression Analysis

Linear regression is a commonly used predictive analysis tool that establishes linear relationships between dependent and independent variables to predict future outcomes. Multiple Linear Regression (MLR) extends this approach by incorporating multiple predictors, providing insights into the correlation and contribution of each variable to variance. MLR is favored in hydrological research due to its simplicity and cost-effectiveness, despite limitations in handling non-linear relationships.

The linear regression equation, represented by:
y = m1x1 + m2x2 + ... + c, includes slope values (m1, m2, ...) and an intercept (c)
The Simple Linear Regression (SLR) involves two variables, whereas, the Multiple Linear Regression (MLR) involves more than two. Correlation types can be positive (positive slope) or

negative (- ve slope), and the slope ranges from 0° to 360°, while the intercept's sign determines the line's position relative to the x-axis. Excel (MS Office 2016) is used in the present study for performing linear regression analysis. The coefficient of determination (R^2) provides the accuracy and can be calculated by the following formula: -

$$R^2 = 1 - \frac{RSS}{TSS}$$

where RSS = sum of squares of residuals, and
TSS = total sum of squares.
If the value of R^2 is near to or equal to zero, then the relationship is not valid as most points don't lie on the trend line. If the value of R^2 is one or approaches one, then the relationship equation is the best fit for the measured values.

4.8. Time Series Analysis

The time series analysis is the graphical representation and identification of the trend of a variable with respect to time. In the present study, the Mann-Kendall Trend Test (Mann, 1945; Kendall, 1975) is used in the time series analysis to detect the trend of the given time series. It is based on the null hypothesis (*H*0) and alternate Hypothesis *H*1. The null hypothesis represents the nonexistence of trend, while the alternate hypothesis represents the existence of a significant falling or rising trend in the data set.

This test analyzes the change in sign of difference between the earlier and later values. The positive or negative change will tell the increase or decrease in the value of the variable with time. The statistic S can be obtained by the following equation: -

$$S = \sum_{k=1}^{n-1} \sum_{j=k+1}^{n} sgn(x_j - x_i)$$

$$sgn(x_j - x_i) = +1, if\ (x_j - x_i) > 0;\ 0, if\ (x_j - x_i) = 0;\ and\ -1, if\ (x_j - x_i) < 0$$

where n = sample size,
j = k+1, k+2, ……, n, and
k = 1, 2, 3, 4, …., n-1.
The variance of S can be calculated as follows: -

$$Var(S) = \frac{n(n-1)(2n+5)}{18}$$

Now, the value of Z-statistic can be calculated by the following formula: -

$$z = \frac{S-1}{\sqrt{Var(S)}}\ if\ S > 0; 0\ if\ S = 0;\ and\ \frac{S+1}{\sqrt{Var(S)}}\ if\ S < 0$$

On the basis of 5% significance level, if _ ≤ 0.05 (s value), i.e., *zs* = 1.96, then the alternate hypothesis is rejected, or the alternate hypothesis is accepted. While _ ≥ 0.05, the null hypothesis is accepted.

In order to interpret the Mann-Kendall Trend test results, the following rules must be followed:

i. If Z>0 then there is increasing trend.
ii. If Z<0 then there is decreasing trend.
iii. If $|Z|>Z(1-\dot{\alpha}/2)$, where $\dot{\alpha}$ is the confidence level, then there is significant trend.

The Sen's slope estimator can be calculated by the following formula: -

$$\beta = Median\left(\frac{x_j - x_i}{j - i}\right)$$

where j>i. If the value of β is more than zero, then there is increasing trend, while the value of β less than zero shows a decreasing trend.

4.9. Forecasting

Forecasting is a crucial process involving the prediction of future values based on current and historical trends, essential for planning activities such as sustainable water management. It encompasses projecting variables like rainfall, temperature, crop prices, water demand, population, and per capita income. With a plethora of methods available, including linear, polynomial, moving average, exponential function, and multivariable analysis, selecting the appropriate approach is paramount before commencing projections.

ARIMA (Autoregressive Integrated Moving Average) is a powerful statistical model extensively for analyzing time series data and forecasting future trends. By scrutinizing past values to anticipate future ones, ARIMA ensures data stationarity through differencing, where stationary data maintains consistent statistical properties over time, such as mean and variance. The process involves partitioning the data into two periods, with the optimal ARIMA model selected based on favorable criterion values.

ARMA (Autoregressive Moving Average) model is similar to ARIMA that serve as statistical tools for time series analysis and forecasting. While ARIMA addresses non-stationary data through differencing, ARMA focuses on stationary data. Leveraging differences between values rather than the values themselves, ARMA facilitates adaptable and robust forecasts by incorporating additional information.

The ARIMA model leverages time series data to understand datasets and predict future trends. Operating on the premise of predicting future values based on past ones, ARIMA consists of an ARMA model fitted on a differenced time series to ensure stationarity. Optimal model selection involves splitting the data into estimation and validation periods, with preference given to models exhibiting the smallest criterion values.

In essence, ARIMA serves as a regression analysis tool, gauging the relationship strength between a dependent variable and changing variables. By analyzing value differences within the series, ARIMA forecasts future time series movements and readily incorporates additional information. Offering a straightforward yet powerful method for time series analysis and forecasting, ARIMA models provide a diverse range of standard structures tailored for effective forecasting

An example of the univariate time series is the Box et al (2008) Autoregressive Integrated Moving Average (ARIMA) models.

Box-Jenkins Analysis is a step-by-step method for understanding and using ARIMA time series models. The steps include checking if the data is stationary, identifying the best model type using autocorrelation and partial autocorrelation functions, creating and fitting a model template to the data, checking the goodness-of-fit of the model, and finally using the model for forecasting future data or simulating different scenarios.

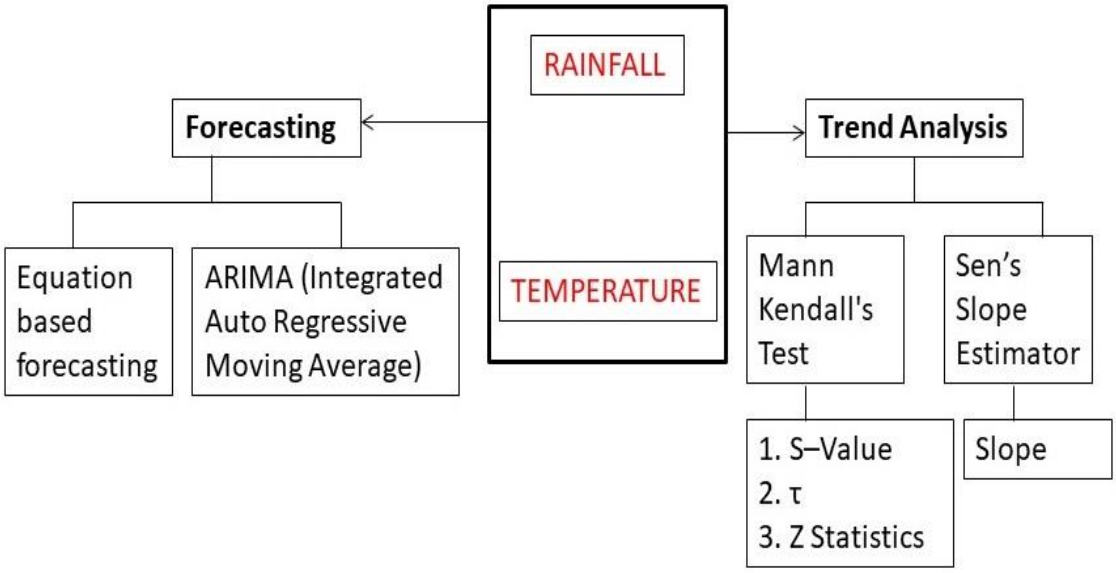

Fig. 4.2: Scheme of approach for forecasting and trend analysis

4.10. Analysis of Rainfall Data

Analyzing rainfall data for drought and wet event periods is of paramount significance in climate studies and water resource management. The developed indices, such as the Rainfall Anomaly Index (RAI), Percentage Departure (D%) from normal, and Standardized Precipitation Index (SPI), offer crucial insights into temporal deviations and severity levels. Identifying drought and wet periods aids in understanding climate change impacts, facilitating adaptation strategies, and assessing vulnerability and risk in water resource management. These analyses are instrumental in preparedness efforts, enabling timely interventions to mitigate the adverse effects of extreme weather events, safeguarding communities, agriculture, and ecosystems against water-related challenges.

a) Rainfall Anomaly Index (RAI)

The following equations developed by Olukayode et al. (1965) are used to calculate the RAI, and to classify the irregularities in the precipitation time series:

$$RAI = \frac{p - p_{med}}{p_{max} - p_{med}}, \qquad \text{For positive anomalies} \qquad (6)$$

$$RAI = \frac{p - p_{med}}{p_{min} - p_{med}}, \qquad \text{For negative anomalies} \qquad (7)$$

Where,

P = current annual precipitation (mm);

P_{med} = mean annual rainfall (mm) of the historical series;

P_{max} = mean of the ten largest annual precipitations (mm) of the historical series

P_{min} = mean of the ten lowest annual precipitations (mm) of the historical series

RAI estimation requires only precipitation data as input. The RAI value varies from ≤-3 to ≥3 with ≤-3 indicating an extremely dry climate and ≥3 indicating extremely humid/wet conditions

Table 4.1: Classification of draught/precipitation severity using Rainfall Anomaly Index (RAI).

	RAI Range	**Classification**
Rainfall Anomaly Index (RAI)	≥3.0	Extremely wet
	2.0 to 2.99	Very wet
	1.0 to 1.99	Moderately wet
	0.5 to 0.99	Slightly wet
	0.49 to -0.49	Near Normal
	-1.0 to -1.99	Moderately dry
	-2.0 to -2.99	Very dry
	≤-3.0	Extremely dry

**Source:* Source: Freitas (2005) adapted by Araújo et al. (2009)

b) Percentage Departure (D%) of Rainfall from the long term normal

The India Meteorological Department (IMD) has classified the precipitation in a region into 6 categories Normal, Deficient, Excess, Large Excess, Large Deficient, and 'No rain' on the basis of rainfall departure (in %) with respect to the long term mean (Table 3) calculated using the following equation:

$$Percentage\ Departure, D\ (\%) = \frac{X_i - X}{X_m} * 100 \qquad (8)$$

where, X_m is the long-term mean annual rainfall and X_i is the annual rainfall.

Table 4.2: Classification of rainfall from percentage departure of rainfall from the long term rainfall.

Rainfall Category	**% Departure (%D)**
Large Excess Rainfall	+60%
Excess Rainfall	+20% to +59%
Normal Rainfall	+19% to -19%
Deficit Rainfall	-20% to -59%
Large Deficient (or Scanty) Rainfall	-60% to -99%
No Rain	-100%

c) Standardized Precipitation Index (SPI)

The Standardized Precipitation Index, the dimensionless quantity SPI, also known as the Standardized Anomaly Index (SI), was created by McKee et al. (1993), and the following equation is used to determine its value:

$$SPI = \frac{x - \mu}{s} \qquad (9)$$

where, x is the observed precipitation data from a long-term record;

μ is the average or mean across all observations; and

s is the standard deviation over the period of observation.

SPI is used to identify and quantify wet and dry events in rainfall time series (Bartczak et al. 2014). Normal rainfall is indicated by SPI values near zero (–0.99 SPI 0.99), intensified wet events by higher positive values, and intensified dry events by higher negative values (Table. 2). SPI may exhibit minor fluctuations on a shorter time scale, but well-defined dry (negative SPI values) and wet cycles (positive SPI values) may be observed over a longer time scale as a result of a regional or sub-continental change in the climate cycles (Ionita et al., 2016).

The SPI value indicates the severity of the drought by displaying the ratio of the magnitude of the drought to its duration. The significance of the SPI values to the severity of the drought or wet (Hayes et al. 2011) is shown in Table 3. SPI values of +ve and –ve indicate either a wet or dry regime. As the severity of wet or dry conditions rises, so does the magnitude of SPI. The classification value of SPI are shown in table 4.

Table 4.3: Classification of rainfall regime as per SPI values

SPI values	Rainfall regime
≥2.00	Extremely wet
1.50–1.99	Very wet
1.00–1.49	Moderately wet
−0.99 to 0.99	Near Normal
−1.00 to −1.49	Moderately dry
−1.50 to −1.99	Severely dry
≤−2.00	Extremely dry

**Source: Hayes et al. ,1999*

d) Percent of Normal Index (PNI)

Percentage of Normal Precipitation (PNI) was described by Willeke et al. in 1994 as a percentage of normal precipitation. It can be calculated for different time scales (monthly, seasonally, and yearly). PNI has been found to be rather effective for describing drought for a single region or/and for a single season (Hayes, 2006). PNI is calculated as following:

$PNI=(P_i/P)$ *100

where P_i is the precipitation in time increment i (mm), and P is the normal precipitation for the study period (mm).

Boughton (2009) calculated streamflow drought characteristics using percent of normal index (PNI) in eastern Australia and found that the severity of droughts increased with average recurrence interval to the limit of the generated data. Salehnia et al. (2017) revealed that the trends of SPI, Decile Indeex, and PNI indices were very similar in the study area. Jokar et al., (2018) studied rainfall pattern in Iran using PNI indices.

4.11 Groundwater Quality

In water quality studies, it is important to find the interrelationship in huge groundwater dataset and extracted the important factors influencing groundwater quality, which was used to infer the hypothetical sources of heavy metals (Narany et al., 2014). Therefore, principal component analysis was used on groundwater quality by trace metals dataset, which also useful to minimized the number of variables with a high loading on each component, thereby facilitating the interpretation of PCA results.

Generally, pollution indices are calculated to determine the appropriateness of water for a specific intended use. In this study the indices namely Water Quality Index(WQI), Heavy Metal Pollution Index (HPI), Heavy metal Evaluation Index (HEI) & Hazard Index (HI) were calculated to define the extent of contamination in groundwater. The HPI and HEI methods used to know the impact of heavy metal concentration on overall quality of groundwater. These indices are evaluated using the ratios of measured values of the parameters and the permissible concentrations of the respective parameters (Bhuiyan et al. 2010). A Hazard Index (HI) is used to calculate the non-carcinogenic risk caused by consumption of heavy metal.

4.12. Drinking Water Quality

i) Water Quality Index (WQI): Water quality index was first proposed by Horton (1965). Generally, WQI is discussed for a particular and intended use of water. In this study, we considered WQI for human consumption. It was calculated in three main steps, i.e., selection of parameters, determination of sub-indices, and finally sub-indices aggregation with mathematical expression (Fernández et al. 2004). We calculated WQI according to Tandel et al. (2011) which was done by using the weighted arithmetic index method. The quality rating scale for each parameter, Qi, was calculated by using the following expression:

$$WQI = \sum_{i=1}^{n} W_i Q_i / \sum_{i=1}^{n} W_i$$

where n = number of variables or parameters, Wi= unit weight for the ith parameter, Qi=quality rating (sub-index) of the i^{th} water quality parameter. The unit weight (Wi) of the various water quality parameters are inversely proportional to the recommended standards for the corresponding parameters.

$$W_i = K / S_n$$

where, Wi=unit weight for the i^{th} parameter, Sn=standard value for i^{th} parameters, K=proportional constant, the value of K has been considered '1′ here and is calculated using the mentioned equation below:

$$K = 1 / \sum (1/ S_n)$$

According to Brown et al. (1972), the value of quality rating or sub-index (Qi) is calculated using the equation as given below:

$$Q_i = 100[(V_o - V_i) / (S_n - V_i)]$$

where V_o = observed value of i^{th} parameter at a given sampling site, Vi = ideal value of i^{th} parameter in pure water, Sn = standard permissible value of i^{th} parameter.

ii) Heavy metal Pollution Index (HPI): Permissible limits for drinking water given by various organisations and countries ascertain the suitability of water based on each metal; however, a cumulative understanding of the pollution level based on all heavy metals is not achieved. Hence many researchers have used HPI as a comprehensive tool to determine the overall quality of water based on heavy metals (Horton 1965; Brown et al. 1970). Weights of each metal are assigned between 0 and 1 which depends on the relative importance of the metal that builds on the standard permissible limit for the metal in drinking water.

$$\mathrm{HPI} = \frac{\sum_{i=1}^{n} W_i Q_i}{\sum_{i=1}^{n} W_i}$$

The unit weight, Wi, is calculated by

$$W_i = K/S_i$$

where K is the proportionality constant, Si is the standard permissible limit in water for the 'i'th heavy metal. The proportionality constant, K is calculated by

$$K = 1/\sum_{i=1}^{n} \frac{1}{S_i}$$

$$\sum_{i=1}^{n} \frac{1}{S_i} = \frac{1}{S_1} + \frac{1}{S_2} + \frac{1}{S_3} \cdots + \frac{1}{S_i}$$

where S_1, S_2, S, etc. represent standards for different heavy metals in water such as silver, arsenic, copper, lead, etc.

The sub-index, Qi, is calculated by

$$Q_i = \sum_{i=1}^{n} \frac{|M_i - I_i|}{(S_i - I_i)} \times 100$$

where Mi is the monitored value of heavy metal of the 'i'th heavy metal, Ii is the ideal value of the 'i'th heavy metal based on international limits for drinking water and Si is the

standard value of 'i'th heavy metal. HPI is classified into three classes, viz., Low (0–15), Medium (15–30) and High (>30) based on its pollution extent (Edet and Offiong 2002; Herojeet et al. 2015).

iii) Heavy metal Evaluation Index (HEI): Heavy metal Evaluation Index(HEI) gives an overall quality of the water with respect to heavy metals (Edet and Offiong 2002) and is expressed as follows.

$$HEI = \sum_{i=1}^{n} \frac{H_C}{H_{MAC}}$$

where Hc monitored value, H_{MAC} maximum admissible concentration (MAC) of the i^{th} parameter.

iv) Hazard Index(HI): A non-carcinogenic risk due to consumption of groundwater containing heavy metals was assessed by calculating hazard index (HI) based on following equations (US EPA 1989).

$$LADD = (C \times IR \times ED \times EF)(BW \times AT)$$

where LADD lifetime average daily dose of ingestion of heavy metal through drinking water (mg/kg/day), C concentration of the heavy metal in water (mg/l), IR ingestion rate of water [250 ml/day for infants, i.e., 0–12 months, 1.5 l/ day for children (Brindha et al. 2016) and 3 l/day for adults (Planning Commission 2011)], EF exposure frequency (days/year), ED exposure duration [66.4 years (UNDESA 2013)], BW body weight [6.9 kg for infants, 18.7 kg for children and 57.5 kg for adults(ICMR 2009)], AT average time (days). This equation was modified with the assumption that the water is consumed throughout the year (exposure frequency) for a lifetime (exposure duration) by an individual. In that case the exposure frequency and duration will be equal to the average time.

Hazard quotient index (US EPA 1989) is calculated as;

$$HQ = LADD/RfD$$

where HQ hazard quotient, RfD Reference dose for a heavy metal that an individual can be exposed to in a day over his/her lifetime without experiencing any deleterious health effect (mg/kg/day). The non-carcinogenic risk given by HI is sum of the HQ of all metals.

$$HI_i = \sum HQ_i$$

4.13. Assessment of Irrigation Water Quality

The Groundwater plays a vital role in agriculture, for both watering and for irrigation of dry season crops. The nature of ground water differs from place to place laterally with the depth of water table. It additionally differs with regular changes and is fundamentally represented by the degree and concentration of dissolved solids present in it. The most important characteristics of water which determine the suitability of groundwater for irrigation purpose are Sodium Absorption Ratio (SAR), Percentage Sodium, Kelly Ratio(KR), Magnesium Hazards(MH), Potential salinity(PS), Permeability Index(PI).

i) Sodium absorption ratio(SAR): SAR is important in supporting agricultural crop production as high SAR values in clay and loam soils will reduce soil permeability, thereby concentrating salts near the surface and inhibiting plant growth. Sodium ion in small amount is good for plants. But excess sodium ions create problem for both plant and soil. Excess sodium ions contributes to salinity and it is toxic for some sensitive crops. SAR value 0-10 indicates low sodium water, 10-18 indicates medium sodium water, 18-26 indicates high sodium water and greater than 26 is very high sodium water.

$$\mathrm{SAR} = \frac{\mathrm{Na^+}}{\sqrt{\frac{(\mathrm{Ca^{2+}} + \mathrm{Mg^{2+}})}{2}}}$$

where all concentrations are expressed as milli equivalents per liter (meq/l).

ii) Percent sodium (%Na) or sodium hazard: The %Na is also used in classifying water for irrigation purpose. Na^+ is important parameter and helps in categorization of any source of water for irrigation uses. Na^+ makes chemical bonding with soil to reduce water movement capacity of the soil (Ayers and Westcot 1985). Percent Na^+ concentration is a factor to assess its suitability for irrigation purposes. Na^+ reacts with CO_3^{2-} and forms alkaline soils, while Na^+ reacts with chloride and forms saline soils. Sodium-afected soil (alkaline/saline) retards crop growth. If concentration of Na^+ in irrigation water is high, then the ions tend toward the clay particles, by removing Ca^{2+} and Mg^{2+} ions through a base-exchange reaction. This exchange process in soil reduces water movement capacity. In this condition, air and water cannot move freely or restricted during wet conditions, and such soils have become hard when dry (Collins and Jenkins 1996; Saleh et al. 1999). The classifcation of water is based on %Na as excellent (<20%), good (20–40%), permissible (40–60%), doubtful (60–80%) and unsuitable (>80%).

$$\%\mathrm{Na} = \frac{\mathrm{Na^+}}{\mathrm{Ca^{2+}} + \mathrm{Mg^{2+}} + \mathrm{Na^+} + \mathrm{K^+}} \times 100$$

All the ion concentrations are expressed in milli equivalents per liter (meq/l).

iii) Permeability index (PI): The permeability index (PI) is an indicator to study the suitability of water for irrigation purpose. Water movement capability in soil (permeability) is infuenced by the long-term use of irrigation water (with a high concentration of salt) as it is afected by Na^+, Ca^{2+}, Mg^{2+} and HCO_3^- ions of the soil. PI formula has been developed by Doneen (1964), to assess water movement capability in the soil as the suitability of any kind of source of water for irrigation.

PI can be categorized in three classes: class I (>75%, suitable), class II (25–75%, good) and class III (<25%,unsuitable). Water under class I and class II is recommended for irrigation.

$$\mathrm{PI} = \frac{\mathrm{Na^+} + \sqrt{\mathrm{HCO_3^-}}}{\mathrm{Ca^{2+}} + \mathrm{Mg^{2+}} + \mathrm{Na^+}} \times 100$$

All the ion concentrations are expressed in milli equivalents per liter (meq/l).

iv) Kelly's ratio (KR) or Kelly's index (KI): A Kelly (1957) was developed the value to assess the groundwater for irrigation purpose. The concentration of Sodium ions measured against Calcium and Magnesium ion concentration in groundwater. A Kelly ratio greater than one indicates a higher concentration of sodium ions in water and it affect the texture of the soil. While those with a ratio less than one is fit for agriculture uses. The following formula is used to calculate the KR Value:

$$\mathrm{KR} = \frac{\mathrm{Na^+}}{\mathrm{Ca^{2+}} + \mathrm{Mg^{2+}}}$$

All the ion concentrations are expressed in milli equivalents per liter (meq/l).

vi) **Magnesium hazard (MH) or magnesium adsorption ratio (MAR):** A Magnesium Hazards Ratio (MAR) is important value to classify the groundwater for irrigation purpose. In generally, Ca^{2+} and Mg^{2+} ion concentration preserves a state of equilibrium in groundwater. Higher Concentration of Magnesium ions in groundwater affects the properties of soil and it resulting in a reduction of crop yield. The value of MH is less than 50 in groundwater is suitable and greater than 50 indicates that unsuitable for irrigation purpose. The following formula is used to calculate the MH Value:

$$\mathrm{MH} = \frac{\mathrm{Mg^{2+}}}{\mathrm{Ca^{2+}} + \mathrm{Mg^{2+}}} \times 100$$

All the ion concentrations are expressed in milli equivalents per liter (meq/l).

A total of one-fifty-nine (159) for major ions and one-forty-two (142) representative groundwater samples were collected from different locations of the study area. Samples were filtered through the 0.45 µm Millipore filter paper using Millipore glass assembly unit in 100 ml PET bottles. The samples were analysed on IC (Ion Chromatography for major ions) & ICP-

OES (Inductively coupled plasma - optical emission spectrometry) for Pb, Cd, Zn, Fe, Mn, Cr, Co, Cu . The Merck's multi-elements ten (10) standard of 0.01, 0.05, 0.1, 0.25, 0.5, 1.0, 2.0, 5.0, 10.0 and 20 mg/l were used for linear curve preparation. Further, run the samples and record the readings. The blank and standards were run at regular intervals for 10 samples and each sample analysed in triplet to maintain the accuracy. First step is heavy metals assessment for potential health effects to human through carcinogenic and non-carcinogenic risk assessment based on USEPA and ICMR guidelines. Carcinogenic risk is calculated based on different indices such as HPI, HEI and non-carcinogenic risk assessment is computed through hazard index. Multivariate Statistical analysis

4.12 Stable Isotope Hydrology

Stable isotopes are variants of elements that have the same number of protons but differ in the number of neutrons. Stable isotope ratios, like those of hydrogen (H) and oxygen (O) in water molecules, provide valuable information about the origin and history of water sources. Delta notation is a common way to express stable isotope ratios, typically denoted as $\delta^{18}O$ and $\delta^{2}H$, representing deviations from a standard reference. These ratios serve as unique "fingerprints" of water sources, as different processes, such as evaporation, precipitation, and groundwater recharge, leave distinct signatures. By analyzing stable isotopes, water movement in the hydrological cycle and its interaction in various hydrological compartments can be traced, aiding in water resource management, environmental studies, and climate research.

The isotope ratio is given by

$$R=\frac{^{18}O}{^{16}O} \quad \text{Or} \quad R=\frac{^{2}H}{^{2}H}$$

The isotope ratio can be used to calculate δ. It can be defined as follows: -

$$\delta^{18}O = \left(\frac{R_{sample}}{R_{sample} - R_{standard}}\right) x\ 1000\ ‰$$

The values of $\delta^{18}O$, and $\delta^{2}H$ is reported in per mill or per mil (‰).

In the present study, stable isotopes (^{2}H or D and ^{18}O) in water were analysed using GV-Isoprime Dual Inlet Isotope Ratio Mass Spectrometer. The measured values are reported as delta (δ) values (Gehre et al., 2004). The precision of measurement for $\delta\ ^{2}H$ is ± 1‰ and that for $\delta\ ^{18}O$ is ± 0.1‰.

Results and Discussion

5. GROUNDWATER RECHAGE POTENTIAL ZONE (GWRPZ)

Groundwater potential refers to the capacity of an area to recharge and sustain groundwater levels, influenced by factors such as surface water availability, soil permeability, and aquifer storage capacity. The recharge potential index, graded from 0 to 100, quantifies this capacity, with higher values indicating optimal conditions for groundwater replenishment. The mapping of recharge potential plays a critical role in groundwater security by identifying areas with varying recharge capabilities. This information is essential for delineating groundwater vulnerable zones, identifying potential sites for artificial recharge measures, implementing strategies for recharge augmentation, assessing risks associated with over-extraction, and ensuring the long-term sustainability and resilience of groundwater resources in the face of water scarcity.

The methodology for the Groundwater Recharge Potential Index (GWRPI) analysis involved three main stages:

(1) Generation of Thematic Maps: Eight thematic maps were generated using ArcMap 10.8, focusing on crucial factors that influence groundwater recharge potential. These factors include: lithology, land use/cover, lineaments, drainage, rainfall, geomorphology, groundwater fluctuation, and slope. The GIS is used to create and store these thematic maps. The groundwater fluctuation is averaged from 1999 to 2017. The integration of diverse datasets, including gridded rainfall data, geological attributes, and remote sensing-based LULC data, adds to the novelty and rigor of the research approach, as these aspects have been rarely addressed in previous studies.

(2) Weight Determination through Analytic Hierarchy Process (AHP): The weights of each class of each map are calculated by the AHP method to prioritize their significance in the Groundwater Recharge Potential Zoning (GWRPZ) analysis.

(3) Overlay Analysis and Site Delineation: With the help of the Weighted Overlay tool in the GIS software, the GWRPZ can be created by performing an overlay analysis to integrate the thematic maps and identify suitable artificial recharge sites. The inclusion of LULC data highlights the importance of understanding the dynamic changes in population and land use patterns within the middle Ganga basin, providing insights into the impacts of human activities and urbanization on groundwater recharge.

The research flowchart (fig 5.1) illustrates the steps and the holistic approach adopted for assessing groundwater recharge potential in the study area. Interpolation was done by Inverse Distance Weighing (IDW)

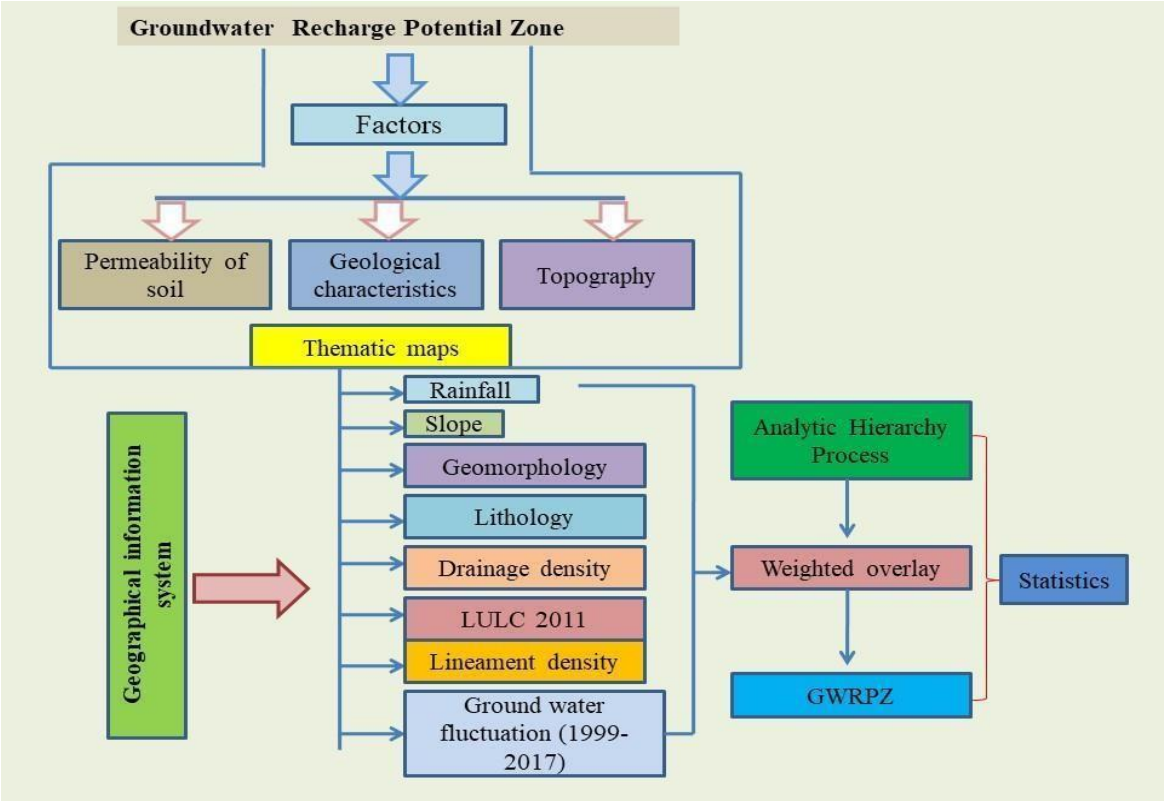

Fig 5.1: The flow chart for mapping GWRPZ.

5.1 Thematic Maps

In this study, eight critical thematic maps were developed using Arc-GIS 10.8. These are; drainage density, lineament density, rainfall, slope, LULC, lithology, groundwater fluctuation, and geomorphology

i) Drainage density

Drainage density is the total length of all the streams and rivers in a drainage basin divided by the total area of the drainage basin. It is sum of the channel lengths per unit area. Mathematically,

$$D = (\sum L)/A_{basin}$$

The higher values of the drainage density indicate lower infiltration rates and higher surface flow velocity. High drainage density is often related to high sediment yield transport trough river network, high flood peaks, steep hills, low suitability for agriculture. A basin with high drainage density, the contribution of surface runoff to stream discharge will be high, while that from base flow will be low. Drainage density is inversely proportional to groundwater recharge. Fig. 5.2(a) presents the variation in drainage density across the study area, measured in kilometers per hectare (km/ha), and reflects the total length of all streams and rivers (in km) per hectare. The drainage density is categorized into six classes from 0.54km/ha to 0.98km/ha. The range of

drainage density values and associated class areas, represented as percentages of the total area is shown in the table. The percentage area, corresponds to the class range 0.76 km/ha to 0.87 km/ha, is observed near the foothills of the Himalayas in the Terai region. Away from the Himalayas in the direction towards SE and SW, the drainage density consistently decreases. The reduced drainage density in regions farther from the Himalayas indicate a smaller proportion of the total area occupied by streams and rivers. Overall, the drainage density of 0.54 to 0.98 km/ha suggests that the middle Ganga basin has a significant network of watercourses that play a crucial role in shaping its hydrological characteristics, including water movement, erosion, sediment transport, and potentially groundwater recharge.

ii) Lineament density

A lineament is a linear feature in a landscape which is an expression of an underlying geological structure such as a fault, fracture zones, shear zones, and igneous intrusions such as dykes etc. The lineament density was defined as the total length of all the recorded lineaments divided by the area under consideration (Edet et al., 1998), with a unit as km/km^2. Generally, lineaments are underlain by zones of localized weathering and increased permeability and porosity. The zones of high lineament intersection density are feasible zones for groundwater prospecting. Lineament density is considered a useful tool to identify "hot spots" of groundwater recharge potentiality. For the present study, the lineament map was taken from the Bhukosh website and is analyzed in the ArcMap software. This map is converted from the raster format to the shape file format. Fig. 5.2 (b) portrays the variation in lineament density within the study area, with a specific emphasis on how this density fluctuates across different sections of the basin. Lineament density measures the total length of linear features, such as faults or fractures, within a unit area, often quantified in kilometers per square kilometer (km/sq. km). It serves as a significant indicator in geology and structural analysis, shedding light on the distribution of linear features across the landscape. The lineament density in the study area is categorized into five classes from a minimum range of 26.36km/ha - 55 km/ha to the maximum range 184.82km/ha - 221km/ha. About 60% of the study area is covered under medium to very high lineament density. The highest lineament density values are observed in the middle section of the basin. This suggests that this region is characterized by a higher concentration of linear features, such as faults or fractures. These linear features might indicate areas of increased groundwater flow [17]. The presence of lineaments leads to better groundwater recharge. The figure highlights that the lineament density is comparatively lower in the upper and lower parts of the basin. This could signify fewer linear features in these regions, which might be due to differences in geological structures, tectonic history, or other factors influencing the distribution of linear features. The significant difference between these two extremes highlights the spatial heterogeneity of the geological and hydrogeological conditions in the Middle Ganga basin. The areas closer to active tectonic boundaries tend to have higher lineament density (221 km/ha) due to the ongoing geological deformation, while regions farther away experience less tectonic stress and consequently lower lineament density (26.35 km/ha). Lineament density is often used as a broad indicator of structural complexity and potential geological activity within a region. It can aid in identifying areas where tectonic forces have been active, which might influence groundwater flow patterns, landscape evolution, and other geological processes.

Table 5.1: - The class value, respective areas and the class weight of the 8 thematic maps used for the analysis of GWRPI (and GWRPZ)

Thematic map (unit); Wt of thematic map	Class No.	Class Name	Class Value	Class Area (in%)	Wt. of class
Rainfall (mm); 0.214	1	Low roinfall	350-600	9.10%	0.033
	2	Medium rainfall	600-850	26.96%	0.063
	3	High rainfall	850-1100	44.22%	0.129
	4	Very high raindall	1100 - 1350	15.10%	0.262
	5	Heavy rainfall	1350 - 1600	4.70%	0.513
	Total			**100.08%**	**1**
Geo-morphology; 0.214	1	Pediment pediplain complex		0.01%	0.753
	2	Older allerial plain		77.78%	0.134
	3	Older floodplain		13.79%	0.077
	4	Active flood plain		3.10%	0.006
	5	Pediment alluvial plain		5.40%	0.03
	Total			**100.08%**	**1**
Slope; 0.073	1	Flat		82.90%	0.388
	2	Gentle		15.56%	0.255
	3	Very mild		1.50%	0.162
	4	Mild		0.09%	0.195
	Total			**100.05%**	**1**
Drainage density (km/ha); 0.021	**1**	Very high	0.54-0.60	4.79%	0.027
	2	High	0.60-0.65	57.58%	0.088
	3	Medium	0.65-0.71	0.15%	0.088
	4	Low	0.71-0.76	19.71%	0.154
	5	Very	0.76-0.87	16.27%	0.24
	6	Extremely low	0.87-0.98	1.48%	0.403
	Total			**99.98%**	**1**
Lineament density (km/ha); 0.118	**1**	Very low	26.36 - 55	22.43%	0.033
	2	Low	55 - 89.71	16.28%	0.063
	3	Medium	89.71-140.60	15.38%	0.129
	4	High	140.60-184.42	22.18%	0.262
	5	Very high	184.42 - 221	23.72%	0.513
	Total			99.99%	1
Lithology; 0.073	**1**	Quaternary allurium		19.68%	0.513
	2	Sandy facies		10.53%	0.351
	3	Clayey facies		69.79%	0.136
	Total			100.00%	1
LULC, yr-2011; 0.073	**1**	Fores		1.72%	0.22
	2	Agricultural land		88.97%	0.144
	3	Bult up land		1.01%	0.025
	4	Shrubland		2.43%	0.11
	5	Fallow land		1.92%	0.135
	6	Wasteland		2.13%	0.025
	7	Waterbodies		0.91%	0.025
	8	Plantations		0.91%	0.316
	Total			**100.00%**	**1.0**

Ground Water Fluctuation (m); 0.214	**1**	Very Largy Fall	(-0.77) to (-0.64)	0.29%	0.016
	2	Large Fall	(-0.64) to (-0.32)	1.04%	0.02
	3	Medium Fall	(-0.52) to (-0.40)	2.68%	0.024
	4	Significant Fall	(-0.40) to (-0.27)	11.61%	0.038
	5	Little Fall	(-0.27) to (0.15)	18.41%	0.046
	6	Small Dip	(-0.15) to (-0.00)	28.81%	0.1
	7	Little Jump	(-0.00) to (0.09)	19.97%	0.125
	8	Significant Rise	(0.09) to (0.21)	11.07%	0.154
	9	Medium Rise	(0.21) to (033)	5.26%	0.193
	10	High Rise	(0.33) to 0.45	0.83%	0.284
	Total			**99.97%**	**1.0**

The lineament density classes ranging from Class 1 (26.36 to 55 km/ha) to Class 5 (184.82 to 221 km/ha) have distinct implications for drainage density, rainfall, and groundwater recharge. Class 1 suggests sparse lineaments, leading to lower drainage density and potentially uniform runoff dispersion. Class 2 features moderate lineament density, contributing to balanced drainage patterns and improved infiltration. Class 3 indicates higher lineament density, resulting in well-defined drainage paths and efficient runoff conveyance. Class 4 showcases substantial lineament density, leading to complex drainage networks and rapid groundwater recharge. Class 5 represents extremely high lineament density, yielding intricate water channel systems and significant groundwater recharge rates. The varying lineament densities within each class range influence the landscape's hydrological behavior, shaping water flow patterns and influencing storage dynamics [26]. The presence of fault lineaments could be connected to the ongoing tectonic activity between the Indian and Eurasian plates. NE and SE alignments of these faults may indicate the primary directions of fault movement, influenced by the stresses from the convergence of the Indian and Eurasian plates along the Himalayan boundary. Join or fracture lineaments could indicate zones where distinct geological formations or units have come together or fractured. In the context of the Himalayas and the Indian-Chinese Plate, these lineaments could represent areas of geologic complexity, potentially associated with the collision and ongoing convergence of the plates.

iii) Land use/ Land cover

Land Use/Land Cover (LULC) refers to the categorization or classification of human activities and natural elements on the landscape within a specific time frame. It provides the ground cover information for baseline thematic maps which is useful in understanding how different parts of the region are utilized and managed for different purposes.. Fig 5.2 (c) provides an overview of land cover distribution within the study area that is sub-categorized into the classes: Forest, Agricultural land, built-up land, shrub land, fallow land, wasteland, water bodies, and plantations. The areas covered by these classes, expressed as percentages of the total study area, are as follows: Forest: 1.7%, Agricultural land: 87.8%, Built-up land: 1%, Shrub land: 2.4%, Fallow land: 1.89%, Wasteland: 2.1%, Water bodies: 0.9%, and Plantations: 0.9%. The presence of Terai forests covering the northern part of the basin is relatively dense forest cover in this region, likely owing to the proximity to the foothills of the Himalayas and the suitable climatic conditions for forest growth. The wetlands are shown to be distributed throughout the entire basin. This could

indicate the presence of natural depressions or areas with high water availability, resulting in the formation of wetlands that contribute to the overall hydrology and biodiversity of the region. Built-up areas are observed within a context of surrounding forests and agricultural land. This arrangement signifies a relationship between urban development and the existing natural and cultivated landscapes. The proximity of built-up areas to forests and agricultural land might have implications for land-use planning and potential ecological interactions.

iv) Rainfall Map

Fig 5.2 (d) presents an overview of the precipitation distribution within the study area, highlighting the variation in rainfall across different parts of the landscape. The data is classified into distinct rainfall ranges. The areas occupied (in percentage) by each range is shown in the **table .** The minimum area 4.7% is covered in the highest rainfall range of 1350-1600 mm followed by the lowest rainfall range 350-600 mm with 9.1% area covered in this range. In general, the rainfall decreases as the distance from the Himalayas increases. This relationship is indicative of the influence of topography on precipitation patterns.

The mountains act as barriers for moist air coming from the Bay of Bengal, causing it to release precipitation on the windward side (facing the mountains) and resulting in drier conditions on the leeward side (away from the mountains) [23, 24].

The rainfall pattern is parallel to the Himalayan mountain ranges. The rainfall map has been divided into five classes from low rainfall to very high rainfall. The rainfall represented in the figure 5.2 is the average rainfall from 1991 to 2020. Rainfall increases from south–west (350 mm to 600 mm) to north–east (1351 to 1600 mm). The northern region receives much higher rainfall (1100 mm to 1600 mm) than the southern region (350 mm to 1100 mm). The average rainfall of the study area is 867.5 mm. The highest rainfall values, exceeding 1350 mm, are observed near the Shiwalik hills, which are the foothills of the Himalayas. This area typically receives the most intense rainfall due to orographic lifting, where moist air is forced to rise over the hills, leading to enhanced precipitation. The basin receives around 80% of its annual rainfall during the monsoon season, originating from the Bay of Bengal. Additionally, notable rainfall during winters, attributed to western disturbances, is observed. These disturbances are weather systems that bring moisture from the Mediterranean region, leading to increased precipitation in some areas.

The annual rainfall classes are linked with drainage density, runoff, and groundwater infiltration. In areas experiencing 350-600 mm of rainfall, drainage density is moderately defined, and runoff is generally mild due to soil absorption. At 600-850 mm, drainage density increases, leading to more significant runoff potential. Rainfall between 850-1100 mm triggers high drainage density, intense runoff, and reduced groundwater infiltration. Heavy rainfall of 1100-1350 mm establishes extensive drainage networks, predominant runoff, and compromised infiltration. In regions with 1350-1600 mm, exceptionally high drainage density corresponds to substantial runoff, heightened flood risks, and minimal groundwater infiltration. These relationships reflect the complex interplay between rainfall, landscape characteristics, and hydrological processes, influencing the distribution of water through streams, soil, and aquifers [18, 25, 29].

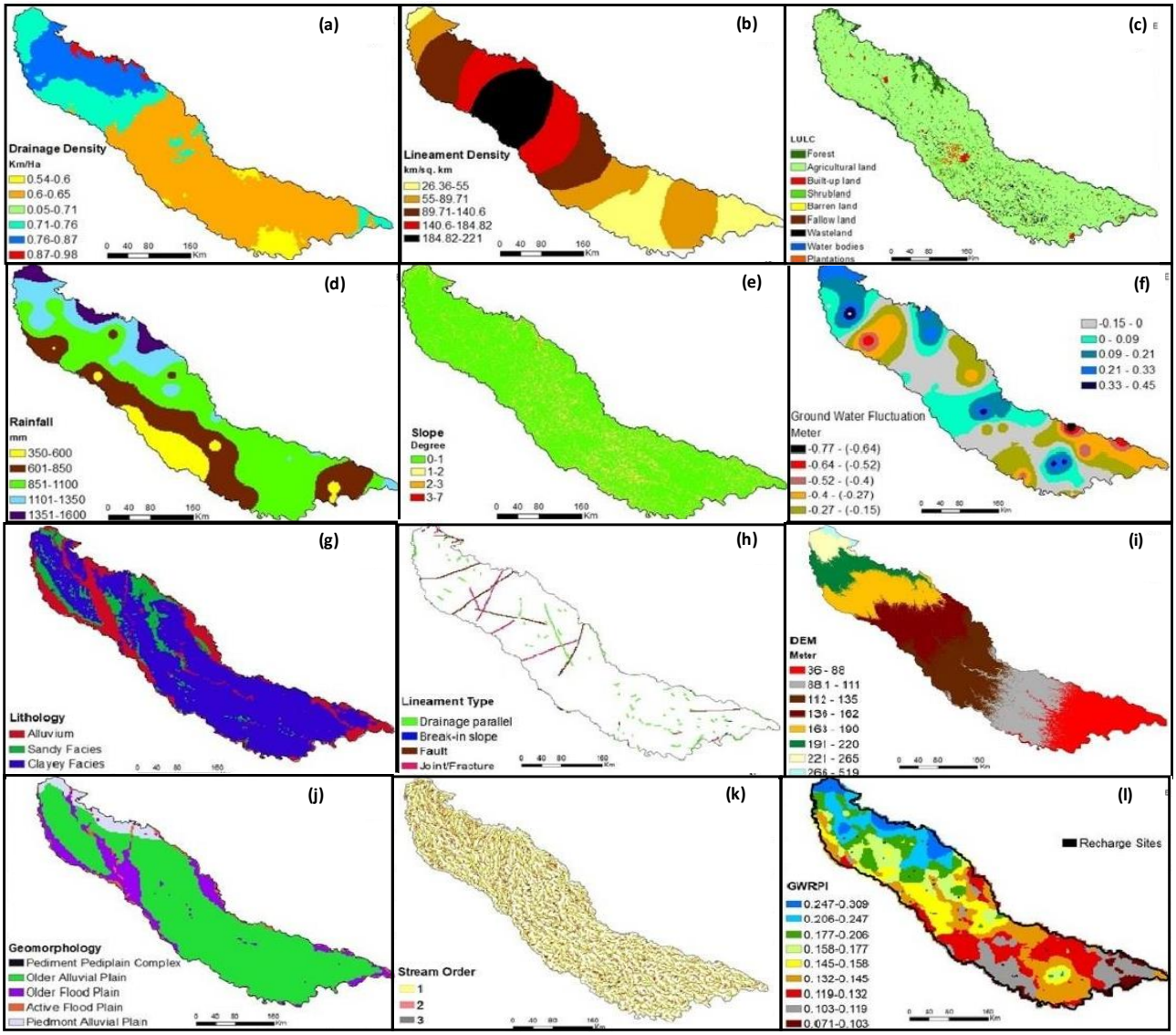

Figure 5.2: Thematic maps and the result (GWRPI map). (a) The drainage density, (b) lineament density, (c) land use land cover, (d) rainfall, (e) slope, (f) groundwater fluctuation, (g) lithology, (h) lineament type, (i) digital elevation model, (j) geomorphology, (k) stream order, and (l) groundwater recharge potential index map or GWRPZ map. The comparison of all these maps with the district map shown in figure 3 can give important information for each district about any of the thematic/spatial maps in this figure.

v) Slope Map

The slope map is created by using the slope tool of ArcGIS and using DEM as the input raster. The DEM raster was converted into the slope raster. The slope map was created using *slope tool* in the ArcMap software which was then reclassified using the *reclass tool* in ArcMap software into five classes from flat to steep. The lower slope areas of the flat terrain allow rainfall infiltration and percolation while the higher slope areas generate quick runoff from the terrain and hence offer little volume of water for groundwater recharge. However, areas with steep slopes have low groundwater level since less time is allowed for storm water to infiltrate, thus rainfall is easily turned into runoff and rapidly flow down the slope. Generally, gentle slopes are prospects of high groundwater potential, more rainfall can percolate into the subsurface. Fig. 5.2 (e) provides insight into the topography of the middle Ganga basin, showcasing the variation in slope across different parts of the landscape. The data is categorized into distinct slope classes, and the areas occupied by each range, expressed as percentages of the total study area, are as follows: 0-1 degrees: 82.90%, 1-2 degrees: 15.56%, 2-3 deg ees: 1.5%, and 3-7 degrees: 0.15%. The figure visually conveys the spatial variation in slope across the study area. Each class area represents the proportion of the total study area covered by a specific range of slope values. The maximum slope is in the Shiwalik hills region in the range height of 500 m to 300 m above msl.

A discernible pattern emerges where the slope decreases as the distance from the Himalayas increases. This aligns with the general topographical trend in mountainous regions, where the steepest slopes are closer to the mountain range, and the terrain gradually becomes flatter as you move away from the mountains. The elevation of the study area is described, ranging from 519 meters in the north to 36 meters in the south. This elevation variation is likely to contribute to the observed slope patterns. The higher elevations in the north, closer to the Himalayas, likely contribute to steeper slopes, while the lower elevations in the south are associated with flatter terrain.

The varying slope conditions in the middle Ganga basin create diverse hydrological environments. Flat terrains can act as potential water storage areas, whereas low to moderate slopes enhance infiltration and groundwater recharge [25, 29]. Steeper slopes, although promoting quicker runoff, can still play a role in recharge if managed sustainably. It's important to consider the relationship between slope, land cover, soil characteristics, and vegetation to fully understand the impact on groundwater recharge potential across the region.

vi) Groundwater fluctuation (GWF)

Groundwater-level fluctuation is an effect related to aquifer type, recharge, abstraction and regional circulation of groundwater in the area. Fig 5.2(f) provides insights into the GWF across the study area, illustrating how water levels change over time in different parts of the landscape. The data is classified into distinct GWF classes, and the areas occupied by each range, expressed as percentages of the total study area, are as follows: -0.77 to -0.64 m: 0.29%, -0.64 to -0.52 m: 1%, -0.52 to -0.4 m: 2.68%, -0.4 to -0.27 m: 11.61%, -0.27 to -0.15 m: 18.41%, -0.15 to 0 m: 28.81%, 0 to 0.09 m: 19.97%, 0.09 to 0.21 m: 11%, 0.21 to 0.33 m: 5.26%, and 0.33 to 0.45 m: 0.83%.

The figure visually represents the spatial variation in groundwater fluctuation across the study area. Each class area indicates the proportion of the total study area affected by a specific range of groundwater level change. The northern Terai region experiences a rise in GWF, as evidenced by the presence of positive values in the GWF classes. This suggests that groundwater levels are

increasing over time in this area. The rise in GWF might be attributed to factors such as higher recharge from precipitation, favorable hydrogeological conditions, and potential proximity to water sources from the Himalayas. Conversely, the southern part of the basin sees a fall in groundwater fluctuation, evident in the presence of negative values in the GWF classes. This indicates that groundwater levels are declining in this region. The fall in GWF could be related to factors like excessive groundwater extraction, lower recharge rates, and potential aquifer depletion.

vii) Lithology

The lithology is a physical description of a rock unit visible at outcrop, in hand or core samples. The physical characteristics include color, texture, grain size, and composition and rock type (alluvium, clay, silt, sand, sandstone, slate, basalt, limestone, igneous, sedimentary, metamorphic, karst, etc). Porosity determines the amount of water that a rock or sediment can contain. In sediments or sedimentary rocks, the porosity depends on grain size, the shapes of the grains, and the degree of sorting, and the degree of cementation. Clay is the most porous sediment but is the least permeable. Clay usually acts as an aquitard, impeding the flow of water. Gravel and sand are both porous and permeable, making them good aquifer materials. Gravel has the highest permeability. Soil permeability measures the time (ml/sec) it takes for water to flow through the soil pores.

Fig. 5.2 (g) provides insights into the sediment distribution across the study area, highlighting the composition of different sediment types in different parts of the landscape. The data is categorized into distinct sediment classes, and the areas occupied by each type, expressed as percentages of the total study area, are as follows: Alluvium: 19.68%, Sandy facies: 10.53%, and Clayey facies: 69.79%. The figure visually conveys the spatial distribution of sediment types across the study area. Each class area represents the proportion of the total study area covered by a specific sediment type.

The presence of Alluvium and Sandy facies predominantly in the northern parts of the basin is observed. This suggests that these sediment types are more prevalent in the areas closer to the Himalayas. Alluvium, in particular, is commonly associated with river deposits, often found in floodplains and areas influenced by river dynamics. majority of the study area is occupied by Clayey facies, constituting nearly 70% of the total area. This sediment type likely indicates fine-grained deposits, which can be associated with slower water movement, lower energy environments, and potentially older geological formations.

viii) Lineament map

Fig 5.2(h) depicts different types of lineaments within the study area and their directional alignment, specifically in the northeast (NE) and southeast (SE) directions. The lineament types include Drainage parallel, break-in slope, fault, and Join/Fracture. In the Himalayas, lineaments running parallel to drainage patterns could be shaped by tectonic and geomorphic processes associated with the Himalayan uplift. The NE and SE alignments of these lineaments may correspond to the compressional forces resulting from the collision between the Indian and Eurasian plates, influencing drainage alignment.

Break-in slope lineaments in the Himalayas often indicate abrupt topographic changes that could be linked to faults or fractures resulting from tectonic activity. The NE and SE orientations

of these lineaments might reflect the dominant stress directions exerted on the landscape due to plate tectonics. Fault lineaments signify fractures in the Earth's crust where movement has occurred.

Lineaments are geological features that can act as preferential pathways for groundwater movement, influencing the direction and speed of subsurface water flow. In areas where lineaments intersect with recharge sites, there is a heightened likelihood of increased groundwater recharge. These intersecting points could facilitate greater infiltration and movement of water through the subsurface, effectively enhancing the recharge potential of the groundwater system. Lineaments can serve as conduits for the rapid movement of water, potentially bypassing recharge sites and leading to reduced opportunities for water infiltration and recharge.

ix) Geomorphology

Geomorphic landform and its changes occur from erosion, transporation and deposition of rocks and sediments. Fig 5.2(i) provides insights into the geomorphological features across the study area, highlighting different landforms and their distribution. These features include; Pediplain (an extensive flat land formed by the coalescence of pediments, and is covered by the thinly discontinuous veneer of soil and alluvium derived from the upward areas); Alluvial plain (formed from deposition of sediment from everine system or systems; Floodplain (sediment deposition along the river flooding reaches); etc. The data is categorized into distinct classes representing various geomorphological features, and the areas occupied by each feature, expressed as percentages of the total study area, are as follows: Pediment Pediplain complex: 0.1%, Older Alluvial plain: 77.78%, Older flood plain: 13.79%, Active flood plain: 3.1%, and Pediment alluvial plain: 5.4%. The presence of a Pediment Pediplain complex indicates a particular type of landform where a gently sloping surface forms between the base of the hills and the adjacent plains. This landform often results from the erosion of rocks from the hills and their deposition on the adjacent plains. The Shiwalik hills could contribute to the materials that form these pediments, and the complex could be influenced by the dynamics of the sediment transport and erosion from the hills.

The significant occupation of the Older Alluvial plain class, suggests that these plains have been formed over an extended period through the deposition of sediments carried by rivers. The Shiwalik hills could play a role in providing the source of sediments that contribute to the formation and gradual expansion of these older alluvial plains. The presence of both Older and Active flood plain classes indicates areas that experience floodplain deposition. These areas could be influenced by the periodic flooding of rivers originating in the Shiwalik hills. The hills might contribute to increased sediment load during floods, leading to the deposition of sediments and the formation of flood plains. The presence of Pediment alluvial plain class signifies a landform that lies between the hills and the adjacent plains, characterized by sediment deposition from the hills. The presence of such a class highlights the interaction between the hills and the adjacent plains in terms of sediment transport and deposition.

x) DEM map

In Fig. 5.2 (j), the Digital Elevation Model (DEM) provides a representation of the elevation variation across the study area, illustrating how elevation changes in relation to distance from the Himalayas. The DEM values vary from 519 meters to 36 meters, with a consistent decrease in elevation as one moves away from the Himalayan region. As one approaches the Himalayas, the land begins to rise significantly due to the tectonic uplift and the presence of high peaks and ranges. These elevations are

typical of the foothills and the lower slopes of the mountains. The lower DEM values, such as the 36-meter elevation, correspond to relatively flat and low-lying areas, which are often found away from mountainous regions. These plains and lowlands are usually characterized by more gradual elevation changes and are the result of sediment deposition over geological time.

Table 5.2: Percentage coverage of the classes represented in the geomorphology map.

S. No.	Class name	Percentage area cover
1	Pediment pediplain complex	0.01%
2	Older alluvial plain	77.78%
3	Older flood plain	13.79%
4	Active flood plain	3.10%
5	Pediment alluvial plain	5.40%
6	River	0.02%
7	Highly dissected structural hills and valleys	0.02%
8	Dam and reservoir	0.02%
9	Waterbodies - unclassified	0.04%

xi) Drainage network & Stream Order

The presence of stream orders 1, 2, and 3 in Fig 5.2(k) with respect to elevation and slope:

1. Stream Order 1 and Elevation: Stream order 1 channels are typically found at higher elevations. These smaller streams often originate from springs, runoff, or minor depressions in the landscape. In the context of the study area, these stream order 1 channels are likely to emerge from the elevated regions, such as the Himalayas. The higher elevations provide the necessary gradient for water to flow downhill, initiating the formation of these smaller channels. The presence of stream order 1 channels in Fig 5.2(i) signifies the widespread distribution of these small streams in the elevated areas.

2. Stream Order 2 and Confluence Zones: Stream order 2 channels result from the merging of multiple stream order 1 channels. These converging points typically occur in areas where slopes become gentler, and water from different directions comes together. In the study area, these stream order 2 channels might be observed as watercourses that have collected flow from smaller, order 1 channels. The confluence zones of these smaller channels contribute to the formation of slightly larger and more well-defined drainage paths.

3. Stream Order 3 and Main Drainage Paths: Stream order 3 channels represent the merging of stream order 2 channels or combinations of stream order 2 and 1 channels. These channels tend to be larger and more significant in terms of water flow. In the context of elevation and slope, stream order 3 channels often follow the main valleys and lowlands, where the terrain is more gradual and the slope is less steep. The convergence of multiple stream order 2 channels in these areas leads to the formation of well-defined and more substantial drainage paths.

xii) Groundwater Recharge Potential Zone (GWRPZ)

Figure 5.2 (l) integrates information from eight thematic maps (drainage density, lineament density, LULC, rainfall, slope, GWF, lithology, and geomorphology) by giving appropriate weights and integrating using AHP to generate the Groundwater Recharge Zone Map. The resulting Groundwater Recharge Zone Map displays Groundwater Recharge Potential Index (GWRPI) values ranges from 0.309 to 0.071; and categorized into 7 classes, representing, different ranges of recharge potential for groundwater recharge within the study area. The variations in GWRPI values reflect the complex nature of groundwater recharge processes and highlight the significance of considering multiple influencing factors when assessing groundwater resources.

Two trends are observed in GWRPI values. First, GWRPI values decrease from NE to SW, implying higher recharge potential in NE. Elevation, precipitation, geology, and land use practices might contribute to this trend. Second, GWRPI values decrease from NW to SE, indicating higher recharge potential in NW.

xiii) Validation

Different empirical relations between the rainfall (P) and the recharge (R) are given in the literature for the Indo-Gangetic Basin. Table 1 displays some of these formulae that are used in the present study.

Table 5.3: A list of empirical formulas used in this study for the calculation of the groundwater recharge. These formulas can provide a rough estimate of the groundwater recharge in a certain area. All formulae estimate recharge 'R' on the basis of rainfall 'P'.

S. No.	Name	Formula
1	UP Irrigation Board formula	$R=1.35(P-15)^{0.5}$ here P = inches, and R=inches.
2	Krishna Rao formula	R=0.30(P-300) here P = mm, and R=mm.
3	Chaturvedi formula	$R=2.0(P-15)^{0.4}$ here P =inches, and R=inches.
4	Braden-Camp formula	R=0.32(P-360) here P = mm, and R=mm.
5	Amritsar formula	$R=2.5(P-16)^{0.5}$ here P = inches, and R=inches.

Figure 5.3 presents a linear relationship between the quantity of groundwater recharge (in inches) and the GWRPI for the study area. The figure also displays various formulas used to calculate GWR based on specific methods: UP Irrigation Board formula in (A), Krishna Rao formula in (B), Chaturvedi formula in (C), Braden-Camp formula in (D), and Amritsar formula in (E). Additionally, regression equations are provided to express the relationship between GWRPI and GWR for each formula.

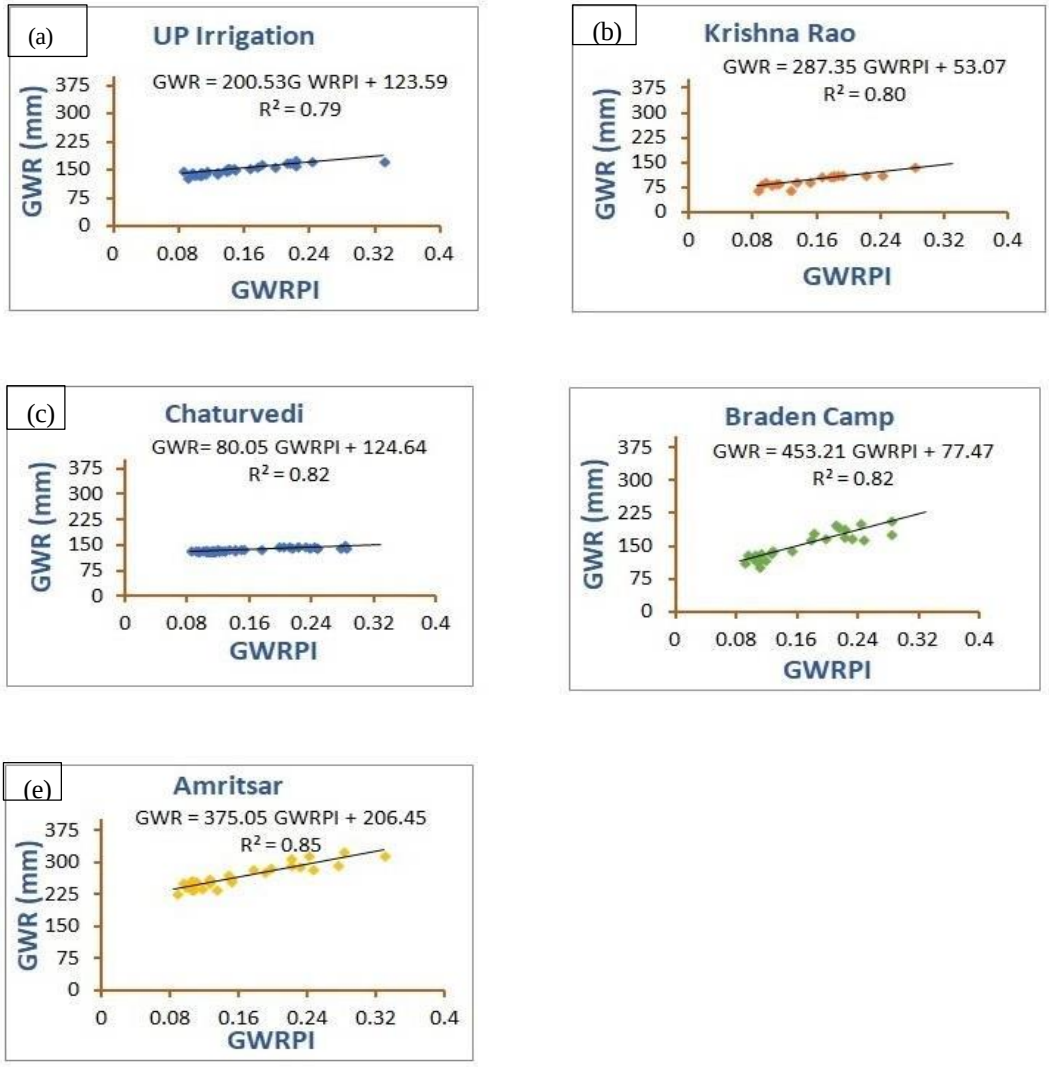

Figure 5.3: - Linear relationship between the quantity of ground water recharge (GWR) and groundwater recharge potential index (GWRPI) of the study area. The various formulas used to calculate the GWR are the UP Irrigation Board formula in (a), Krishna Rao formula in (b), Chaturvedi formula in (c), Braden-Camp formula in (d) and Amritsar formula in (e).

When the coefficient of determination (R^2 value) for the regression lines are compared (Fig. 5.3), the Amritsar formula has the highest coefficient of determination (R^2=0.85), followed by Braden Camp (R^2=0.82) and Chaturvedi Formula (R^2=0.82) implying a relatively better fit of the linear regression model compared to the Krishna Rao and UP Irrigation formula. The high R-squared values indicate that the GWRPI, as derived from the integration of multiple thematic maps and assigned AHP weights, correlates well with the calculated groundwater recharge.

The slope of the regression line indicates the strength of the relation between GWR and GWRPI. A steeper slope of the regression line indicates a stronger relationship between GWRPI and GWR.

Accordingly, Braden camp (slope=453.21) and Amritsar Formula (Slope = 375.05) show a stronger relation compared to the remaining regressions.

Combining the slope and goodness of fit Braden Camp (R2=0.85, Slope = 453.21) and (Amritsar formula (R^2=0.85, Slope =375) appears to best correlated with be GWRPI.

xix) Site suitability for Artificial Recharge Measures:

Fig 5.4 depicts the sites suitable for artificial recharge measures. Total 92 recharge sites have been identified. These sites are located along the point of cross section of third-order streams and lineaments. The lieaments help to swift the flooding water and to recharge it to the groundwater. The identified ninty-two sites are split in to two categories (62 and 30) as per their locations in the zones characterized according to the groundwater recharge potential index and the trend of groundwater fluctuation.

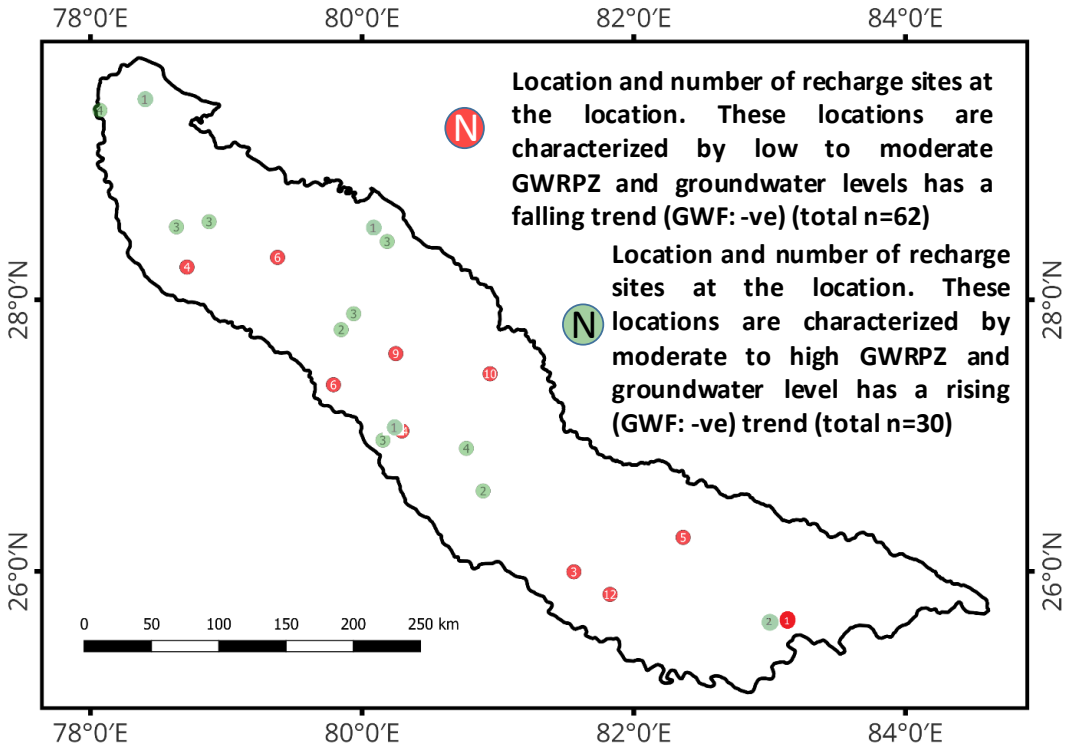

Fig 5.4: Recharge sites for artificial recharge measures. Of the total identified 92 sites, 62 are located in the zones characterized by low to moderate GWRPZ and falling trend in groundwater level whereas, 30 are located in the areas characterized by high GWRP and rising groundwater level zones. (GWF: Groundwater fluctuation)

xx) Significance

Considering water crises under the increasing water demand and the impact of climate change, states and the Central government are running large scale schemes and programs to bring awareness among the public on the importance of water conservation and to implement programs for development, augmentation, and conservation of water resource. At the country level, these program exceeds a total budget of ten lakh crore rupees. Some such programs that are getting implemented in the state of Uttar Pradesh include schemes like **Atal Bhujal Yojana** (Total Budget:

Rs 6,000 crores), **Jal Jeevan Mission** (Budget: Rs 3.,60 lakh crores), **Khet Talab Yojana** (Rs 204 crores), **Pradhan Mantri Krishi Sinchayee Yojana** (Budget: Rs 93069 crores), **Mission Amrit Saroar** (Budget Rs 3.0 lakh crores), **Mukhyamantri Jal Bachao Abhiyan**. Various thematic maps that are developed in the present study including the map of groundwater recharge potential zone and the indentified sites for artificial recharge measures provide scientific input to these missions.

6. LONG-TERM TREND ANALYSIS OF CLIMATE VARIABLES

Due to increase in industrialization, the greenhouse gas concentration has increased in the atmosphere. This has warmed the surface of the earth. An increase in the temperature is observed in the study area, especially in the case of night temperature. Because of higher levels of carbon dioxide, the trapped solar heat during the day is not able to escape in the night. This results in the increased earth temperature. The increase in the earth temperature leads to increased evapotranspiration. This further reduces the groundwater level.
The detection, estimation and prediction of trends and associated statistical and physical significance are important aspects of climate research.

6.1 Temperature Distribution

The lowest temperature recorded-diurnally, monthly, seasonally, or annually, or the lowest temperature of the entire record. Daily air temperature minima are recorded by the screen minimum thermometer. The process of evaporation also takes place at night but at a very slow rate. This is because even after sun set some amount of heat still exists in the environment. This small amount of heat is sufficient to carry out the process of evaporation. Atmospheric surface temperature in India has increased in the last century by about 1°C and 1.1°C during winter and post-monsoon months respectively.

In the present study, the maximum temperature was calculated by averaging the maximum temperature values recorded on all days from January 1, 1991, to December 31, 2020. Similarly, the minimum and average temepratures are calculated for the each grid point data.

The average maximum temperature ranges from 27°C to 33°C across the study area. Lower temperatures (27°C to 30°C) are predominantly observed near the Shiwaliks or the outer Himalayas, while relatively higher temperatures (31°C to 33°C) are observed in areas farther away from the Shiwaliks. The higher-temperature regions of the basin are located outside the Terai region. In a significant portion of the study area, the maximum temperature exceeds 31.80°C, and in 90% of the study area, the annual average maximum temperature exceeds 30°C. The maximum temperature generally occurs at 2:00 p.m. The temperature increases from north to south and from west to east. The higher temperatures are mostly observed in the plains of the study area. The average annual maximum temperature for the entire study area is 31.35°C.

Long-term temperature change analysis is pivotal for comprehending the intricate interplay between regional or global temperature fluctuations and their impact on water resources. Beyond influencing sea surface temperatures (SST) and vapor quantity through evaporation, these changes profoundly shape phenomena like El Niño, La Niña, and monsoon intensity.

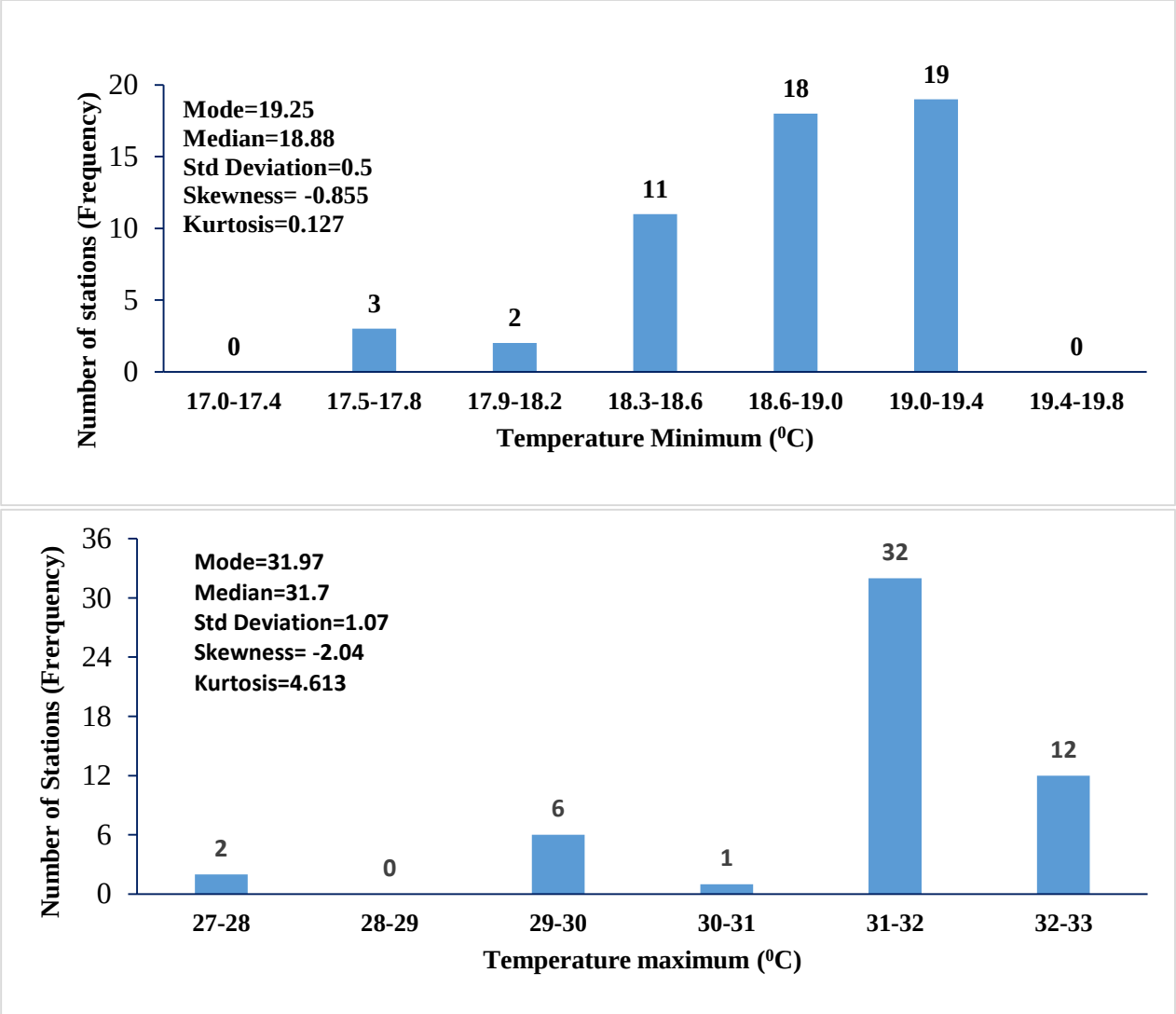

Fig 6.1: Histogram of long-term annual average temperature (minimum and maximum) for total 53 number of locations taken over the period from 1991 to 2020

Moreover, they intricately control vapor pressure, thus modulating cloud dynamics and fostering conditions for enhanced evaporation and transpiration. Ultimately, such shifts reverberate through surface water bodies, soil moisture, and vegetation, underscoring the critical need for sustained temperature monitoring in water resource studies. As dawn breaks, the Earth begins to warm, reaching its peak temperature by the afternoon. Cooling sets in as the sun sets, eventually reaching its lowest point just before dawn. Exceptions to this happen during unusual wind events, where warm or cold air moves over the surface. The highest temperature of a day is termed as a 'maximum temperature ($Temp_{max}$)', and the lowest temperature that attains just before the dawn as the 'minimum temperature ($Temp_{min}$)'. The long-term trends of the annual average maximum temperature and the annual average minimum temperature provide insights into the prolonged patterns of daytime warming and nighttime cooling within a region

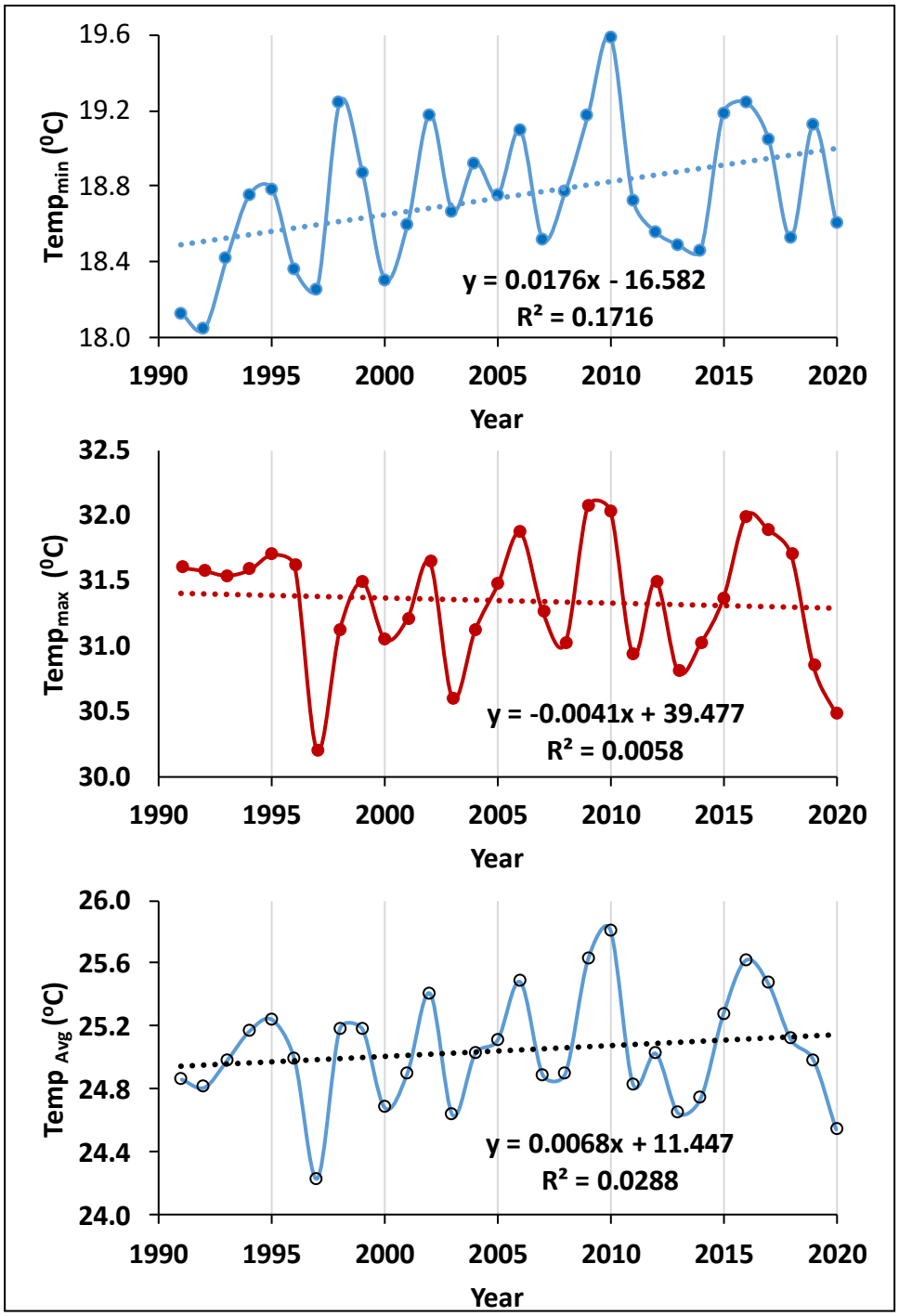

Figure 6.2: The time series of the minimum temperature, the maximum temperature and the average temperature of the middle Ganga basin

The observed results from the study area in the middle Ganga Basin reveal the following temperature trends: The average values for temperature series are as follows: $Temp_{min}$=18.75±0.37 °C; $Temp_{max}$=31.35±0.47 °C; $Temp_{avg}$=25.05±0.35 °C. In both $Temp_{min}$ and $Temp_{max}$ series, the years exhibiting troughs and crests coincide, except for 2005 and 2018, where disparities are noted. In the $Temp_{min}$ series, the increasing magnitude of crest strength relative to trough strength leads to a progressive increase in the $Temp_{min}$ at a rate of 0.176°C per decade. Conversely, in the $Temp_{max}$ series, the strengthening of troughs surpasses that of peaks, resulting in a decreasing trend with a rate of decrease of 0.04°C per decade. As the rising trend of the $Temp_{min}$ series exceeds the decreasing trend of $Temp_{max}$, the resultant $Temp_{avg}$ series indicates a rising temperature trend, at a rate of 0.06°C per decade. Consequently, the region's temperature is increasing at a rate of 0.06°C per decade. Notably, the rise primarily stems from an increase in nighttime temperatures ($Temp_{min}$), suggesting a potential amplification of the atmosphere's thermal capacity, likely attributable to rising greenhouse gas concentrations, alterations in dust composition, and other contaminants.

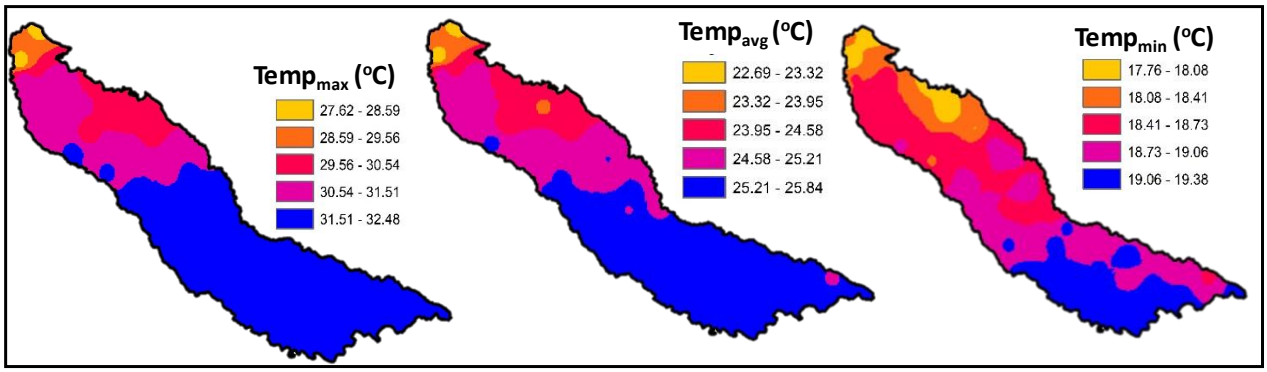

Figure 6.3: The spatial distribution map of the minimum temperature of the middle Ganga basin, UP.

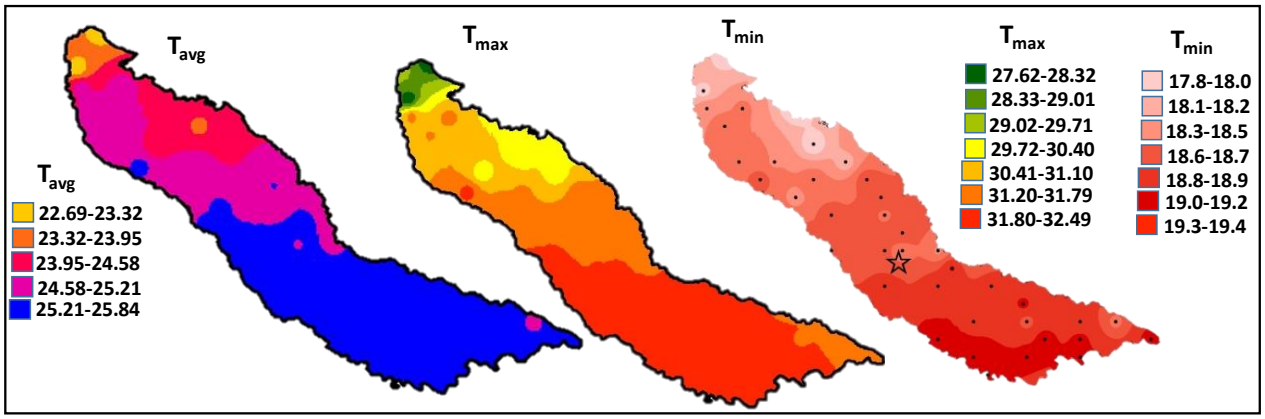

Fig 6.4: Spatial variation of temperature in ^{0}C (average, maximum and minimum) in the study area averaged over the period from 1991-2020. Grid points for the temperature data is shown in the fig for $T_{min.}$ Symbol star in the Tmin map indicates the location of city Lucknow

(a) Spatial and Temporal Variation of Maximum Temperature

The spatial distribution of the annual maximum temperature (which is generally observed at 2:00 PM in the entire day) for the periods 1991–2000, 2001–2010, and 2011–2020 is shown in the fig XXX. The average maximum temperature varies from 27.1°C to 32.5°C. The lower temperatures (27°C to 29°C) are observed mostly near the Shiwaliks, whereas, higher temperatures (31°C to 32.5°C) are observed in the areas which are very far from the Shiwaliks. In a large part of the study area, the maximum temperature is higher than 31.50°C. . In 90% of the study area, the annual average maximum temperature is more than 30°C. Significant changes can be seen in the distribution and range of temperatures distribution pattern over the three decades. The spatial distribution of maximum temperature for 1991–2000 appears largely similar to that of 2011–2020. However, the dark red temperature range covers a larger area in 1991–2000 (approximately 60%) compared to 2011–2020 (approximately 50%). These changes in the annual maximum temperature are primarily observed in the central portion of the study area.

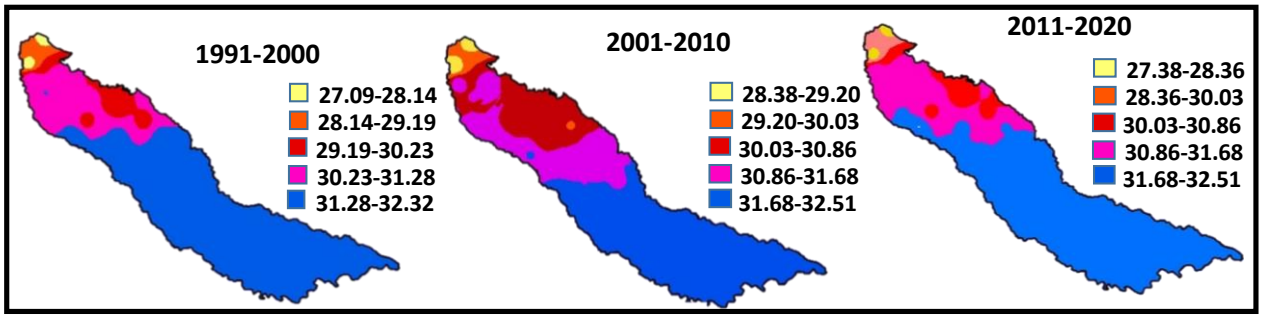

Figure 6.5: The decadal comparison of the maximum temperature of the study area of the decades 1991-2000, 2001-2010, and 2011-2020.

The spatial distribution of the average monthly maximum temperature is shown in Figure 14. The annual average temperature of the study area systematically increases from January onward, peaking in May and then decreasing till December-January. The temperature ranges for each month are as follows: January (17°C to 23.2°C), February (20°C to 29°C), March (25°C to 34°C), April (30°C to 38°C), May (34°C to 43°C), June (33°C to 40°C), July (32°C to 37.5°C), August (29°C to 33.2°C), September (28°C to 34.2°C), October (23°C to 29°C), November (19°C to 24.4°C), and December (19°C to 24.4°C).

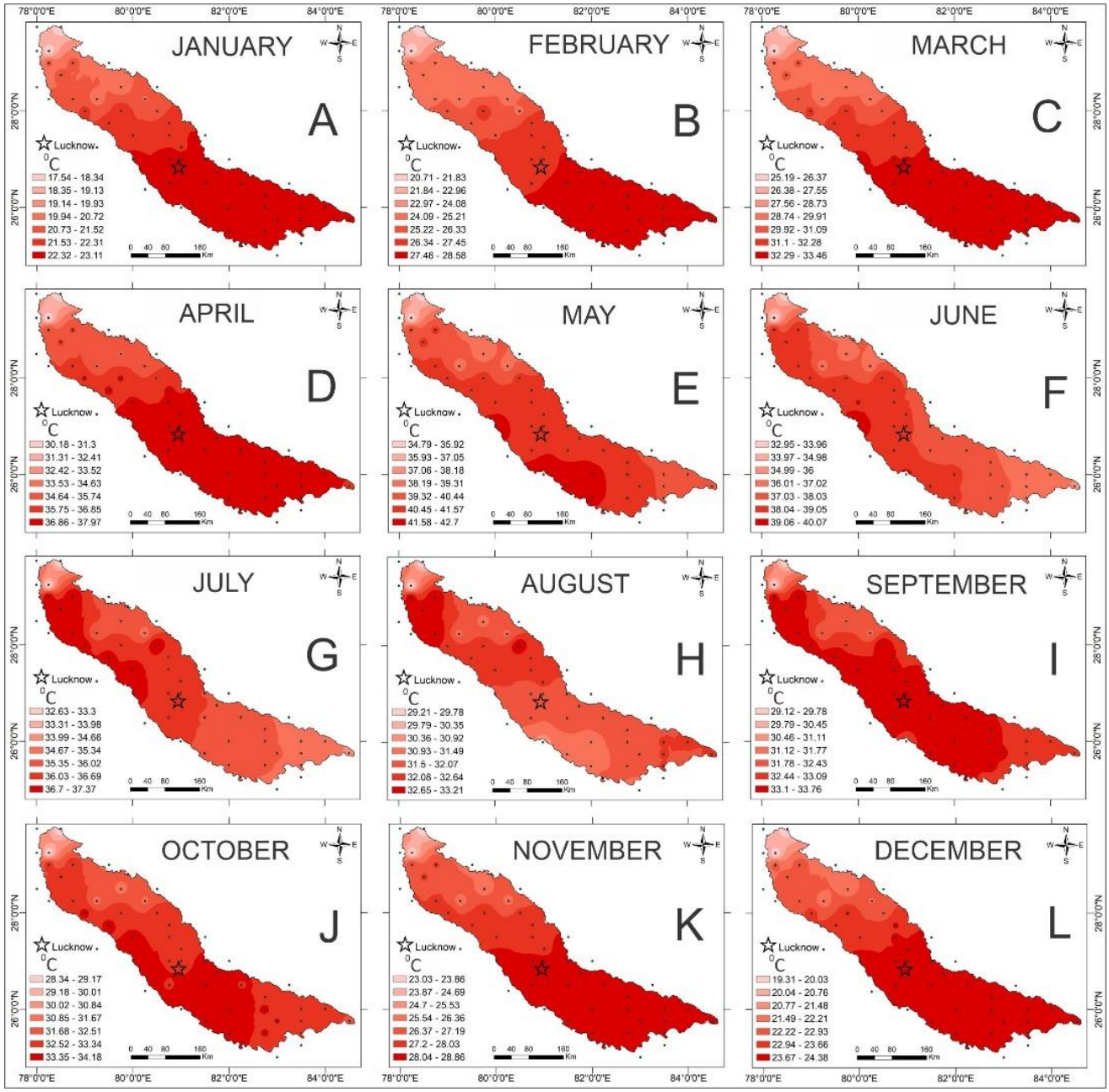

Fig. 6.6: Spatial distribution of the average monthly maximum temperature from January (A) to December (L) for 12 months (°C).

(b) Spatial and Temporal Variation of Minimum Temperature

The spatial variation of the annual average minimum temperature is shown in Fig. 15. The minimum temperature was calculated by averaging the minimum temperature values recorded on all days from January 1, 1991, to December 31, 2020. The values shown in Figure 15 represent the average minimum temperature calculated over a 30-year period.

The average minimum temperature ranges from 17°C to 19.5°C across the study area. Lower temperatures (17°C to 18.5°C) are predominantly observed near the Shiwalik hills, while relatively higher temperatures (above 18.5°C) are observed in areas farther away from the Shiwalik hills. In general, the temperature was observed to increase in the southeast direction. In a significant portion (approximately 75%) of the study area, the minimum temperature exceeds 18.5°C. The minimum temperature generally occurs at 4:00 a.m. The capital city of Lucknow, situated in the plains, falls under the temperature range of 18.8°C to 18.9°C. The average annual minimum temperature for the entire study area is 18.75°C.

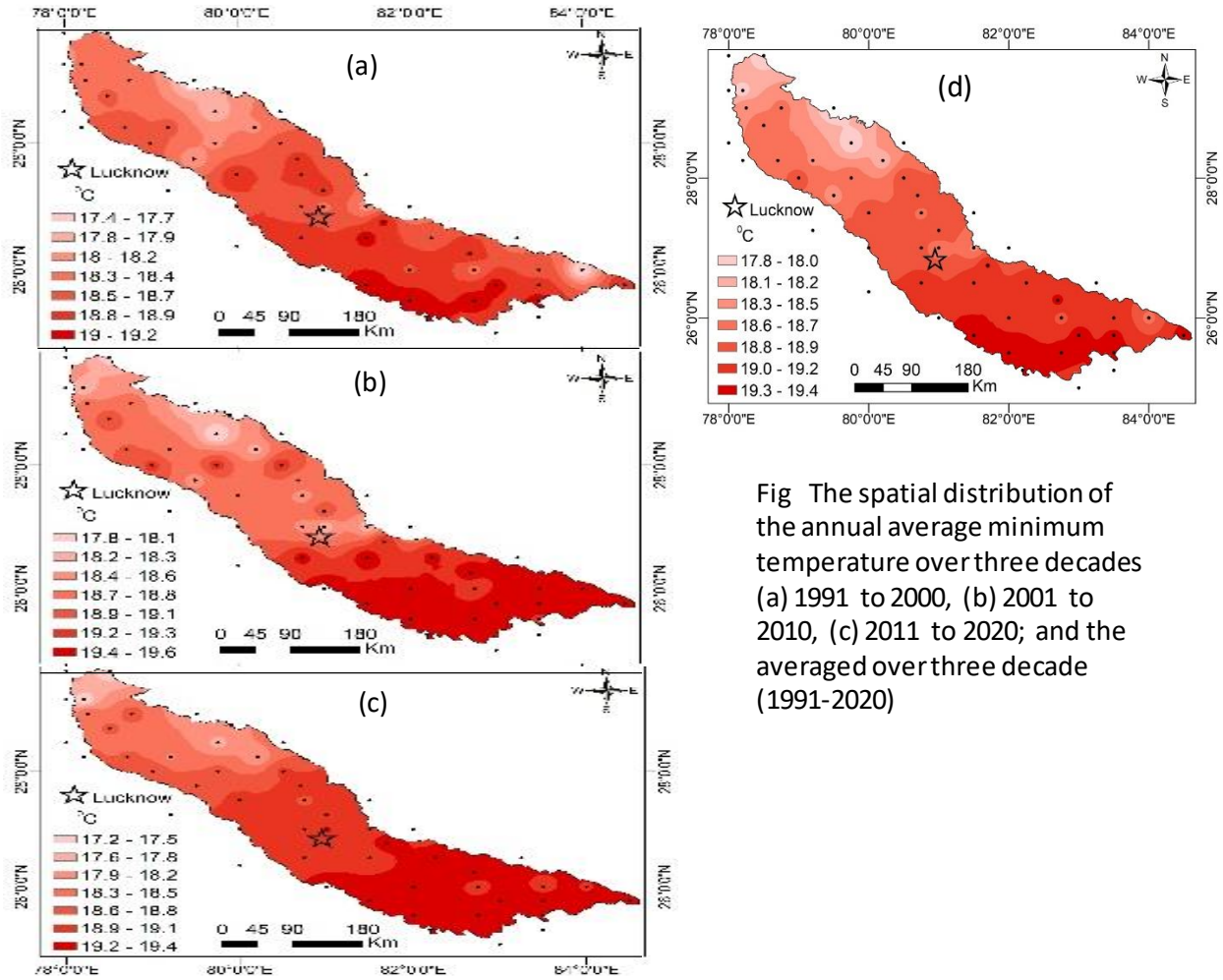

Fig The spatial distribution of the annual average minimum temperature over three decades (a) 1991 to 2000, (b) 2001 to 2010, (c) 2011 to 2020; and the averaged over three decade (1991-2020)

The decadal averaged annual minimum temperature for the periods 1991-2000, 2001 2010, and 2011-2020, shows large part of the southern portion of the study area covered by the darkest red zone; and this region is larger in the decade 2011-2020 compared to the decade 1991-2000. In the state capital Lucknow (shown by star in the figure), the temperature range changes from 18.5°C-18.7°C in 1991-2000 to 18.4°C-18.6°C in 2001-2010, and again to 18.6°C-18.8°C in 2011-2020. There is an increase of 0.1°C in the minimum temperature in the period 2011-2020 compared to

1991-2000. The annual minimum temperatures for 1991-2000, 2001-2010, and 2011-2020 are 18.52°C, 18.93°C, and 18.80°C, respectively.

Figure 17 displays the spatial distribution of the average monthly minimum temperature averaged over three decades, 1991-2020. The distribution pattern in the annual temperature shows an increase in the mean monthly temperature from January to July, and thereafter a systematic decrease till December. The temperature ranges for each month are as follows: January (6.78°C to 10.2°C), February (9.1°C to 13.4°C), March (9.1°C to 13.4°C), April (13.21°C to 18.36°C), May (18°C to 24°C), June (21.5°C to 27.7°C), July (23.1°C to 29.1°C), August (23.25°C to 27.58°C), September (23°C to 27°C), October (21.5°C to 25.7°C), November (17.1°C to 22.3°C), and December (12.2°C to 16.5°C).

Table 7 presents the results of the Mann-Kendall trend test and Sen's slope estimator. The Mann-Kendall trend test indicates that, out of the total data points (53), the average maximum temperature shows a decreasing trend over time at five stations (as observed from the S-value). The rate of decrease ranges from -0.05 °C/year to -0.001 °C/year (Sen's slope) across these 12 stations. Conversely, the remaining points (41) exhibit an upward trend in the average maximum temperature. The rate of increase varies from 0.0028 °C/year to 0.073 °C/year based on Sen's slope estimation. Out of the total data points (65), the average minimum temperature shows a decreasing trend over time at 26 stations (as observed from the S-value) according to the Mann-Kendall trend test. The rate of decrease ranges from -0.05°C/year to -0.01°C/year (Sen's slope) across these nine stations. Conversely, the remaining points (39) exhibit an upward trend in the average minimum temperature. The rate of increase varies from 0.01°C/year to 0.07°C/year based on Sen's slope estimation. There are five stations where the minimum temperature shows no significant trend (Sen's slope ~ 0).

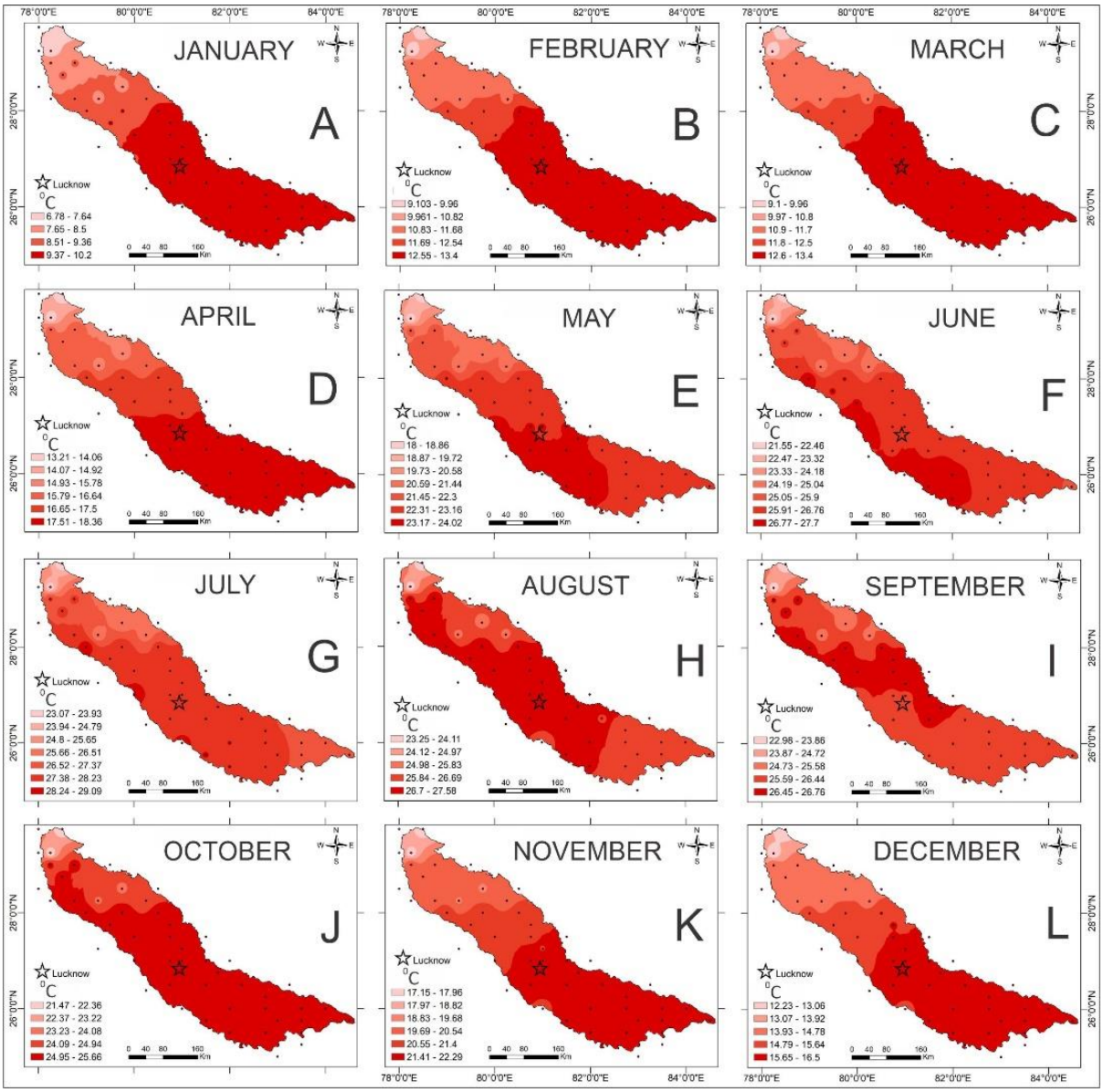

Fig. 6.8: Spatial distribution of average monthly minimum temperature from January to December for 12 months (°C).

Table 6.1: Mann-Kendall trend test and Sen's slope for the annual temperature data

S. No.	Lat.	Long.	For Annual Maximum Temperature				For Annual Maximum Temperature			
			Sen's slope	S value	Z Statistic	Trend	Sen's slope	S-value	Z-statistic	Trend
1	25	83	0.02	0	-0.02	Decreasing	0.022	-3	-0.04	Decreasing
2	25.25	82.25	0.02	4	0.05	Increasing	0.019	1	0	No trend
3	25.25	83.5	0.02	0	-0.02	Decreasing	0.024	5	0.07	Increasing
4	25.5	82	0.02	2	0.02	Increasing	0.015	-3	-0.04	Decreasing
5	25.5	82.75	0.02	2	0.02	Increasing	0.019	-3	-0.04	Decreasing
6	25.5	83.5	0.02	2	0.02	Increasing	0.018	5	0.07	Increasing
7	25.75	81.5	0.02	4	0.05	Increasing	0.016	1	0	No trend
8	25.75	83	0.03	-2	-0.02	Decreasing	0.034	1	0	No trend
9	25.75	83.5	0.02	-2	-0.02	Decreasing	0.018	5	0.07	Increasing
10	25.75	84.5	0.03	0	-0.02	Decreasing	0.027	5	0.07	Increasing
11	25.75	84.75	0.02	0	-0.02	Decreasing	0.019	-1	0	No trend
12	26	81	0.03	4	0.05	Increasing	0.026	-1	0	No trend
13	26	82	0.02	2	0.02	Increasing	0.015	-1	0	No trend
14	26	82.75	0.01	0	-0.02	Decreasing	0.014	5	0.07	Increasing
15	26	83.5	0.01	0	-0.02	Decreasing	0.013	5	0.07	Increasing
16	26	84	0.03	0	-0.02	Decreasing	0.028	3	0.04	Increasing
17	26.25	82.75	0.04	2	0.02	Increasing	0.036	1	0	No trend
18	26.38	80.25	0.02	4	0.05	Increasing	0.022	1	0	No trend
19	26.5	80.75	0.02	4	0.05	Increasing	0.025	-5	-0.07	Decreasing
20	26.5	81.5	0.03	0	-0.02	Decreasing	0.032	1	0	No trend
21	26.5	82.25	0.01	2	0.02	Increasing	0.015	3	0.04	Increasing
22	26.5	83.25	0.03	2	0.02	Increasing	0.033	3	0.04	Increasing
23	26.75	81.75	0.04	4	0.05	Increasing	0.037	1	0	No trend
24	27	80	0	2	0.02	Increasing	-0.002	-1	0	No trend
25	27	80.75	0.01	4	0.05	Increasing	0.015	-5	-0.07	Decreasing
26	27	81	0.01	4	0.05	Increasing	0.009	-5	-0.07	Decreasing
27	27	81.5	0.02	2	0.02	Increasing	0.015	-1	0	No trend
28	27	82	0.03	0	-0.02	Decreasing	0.032	1	0	No trend
29	27.25	79.25	0.04	0	-0.02	Decreasing	0.039	-1	0	No trend
30	27.25	81	0.02	0	-0.02	Decreasing	0.017	-5	-0.07	Decreasing
31	27.5	80	0.02	0	-0.02	Decreasing	0.019	-3	-0.04	Decreasing
32	27.5	80.75	0.03	6	0.09	Increasing	0.027	-5	-0.07	Decreasing
33	27.5	81.5	0.03	2	0.02	Increasing	0.029	-5	-0.07	Decreasing
34	27.75	79.5	0.05	4	0.05	Increasing	0.052	-3	-0.04	Decreasing

35	**27.75**	**80.75**	**0.07**	**-2**	**-0.02**	**Decreasing**	**0.073**	**-3**	**-0.04**	**Decreasing**
36	**28**	**79**	**-0.01**	**4**	**0.05**	**Increasing**	**-0.008**	**-5**	**-0.07**	**Decreasing**
37	**28**	**79.75**	**-0.01**	**4**	**0.05**	**Increasing**	**-0.008**	**-1**	**0**	**No trend**
38	**28**	**80.5**	**-0.03**	**2**	**0.02**	**Increasing**	**-0.029**	**-1**	**0**	**No trend**
39	**28.25**	**78.25**	**-0.03**	**2**	**0.02**	**Increasing**	**-0.027**	**-1**	**0**	**No trend**
40	**28.25**	**78.75**	**0.02**	**2**	**0.02**	**Increasing**	**0.016**	**-3**	**-0.04**	**Decreasing**
41	**28.25**	**79.25**	**0**	**2**	**0.02**	**Increasing**	**-0.004**	**-5**	**-0.07**	**Decreasing**
42	**28.25**	**80.25**	**-0.02**	**0**	**-0.02**	**Decreasing**	**-0.015**	**-3**	**-0.04**	**Decreasing**
43	**28.5**	**78**	**0.01**	**0**	**-0.02**	**Increasing**	**0.006**	**-3**	**-0.04**	**Decreasing**
44	**28.5**	**79.75**	**0.01**	**2**	**0.02**	**Increasing**	**0.014**	**-7**	**-0.11**	**Decreasing**
45	**28.5**	**80.5**	**0.03**	**2**	**0.02**	**Increasing**	**0.029**	**-5**	**-0.07**	**Decreasing**
46	**28.75**	**78.5**	**0.03**	**2**	**0.02**	**Increasing**	**0.027**	**-1**	**0**	**Decreasing**
47	**29**	**78.25**	**-0.02**	**4**	**0.05**	**Increasing**	**-0.022**	**-3**	**-0.04**	**Decreasing**
48	**29**	**78.75**	**-0.04**	**2**	**0.02**	**Increasing**	**-0.043**	**-7**	**-0.11**	**Decreasing**
49	**29**	**79.5**	**0**	**2**	**0.02**	**Increasing**	**-0.005**	**-3**	**-0.04**	**Decreasing**
50	**29.25**	**78**	**-0.05**	**4**	**0.05**	**Increasing**	**-0.051**	**-3**	**-0.04**	**Decreasing**
51	**29.25**	**78.25**	**-0.01**	**-2**	**-0.02**	**Decreasing**	**-0.011**	**3**	**0.04**	**Increasing**
52	**29.75**	**78**	**0**	**4**	**0.05**	**Increasing**	**0.003**	**-3**	**-0.04**	**Decreasing**
53	**29.75**	**78.5**	**0**	**-2**	**-0.02**	**Decreasing**	**0.003**	**-3**	**-0.04**	**Decreasing**

In the study area, the average temperature varies from 22.69°C to 25.84°C from north to south. The surface temperatures over a given region vary seasonally and annually depending upon latitude, altitude and location with respect to geographical features such as a water body (river, lake or sea), mountains, etc.

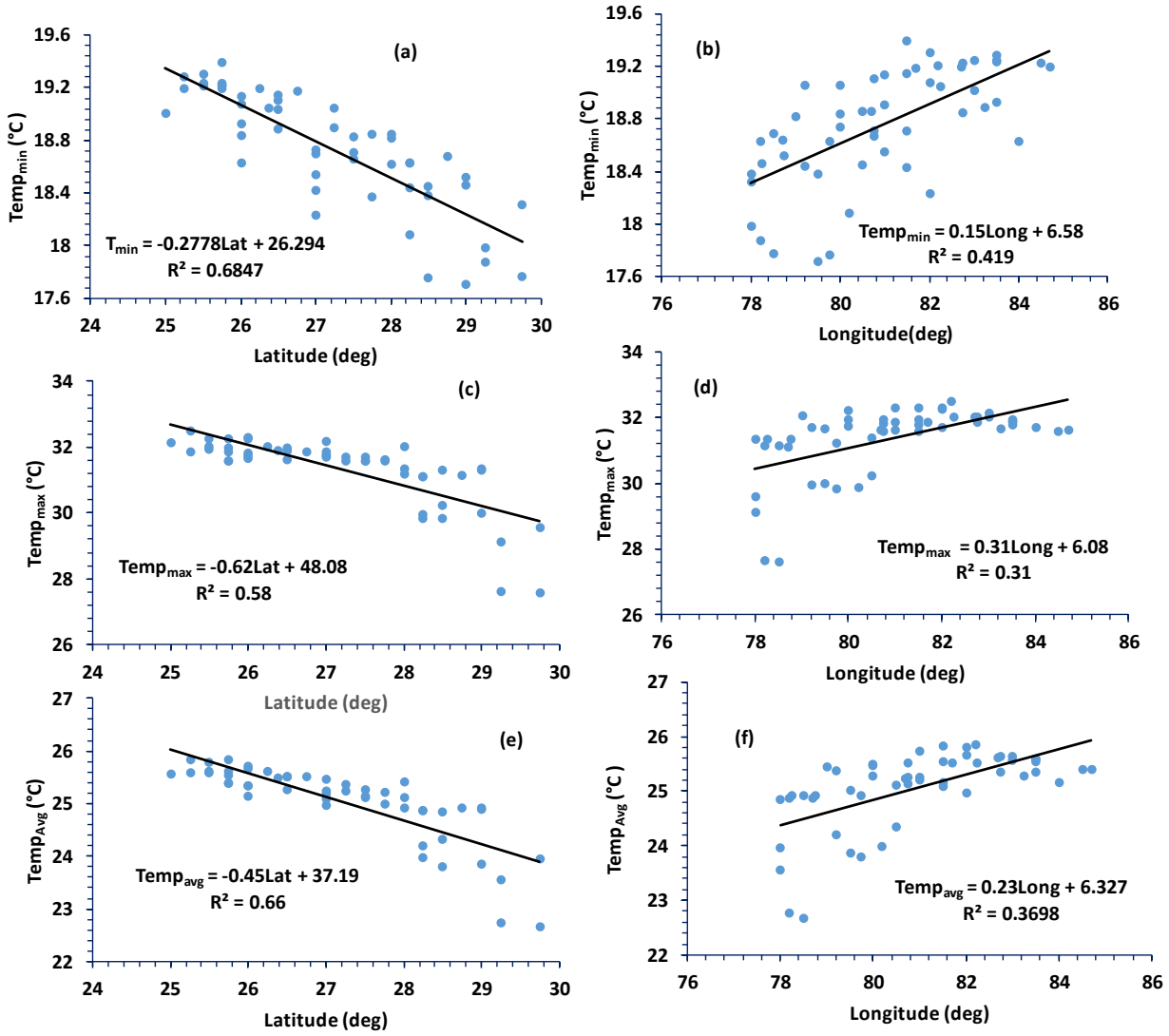

Fig 6.9: Geospatial temperature modeling. (a) & (b): Longitudinal and latitudinal dependency of T_{min}. (c) & (d): Longitudinal and latitudinal dependency of T_{max}. (e) & (f): Longitudinal and latitudinal dependency of T_{avg}

Table 6.2. Longitudinal and latitudinal temperature gradient

Temerature	Rate of rise (+)/fall(-) in temperature (in ^{0}C) per degree increase in the	
	Lattitude	Longitude
Night temperature (T_{min})	-0.28 ^{0}C/Lat	+0.15 ^{0}C/Long
Maximum Temperature	-0.62^{0}C/Lat	+0.31 ^{0}C/Long
Avg Temperature	-0.45^{0}C/Lat	+0.23 ^{0}C/Long

Fig. 20 shows the temporal variation of average annual night and day temperatures across the entire study area. Similar to the rainfall plot, it displays observed temperature values from 1991 to 2020 and forecasted values from 2021 to 2044 using the ARIMA model.

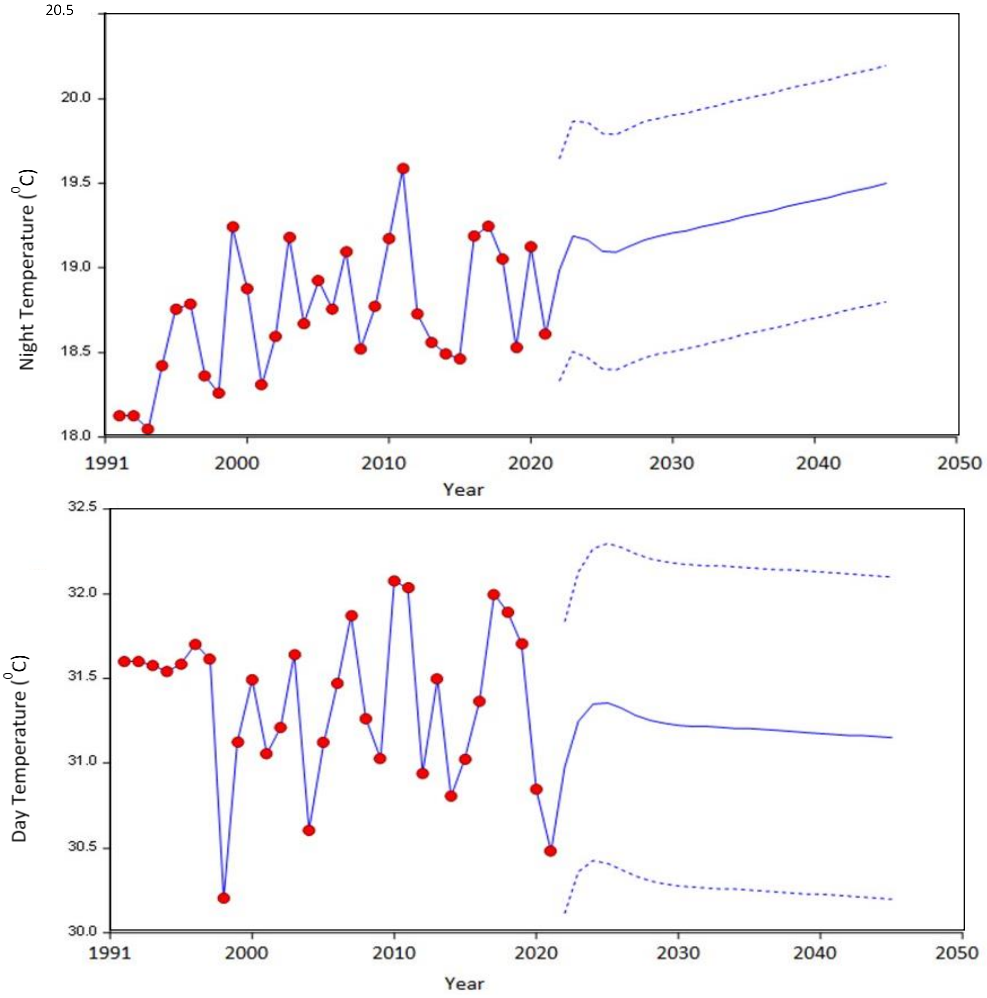

Fig. 6.10.: Time series trend and forecast of the night temperature (°C) and the day temperature (°C) of the entire study area using ARIMA model.

The upper and lower dashed lines represent the upper bound limit and the lower bound limit, respectively, providing a 95% confidence interval. The ARIMA model suggests a rapid increase in nighttime temperatures and a decrease in daytime temperatures throughout the study area. The upper and lower bound limits provide insights into the potential range of fluctuation around the mean night and day temperatures. Both observed and forecasted values of maximum (day) and minimum (night) temperatures exhibit considerable variability compared to the mean rainfall.

The detrend analysis of temperature time series shows maximum fluctuation in $Temp_{min}$ series in the years 1999, 2010, and 2011; $Temp_{max}$ series in the years 1997, 2003, 2009 and 2010; and $Temp_{Avg}$ series in the years 1999, and 2011.

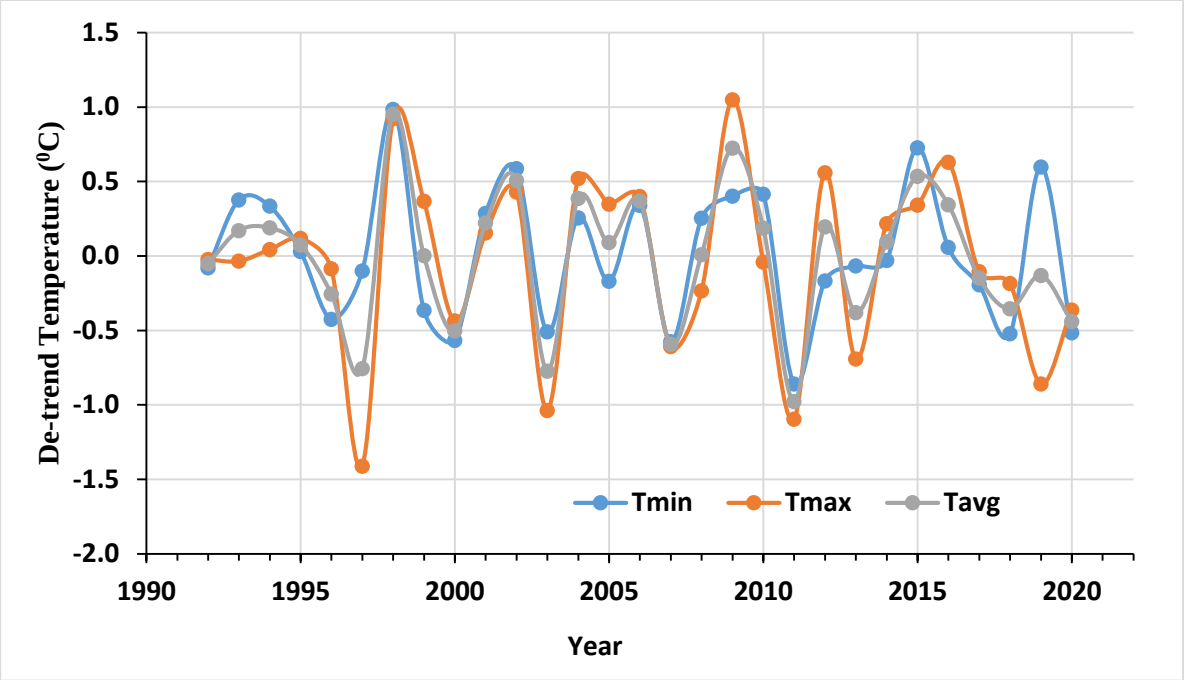

Fig. 6.11: The time series of the de - fluctuation of the temperature ($Temp_{min}$, $Temp_{max}$ and $Temp_{Avg}$)

6.2. Spatio-temporal analysis of Rainfall

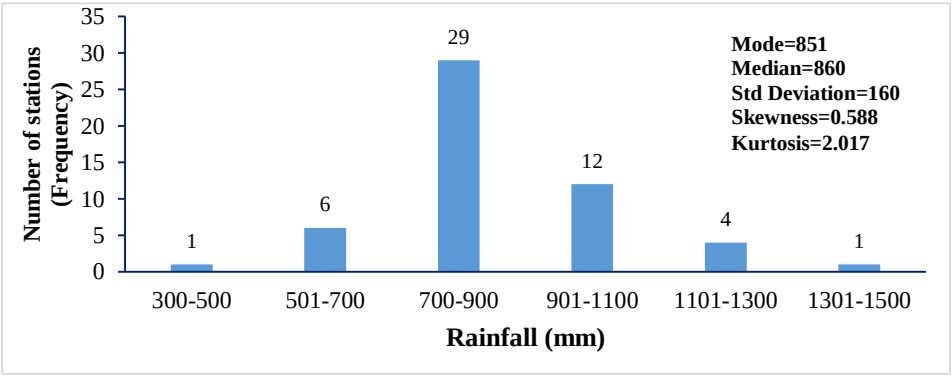

Fig 6.12: Histogram of rainfall of all 53 stations of the study area. The data for each location is represents mean annual rainfall over the period from 1991-2020

The spatial distribution map of the rainfall has been created using ArcGIS software by averaging the rainfall for the period 1991-2020 at all the gtid points in the study area. The data interpolation was done by the Inverse Distance Weighted (IDW) method. The average rainfall in the middle Ganga basin varies from 508 mm to 1325 mm with the average about 867mm which is 26.5% lower than the average rainfall in India (which is 1180 mm). The variation of the rainfall

is parallel to the Himalayan mountains. Rainfall decreases with an increase in the distance from the Himalayan mountains.

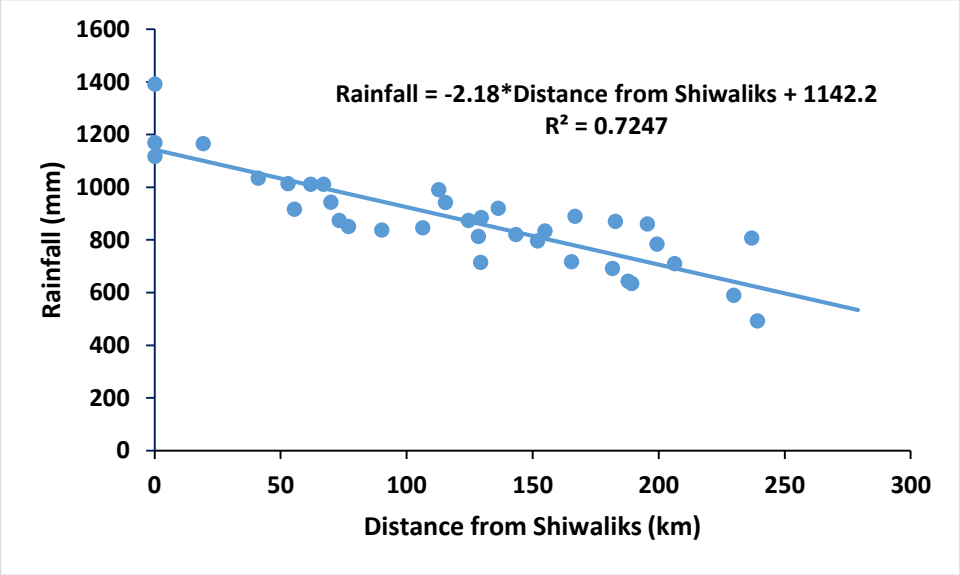

Fig. 6.13. Trend of rainfall with the distance away from the Siwalik foothills

The monthly average rainfall for 30 years from January to December shows a general form of increasing rainfall in the direction from west to east, and south to north (Fig XXX). The average annual rainfall of the study area is 868mm with the monthly distribution is: Jan: 15±6mm, Feb: 18±9mm, Mar: 10±5mm, Apr: 7±3mm, May: 21±9 mm, June: 111±30mm, July: 253±46mm, Aug: 240±47mm, Sept: 160±25mm, Oct: 25±8mm, Nov: 3±2mm, and Dec: 4±2mm. The average monsoon season (June to September) rainfall is 763 mm which is 88% of the average yearly rainfall.

The rainfall class interval 1209 mm to 1325 mm covers more area in the decade 2001 to 2010 in comparison to 1991 to 2000 interpretable from figure 9 (A) and figure 9 (B). All the rainfall classes 508 mm to 624 mm, 625 mm to 741 mm, 742 mm to 858 mm, 859 mm to 975 mm, 976 mm to 1092 mm, 1093 mm to 1208 mm, and 1209 mm to 1325 mm change their position and area on the map in the three decades.

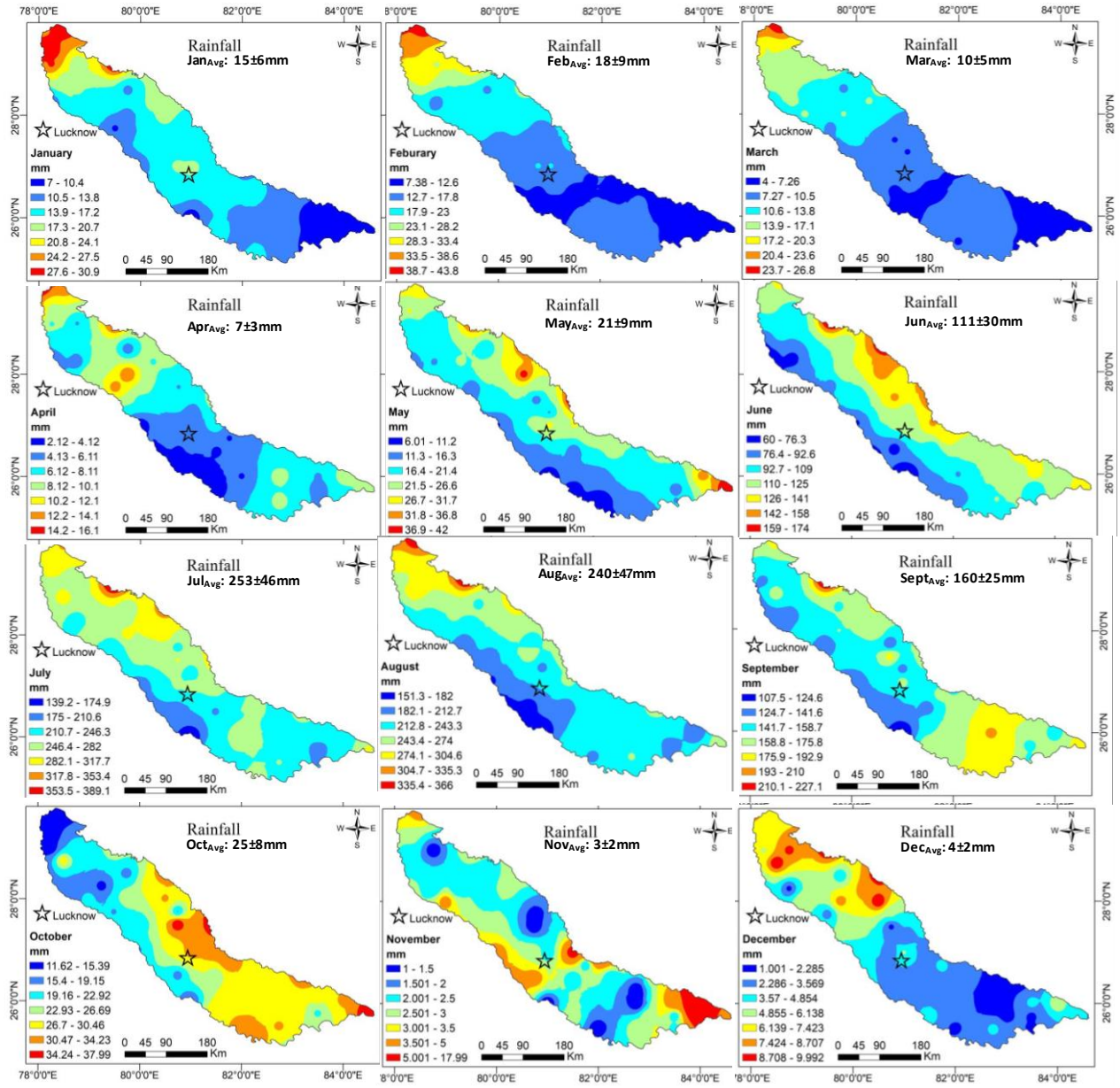

Fig 6.14: Thirty years (1991-2020) average monthly rainfall spatial distribution pattern in the study area

For the trend analysis of rainfall, the study area, on the basis of the spatial distribution pattern of rainfall, is divided into four zones: - Zone 1 (350mm-600mm), Zone 2(600mm-850mm), Zone 3 (850mm-1100mm) and Zone 4(1100mm-1350mm) as shown in figure 8. The rainfall in the four zones vary in the trend: Zone 1<Zone 2<Zone 3<Zone 4. The area covered in different zones are in the order of Zone 1<<Zone4<<Zone 2<Zone 4

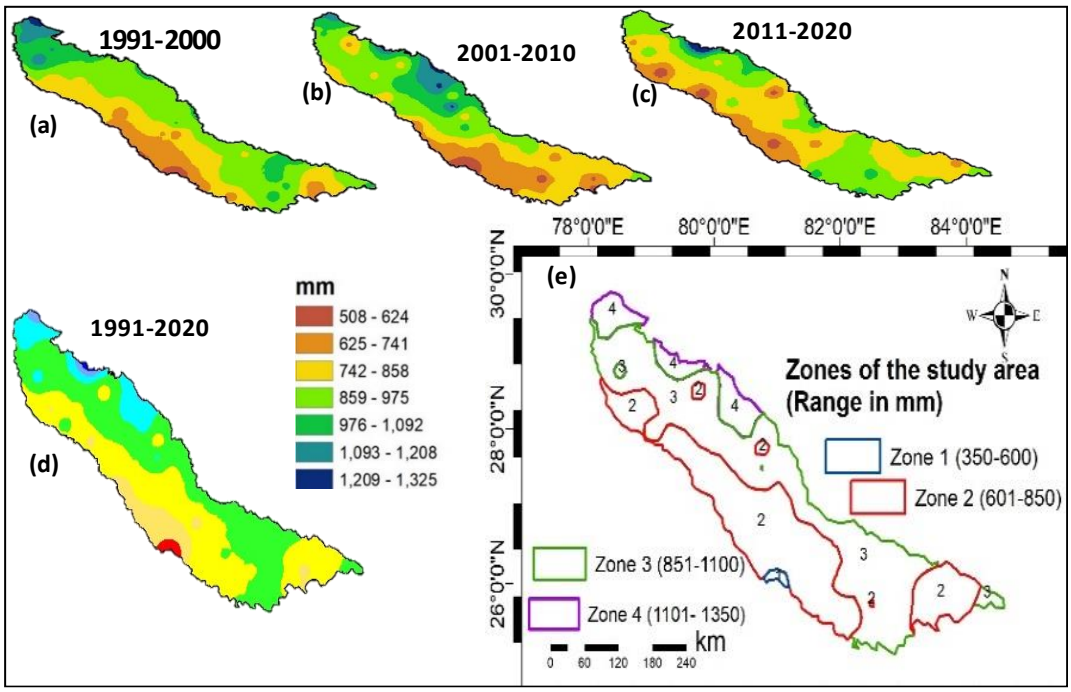

Fig.6.15.: The spatial distribution pattern of rainfall during the decades (a) 1991-2000, (b) 2001-2010, and (c) 2011-2020. The spatial map (C) shows three-decade average rainfall distribution pattern. The spatial map (e) shows the rainfall sub-division units 1,2,3 and 4.

Table 6.3: Rainfall zones, ranfall range and the zone area

Zone	Rainfall range	Area (km^2)
Zone 1	350 mm – 600 mm	527.47
Zone 2	600 mm – 850 mm	38292.73
Zone 3	850 mm – 1100 mm	44258.97
Zone 4	1100 mm – 1350 mm	8661.52

The groundwater levels in these zones were analyzed for the period from 1999-2017. No fall in groundwater level is observed in Zone 1. In the remaining zones, groundwater exhibited a falling trend at the rate of 10 cm/year (as observed from Sen's slope). It may be noted that the Zones 2, 3, & 4 constitute more than 97% of the study area. This means, in 97% of the study area, groundwater has depleted by a meter in a decade**.**

Using the rainfall data for the period from 1991 to 2020; the average annual rainfall for Zones 1 to 4 is estimated; and is observed to be Zone 1:475mm, Zone 2:725mm, Zone 3: 975mm, and Zone 4: 1225mm. The rainfall data showed a decreasing trend (as per Sen's slope) in Zone 1

and Zone 3 at the rate of 2.1 mm/year and 0.5 mm/year respectively. In Zone 2, the rainfall exhibited an increasing trend (as per Sen's slope) at the rate of 0.5 mm/year. In Zone 4, Sen's slope indicated an increasing trend in rainfall (at the rate 0.4 mm/year) whereas, the linear regression showed a decreasing trend (R^2 = 0.0001). The forecasted values of climate variables showed an increase in average night temperature and a decrease in the average rainfall. The details of Sen's slope and regression analysis is shown in the figure 5.54.

Due to an increasing trend in the value of the night temperature, the average temperature of the day is on an increasing. The increased temperature can cause a significant increase in the water demand and the rate of evapotranspiration of the green vegetation. The significant rise in temperature can be the result of increase in greenhouse gases, vehicular emissions and industries. The climate variables significantly affect the groundwater hydrology of the middle Ganga basin.

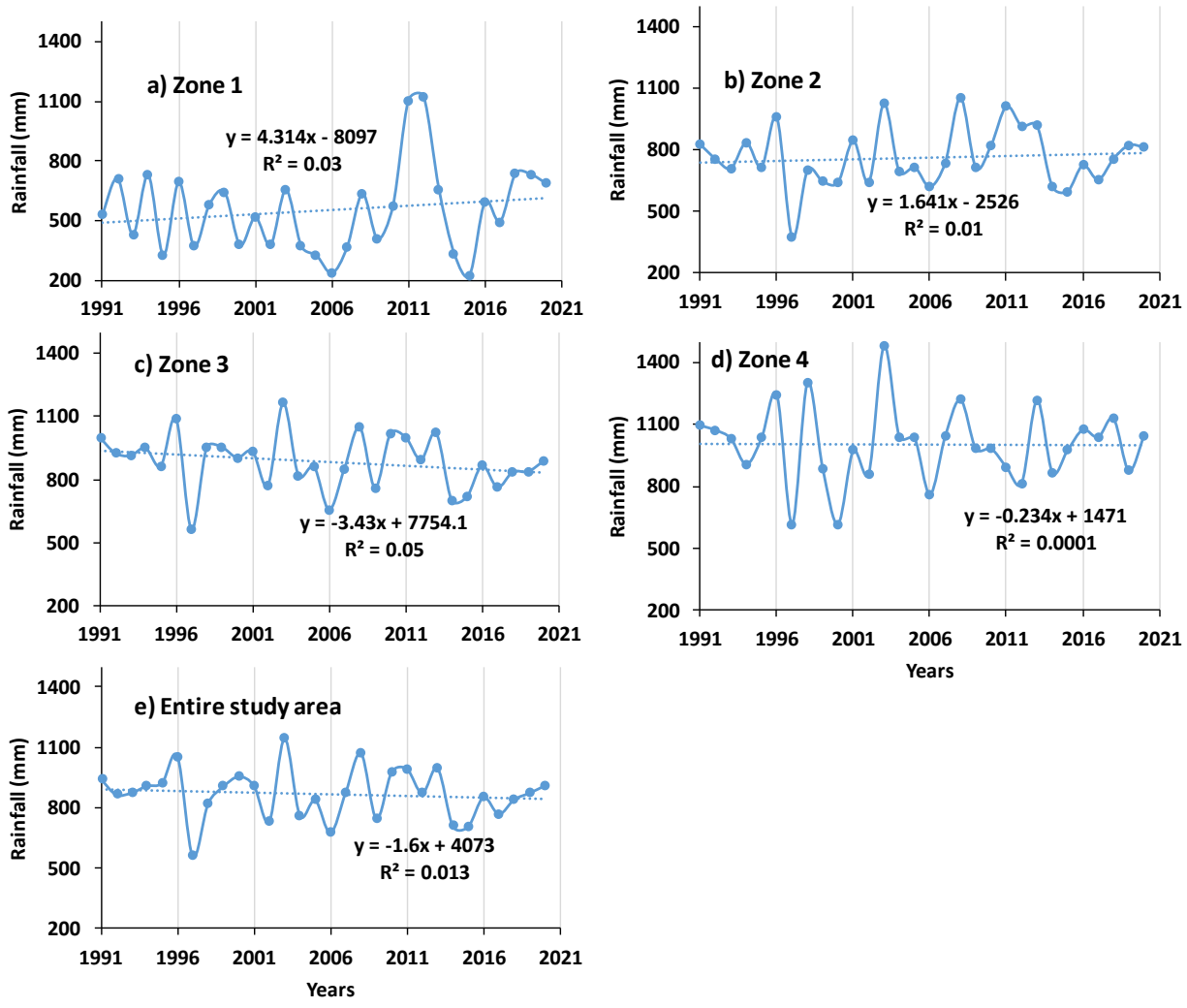

Fig. 6.16: Rainfall trend in the four zones and for the entire study area

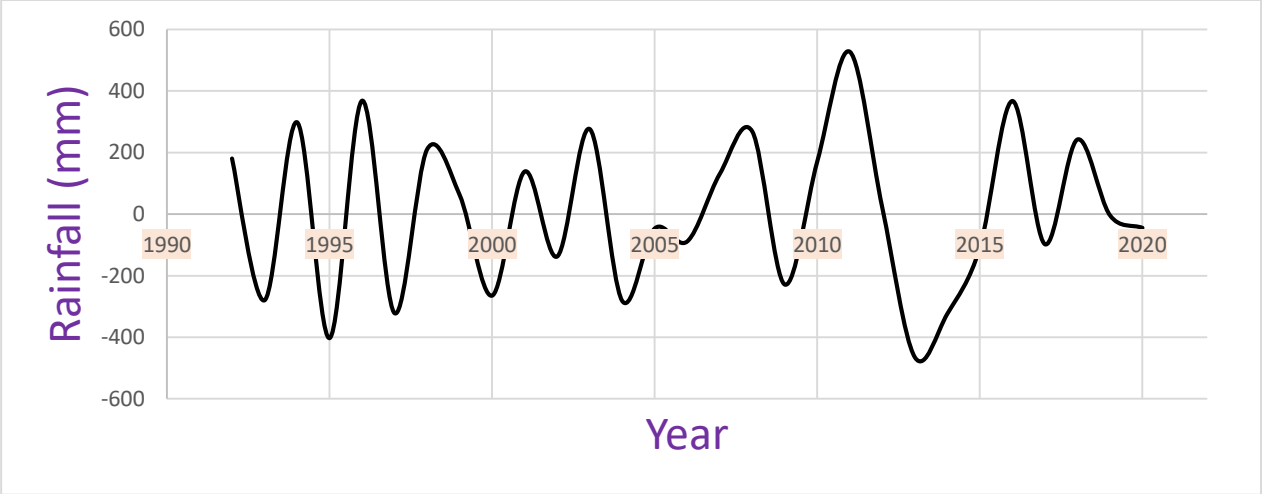

Fig. 6.17. Rainfall variation averaged over the entire study area for the period from 1993-2020

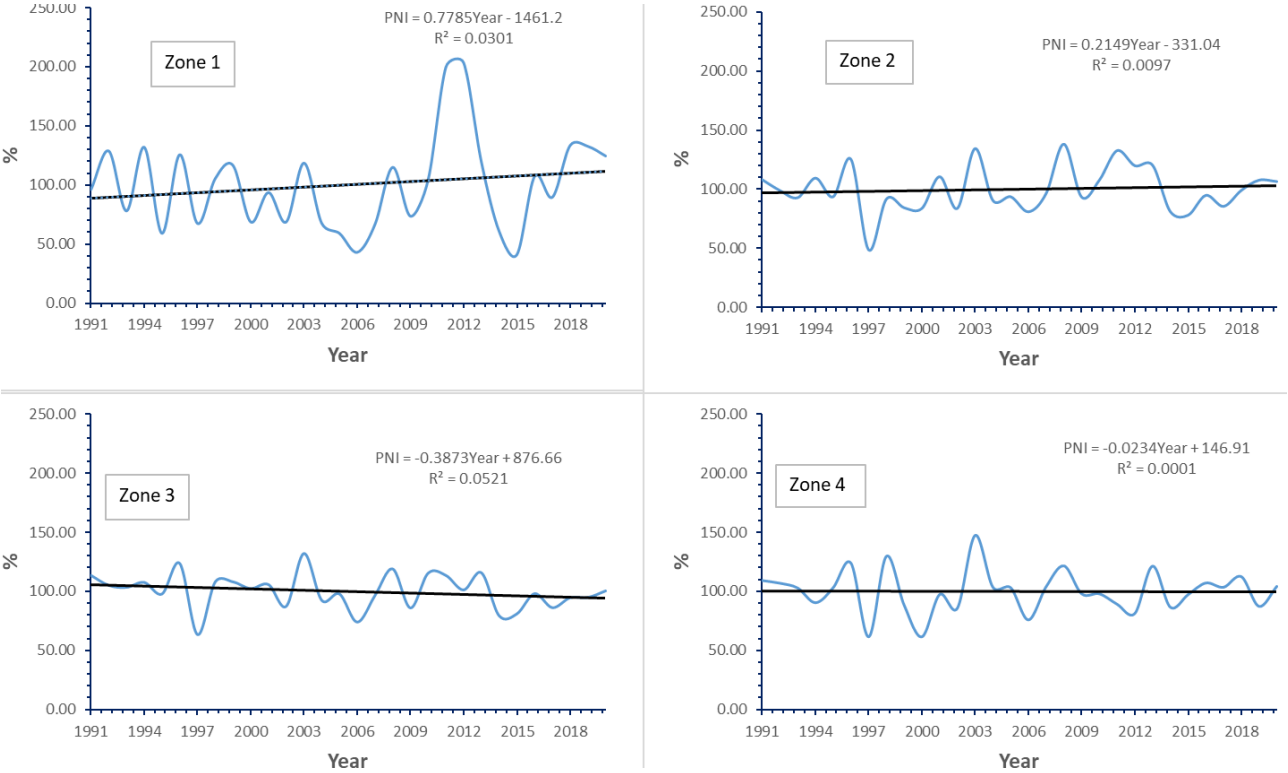

Fig. 6.18: The percent of normal index (PNI) of zone 1, zone 2, zone 3, and zone 4 of the study area is shown.

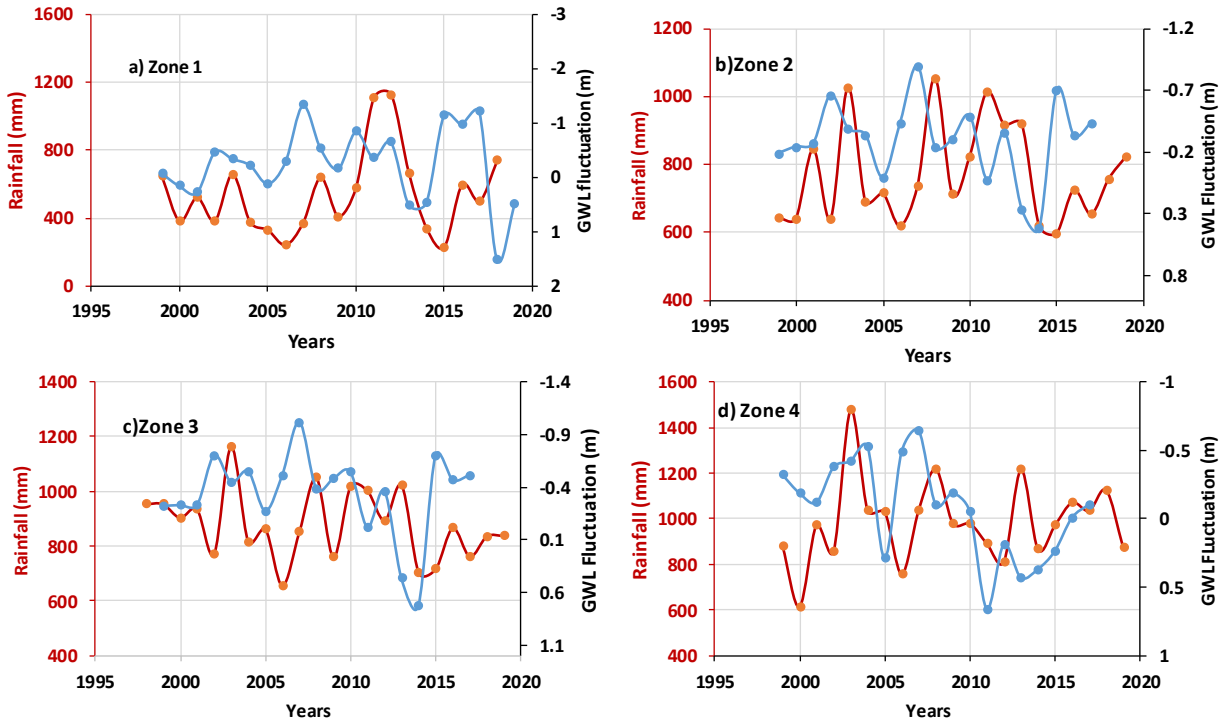

Fig 6.19: Relation between rainfall and groundwater level fluctuation. (GWL fluctuation = (Post-pre)$_{monsoon}$). Fluctuation –ve indicates rising and +ve as falling water table.

Table 6.4: The Mann-Kendall trend test with Sens' slope estimator results for the average rainfall

Zone	S	kendall's tau	sens's slope	P-value	Var(S)	Standard deviation
1	31.0	0.071	-2.1	0.592	3139.67	218.85
2	14.0	0.032	0.50	0.817	138.67	146.9
3	-86.0	-0.198	-0.50	0.129	3138.67	-4.31
4	-7.0	-0.016	0.40	0.915	3137.67	185.42

Rainfall spatial distribution with time

The variation in the climate variable of rainfall can be seen both in space and time. With passing years, the amount of rainfall changes at a particular location. The rainfall amount may increase or decrease at a station. This changes the entire pattern of rainfall in the study area. The rainfall data from 1991 to 2020 has been used to create thematic maps of rainfall 1991 to 2000, 2001 to 2010, and 2011 to 2020. The rainfall quantity can be seen to vary in the three decades at most of the places within the confined region.

As it can be seen in the figure 5.10, the rainfall amount has changed in the last three decades. But the overall pattern remains the same: the rainfall increases from south–west to north–east. The pattern is expected to modify further in the upcoming years. The temporal change in the rainfall can be attributed to the factors like anthropogenic activities. The climate change can affect the

rainfall pattern. It has been observed that the number of dry years in the decade 2011-2020 has increased in comparison to the decade 2001 – 2010. The rainfall extremes are more frequent in the recent years. Either it is flood or drought each year. Very few years witness normal rainfall. Both kinds of rainfall are detrimental to crops and can cause disasters.

Zone1-2 = {(2-1)x100}/1

In the study area, the minimum temperature varies from 17.76°C to 19.38°C from north to south. This makes sense because at higher temperatures, more molecules are moving faster; therefore, it is more likely for a molecule to have enough energy to break away from the liquid to become a gas.

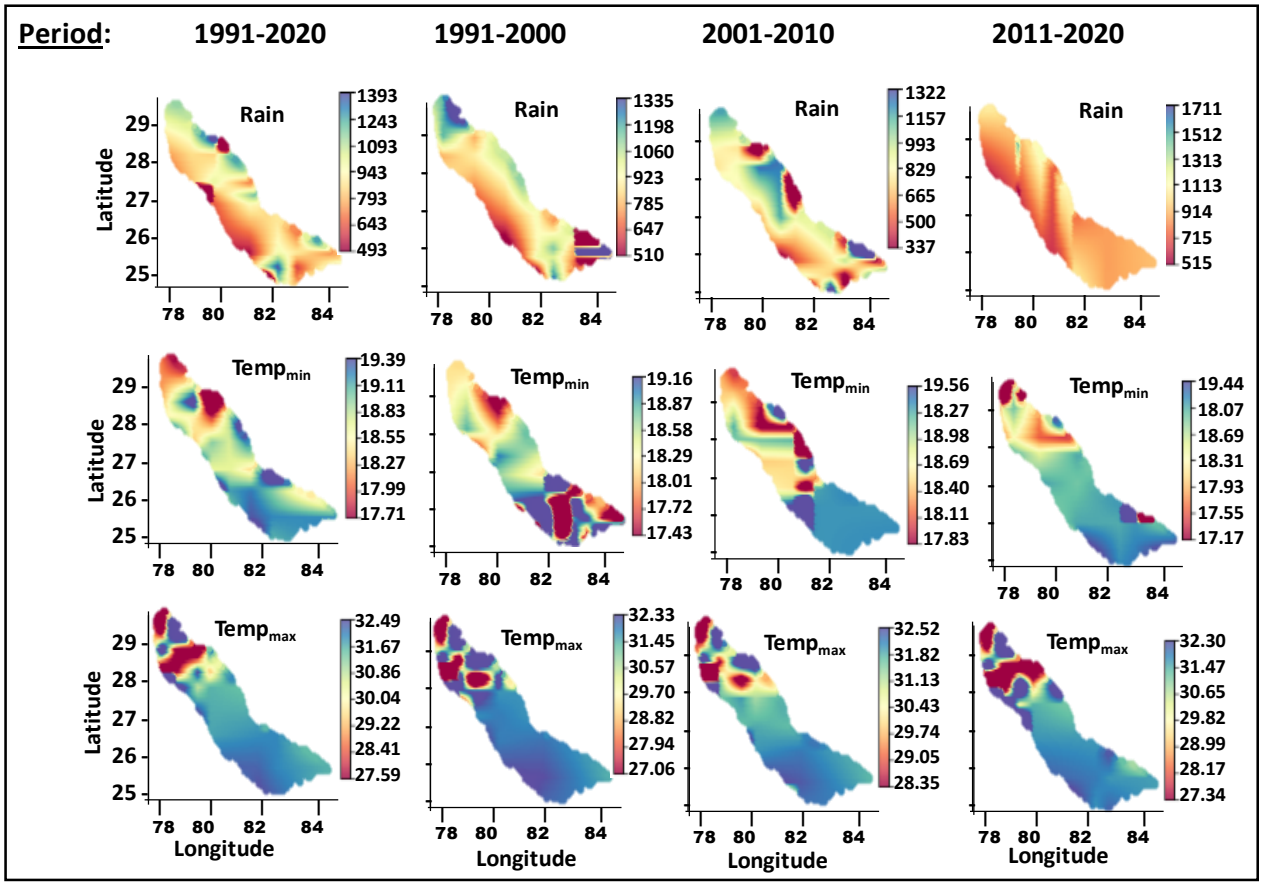

Fig. 6.20. Long-term averaged, temporal and spatial variation of climate parameters. Climate parameters; Rainfall is shown in the top row, $Temp_{min}$ is shown in the middle row, and $Temp_{max}$ is shown in the bottom row. The temporal average is taken over four periods as: (i) 1991-2020, (ii) 1991-2000 (iii) 2001-2010, and (iv) 2011-2020.

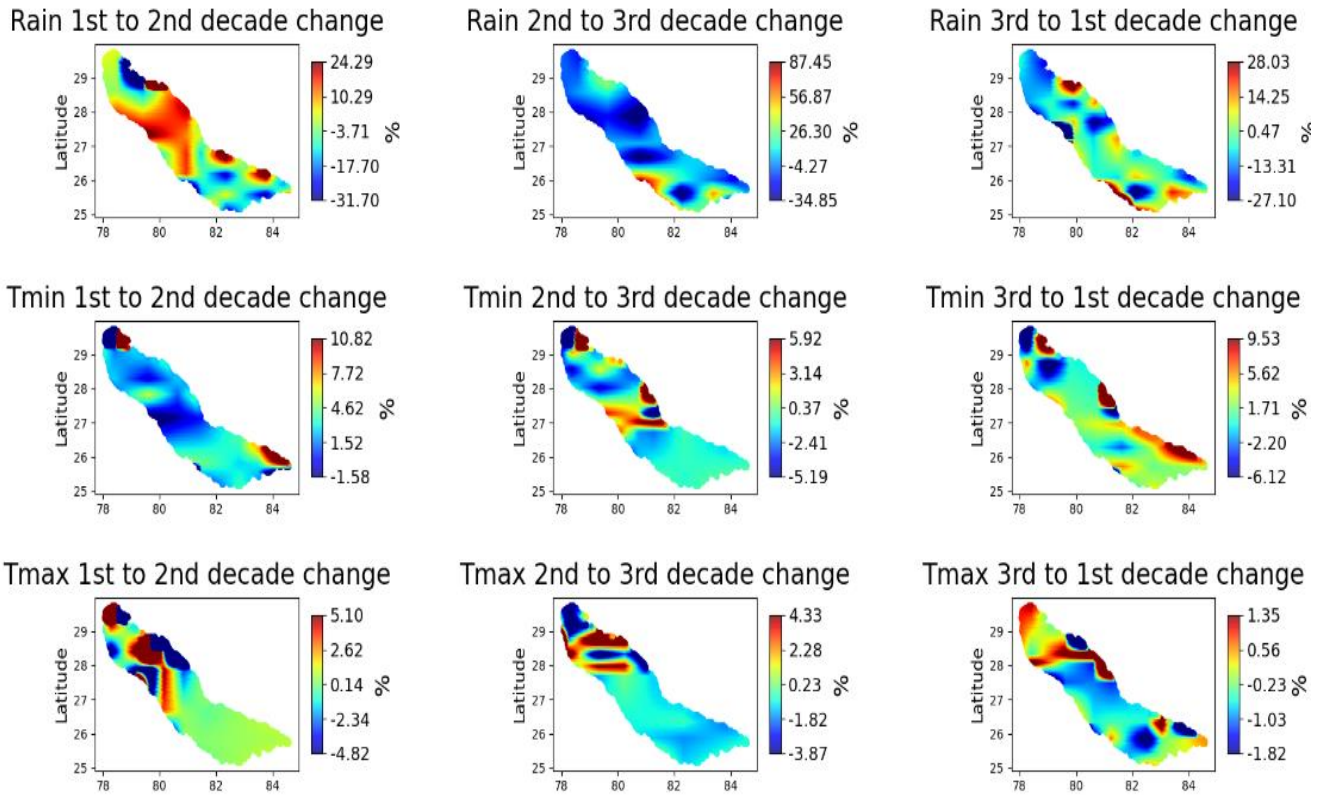

Fig.6.21: Percentage change in rainfall, Tmin, and Tmax from 1st decade (1991-2000) to 2nd decade (2001-2010), and 2nd decade (2001-2010) to 3rd decade (2011-2020), and 3rd decade (2011-2020) to 1st decade (1991-2000).

6.3 Trends in Rainfall

The Mann-Kendall (MK) test was conducted on rainfall data from 1991 to 2020 for all the 53 stations in the study area. The MK test result, the calculated s-value and z-statistic results are presented in Table XXX. The results indicated increasing rainfall trend in 34 locations, and decreasing rainfall trend in 19 locations of the study area. Negative s-values indicating decreasing rainfall trend is observed at 5 locations, no change in the rainfall trend (s=0) in 14 locations, marginal increasing rainfall trend (s=+2) at 19 locations, moderately increasing rainfall trend (s=+4) at 14 locations, and high increasing trend (s=+6) at one location. The Sen's slope of the 20 positive trend stations varies from 0.079 mm/year to 29.74 mm/year; and 33 stations exhibiting a negative trend from -18.74 mm/year to -0.014 mm/year.

The calculated z-statistic confirmed a decreasing trend in rainfall at 19 stations, and increasing trend at 34 stations. Conversely, 34 stations showed an increasing trend, with Sen's slopes ranging from 0.079 mm/year to 29.74 mm/year. Notably, the stations with positive or

negative trends were located at elevations above 100 m, while stations below 100 m exhibited no significant rainfall trend. The stations with no rainfall trend are located below 100 m msl.

Table 6.4: Mann-Kendall trend test and Sen's slope for the annual rainfall. This table interprets the rainfall trend in the study area.

S. No.	Latitude	Longitude	Sens' slope	S-value	Z-Statistic	Trend
1	25.00	83.00	3.45	0	-0.02	Decreasing
2	25.25	82.25	8.86	4	0.05	Increasing
3	25.25	83.50	-4.02	0	-0.02	Decreasing
4	25.50	82.00	5.36	2	0.02	Increasing
5	25.50	82.75	-9.21	2	0.02	Increasing
6	25.5	83.5	14.12	2	0.02	Increasing
7	25.75	81.50	15.22	4	0.05	Increasing
8	25.75	83.00	-8.30	-2	-0.02	Decreasing
9	25.75	83.50	8.63	-2	-0.02	Decreasing
10	25.75	84.50	-2.85	0	-0.02	Decreasing
11	25.75	84.75	8.62	0	-0.02	Decreasing
12	26.00	81.00	-0.01	4	0.05	Increasing
13	26.00	82.00	-1.02	2	0.02	Increasing
14	26.00	82.75	-12.86	0	-0.02	Decreasing
15	26.00	83.50	-1.24	0	-0.02	Decreasing
16	26.00	84.00	-9.74	0	-0.02	Decreasing
17	26.25	82.75	-13.40	2	0.02	Increasing
18	26.38	80.25	5.15	4	0.05	Increasing
19	26.50	80.75	-5.36	4	0.05	Increasing
20	26.50	81.50	-5.78	0	-0.02	Decreasing
21	26.50	82.25	-3.47	2	0.02	Increasing
22	26.50	83.25	-9.05	2	0.02	Increasing
23	26.75	81.75	-2.52	4	0.05	Increasing
24	27.00	80.00	-3.48	2	0.02	Increasing
25	27.00	80.75	3.30	4	0.05	Increasing
26	27.00	81.00	12.01	4	0.05	Increasing
27	27.00	81.50	3.79	2	0.02	Increasing
28	27.00	82.00	-0.77	0	-0.02	Decreasing
29	27.25	79.25	-10.01	0	-0.02	Decreasing
30	27.25	81.00	-4.19	0	-0.02	Decreasing
31	27.50	80.00	12.39	0	-0.02	Decreasing
32	27.50	80.75	-4.56	6	0.09	Increasing
33	27.50	81.50	3.97	2	0.02	Increasing
34	27.75	79.50	-7.87	4	0.05	Increasing
35	27.75	80.75	-18.74	-2	-0.02	Decreasing
36	28.00	79.00	0.08	4	0.05	Increasing

37	28.00	79.75	-1.75	4	0.05	Increasing
38	28.00	80.50	2.90	2	0.02	Increasing
39	28.25	78.25	-8.31	2	0.02	Increasing
40	28.25	78.75	-13.10	2	0.02	Increasing
41	28.25	79.25	1.94	2	0.02	Increasing
42	28.25	80.25	3.24	0	-0.02	Decreasing
43	28.50	78.00	-8.54	0	-0.02	Decreasing
44	28.50	79.75	-3.53	2	0.02	Increasing
45	28.50	80.50	7.34	2	0.02	Increasing
46	28.75	78.50	-8.15	2	0.02	Increasing
47	29.00	78.25	-15.39	4	0.05	Increasing
48	29.00	78.75	-13.07	2	0.02	Increasing
49	29.00	79.50	29.74	2	0.02	Increasing
50	29.25	78.00	3.20	4	0.05	Increasing
51	29.25	78.25	-5.78	-2	-0.02	Decreasing
52	29.75	78.00	-0.11	4	0.05	Increasing
53	29.75	78.50	-16.64	-2	-0.02	Decreasing

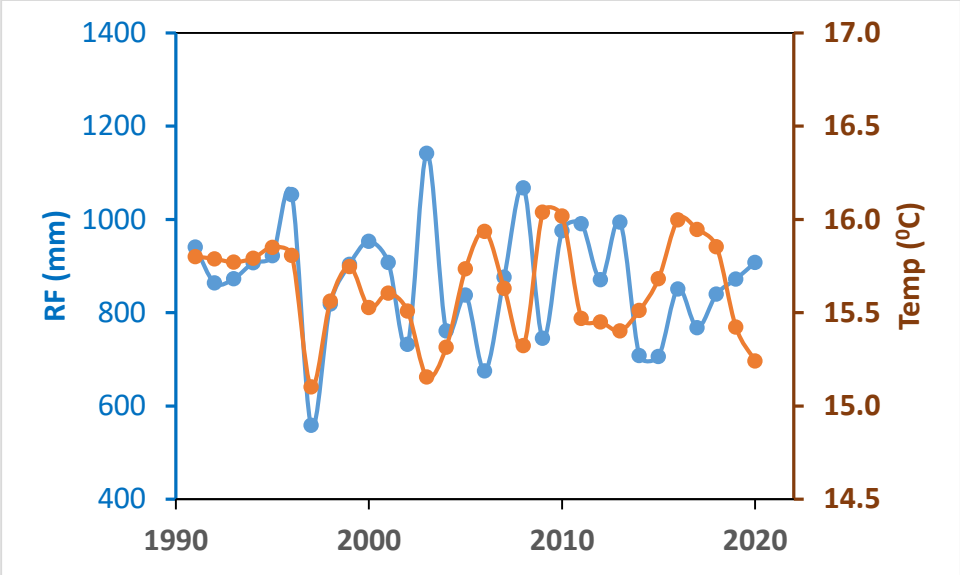

Fig.6.22: Interrelation rainfall and the average temperature pattern

In 80% of the data points, rainfall show a positive correlation with the regional temperature. Remaining 20% that show a negative correlation probably indicate subcontinental or non-regional control on meterological parameters.

The temporal variation of average rainfall across the entire study area is shown in Fig. 18. The plot includes observed rainfall values from 1991 to 2020 as well as forecasted values from 2021 to 2044 using the ARIMA model. The upper and lower dashed lines represent the upper bound limit and the lower bound limit, respectively, providing a 95% confidence interval.

The ARIMA model suggests a slight decrease in rainfall quantity, followed by relatively stable values (the mean line). However, the upper and lower bound limits indicate the potential range of fluctuation around the mean rainfall, spanning approximately 1150 mm and 600 mm, respectively. Both observed and forecasted rainfall values exhibit considerable variability compared to the mean. Additionally, the partial autocorrelation function, shown in Figure 19, indicates that most residual values are close to zero.

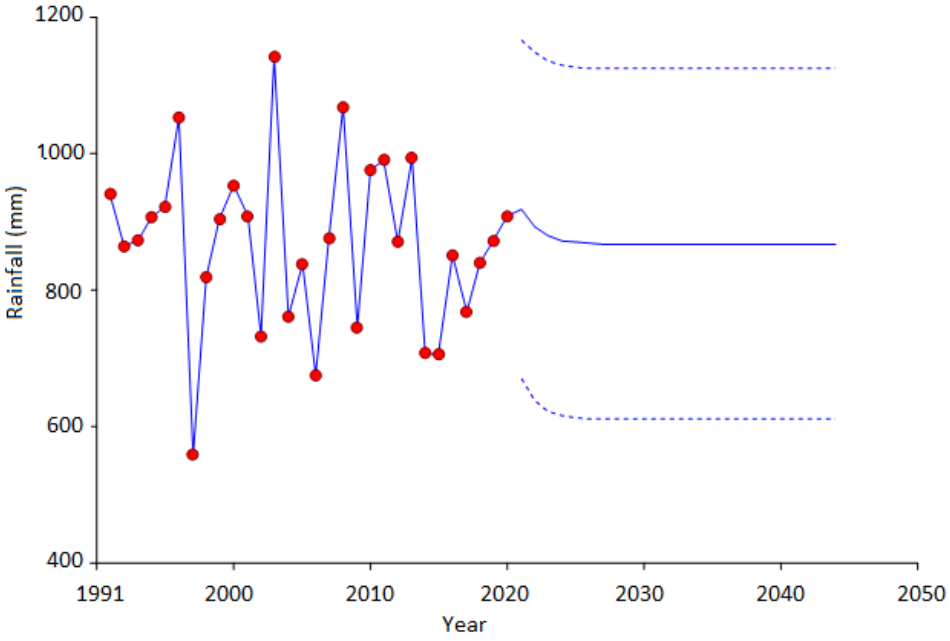

Fig.6.23: Time series trend and forecast of the average rainfall of the entire study area using the ARIMA model.

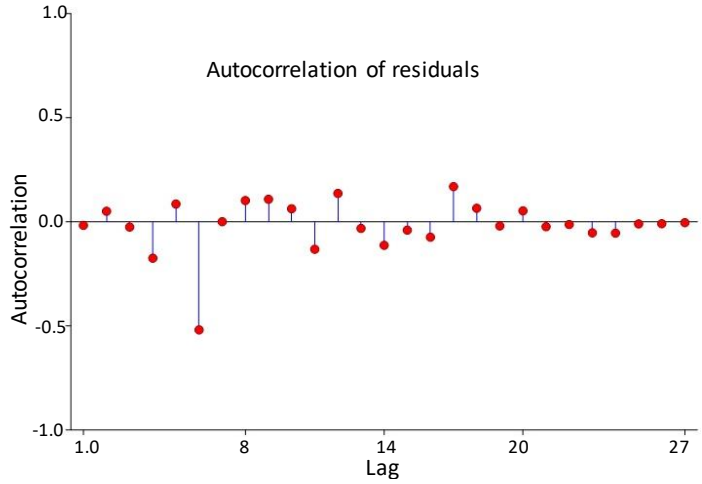

Fig.6.24: The auto-correlation function plotted for rainfall.

Figure XXX depicts the spatial pattern of Mann-Kendall trend test and Sen's slope estimator analysis conducted on rainfall, minimum temperature (T_{min}), and maximum temperature (T_{max}) data from 1991 to 2020. For rainfall, the figure displays the Mann-Kendall Z-statistic, which identifies trends, ranging from -3.8 to 4.12, and Sen's slope estimator, quantifying trend

magnitude, ranging from -10.71 to 16.96 mm/year. The Tau-value indicates trend strength and direction (ranging from -0.5 to 0.54), while the p-value assesses trend significance (ranging from 0 to 0.97). Similarly, for T_{min}, Z-statistic values range from -1.53 to 3.28, Sen's slope values from -0.05 to 0.07 degrees Celsius/year, Tau-values from -0.2 to 0.43, and p-values from 0 to 0.89. For T_{max}, Z-statistic values range from -1.52 to 0.21, Sen's slope values from -0.1 to 0.01 degrees Celsius/year, Tau-values from -0.19 to 0.03, and p-values from 0.13 to 1.0.

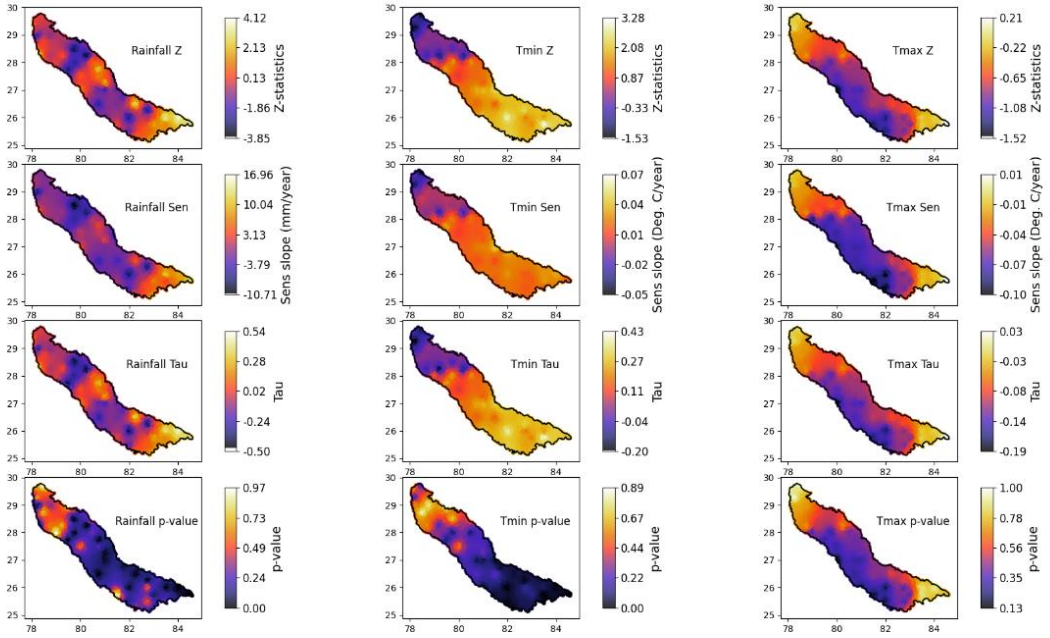

Fig. 6.25: Mann-Kendall Z-statistic and Sen's slope for rainfall, T_{min} and T_{max} for the time period 1991 to 2020.

6.4. DROUGHT INDEX

The following drought indices have been used in the present study:

1. Percent of Normal Index (PNI)
2. Standardized Precipitation Index (SPI):
3. The Rainfall Anomaly Index (RAI):
4. Percentage Departure (D%) from the long term normal (IMD)

Claculation for these indices and the value range of indices for drought/wet classification is briefly given below

$$\text{Percent of Normal Index (PNI)} = \frac{Pi}{P} \times 100$$

Pi = total of precipitation in each year; P = average of precipitation in the period

Table 6.5: Categorizing intensity of drought using Percent Normal Index (PNI)

PNI Classification		
Class	PNI Value	Drought Category
1	>120	Wet
2	80-120	Normal
3	70-80	Slightly Dry
4	55-70	Moderately Dry
5	40-55	Severe Dry
6	<40	Very Severe Dry

Standardized Precipitation Index (SPI):

SPI=(x-μ)/s

Where, x is the observed precipitation data from a long-term record; μ is the average or mean across all observations; s is the standard deviation over the period of observation

Table 6.6: Classification of drought and wet periods using Standardized Precipitation Index (SPI)

SPI values	**Rainfall regime**	**SPI values**	**Rainfall regime**
≥2.00	Extremely wet	−1.00 to −1.49	Moderately dry
1.50–1.99	Very wet	−1.50 to −1.99	Severely dry
1.00–1.49	Moderately wet	≤−2.00	Extremely dry
−0.99 to 0.99	Near Normal		

The Rainfall Anomaly Index (RAI):

$$RAI = 3 \times \frac{p - p_{med}}{p_{max} - p_{med}} \quad \text{For positive anomalies} \quad \text{---------(1)}$$

$$RAI = -3 \times \frac{p - p_{med}}{p_{min} - p_{med}} \quad \text{For negative anomalies} \quad \text{----------(2)}$$

Where,
P = current annual precipitation (mm); P_{med} = mean annual rainfall of the historical series (mm); P_{max} = mean of the ten largest annual precipitations of the historical series (mm) and P_{min} = mean of the ten lowest annual precipitations of the historical series (mm).

Table 6.7.: Classification of draught/precipitation severity using RAI

RAI Range	Classification
> 4	Extremely humid
2 to 4	Very humid
0 to 2	Humid
-2 to 0	Dry
-4 to -2	Very Dry
<-4	Extremely dry

Percentage Departure (D%) from the long term normal (IMD):

$$D\% = \frac{X_i - X_m}{X_m} \times 100$$

Where, X_m is the long-term mean annual rainfall and X_i is the annual rainfall

Table 6.8: Rainfall classification using %Departure from the long-term normal

Rainfall Category	**% Departure**
Large Excess Rainfall	+60%
Excess Rainfall	+20% to +59%
Normal Rainfall	+19% to -19%
Deficit Rainfall	-20% to -59%
Large Deficient (or Scanty) Rainfall	-60% to -99%
No Rain	-100%

Results

6.4.1 Percent of Normal Index (PNI)

The PNI is calculated for the study area by integrating annual rainfall data for all the sites for each year for the data period from 1991 to 2020. The Percent of Normal Index, table for the categorized precipitation years (Wet, Normal, Slightly Dry, and Moderately Dry yeears) and the plot showing rainfall trend for the Middle Ganga basin is shown below.

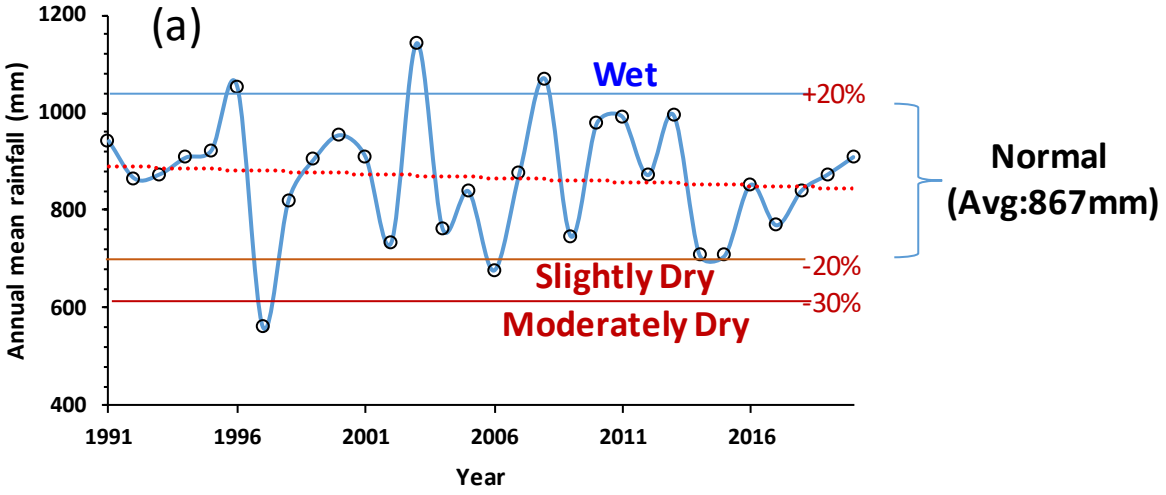

(b)

PNI Classification		
Class	Percent of Normal Index (PNI)	Category
1	>120%	Wet
2	80-120 %	Normal
3	70-80 %	Slightly Dry
4	55-70 %	Moderately Dry
5	40-55%	Severe Dry
6	<40%	Vere severe

Fig 6.26: Characterizing meterological drought using Percent of Normal Index (PNI). (a) Each point in the plot indicates PNI averaged for all the all the grid points of the rainfall locations. The data points in the PNI plot are categorized into four classes (1-4) based on the class details as shown in the adjoining table (b). The dotted red line marks the average decreasing rainfall trend. The linear trend line of decreasing average rainfall shows that overall, the annual mean rainfall in the study area is decreasing at a rate of 1.6 mm per year.

In the case of the indices SPI, RAI and %D, number of extreme wet and dry years falling in the rainfall time series (1991-2020) at each of the grid-points in the study area were calculated for the respective indices. A spatial distribution maps depicting number of observed extreme dry and wet years were prepared for each of these indices and were compared (Fig.). For illustration purposes, plots of extreme rainfall years at a few locations are also shown and compared for each of the indices (SPI, RAI and %D).

6.4.2 SPI Index:

In the case of SPI, the spatial distribution maps of points where each point indicates the number of years a location experienced severe to extreme wet or dry years (SPI>1.5; SPI <-1.5) is plotted (Fig XXX). Beside to the spatial distribution plot, for illustration purposes, for three locations (location number 21, 41, 42) SPI time series are shown. The location number 41 experienced four very wet rainfall years (SPI>1.5) during 1991-2000 that were occurred during the years 2000, 2003, 2010, and 2011. Location number 44 received two very wet rainfalls (SPI>1.5) during the years 2003 and 2011, and three very dry-spell years during 1997, 2006, and 2014. Location number 21 received four extreme dry spells during the years 1998, 1999, 2006, and 2015. Spatial distribution map shows large part of the study area covered by both severe to extreme wet years, and also by severe dry to extremely dry years. It means, large part of the area experienced and susceptible to extreme rainfall years (wet or dry).

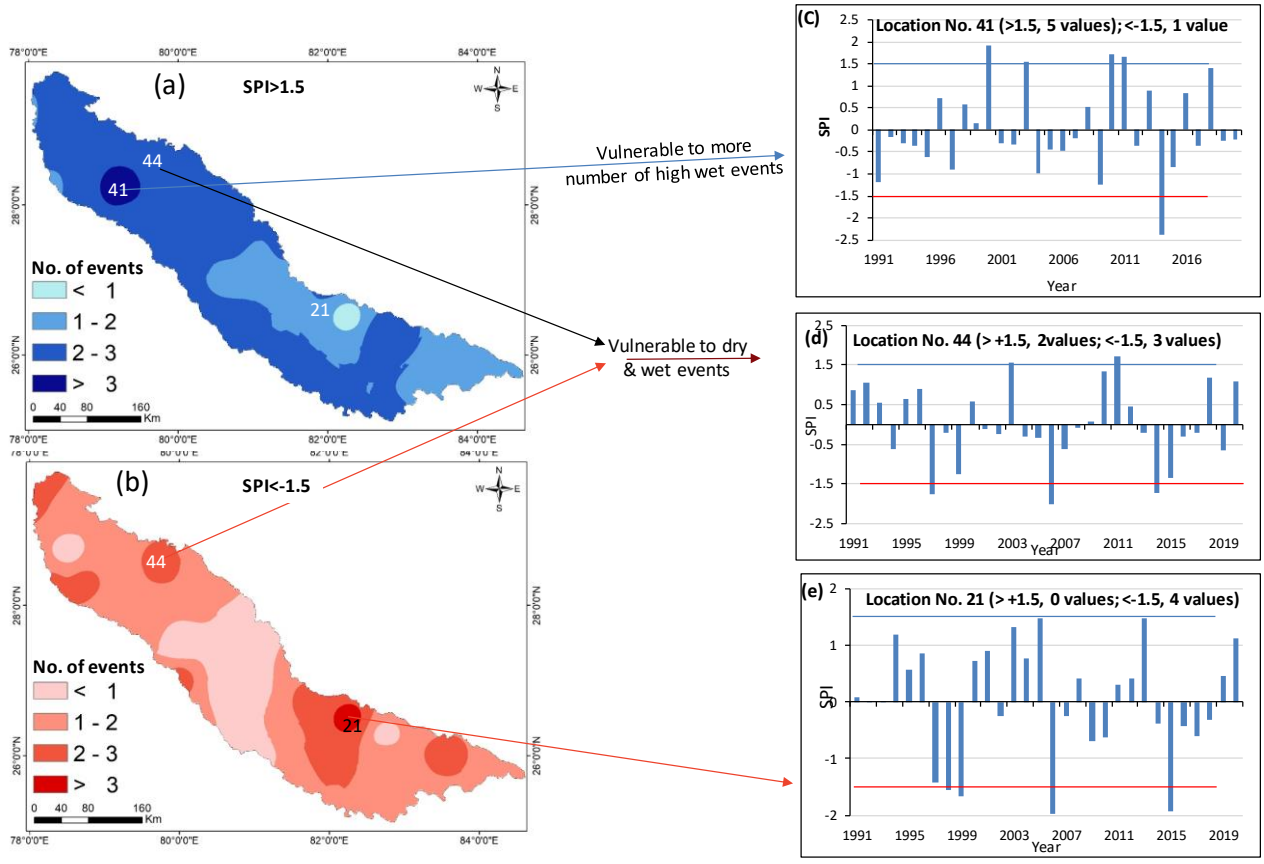

Fig 6.27. Spatial distribution map and plots of Standardized Precipitation Index (SPI) for the period averaged over 1992-2020, and the SPI time series. (a) Spatial maps of area showing severe to extreme wet years (i.e., SPI>1.5); (b) Spatial map of area feature that experienced severe dry to extremely dry years (i.e., SPI <-1.5). (c), (d), and (e) are the bar diagrams of SPI plotted for the locations 41, 44 and 21. Within the plot a red line and a blue line is given to identify points that crosses the limit of SPI>1.5 and SPI<-1.5

6.4.3 Rainfall Anomaly Index (RAI)

Similar to the SPI, for the Rainfall Anomaly Index (RAI), spatial distribution plot of RAI for very wet to extremely wet climate (RAI>3) and severely dry to extremely dry rainfall years (RAI <-3) is plotted (Fig XXX). Beside to this figure, the corresponding bar diagrams illustrating RAI time series is also plotted for the location numbers 5, 7 and 9.

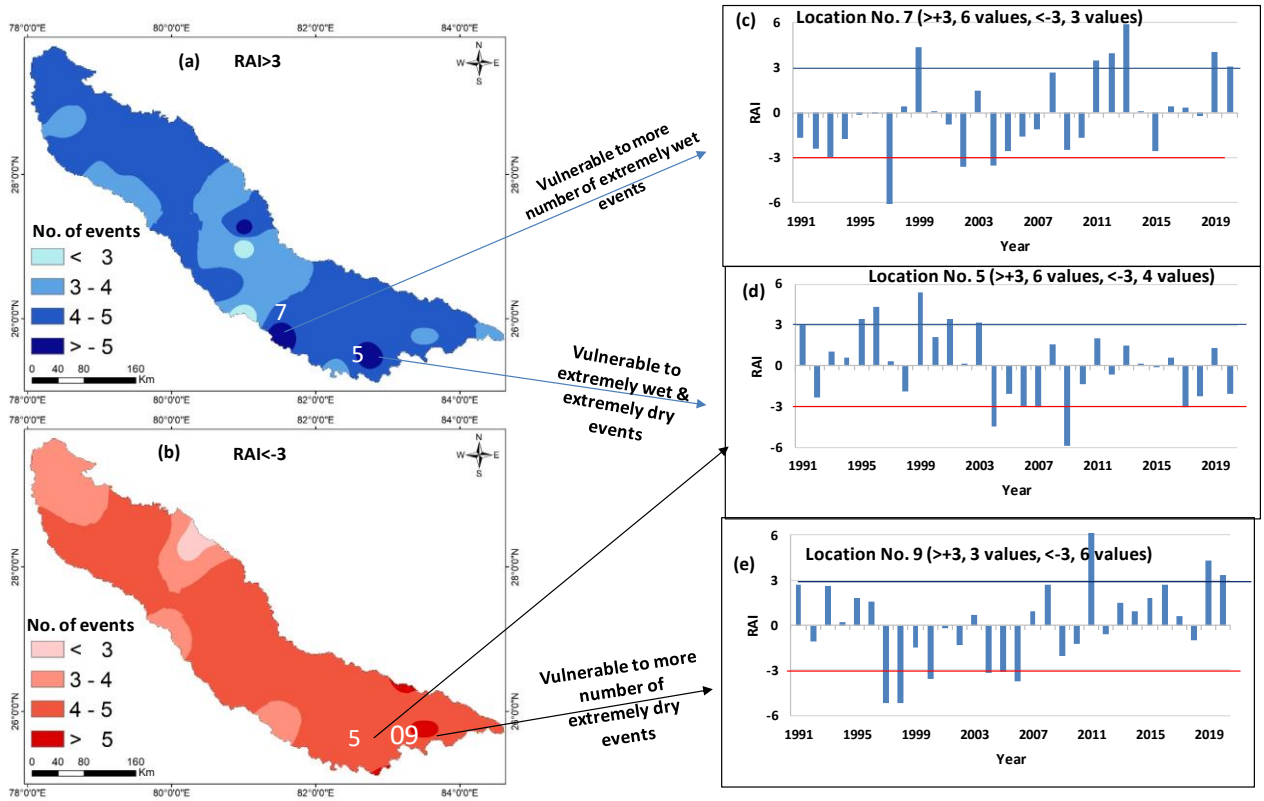

Fig 6.28: Spatial distribution map and plots of Rainfall Anomally Index (RAI) for the period averaged over 1992-2020, and the RAI time series. (a) Spatial map showing area distribution experienced very wet to extremely wet years (i.e., RAI>3); (b) Spatial map showing area distribution that experienced severely dry to extremely dry rainfall years (i.e., RAI <-3). (c), (d), and (e) are the bar diagrams of RAI plotted for the locations 7, 5 and 9. Within the plot a red line and a blue line is given to identify points that crosses the limit of RAI>3 and RAI<-3.

The location number 7 that falls in the RAI>3 experienced 6 very wet to extreamly wet years that ocured during 1999, 2011, 2012, 2013, 2019 and 2020. Location number 5 that fall both in RAI >3 and RAI<-3 experienced 6 very wet to extreamly wet years that occurred during 1991, 1995, 1996, 1999, 2001 and 2003; and severerly dry to extreamly dry years during 2004, 2006,

2007, and 2009. The location number 09 that falls in RI<-3 zone experienced 6 severely dry to extreamly dry years during 1997, 1998, 2000, 2004, 2005, and 2006.
Similar to the SPI distribution map, the RAI spatial distribution map also shows large part of the study area experienced both severe to extreme wet and dry years.

6.4.4 Percentage Departure (D%) from the long term normal (IMD):

Similar to SPI and RAI, the spatial distribution maps of occurrence of 20% rainfall excess with respect to the normal rainfall and 20% deficient rainfall years were plotted, and beside these figures also plotted the number of times such excess and deficient rainfall events were occurred at all the observed location points in the study area.

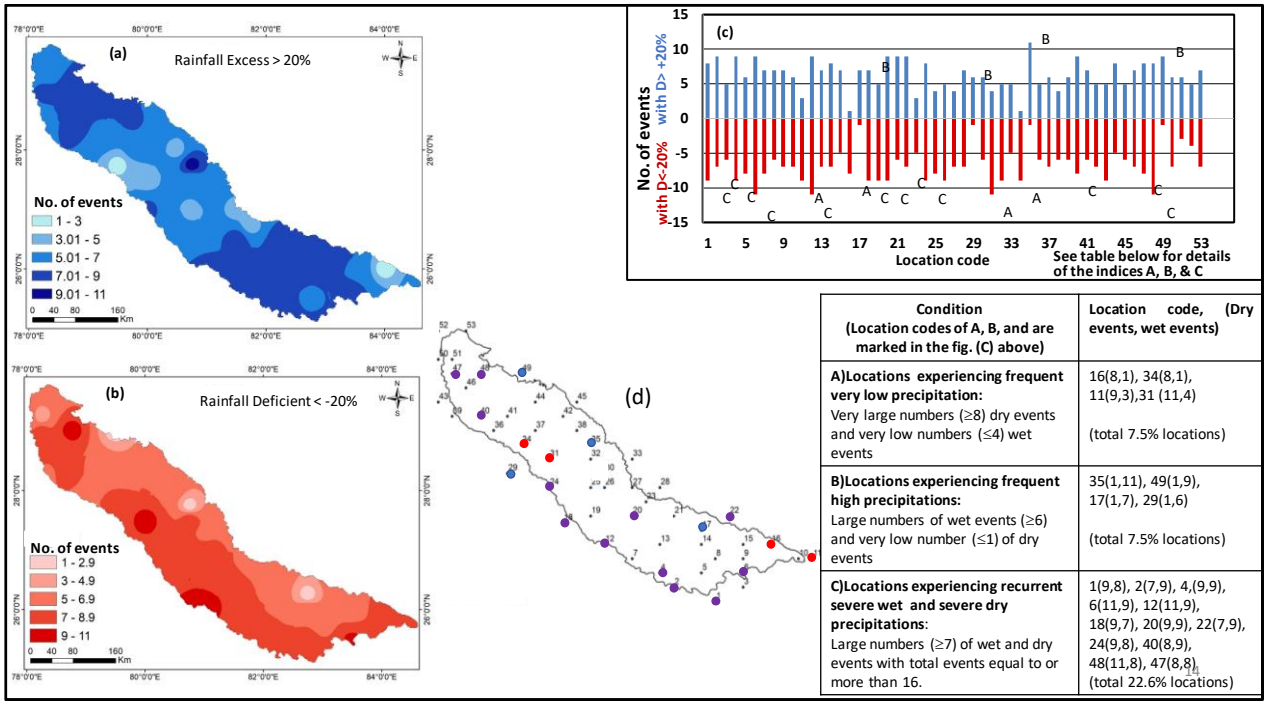

Condition (Location codes of A, B, and are marked in the fig. (C) above)	Location code, (Dry events, wet events)
A)Locations experiencing frequent very low precipitation: Very large numbers (≥8) dry events and very low numbers (≤4) wet events	16(8,1), 34(8,1), 11(9,3),31 (11,4) (total 7.5% locations)
B)Locations experiencing frequent high precipitations: Large numbers of wet events (≥6) and very low number (≤1) of dry events	35(1,11), 49(1,9), 17(1,7), 29(1,6) (total 7.5% locations)
C)Locations experiencing recurrent severe wet and severe dry precipitations: Large numbers (≥7) of wet and dry events with total events equal to or more than 16.	1(9,8), 2(7,9), 4,(9,9), 6(11,9), 12(11,9), 18(9,7), 20(9,9), 22(7,9), 24(9,8), 40(8,9), 48(11,8), 47(8,8), (total 22.6% locations)

Fig 6.29: Spatial distribution map and plots of Rainfall Excess (D>20%) and Rainfall Deficient (D < 20%) data-set. In the spatial maps, the data is averaged for the period from 1992-2020. (a) Spatial map showing area distribution that experienced rainfall-excess more than 20% the normal; (b) Spatial map showing area distribution that experienced 20% deficient rainfall. The plot (c) shows number of 20% excess rainfall years (blue portion of the bar) and 20% deficient rainfall years (red portion of the bar) at each location during the period 1992-2020. In the table shown in the figure, the location points are filtered into three categoriez 'A', 'B' and 'C' according to whether these locations experienced more/less/equal wet years or dry years; as; A: >8 dry years and ≤ 4 wet years; B: >6 wet years and ≤1 dry spell years; and C: ≥7 wet and dry spell years. The sub-fig (d) is a spatial points distribution map in which the locations categorized into 'A', 'B' and 'C' are shown in red dot, blue dot, and violet dot respectively.

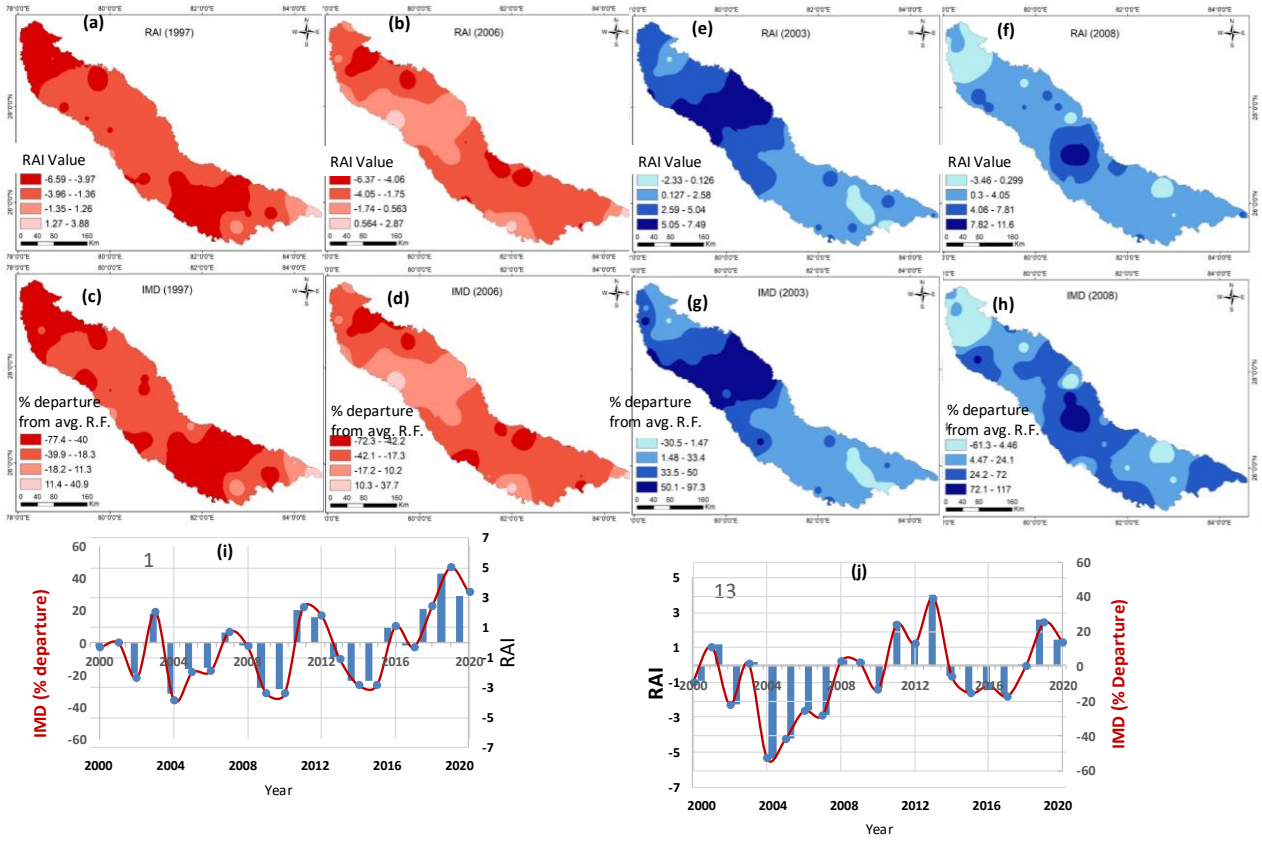

Fig. 6.30: Correlation between the results obtained using RAI vs %D. The spatial maps for RAI and %D are compared for the two drought years 1997 and 2006, and two wet years 2003 and 2008. The RAI and %D time series plots are compared for two location points 1 and 13. The locations of these points in the study area are also shown in the sub-fig (d) of FigXXX. In the sub-fig i & j, Red contour marks the %D data whereas, the blue bars marks RAI.

In the plot, the indice 'C' indicating locations where both severe wet as well as severe dry spell years experienced, are 12 locations out of the total 53 observation points. These 12 points fall on both the spatial distribution maps (a & b in Fig XXX). These 12 points are also marked in the sub-fig (d) of the fig XXX as violet colour points.

7. Groundwater Fluctuation

Groundwater depletion is a pressing global issue, driven by the increasing demand for water to support food and energy production, as well as betterment in the lifestyles. As this precious water resource is continuously depleting, the risks to food and energy security are escalating, and also the demand for enhancing the water productivity (productivity in dollars per m^3 of water consumption). In the long run, unchecked groundwater depletion may develop into a critical survival challenge for many communities. To address this problem effectively, it is important to thoroughly assess the key factors contributing to groundwater depletion and quantify the magnitude of their impact. Results below shows the groundwater depletion in the studied area and a few factors that are impacting the groundwater resources.

A) Spatial variation in groundwater depletion/rising zones: Fig XXX shows the spatial variation in the groundwater depletion and rising conditions during the assessment period 2010-17, the corresponding quantitative details are given in the Table XXX. From the figure it can be observed northwest parts close to the river Ganga flood plain is covered by the groundwater depletion up to 8 meter. Safe conditions are located mainly near the Shiwalik foot hill regions and in the southeastern parts of the study area.

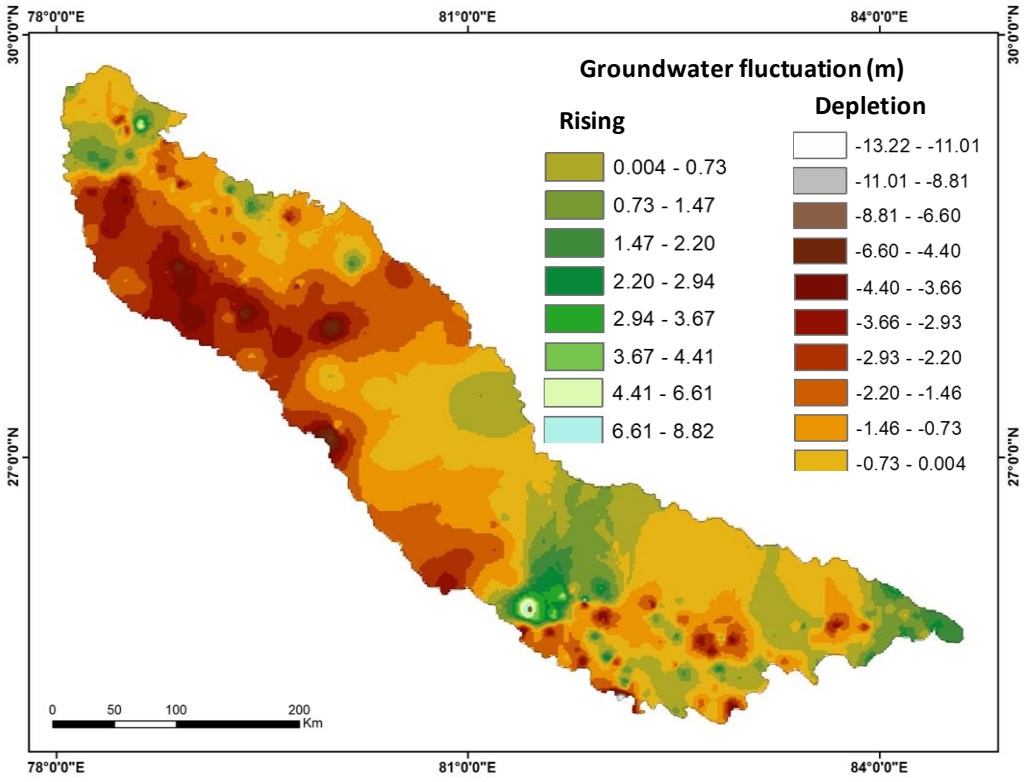

Fig. 7.1: Change in groundwater level data during pre-monsoon over 7 years (2010 to 2017). Groundwater level of 2010 is taken as the groundwater averaged over 2009 to 2011, and that of 2017 as the data average of 2016 to 2018

The data provided in Table XXX indicates that in a 19.7 km^2 area, groundwater levels depleted by over 12 meters during the 2010-2017 period. Additionally, in 58,000 km^2 area, groundwater levels declined within the range of 1.1 to 1.8 meters. On the contrary, the same timeframe also witnessed rising groundwater tables, with increases ranging from 0.37 to 1.84 meters, observed across a 14,000 km^2 area. Overall, the analysis suggests that the study area is experiencing significant annual aquifer volume depletion of 120,111 Mm^3, which corresponds to an average groundwater level decline of 12.54 cm per year.

Table 7.1: Average change in groundwater level during 2010 to 2017, and the corresponding volumetric change computed using area calculated for the respective contour intervals from Fig XXX.

Average change in GW level (m)	**Area (km^2)**	**Volumetric change (Mm^3)**	**Total Area (km^2)**	**Total Volumetric change (Mm^3)***	**Average Groundwater level fluctuation**
-12.12	19.70	-238.67			
-9.91	3.90	-38.65			
-7.71	31.55	-243.09			
-5.50	485.00	-2667.50			
-4.03	1198.00	-4827.94	95781.15	-84075.04	-0.88m
-3.30	4850.00	-15980.75			
-2.57	8889.00	-22800.29	Average change per year	-12010.72Mm^3 per **year**	-12.54 cm/year
-1.83	14588.00	-26696.04			
-1.10	19139.00	-20957.21			
-0.37	24357.00	-8890.31			
0.37	13448.00	4908.52	Average Change per year per km^2	-0.1254 Mm^3	----
1.10	5391.00	5930.10			
1.84	1873.00	3436.96	*Actual change in water volume need multiplication with specific yield		
2.57	741.00	1904.37			
3.31	441.00	1457.51			
4.04	161.00	650.44			
5.51	134.00	738.34			
7.72	31.00	239.17			

B) Relative changes Between the Rainfall and Groundwater fluctuation: Rainfall stands as the primary source of groundwater, establishing an inherent connection between the two. The correlation between rainfall and groundwater fluctuation across four distinct rainfall zones, as well as for the entire study area, is illustrated in Figure XXX. Notably, a strong correlation is observed between rainfall and groundwater fluctuation in Zone 1 (refer to Fig. a, XXX) and across the entire study area (refer to Fig. e, XXX). However, the remaining zones display a weak correlation between these variables, often accompanied by a discernible time lag.

For instance, in Zone 4, groundwater fluctuation exhibited a significant valley between 2008 and 2017, contrasting with a pronounced peak in the rainfall spectrum occurring in 2013. Similarly, in Zone 2, there appears to be one fewer peak in the groundwater fluctuation spectrum compared to the rainfall spectrum over the period from 1999 to 2019. These observations suggest that factors beyond mere rainfall quantity influence groundwater fluctuation.

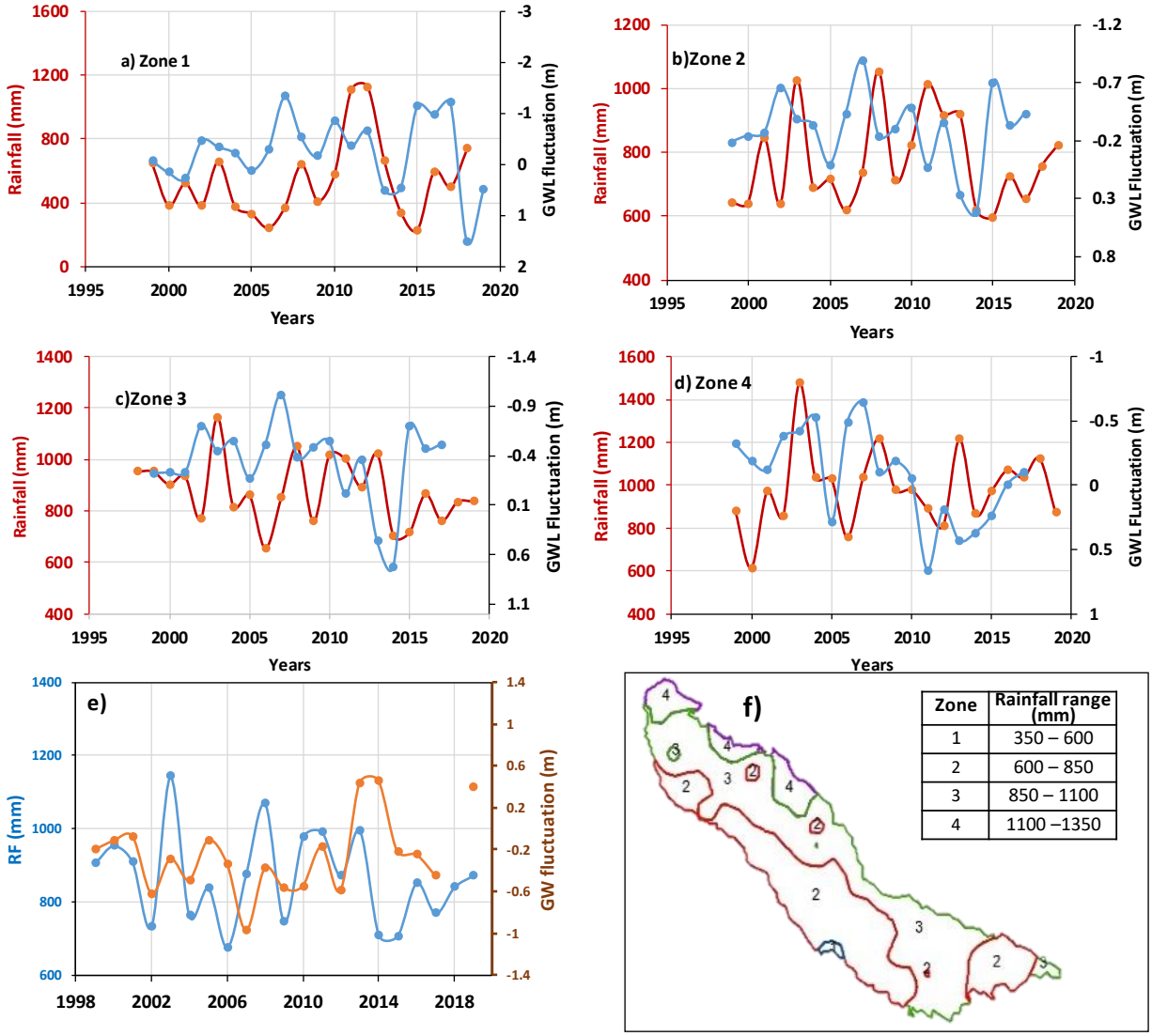

Fig 7.2: Groundwater fluctuation and its relation with rainfall. The spatial pattern of the demarcated four rainfall zones is shown in the figure (f). The relation between the rainfall and groundwater level in these four zones is shown in the plots (a) to (d); and for the relation of rainfall to groundwater for the entire study area is shown in the plot (e).

Considering the escalating water demand with rising temperatures, the examination of groundwater fluctuation concerning temperature is imperative. The observed relationship is depicted in Figure XXX (Fig. a of XXX). While the correlation is relatively weak (R2=0.2), it broadly indicates an increasing depletion of groundwater with temperature rise.

Further exploration of the correlation between rainfall and groundwater levels during pre- and post-monsoon periods is conducted. The correlation between these parameters is illustrated in Figure XXX (Fig. b of XXX).

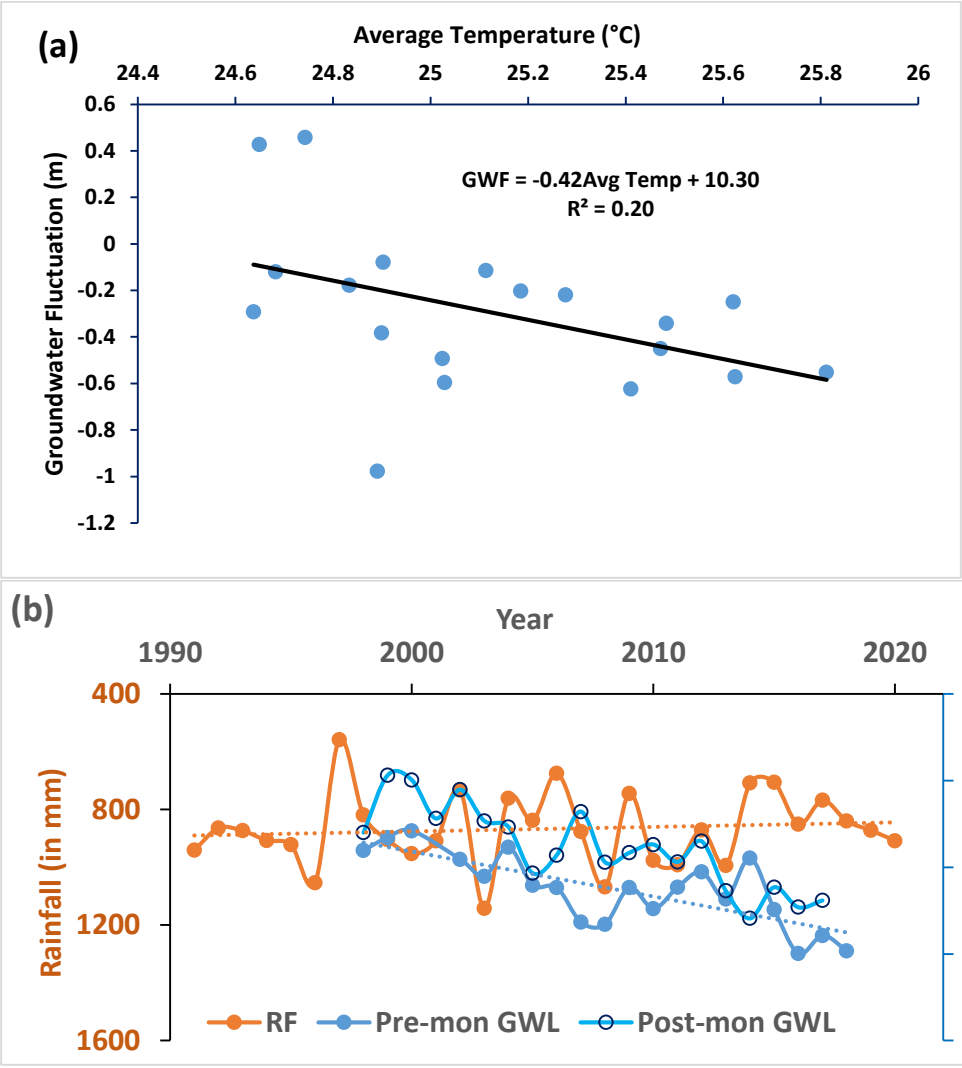

Premonsoon GWL = 0.1039Year - 202.2; R² = 0.582
Post-monsoon GWL=0.1366Year-268.65; R2=0.715
Rainfall = -1.6xYr + 4073

Fig 7.3: (a) Variation in groundwater fluctuation with increasing average temperature (b) Variation in rainfall and its relation with pre-monsoon and post-monsoon groundwater level. Note the reverese order of the Y-axes.

Between 1991 and 2018, rainfall decreased at an approximate rate of 1.6mm per year, while groundwater levels deepened at rates of 10cm/yr and 14cm/yr for pre-monsoon and post-monsoon periods, respectively.

The timing of rainfall peaks, both pre- and post-monsoon, broadly correlates. However, the difference (in meters) between pre- and post-monsoon groundwater levels is non-uniform. For instance, in 2007, the difference between pre- and post-monsoon levels was 2.55m, while in 2005, it was 0.28m. Conversely, in 2014, the post-monsoon level was 1.38 meters deeper than the pre-monsoon level. This varying disparity in groundwater depth likely contributes to the lack of strong correlation between rainfall and groundwater fluctuation observed in various zones in Figure XXX.

It's worth noting that declining groundwater levels can also result from rising water demand for irrigation, domestic use, and industrial activities, including power production; that is, due to the combined effect of an increase in per capita water demand and population growth. To examine this, groundwater depletion over three decades versus population density is evaluated (refer to Fig XXX). Each point indicate the district population density and the groundwater fluctuation recorded in the district. The plot broadly depicts depletion exceeding 0.7m in the southeastern zone (Zone C and D of Fig XXX) that has a population density of more than 900 persons/km², groundwater fluctuation less than 0.2m in the zone A, which falls near the foothill region with a population density in the range of 715 persons/km², and for the rest of the area, fluctuation ranges from 2m to 4m. One of the reason for the low depletion of groundwater in this zone could be due to surface water support from the dense canal network in these district area (for example see the location of point numbers 3, 7, 9, 10, 11, 12, 13, etc.) or that these districts are located along the river Ganga flood plain (district number 6). and therefore,

Across the study area, from northwest to southeast, as longitude increases and latitude decreases, groundwater fluctuation increases. This aspect is illustrated in a plot in Figure XXX.
From the above analysis, it's evident that forecasting and addressing the falling trend in groundwater fluctuation require consideration of multiple parameters, including rainfall, temperature, population density, and location with respect to the Shiwalik range (geo-coordinates), among others. Implementing multiple strategies is essential to control declining groundwater levels. These include enhancing water use efficiency, increasing water recycling across all water-consuming sectors, implementing effective groundwater governance, and exploring groundwater augmentation methods.

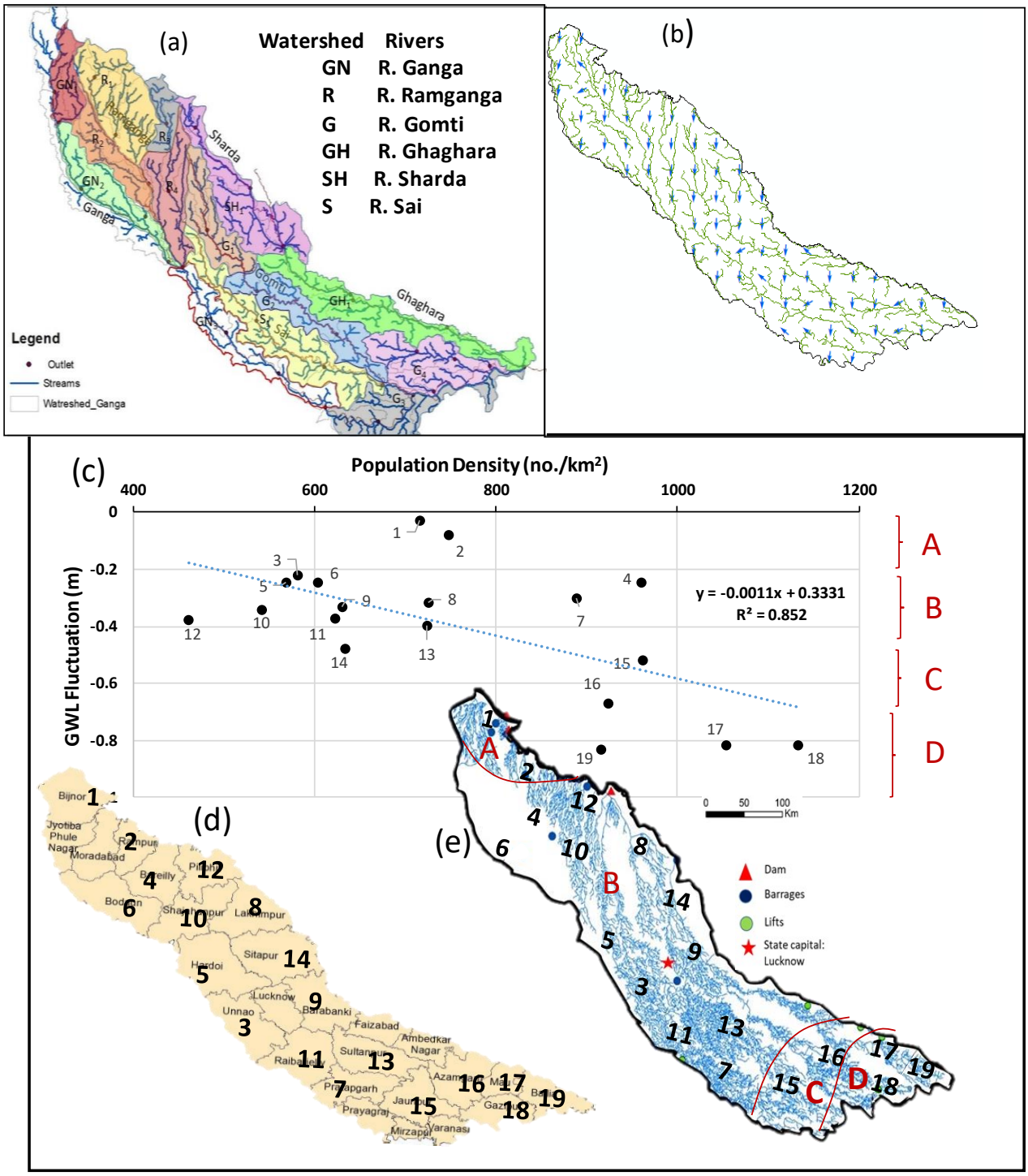

Fig. 7.4: Surface water and groundwater conditions. Relation between groundwater fluctuation with population desnity. (a) Watersheds in the study area, (b) groundwater flow pattern overlaid on the river network (c) cross-plot between groundwater level fluctuation (post-monsoon – pre-monsoon) vs population density, (d) distribution of points on the cross-plot in (c) are shown in the district map of the study area (e) distribution of points on the cross-plot in (c) is shown on the spatial distribution map of the canal network. Also shown the three zones A, B, C, and D to correlate the appearance of these zones in the cross-plot with that on the spatial distribution pattern.

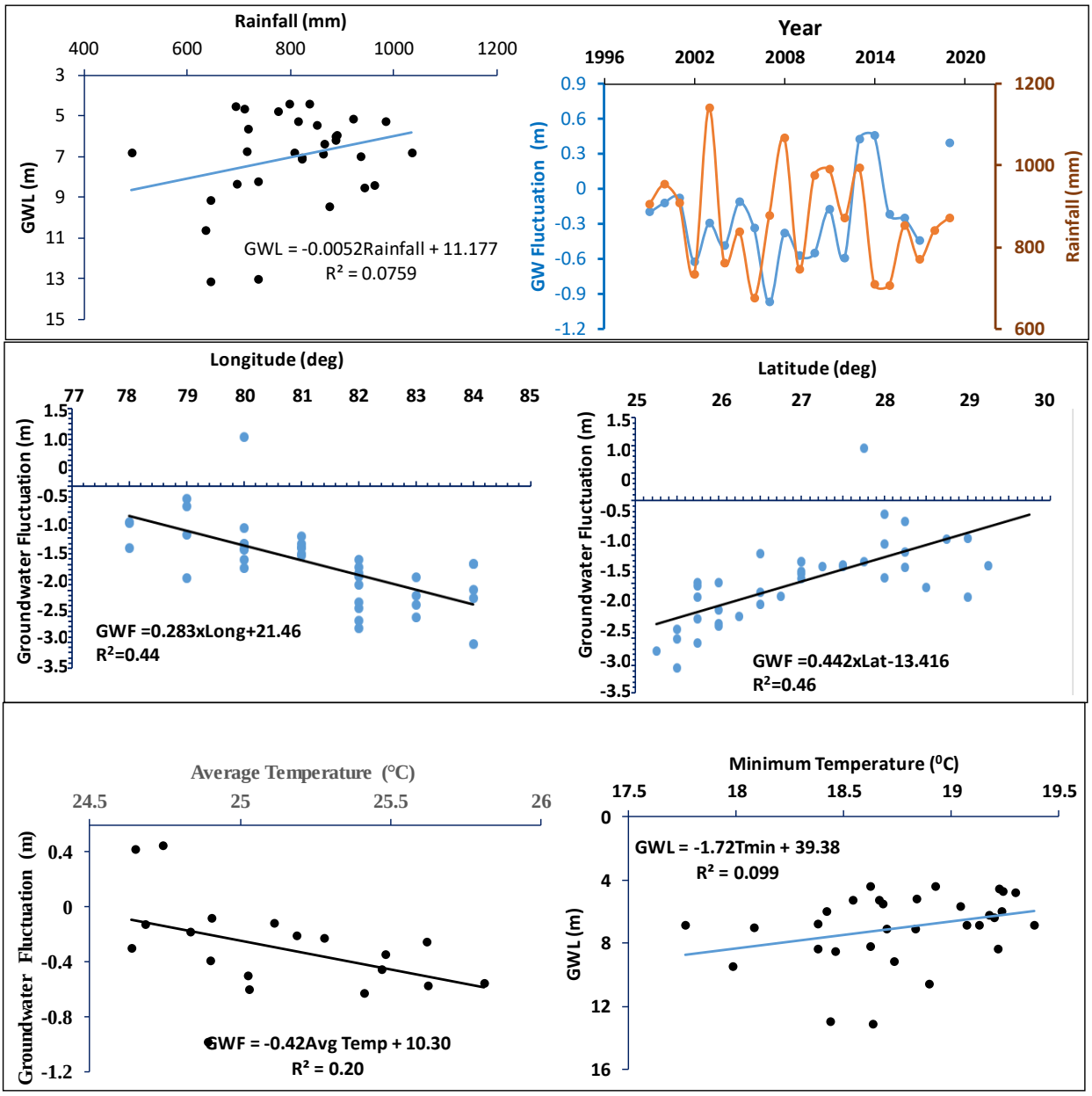

Fig. 7.5. Dependence of groundwater fluctuation on various hydrometerological parameters

C) Comparison of Mann-Kendall trend test results for rainfall and GWL

The Kendall' tau is nearly zero with negative value of -0.078. It means that there is vary less correlation between the rainfall values of sequential years. The Sen's slope value (-2) explains the the monotonous decrease in the rainfall in the entire study area. The Standard deviation 125.6 explians the large fluctuation in the rainfall about its mean value. The value of Sen's slope for pre

– monsoon groundwater level and post – monsoon groundwater level is same and is equal to -0.086. This is less negative than the rainfall of the study area which is -2.0.

Table 7.2: The Mann-Kendall trend test with Sen's slope estimator results for rainfall, pre monsoon GWL and post-monsoon GWL for the entire study.

S. No.	Parameter	S – value	Kendall's tau	Sens's slope	p-value	Var(S)	Standard deviation
1	Rainfall	-34.000	-0.078	-2.000	0.556	3140.667	125.616
2	Pre-monsoon GWL	254.000	-0.086	-0.086	<0.0001	2776.667	2.463
3	Post-monsoon GWL	269.000	-0.639	-0.086	<0.0001	3076.333	2.75

8. GROUNDWATER QUALITY AND ISOTOPIC INVESTIGATIONS

A total of 159 water samples (Fig 70) were collected for analysis of major cations and anions, including 55 deep groundwater samples (depth >120 ft) and 104 shallow groundwater samples (depth <120 ft). The study area, spans over 700 km in Uttar Pradesh, exhibiting distinct variation in topography, soil type, soil textue and drainage characteristic. To make water quality analysis more focused and comprehensive, the study area has been divided into three elevation zones: (i) 35 m to 130 m, (ii) 130 m to 165 m, and (iii) regions above 165 m (Fig XXX).

According to the charge balance verification of all hydro-chemical data, the ionic balance error was within the limit value of ±5%, indicating the accuracy of our data. The analysed cationic compositions follow the pattern of $Na^+ > Ca^{2+} > Mg^{2+} > K^+$. In 29% sample, the most predominant cation Na^+ exceeds the contamination level (WHO, 2011). The ion exchange as well as dissolution of clay minerals and the presence of sodic plagioclase contribute to excess Na^+ ion in groundwater. Comparing all cations, a low level of K^+ (0.149–5.179 mg/L) ion signifies weak mobility in groundwater samples. High Ca^{2+} concentration than Mg^{2+} suggests carbonate mineral dissolutions.

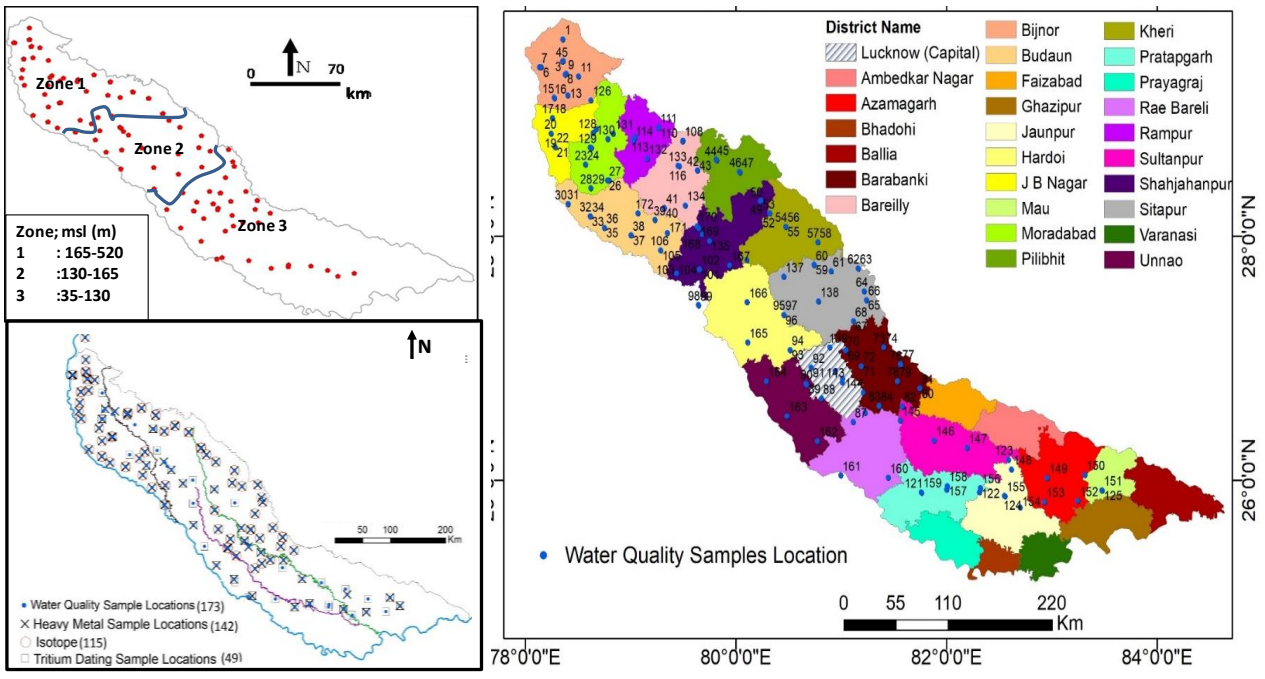

Fig 8.1. Water sampling location map shown with respect to (a) elevation range (b) district-wise distribution (c) along with major rivers in the study area

Table 8.1: Graphs and their relevance for water quality analysis and interpretation

Graph	Purpose
TDS vs TH	**Water quality (salinity & hardness)**
Na/Cl vs Sample No	**Halite dissolution, anthropogenic contamination, evaporation, rock-water interaction**
Ca+Mg vs (SO4+HCO3)	**For information on dissolution of various ions Ca, Mg, SO4, HCO3 and silicate weathering.**
TZ+ vs (Na+K) **(Ca+Mg) vs TZ+** **HCO_3/Na vs Ca/Na** **Mg/Na vs Ca/Na**	**For information about silicate and carbonate weathering processes.**
HCO3 vs (Ca+Mg)	**To assess the relationship between calcium (Ca) and magnesium (Mg) and their concentrations in groundwater samples.**
Ca/Mg vs Sample Number	
Chlor-Alkaline Indices	**To analyze the degree of ion exchange, freshening and salinization of groundwater**
Piper Diagram (Chadha Diagram)	**Hydrochemical facies**
Gibb's Diagram	**Rock-water interaction, evaporation enrichment of salts, etc**
Water quality index and Heavy Metal Indices	
Isotopic analysis	**Identification of source water and mixing process**

8.1 TDS vs TH:

In TDS vs TH plot, 50% of the data points fall in the range of <270 mg/l, representing a soft to moderately hard water. The remaining data points exhibit TH values ranging from 270-1000 mg/l, indicating a hard to excessive hardness. The hard water belongs mainly to the zone II and Zone III. These variations in TH values across the region signify spatial differences in Ca-Mg type mineral composition, although there is an overall higher level of Ca-Mg mineral composition compared to sodium-rich minerals.

This observation is consistent with the interpretation of Parson's plot, which has indicated two water types: Ca-Mg-SO4 and Ca-Mg-Cl, with low sodium content in the samples due to reverse ion exchange processes. The combined Parson's and TDS vs. TH plots indicate the dominance of Ca-Mg-SO4 and Ca-Mg-Cl water types and sulfate and chloride-rich sources in the study area.

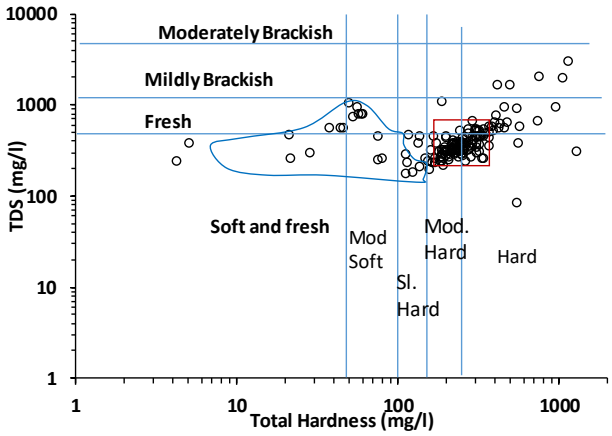

TH (mg/l)	Hardness	TDS (mg/l)	Water type
<50	Soft	<500	Drinking water
50-100	Moderately soft	<1000	Fresh water
100-150	Slightly Hard	1000-5000	Mildly Brackish water
150-250	Moderately Hard	5000-15,000	Moderately brackish water
250-350	Hard	15,000-35,000	Heavily brackish water
>350	Excessively Hard	>35,000	Seawater

Fig 8.2: TDS Vs TH plot. The blue polygon encloses data points are from Zone 1. The distribution of points from Zone 2,3 & 4 overlaps and cover the area outside the blue polygon. The red square indicates zone of 90% data points, and these are hard and soft to fresh water. (Abbreviations used: Mod. Soft: Moderately soft; Sl. Hard: Slightly Hard; Mod Hard: Moderately hard). Also shown the table of classification of water on the basis of TH and TDS concentration.

8.2 Parsons Diagram:

The analysis of groundwater quality data using Parson's plot revealed the predominance of two types of groundwater as: Ca-Mg-SO_4 (~40%) and Ca-Mg-Cl (~55%). The water quality indicates Cl/SO_4 ratio in the range from 0.8 to 2.5. The Na/(Ca+Mg) ratio ranges from 0.2 to 0.8 indicating a relatively lower sodium content compared to the combined concentrations of calcium and magnesium ions. This suggests moderate to higher proportion of (Ca+Mg) compared to Na. These ratios indicate that the water quality is controlled by dissolution of sulfate-bearing rocks (for example gypsum or unhydrite), carbonate and magnesium bearing rocks (such as calcite and dolomite) and silicate bearing rocks. On the other hand, Ca-Mg-Cl-type water is characterized by a higher concentration of chloride ions relative to sulfate ions, as indicated by a Cl/SO_4 ratio ranging from 1.5 to 3. This suggests the influence of chloride-rich sources on groundwater chemistry. The Na/(Ca+Mg) ratio ranging from 0.15 to 0.4 indicates a lower proportion of sodium compared to the combined concentrations of calcium and magnesium ions.

The presence of high chloride but low sodium suggests that halite dissolution is not the primary process governing the water chemistry in the study area. This type of water can be explained by a combination of processes, including reverse ion exchange and the dissolution of chloride-rich minerals. Reverse ion exchange involves the rocks with higher affinity for sodium, such as zeolite, clays, and certain sedimentary rocks, retaining sodium and releasing calcium and

magnesium ions into the aqueous solution. Additionally, the high chloride concentration can be attributed to the dissolution of chloride-rich minerals.

Furthermore, approximately 5% of groundwater samples exhibit $NaSO_4$ type groundwater. These samples have an ionic ratio of Na/(Ca+Mg) between 1.5 and 3.0 and a (Cl/SO_4) ratio ranging from 0.2 to 0.9, indicating rock-water interaction with sodium- and sulfate-rich rocks. Overall, Parson's plot suggests the dissolution of sulfate-bearing minerals, the presence of chloride-rich sources, and the occurrence of a reverse ion exchange process.

8.3 Gibbs Diagram:

The Gibbs diagram of groundwater (Fig XXX) reveals that 95% of the data points exhibit rock-water interaction, as evident from their distribution in both the TDS vs. [Cl/(Cl+HCO3)] and TDS vs. [Na/(Na+Ca)] axes. Examining the axis representing [$Cl/(Cl+HCO_3$)], it is observed that 95% of the data points have values below 0.18, indicating a low chloride content in the groundwater. Similarly, in the axis for [Na/(Na+Ca)], the data points are distributed as follows: 60% between 0.15 to 0.36, 25% between 0.36 and 0.6, 5% between 0.08 and 0.15, and the remaining 10% between 0.6 and 0.96. This distribution signifies the composition of the groundwater samples, with 65% predominantly containing calcium, 25% having an equal proportion of calcium and sodium, and 10% mainly consisting of sodium. This suggests that the majority of the groundwater samples have undergone dissolution processes involving minerals or rocks that are not chloride-rich but, rich in calcium and to minor extent by sodium. Such mineral matrix includes rock types dominant proportion of limestone or dolomite and to minor level by sodium-rich minerals such as halites or sodium feldspars.

8.4 Chadha Diagram:

Almost 82% of the data points belong to Ca-Mg-HCO_3 which is the characteristic of recharging water, and quite safe for drinking. Also, 5% of data points belonging to Na-HCO_3 indicate base ion exchange. 3% of the data points belonging to the NaCl type indicate seawater-type groundwater, and 2.5% of the data points belonging to the Ca-Mg-Cl type facies indicate reverse ion exchange, but the overall groundwater is uncontaminated and recharging according to the Chadha diagram.

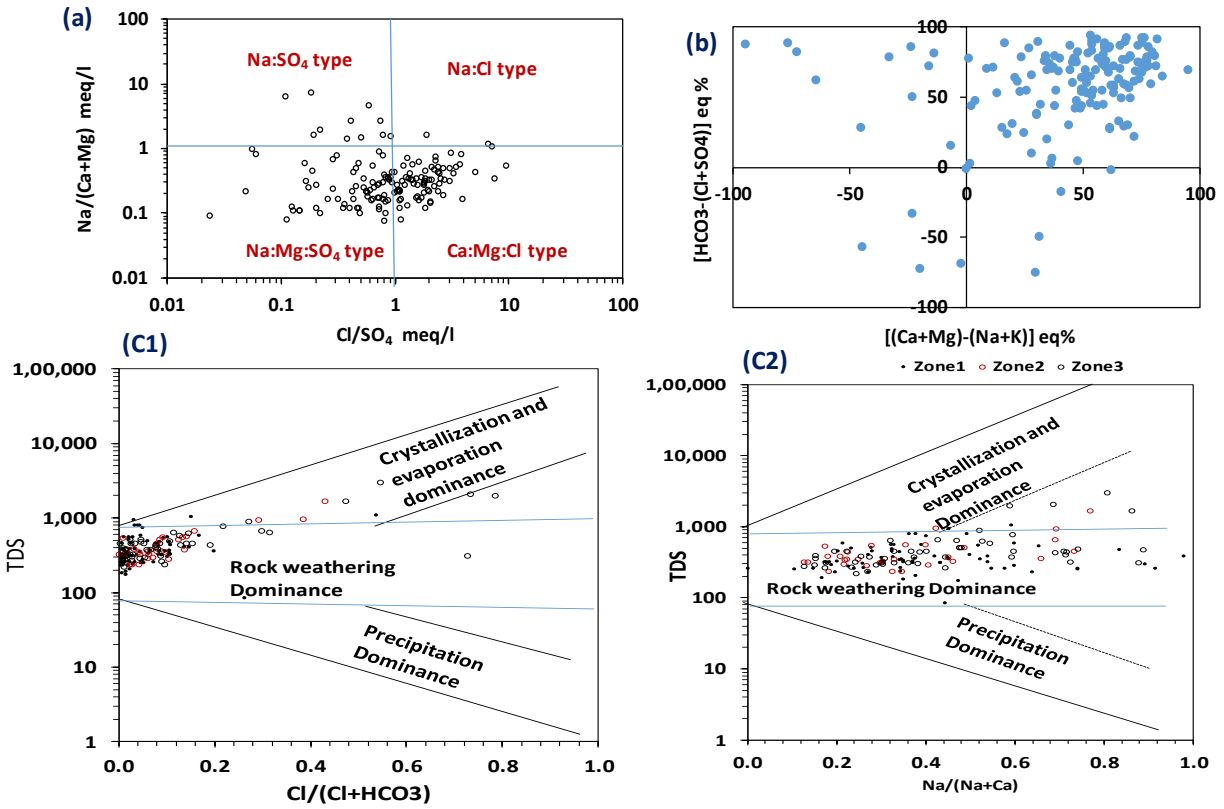

Fig 8.3: Statistical plots of water quality. (a) Parson's diagram; (b) Chadha Diagram; (C1 & C2): Gibb's plot

8.5 Piper Dagram:

The distribution of data points in the Piper Diagram (Cation and Anion ternaries, and in the Central Diamond Faices) is shown in the fig XXX, and the spatial distribution of map of the Piper Diagram based interpreted water type is shown in the Fig XXX.

Piper plot shows 85% of the samples in the shallow groundwater are of Ca Mg HCO_3 type and Ca- HCO_3 type & remaining are of mixed Ca-Mg -Cl type. In the deep groundwater, (95%) are falling in the field of Ca Mg HCO_3 type and Ca- HCO_3 type and the remaining 5% of samples are of mixed Ca Mg Cl type and Na- K -HCO_3 type thus depicting more fresh water conditions in deeper aquifers. ()

The spatial distribution pattern of $CaHCO_3$ shows that these points are widely distributed across the entire upper half of the study area, extending from the central region to the northwest.

About 10% of the $CaMgHCO_3$ water-type points are located just below the central portion, stretching towards the southeast along the Siwalik foothills.

The points classified as $CaMgHCO_3$ with mixed cations and bicarbonate-rich anions show a similar spatial distribution to the $CaHCO_3$ type. However, about 20% of these mixed cation type points are located below the central region, extending further towards the southeast.

(Na+K):Bicarbonate type points are are about 5% of the total, and these points are distributed along the southern boundary of the study area, extending in a northwest to southeast direction.

The predominance of the $CaMgHCO_3$ type, especially the $CaHCO_3$ type, indicates that the groundwater in the Middle Ganga Basin is primarily influenced by the weathering and dissolution of carbonate and dolomite minerals. The interpretation suggests presence of widespread carbonate-rich formations in the study area, and significant precipitation recharge along the Siwalik foot-hills along with dissolution of these carbonate-rich minerals.

The distribution of the mixed cation type points, and (Na+K):bicarbonate type water in the southeast, suggests a minor variation in geological formations in the southeast zone or additional geochemical processes influencing the water chemistry in this direction.

Wide occurrence of carbonate minerals (e.g., calcite, dolomite), and its dissolution along the groundwater flowpaths especially in the upper half of the study area lead to the enrichment of calcium (Ca), magnesium (Mg), and bicarbonate (HCO3-) ions in the groundwater. In addition to the dissolution, mixed cation type water in southeast regions indicates the influence of additional geological formations or geochemical processes like ion exchange reactions, or the mixing of groundwater from different sources that are passed through silicate (Na-feldspar) weathering reactions.

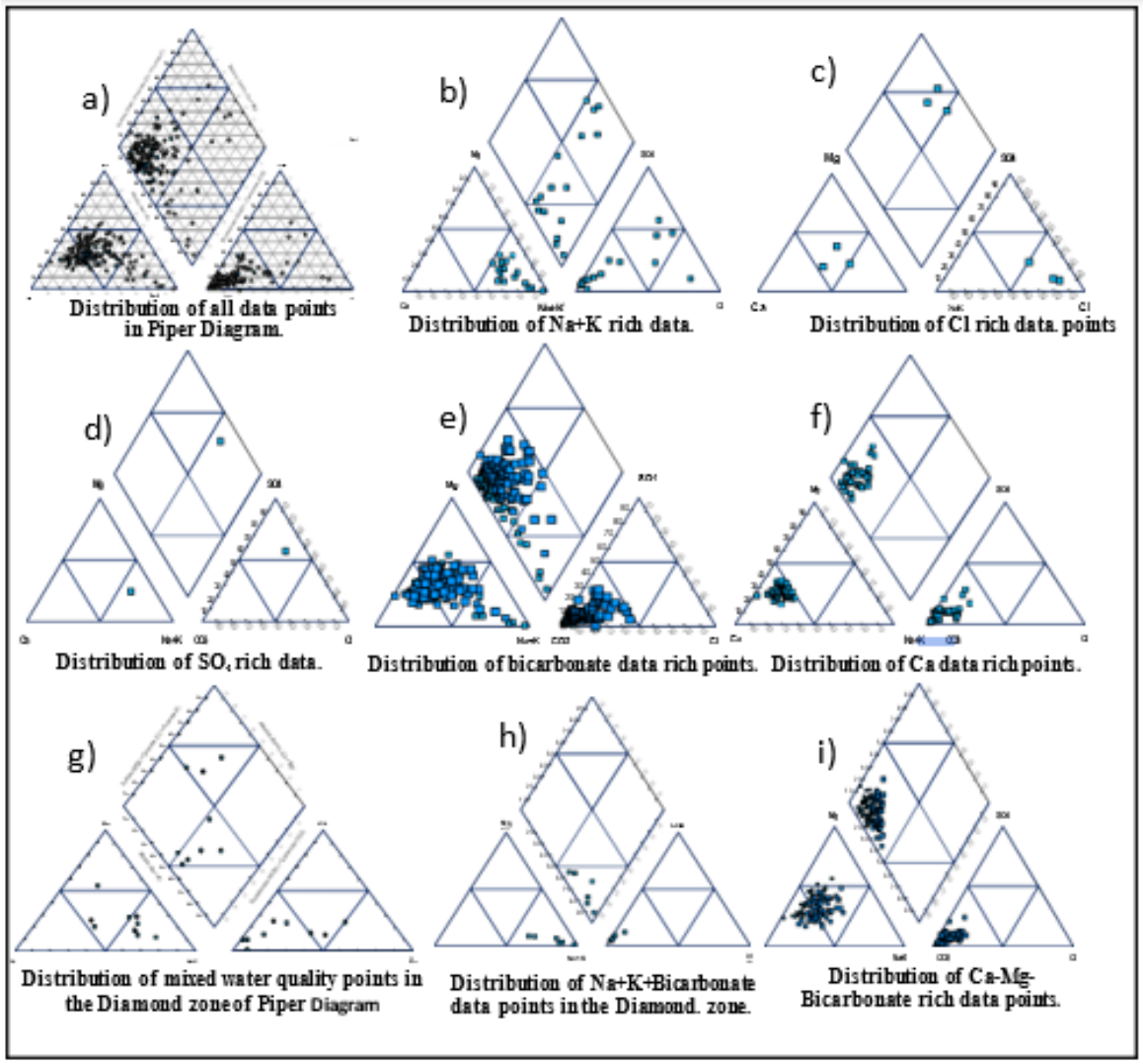

Fig. 8.4.: The hydrochemical classification of the Middle Ganga Basin in the UP-state, analysed using the Piper Diagram. (a): All data points (b) to (f) were resolved on the basis of hydrochemical facies using the cation and anion triangles; (g) to (i) were resolved on the basis of hydrochemical facies in the Diamond zone of the Piper Diagram

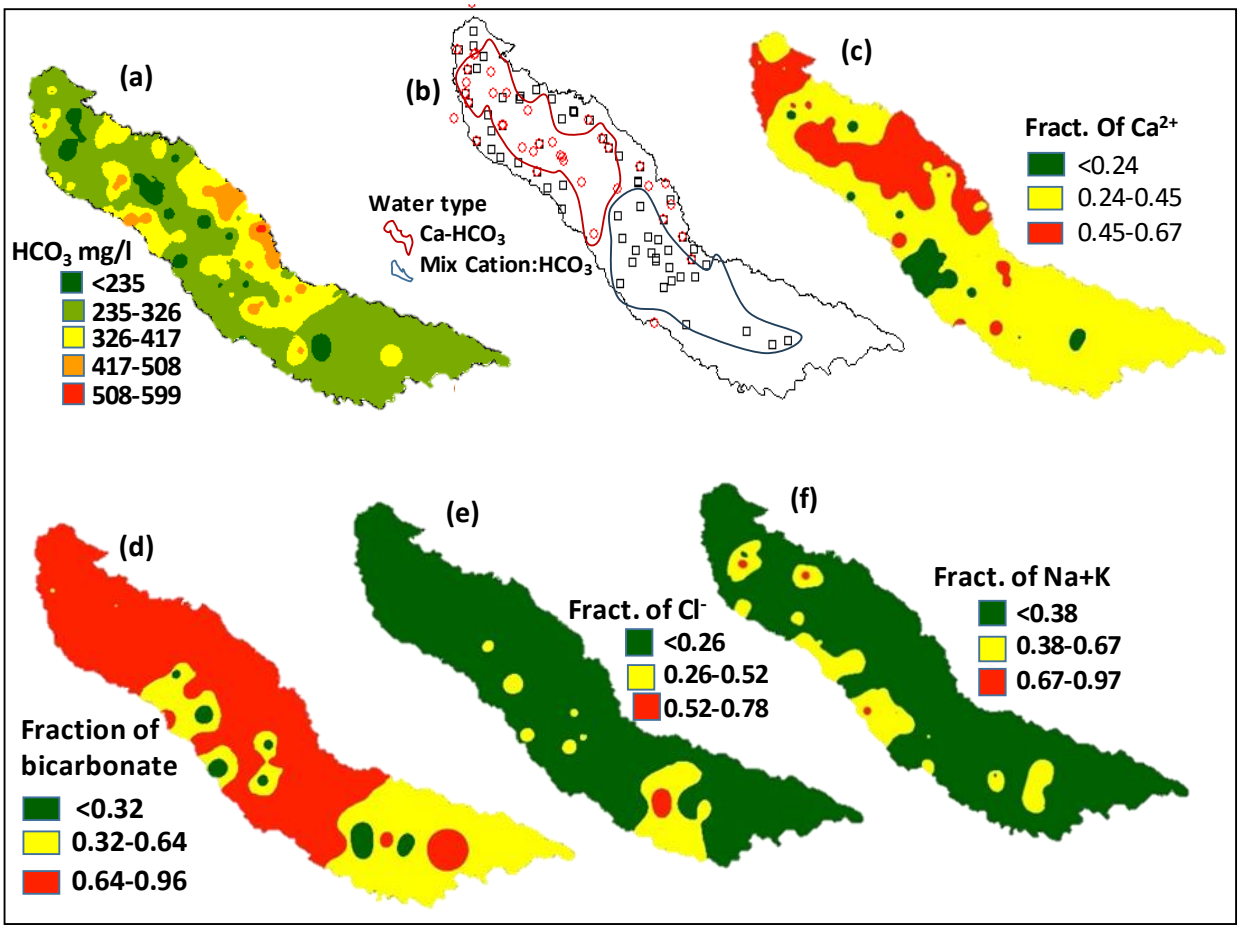

Fig. 8.5: Spatial variation of water quality. (a) Concentration of HCO_3^- (b) Water type (Ca-HCO_3 & Mix Cation:HCO_3^-) as identified from the Piper Diagram; (c), (d), (e) and (f) respectively are the spatial distribution maps of molar fraction of Ca^{2+}, bicarbonate, Cl^-, and Na^++K^+

8.6 Analyzing the Rock-Weathering Processes

To understand the interaction, recharge sources, contamination in shallow and deep aquifers 32 different water quality parameters along with isotopes were analysed and the sample locations are marked in Figure 10.

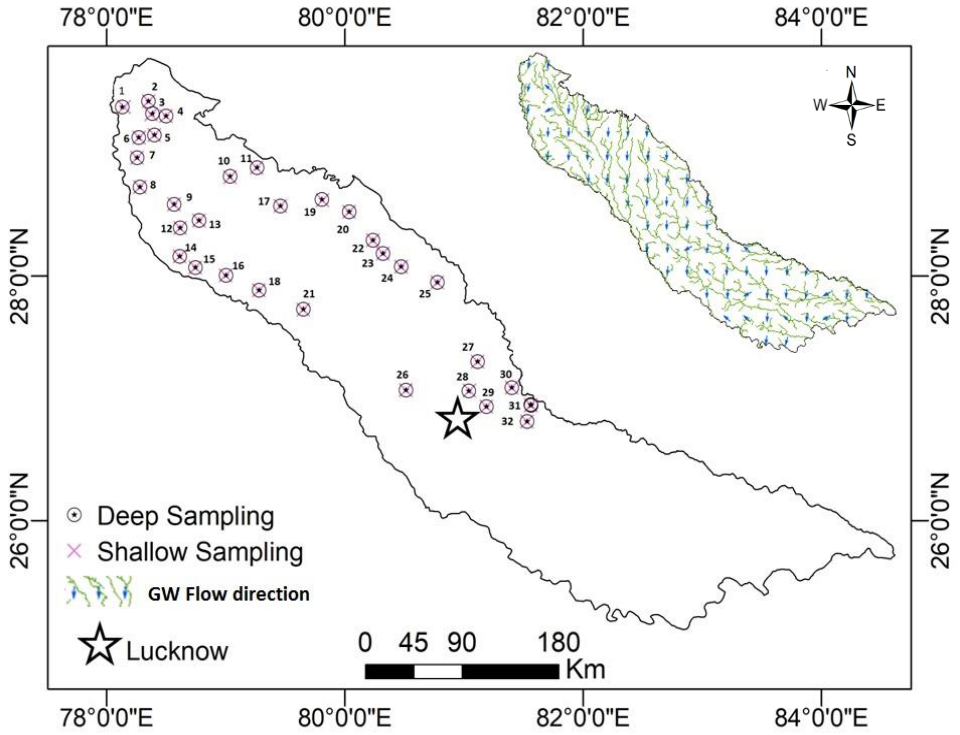

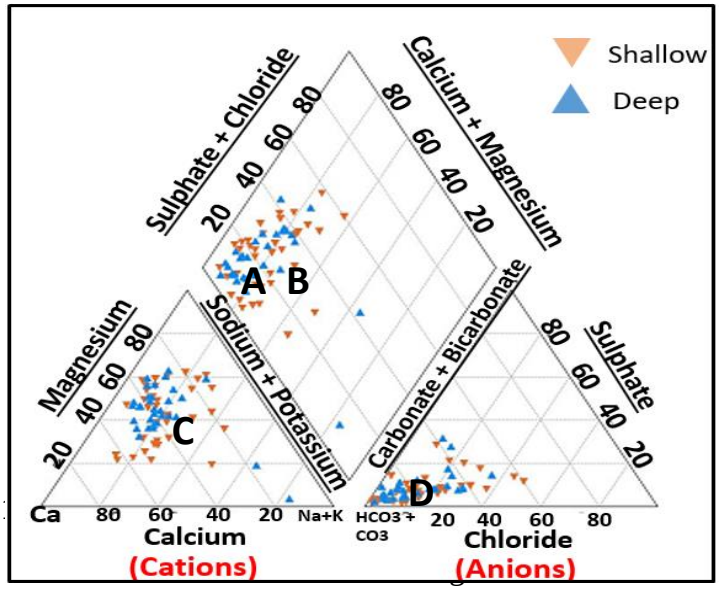

Fig. 8.6: 1) Sampling locations from shallow (d<120 ft) & deep (d>120 ft) groundwater.

2. Piper plot for shallow and deep samples

4.11. through rock weathering and various hydrochemical processes. Groundwater hydrolysis reactions, influenced by factors such as pH, temperature, solubility levels, and the mineral concentration in rock-forming minerals or the soil

matrix, result in the dissolution of various ions, silica, heavy metals, and other elements. The hydrochemical reactions increases the total dissolved solids (TDS) and electrical conductivity (EC) of the water, while also affecting its pH.

Investigating these hydrochemical processes is commonly conducted using ionic bi-plots. These bi-plots help interpret the standard hydrochemical reactions taking place in the groundwater system. A summary of some of the most important hydrochemical reactions is presented in Table XXX.

Table 8.2: Common Mineral Dissolution Reactions

Dissolution of calcite:

$CaCO_3 + H_2CO_3 \rightarrow Ca2+ + 2HCO3$

$CaCO_3 + H+ \rightarrow Ca^{2+} + HCO_3^-$

Congruent Dolomite dissolution (Magnesium calcite dissolution):

$CaMg\ (CO_3)_2 + 2H_2CO_3 \rightarrow Ca^{2+} + Mg^{2+} + 4HCO^-_3$

Incongruent dolomite dissolution:

$CaMg(CO_3)_2 + H_2CO_3 \rightarrow CaCO_3 + Mg^{2+} + 2HCO_3^-$

Cation Exchange Process:

$Ca^{2+}_{(aq)}$ or $Mg^{2+}_{(aq)}$+ 2Na-X or 2K-X → $2Na^+_{(aq)}$ or $2K^+_{(aq)}$ + Ca-X_2 or Mg-X_2
Replacement of Ca^{2+} and Mg^{2+} by Na^+ and K^+ ions decreases the concentration of Ca^{2+} and Mg^{2+} and increases the concentration of Na^+ and K^+ ions

Reverse Ion Exchange:

$Mg - Ex + Ca^{2+}(aq) = Mg^{2+}(aq) + Ca - Ex$

Silicate weathering:

$NaAlSi_3O_8$ (Albite)+$2H_2CO_3$+$9H_2O$ → $Al_2Si_2O_5(OH)_4$(Kaolinite)+$2Na^+$+$4H_4SiO_4$+$2HCO_3$
Albite dissolution increases the concentration of HCO_3^- and (Na^++K^+)
Ca $Mg(Si_2O_6)$ (Pyroxene) + $4CO_2$ + $6H_2O$→ Ca^{2+} + Mg^{2+} + $4HCO_3^-$ + $2Si(OH)_4$
Albite dissolution increases the concentration of HCO_3^- and (Ca^{2+}+Mg^{2+})

Dissolution of gyspum

$CaSO4.2H2O \rightarrow Ca_{(aq)}^{2+} + SO^{2-}_{4(aq)} + 2H2O$

i) **Mg/Na vs Ca/Na, and Ca/Na vs HCO_3/Na:** These bivariate plots in which the axes are normalized with Na provides the relative contribution of three weathering mechanisms (silicate, carbonate and evaporate) to solute concentration of groundwater (Nasher and Ahmed, 2021). The fig (a of XXX) shows 10% data that has undergone silicate weathering and 80% undergone combination of silicate and carbonate weathering processes, and 5% evaporate dissolution.

ii) **Ca vs HCO_3:** The scatter diagram of Ca versus $HCO3^-$ if plots along 1:2 line, it indicates calcite weathering, if plots near and above the 1:4 line suggests dolomite weathering

$$CaCO_3 + H_2CO_3 \rightarrow 2HCO_3^- + Ca^{2+}$$

In the present study the points scatter mostly along 1:2 line indicating calcite dissolution. However, some points also fall below the 1:2 line indicating low calcium. Such depletion of Ca^{2+} usually result due to replacement with Na when silicate dissolution occurs. Therefore, the data points indicate both calcite as well as silicate dissolution.

iii) **Ca^{2+}/Mg^{2+} vs Sample number:** The Ca^{2+}/Mg^{2+} molar ratio indicates calcite and dolomite dissolution in groundwater. $Ca^{2+}/Mg^{2+} = 1$ indicates dolomite dissolution, $1 < Ca^{2+}/Mg^{2+} < 2$ signifies calcite dissolution, and $Ca^{2+}/Mg^{2+} > 2$ indicates silicate dissolution. In the present study, 40% points have their ionic ratio in the range 0.5 to 1.0 indicating dolomite dissolution; 35% in the range 1.0 to 2.0 indicating calcite dissolution, and the remaining 25% with their ratio more than 2.0 indicate silicate dissolution.

iv) **(Ca+Mg) vs HCO_3**: Points on the equilline indicate carbonate dissolution. Points below the calcite dissolution line are due to reduction of Ca and Mg which can happen due to replacement of Ca and Mg by Na when Na gets released from clay and replaces these ions. This can also happen by HCO_3 enrichment due to silicate weathering. Points above the line indicate additional sources for Ca and Mg, such as reverse ion exchange (Krishanraj et al., 2011). In the present case 90% data points show excess HCO3 compared to (Ca+Mg). The excess HCO_3 may be due to silicate weathering resulted into release of Na ions which has has replaced (Ca+Mg) thereby increase in HCO_3 with respect to (Ca+Mg) ion concetration.

v) **(Ca+Mg) vs (SO_4+HCO_3)**: Datta and Tyagi (1996), explained that, in the (Ca+Mg) vs (HCO3+SO4) diagram, the equiline indicate simultaneous dissolution of gypsum, calcite and dolomite, points falling above the equiline are due to carbonate weathering (Paul et al. 2019). Excess (Ca+Mg) arise under ion exchange process thereby the points shift above the equiline. Under the reverse ion exchange (Ca+Mg) decreases thereby the points shift below the equiline. In the present case, 60% points lie along the equilline indicating simultaneous dissolution of calcite, gypsum and dolomite, 20% points show ion exchange and the remaining 20% the reverse ion exchnage.

vi) **(Na+K) vs TZ^+:** The equiline (Na+K)=TZ^+ indicate involvement of silicate weathering in the geochemical process. In the silicate weathering, Na^+ arise from weathering of sodium feldspar (Albite) and K^+ from potashium feldspars (Orthoclase and Microcline).

vii) **(Ca+Mg) vs TZ^+:** This accounts to identify the proportion of (Na+K) and (Ca+Mg) in the total cation (TZ^+) contribution. (Ca+Mg) lower than 0.5 indicate alkali (Na+K) enrichment due to silicate weathering or from other common compounds like Na_2SO_4, K_2SO_4. High (Ca+Mg) with respect to (Na+K) indicates calcite weathering, and if it is low [(Ca+Mg)<(Na+K)] in the total cation (TZ^+) then it indicates silicate weathering.

viii) **Na/Cl Vs EC:** In the case of evaporation with no precipitation of any species, the Na/Cl ratio remains unchanged but EC increases. Therefore, a horizontal line parallel to EC axis with no change in Na/Cl would indicate evaporation associated concentration of ions. and evapotranspiration (Fig. 7). Further, in the case of halite dissolution Na/Cl ~1. Higher value (Na>Cl) indicate silicate weathering and ion exchange reaction. In the present case, Na/Cl vs EC shows random points up to EC=1000μS/cm, and Na/Cl is more than 1 for most of the sample points indicating ion exchange and silicate weathering as the operating hydrochmeical process

ix) **CAI-1 vs CAI-2:** Schoeller (1965, 1967) proposed chloro-alkaline indices (CAI-1 and CAI-2) to identify base ion exchange processes governing groundwater chemistry. During ion exchange, Ca^{2+} and Mg^{2+} ions present in groundwater react with clay minerals to release Na^+ ions. Na^+ and K^+ ions in the water are exchanged with Mg^{2+} and Ca^{2+} ions, if the indices values are positive, which indicates base-exchange reaction, whereas negative values indicates chloro-alkaline disequilibrium. The reaction is known as cation exchange reaction. During this process, the host rocks are the primary sources of dissolved solids in the water. The CAIs were computed by the following equations:

Chlor-alkaline indices:

CAI-1: $[Cl^- - (Na^+ + K^+)]/Cl^-$

CAI-2 : $[Cl^- - (Na^+ + K^+)]/[SO_4^{2-} + HCO_3^- + CO_3^{2-} + NO_3^-]$

The CAI-1 and CAI-2 would be negative [Cl <(Na+K)] if the hydrochemistry is dominantly affected by the normal cation-exchange process i.e., a fraction of Ca^{2+} is replaced by Na^+that was previous in the clay matrix. On the other-hand these would be positive [Cl > (Na+K)] if reverse cation-exchange process takes place.

Reverse ion exchange process: $2Na^+ + [Ca(Mg)\ Clay] \leftrightarrow [Na - Clay] + Ca^{2+}(\ Mg^{2+})$

In the present study, out of 158 points only 8 points show positive values indicating normal ion exchange as the dominant process. The remaining points show normal cation-exchange process. Points are confined mainly in the range 0 to -20 for the case of CAI-1 and 0 to -1 in the case of CAI-2. This suggest $(Na^+ + K^+) > Cl^-$, and CAI-2 suggest that $Cl^- << [SO_4^{2-} + HCO_3^- + CO_3^{2-} + NO_3^-]$. That is, it is a low chloride, normal cation-exchange hydrochemical evolution of groundwater.

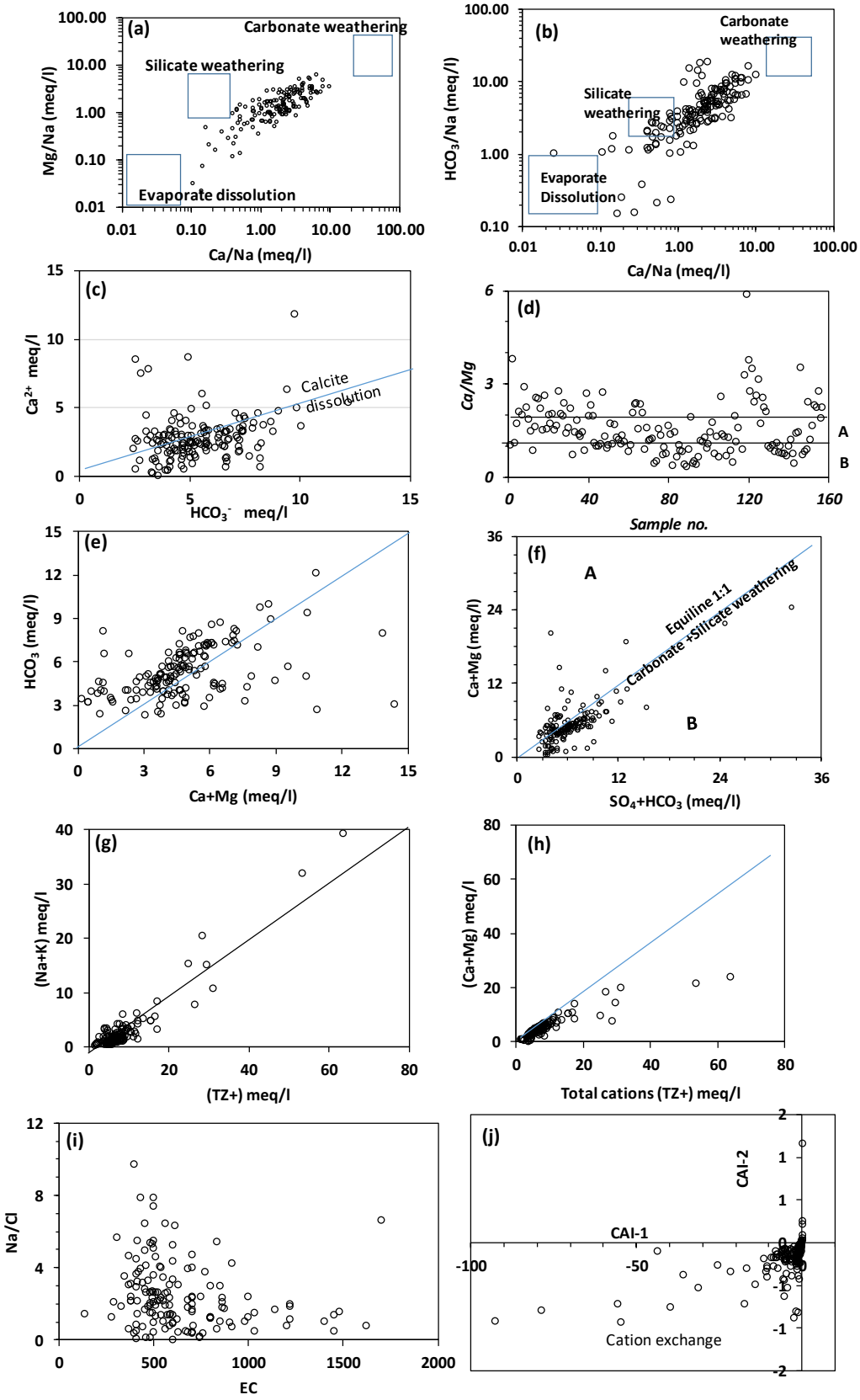

Fig 8.7: Scatter plots for interpreting hydrogeochemical evolution of groundwater

8.10 Groundwater suitability for drinking

Water quality index (WQI) is defined as a rating reflecting the composite influence of different water quality parameters on the overall quality of water. It indicates the quality by an index number, which represents the overall quality of water for any intended use. Water quality index (WQI) was prepared using water quality parameters F, Cl, SO_4, NO_3, Na, NH_4, K, Ca & Mg. It shows that 74% area (71084 km2) portion is having excellent quality of groundwater while very poor (75–100) to unsuitable (>100) quality is prevailing in small pockets in North and south west regions within area of 2795km2. Hardness was found to be hard in 60% area and very hard in 30 % of the study area. Different water quality parameters along with minimum and maximum values are shown in Table 1.

Water quality parameters with the areas which are above permissible limits for drinking purposes are identified as; Flouride in Prayagraj, Ajamgarh and Jaunpur, Magnesium in border areas of Lucknow&Unnao, border areas of Hardoi& Lucknow, Pratapgarh, Nitrates in Shahjahanpur, Lucknow, Hardoi, Unnao, Pratapgarh, Prayagraj,Sulphates in Lucknow, Unnao, Jaunpur, Chloride in Lucknow, Unnao, Prayagraj, Pratapgarh, Jaunpur, Hardoi and Calcium in Lucknow, Barabanki, Sitapur, J P Nagar, Pilibhit, Shahjahanpur, Hardoi, Pratapgarh, Prayagraj, Sultanpur, Ambedkar Nagar, Mirjapur found above the acceptable limits but both were under the permissible limits. (Locations *samples shown in figure 5.57).*

Table 8.3: Variables of water quality with their Min, Max, Avg and SD values

Variables	Min	Max	Avg	SD
EC	130.00	4700.00	729.36	543.15
PH	6.90	10.10	7.70	0.36
HCO_3^-	0.00	744.77	307.83	133.34
F^-	0.00	8.86	0.37	0.74
Cl^-	0.32	903.31	49.44	108.02
SO_4^{2-}	0.00	1299.71	49.53	127.16
NO_3^-	0.00	400.97	15.25	41.68
Li^+	0.00	0.47	0.01	0.05
Na^+	0.00	854.28	62.29	114.52
NH_4^+	0.00	34.46	1.13	4.54
K^+	0.03	106.19	6.90	12.93
Mg^{2+}	0.18	219.48	28.67	25.77
Ca^{2+}	0.98	237.81	57.05	34.31
Total hardness as $CaCO_3$	4.06	1202.10	260.13	174.24

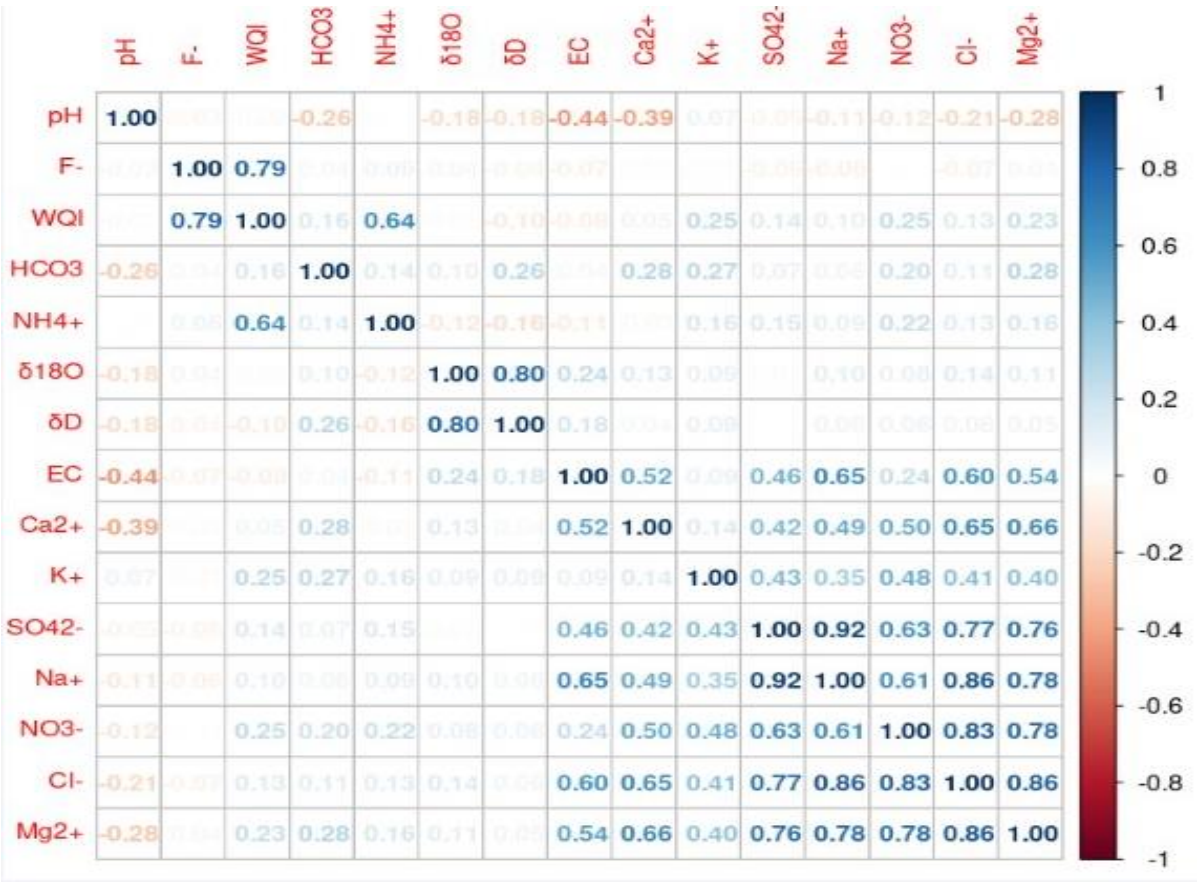

Fig.8.8: Correlation Matrix for 159 water quality samples

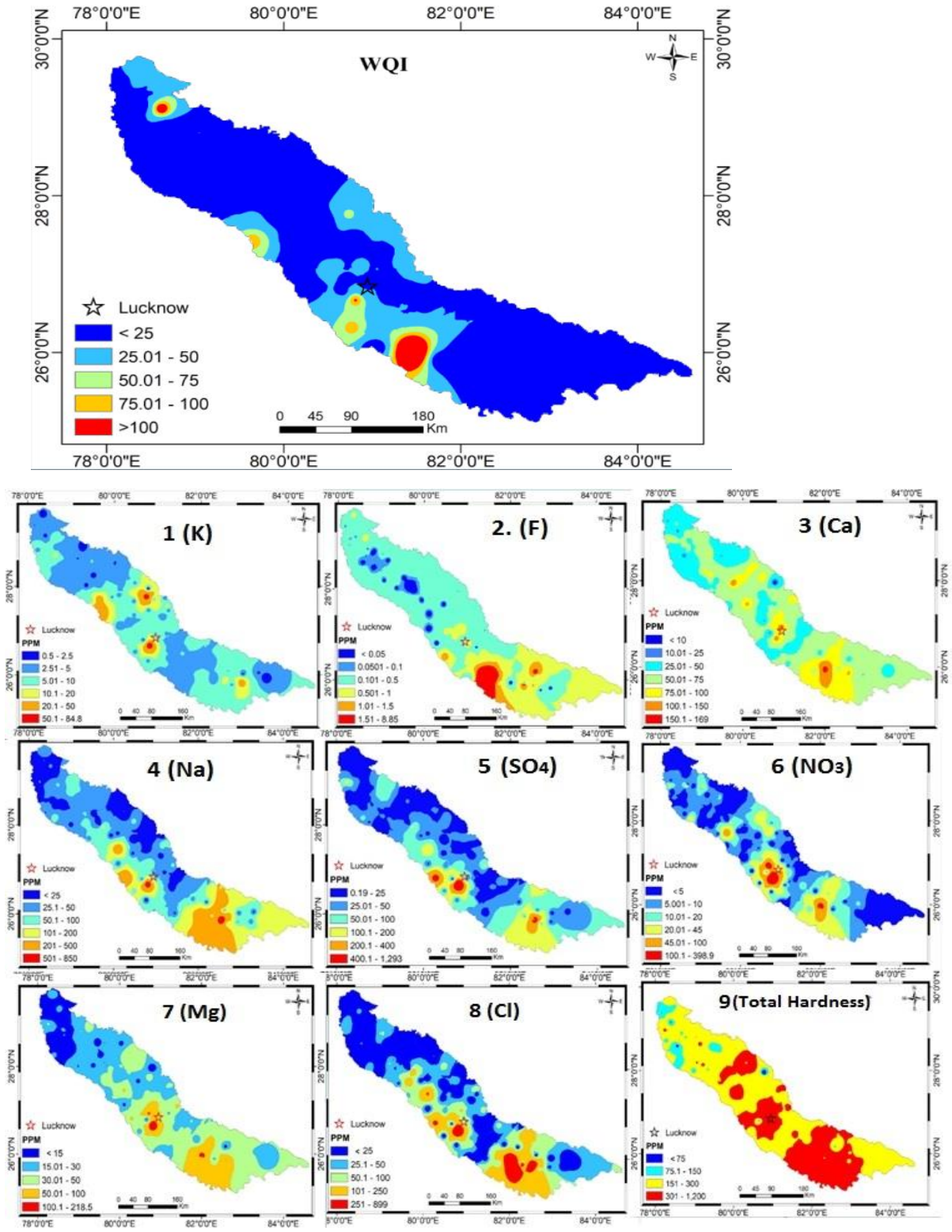

Fig. 8.9: Spatial Variation of Water Quality Index, major ion concentration, and the Total Hardness 1): WQI (Water Quality Index), (2-9): Spatial variation of K, F, Ca, Na, SO_4, NO_3, Mg, Cl, and Total Hardness

8.8 Heavy Metal Contamination and Health Risk Assessment

Trace elements distribution and occurrence in the groundwater depends on degree of weathering and mobility of these elements (Handa 1986). Large aluminum intake may negatively influence health. This was connected with nerve damage. Particularly people with kidney damage are susceptible to aluminum toxicity. There is a risk of allergies. Aluminum is probably mutagenic and carcinogenic. The main sources are Rock and soil leaching. Aluminum was found above permissible limit of 30 µg/l for 13% of the groundwater samples with concentration varying from 0 to 2403.73 µg/l with an average of 118.11 µg/l. The source of Arsenic in groundwater is from Leaching from natural deposits, Wood preservatives, pesticides, industrial deposits, Petroleum production, Semiconductor manufacture & Coal power plants. Arsenic in study area varies from 0 to 147.63 µg/l with an average of 6.31 µg/l. 1% of samples were found to be above permissible limit which can cause serious skin problems, endocrine disruptor, cancer - skin, bladder, lung, kidney, liver, prostate, Harms cardiovascular & nervous systems.

The lead concentration ranges from 0 to 43.81 µg/l with an average 05.38 µg/l . As compared with BIS standards, 14 % groundwater samples exceed the desirable limit (10 µg/l). Lead content is generally derived from use of lead containing fertilizers and pesticides (Aldrin, Deieldrin, Endosulfan etc.,) applied in the agricultural field. The Zinc value varies from 0 to 12239 µg/l with an avg. 577.96. Only 1 sample was found to above desired limit as BIS standards imparting the miniature industrial activities in the study area. The Iron (Fe) is one of the most abundant elements found in earth crust. Iron and Manganese plays an important role in regulation of the biochemical cycle in plants and animals (Ballukarya and Ravi 1999). The Fe concentration ranges 0 to 3029.27 µg/l with an average 140.51 µg/l. It is observed that 11.9% samples exceed the desirable limit (300 µg/l) of the BIS reflecting the impact of agriculture and domestic activities as a possible source (Table 3). Beyond this limit taste/ appearance, domestic utility, water supply structures are affected and promote growth of iron bacteria (BIS 2012). The Mn concentration varies from 0 to 12618.4 µg/l with an average 276.61 µg/l) (Table 3). 15% sample breached the safe limit of 100 µg/l (Table 3). Naturally, chromium occurs in chromite mineral and it replaces Fe^{3+} and Al^{3+} (Faust and Aly 1981). Cr content ranges from 0 to 5.5 µg/l (Avg. 0.83 µg/l) & all of them were under the allowable limit of 50 µg/l set by BIS (10,500:2012). Copper (Cu) plays an important role in production of blood hemoglobin, seed production, disease resistance and regulation of water in plants and humans (Davies and Jones 1988).

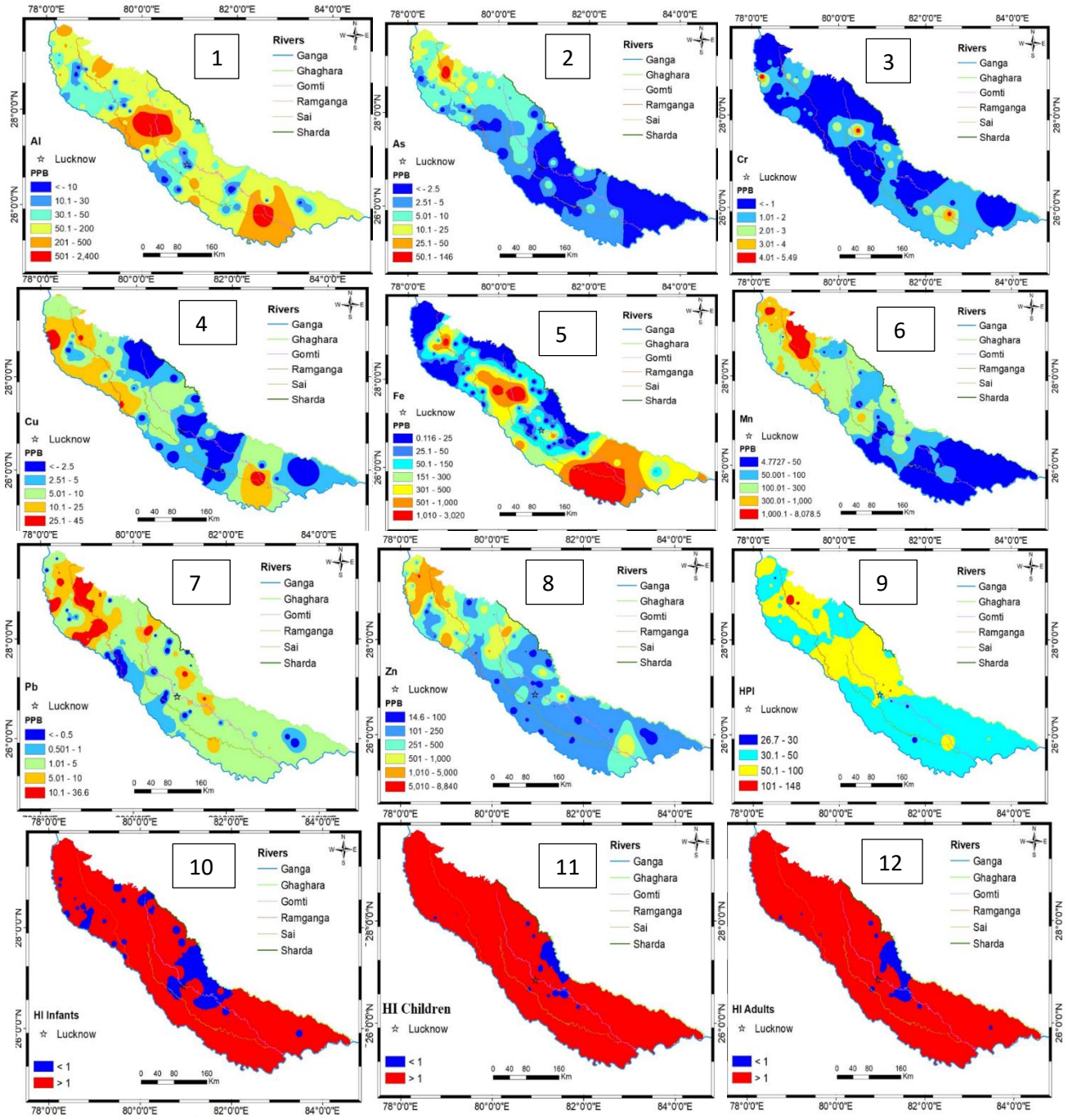

Fig. 8.10. Spatial variation of heavy metal concetration, and the pollution indices HPI and HI. Spatial variation of Al, As, Cr, Cu, Fe, Mn, Pb, Zn, HPI, HI(Infants), HI(Children)& HI(Adults) in figure 1,2,3,4,5,6,7,8,9,10,11 & 12 respectively.

In the study area, copper ranges from 0 to 90.67 µg/l with an average 9.77 µg/l. As per the BIS limit 2.11% samples exceeds the desirable limit due to waste dumps, domestic waste water, fossil fuels combustion, wood production and phosphate containing fertilizers.

According to the (Heavy metal pollution index values of HI (Hazard Index) for infants, children and adults were found exceeding 1 in 52%,71% & 69% of samples, and Children were found at risk more than infants and adults. Iron, Aluminum & Arsenic metal content contributed to larger percentage in HI. (Heavy metal evaluation index) HEI results shows most of the groundwater samples fall in low pollution extent category. The spatial distribution map of heavy metal pollution indices are plotted in (Fig 73).

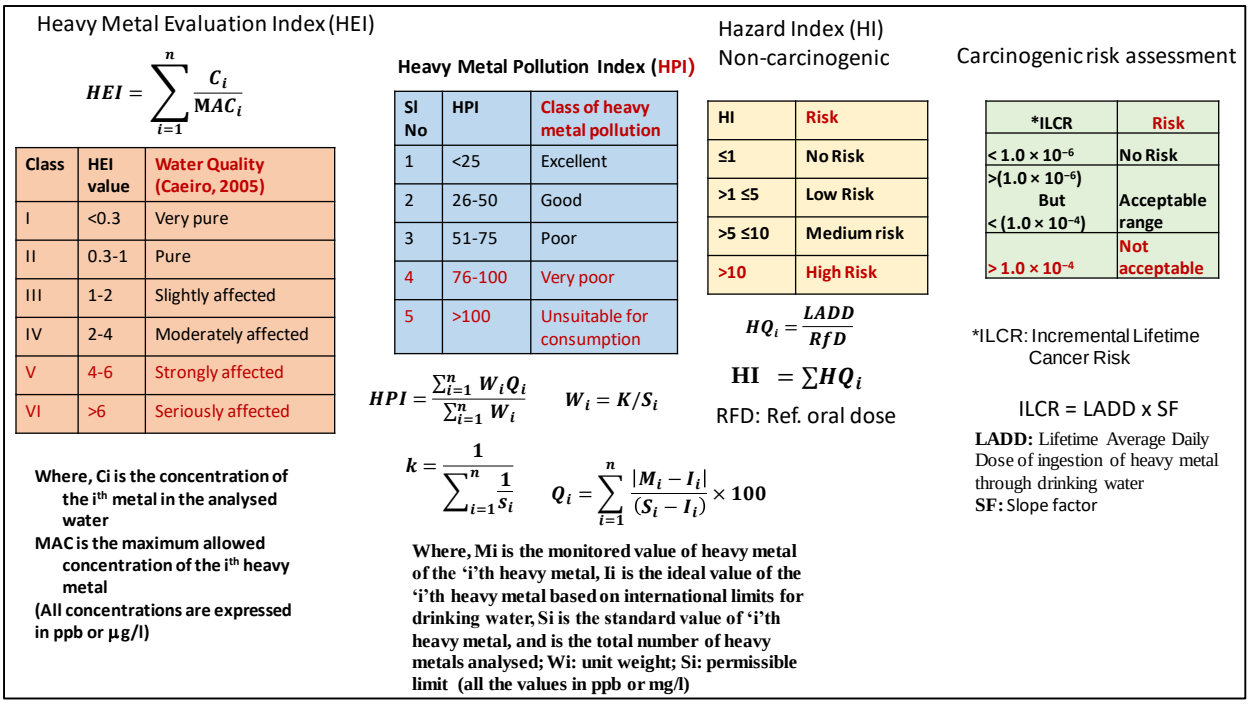

Fig. 8.11: Indices of Water Pollution due to contamination from heavy metals, categorization of water types, and the relevant equations for the analysis

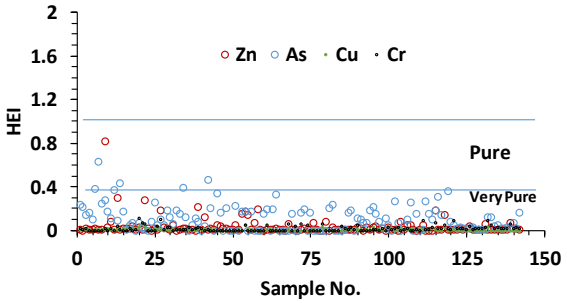

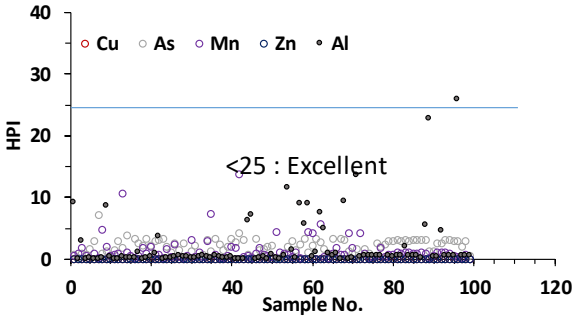

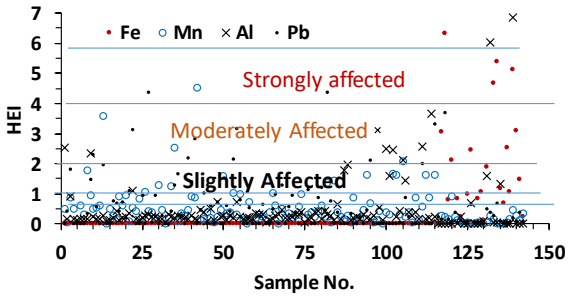

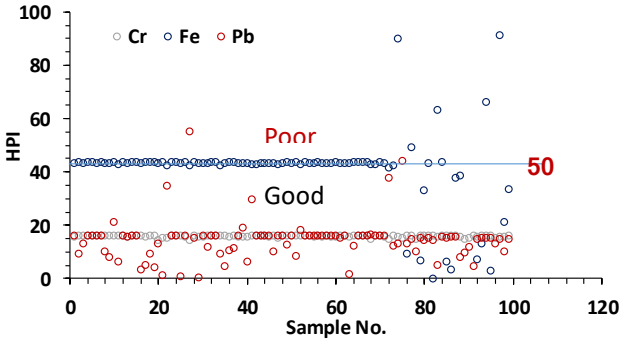

Non-Carcinogenic Metalloid Risk

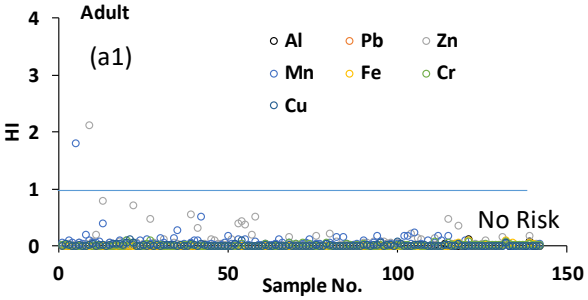

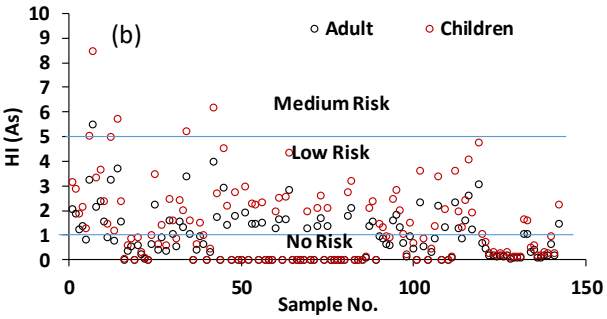

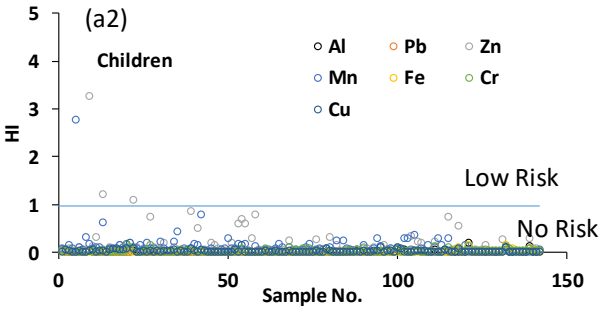

Fig: Hazard Index (HI). (a) for the heavy metals Al, Pb, Zn, Mn, Fe, Cr, and Cu in adults (a1) and in children (a2); and (b) Hazard index for arsenic in adults and children

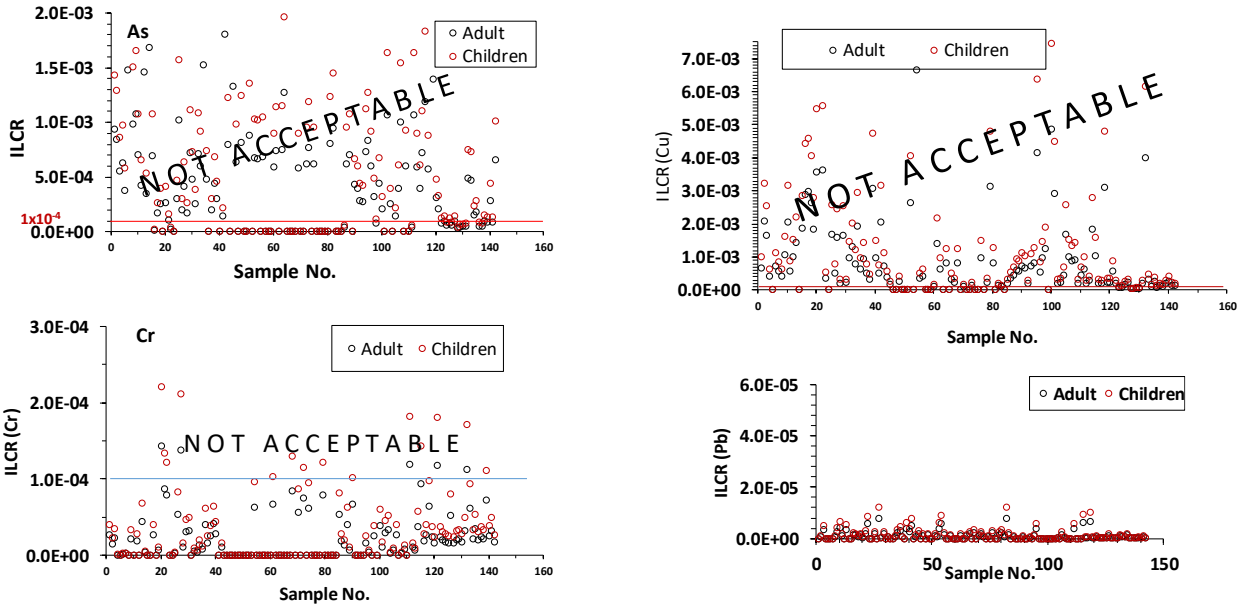

Fig. 8.13. Health hazard due to Incremental Life Time Cancer Risk (ILCR) due to heavy metal contamination

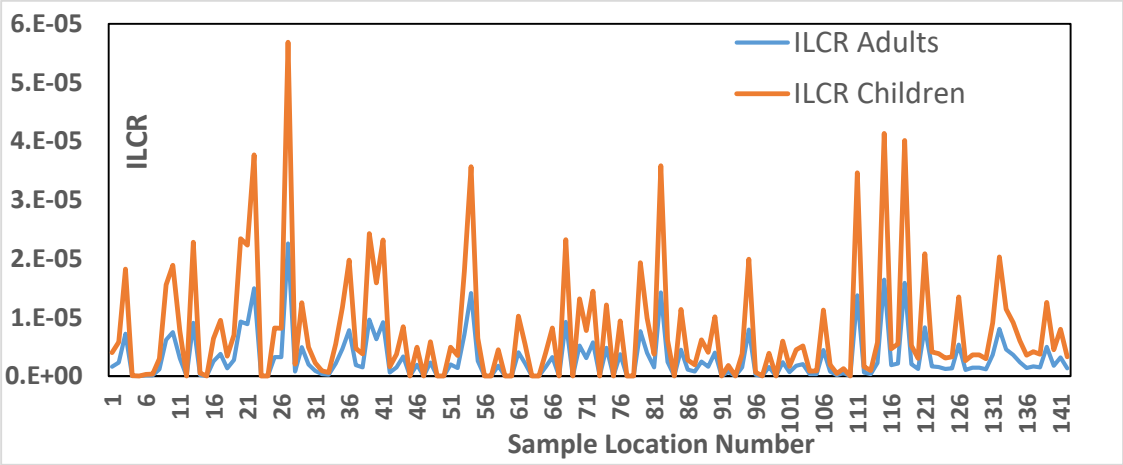

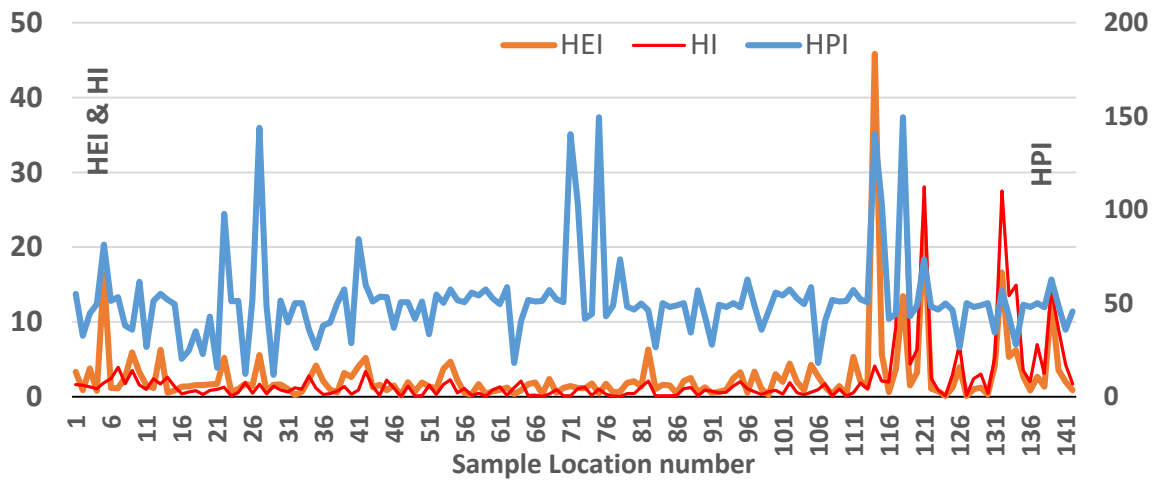

Fig. 8.14: Cross-plot of sample numbers and the heavy-metalrelated health hazard (ILCR, HEI, HPI and HI). a) ILCR in adults and children, b) HEI, HPI and HI values (critical limit of ILCR for adults and children is 10^{-4})

ILCR (Incremental Lifetime Cancer Risk) is less than the critical limit of 10^{-4} for both adults and children. Areas were identified where the ILCR (Incremental Lifetime Cancer Risk) value can exceed the critical limits in nearby future, these are locations number 9,13,22,27,54,82,111,115,118,132. Appropriate measures should be taken to contain the health hazard risk in above mentioned locations.

Table 8.4: Heavy metal pollution in various districts of study area

Place	No. of samples	Approx Conc.	H.M. Pollution	Permiss. Limit
Pinsawa, Dist Sitapur	1	2000 µg/l	Al	200 µg/l
Bargadia, Dist. Sitapur	2	600µg/l	Al	
Ruiya Garhi, Dist Shahjahnpur	1	*1200*µg/l	*Al*	
Luduka, Dist, Jaunpur	1	1200µg/l	Al	
Rampur	1	*700*µg/l	*Al*	
Prilaspur, Dist, Rampur	2	*500*µg/l	*Al*	
City Najibabad	1	500 µg/l	Al	
Tazpur Mafi, Dist Moradabad	1	140 µg/l	As	50 µg/l
Luduka, Dist, Jaunpur	2	2800µg/l	Fe	300µg/l
Tazpur Mafi, Dist Moradabad	2	1800µg/l	Fe	
Lakshmanpur, Dis Pratapgarh	1	1500µg/l	Fe	

Ruiya Garhi, Dist Shahjahnpur	**2**	***1500µg/l***	***Fe***	
Chilbila, Dist Bela Prapagarh	**2**	**1350µg/l**	**Fe**	
City Rampur	**3**	***अत्यधिक***	***Mn***	**300 µg/l**
Nagina, Dist Bijnaur	**1**	**4000µg/l**	**Mn**	
Nurpur, Dist Bijnaur	**2**	**1000µg/l**	**Mn**	
Devchara, Dist Baraily	**1**	**1250µg/l**	**Mn**	
Dahgavan, Dist Badayun	**1**	**700µg/l**	**Mn**	
Chandausi, Dist Sambhal	**1**	**40µg/l**	**Pb**	**10 µg/l**
Radauli, Dist Ayodhya	**1**	**40µg/l**	**Pb**	
Tazpur Mafi, Dist Moradabad	**3**	**35µg/l**	**Pb**	
City Rampur	**4**	***30µg/l***	***Pb***	
Thurbpur, Dist Shajahanpur	**3**	***30µg/l***	***Pb***	
Hasanpur, Dist Amroha	**1**	**30µg/l**	**Pb**	
Devchara, Dist Baraily	**1**	**30µg/l**	**Pb**	

Table 8.5: Health-risk due to groundwater pollution from various heavy metals

Indices	Heavy metals and their level of pollution (No pollution observed from As, Cr, Cu, Zn and Pb)
Heavy Metal Evaluation Index (HEI)	**Moderately level risk due to : Al, Fe, Mn, Pb**
Heavy Metal Pollution Index (HPI)	**Low to moderately level risk due to: Pb, Fe**
Non-carcinogenic metalloid Risk	**Low to moderate level risk: As**
Incremental Lifetime Cancer Risk (ILCR)	**Beyond acceptable limit: As (60%), Cr (5%), Cu (70%)**

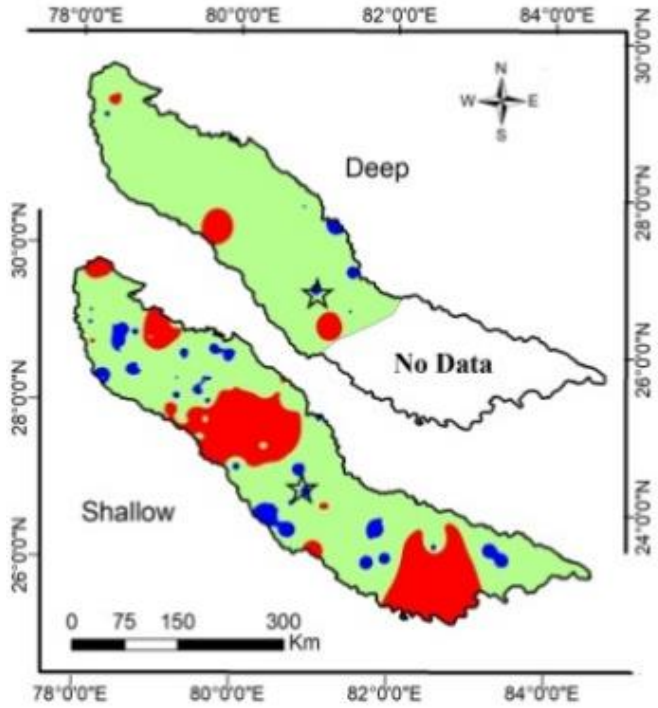

Aluminium

Acceptable limit (PPB) = 30
Permissible limit (PPB) = 200

☆ Lucknow

Classes	Area (Km²)	
	Deep	Shallow
< 30	751.69	5462.25
30.1 - 200	57667.49	64521.57
>200	2784.04	25812.57

Min	Max	Mean	Median	SD
NA	2403	145.46	39.72	332.37
NA	470.99	69.29	44.28	87.52

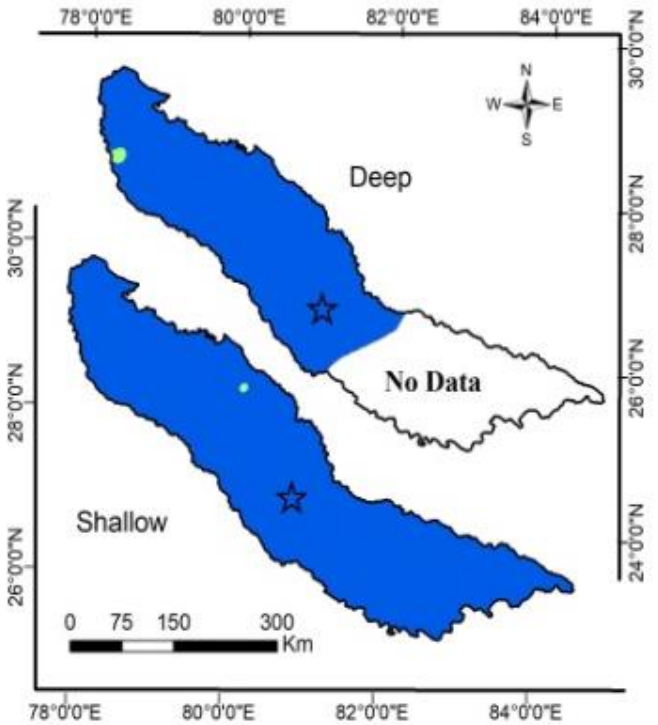

Copper

Acceptable limit (PPB) = 50
Permissible limit (PPB) = 1500

☆ Lucknow

Classes	Area (Km²)	
	Deep	Shallow
< 50	60884.32	95685.97
50.1 - 75	318.90	110.43

Min	Max	Mean	Median	SD
NA	74.8	9.58	3.83	13.78
NA	90.67	10.1	5	15.14

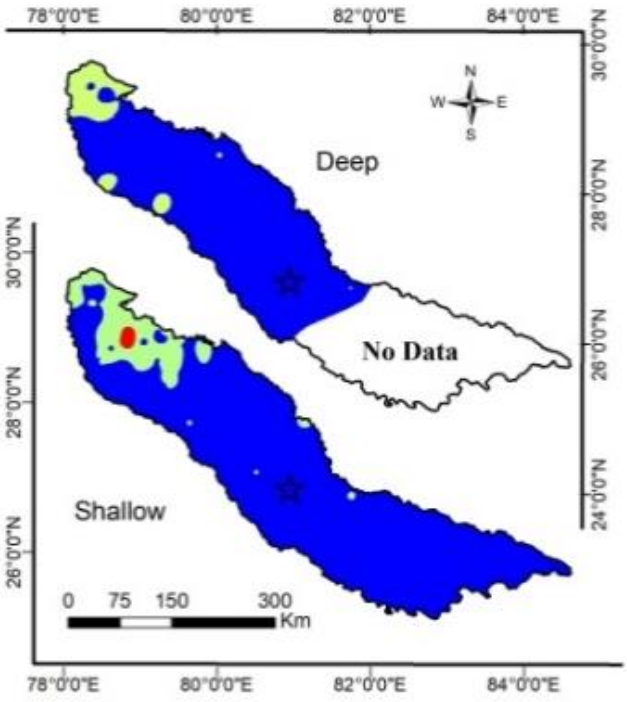

Arsenic

Acceptable limit (PPB) = 10
Permissible limit (PPB) = 50

☆ Lucknow

Classes	Area (Km²)	
	Deep	Shallow
< 10	55890.77	84619.49
10.01 - 50	-	10707.58
> 50	5312.45	469.32

Min	Max	Mean	Median	SD
NA	147.63	6.24	3.23	15.88
NA	31.77	6.43	7.47	6.638

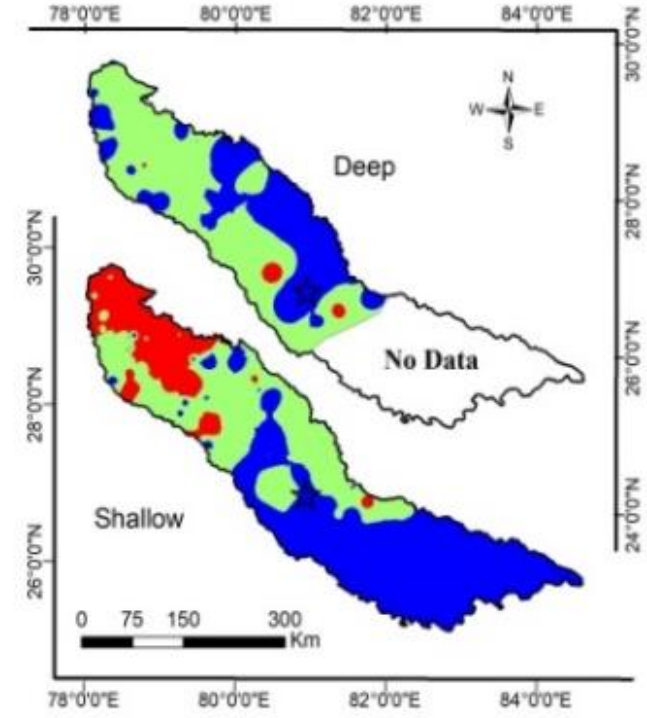

Maganese

Acceptable limit (PPB) = 100
Permissible limit (PPB) = 300

☆ Lucknow

Classes	Area (Km²)	
	Deep	Shallow
< 100	23092.31	48119.05
100.1 - 300	37164.34	32667.01
> 300	946.57	15010.34

Min	Max	Mean	Median	SD
NA	12618.4	366.11	112.28	1405
NA	494.15	116.91	75.98	108.7

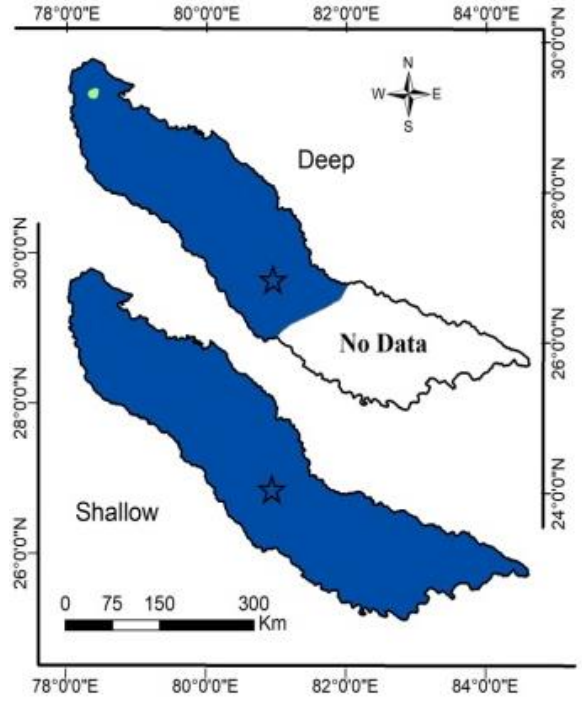

Zinc

Acceptable limit (PPB) = 5000
Permissible limit (PPB) = 15000

☆ Lucknow

Classes	Area (Km²)	
	Deep	Shallow
< 5000	61036.17	95796.40
> 5000	167.04	-

Min	Max	Mean	Median	SD
NA	54345.7	597.2	198.03	926.4
NA	12239	404.41	124.17	1702

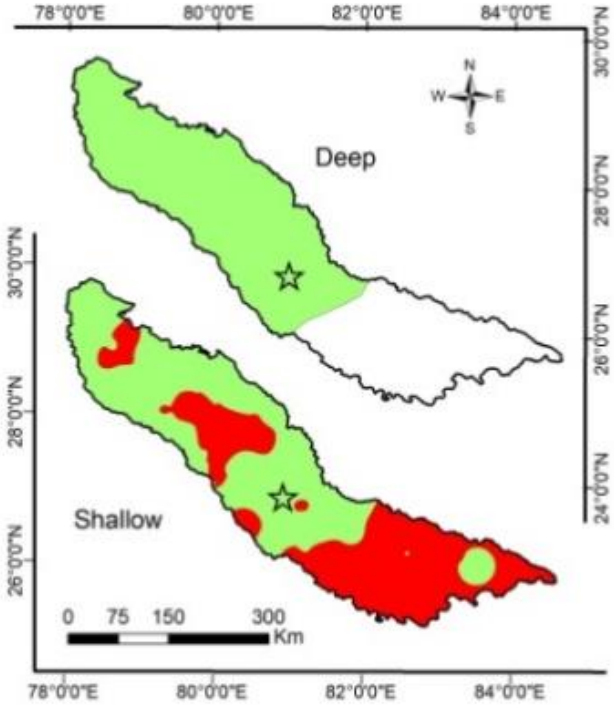

Iron

Acceptable limit (PPB) = 300
Permissible limit (PPB) = 300

☆ Lucknow

Classes	Area (Km²)	
	Deep	Shallow
< 300	61203.21	53253.96
> 300	-	42542.43

Min	Max	Mean	Median	SD
NA	3029.27	218.15	1.75	559.5
NA	70.76	1.96	0.23	108.7

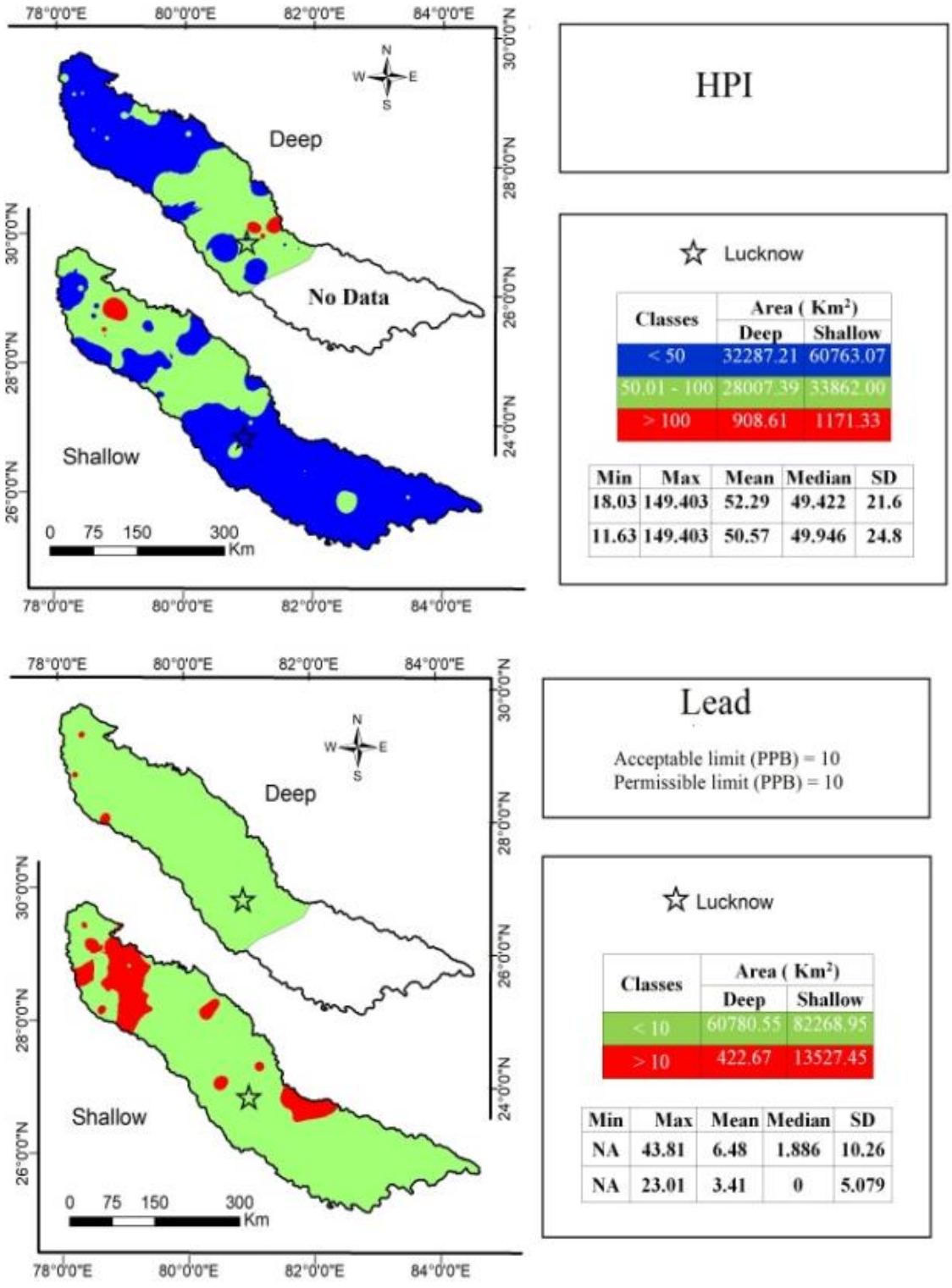

Fig. 8.15.: Spatial distribution maps of the study area affected by heavy metal contamination

8.9 Statistical Analysis

Principal Component Analysis

PCA1: The first principal component increases with decreasing Zn, Al values, amongst other variables. The first principal component increases with increasing Mn and Fe. This suggests that these two criteria vary together. If one increases, then the remaining ones tend to increase as well.

PCA-2: The second principal component increases with decreasing of Mn. This component can be viewed as a measure of how polluted the location is in terms of Mangnese.

Screeplot shows that, principal components 1 and 2 that explains more than 90% variances.

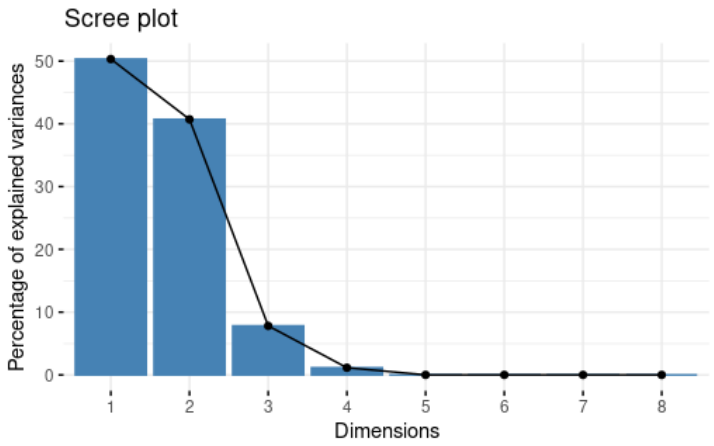

Fig. 8.16: Scree plot

Table 8.6 : *Principal component planes of heavy metals*

	PC1	PC2	PC3	PC4
Al	-0.01699	-4.0378e-02	-0.41482	-0.90861
As	-0.00123	-1.7405e-05	-0.00538	0.02366
Cr	-0.00016	-3.1199e-05	-0.00104	-0.00063
Cu	-0.0019	-6.9903e-04	-0.00219	-0.0059
Fe	0.008964	2.509e-02	-0.9099	0.4138
Mn	0.030993	-9.9842e-01	-0.00605	0.04653
Pb	-0.00334	1.7319e-04	-0.0005	0.00544
Zn	-0.99933	-3.005e-02	-0.0013	0.02056

Table 8.7: Correlation matrix (CM) of heavy metals

	Al	As	Cr	Cu	Fe	Mn	Pb	Zn	HPI	HEI	HI
Al	1	-0.052	0.42	0.13	0.62	0.16	-0.02	0.081	0.14	0.6	0.53
As		1	0.046	0.15	0.25	0.0 61	0.26	0.12	0.31	0.17	0.56
Cr			1	0.39	0.41	0.025	0.35	0.17	0.24	0.35	0.39
Cu				1	0.054	0.049	0.37	0.17	-0.0008	0.18	0.13
Fe					1	-0.057	0.035	-0.025	0.13	0.47	0.94
Mn						1	-0.038	-0.007	0.35	0.8	0.012
Pb							1	0.47	0.3	0.19	0.16
Zn								1	0.13	0.12	0.061
HPI									1	0.43	0.24
HEI										1	0.52
HI											1

The Pearson's correlation coefficient matrix is used to know the relationship among various metals. The correlation results were compared with the PCA to recognize the inter-parameters relationships. A significant positive correlation of Al has been observed with Fe (0.62)) indicating a similar source of PC1;HI is positively correlated to Fe,Al and As, suggesting increase of non cancareous hazard if Fe,Al and As values increases in the study area. HEI also positively correlated to Mn and Al, accounting for increase in pollution extent if Mn and Al are increased. It is confirmed that, Mn, Al,Fe,Zn are the significant attributers to elevate the health risk from groundwater.

PCA, CR and pollution indices analysis corroborate that, high contents of heavy metals in groundwater of middle Ganga basin is due to industries, sewage water and pesticides, which are poisoning the aquifer systems.

8.10 Groundwater suitability for irrigation

Many parameters are estimated to ensure reliable results for the quality of irrigation water of the aquifers. These parameters include electrical conductivity (EC), sodium absorption ratio (SAR), kelly's ratio(KR) etc. The parameters are mathematical expressions that convert water quality concentrations component into a numeric measure to describe the irrigation water quality. Sodium absorption ratio (SAR) means a value representing the relative amount of sodium ions to the combined amount of calcium and magnesium ions in water using the formula: SAR = $[Na^{+}]/(([Ca^{2+}] + [Mg^{2+}])/2)1/2$, where all concentrations are expressed as milli equivalents per liter. SAR is important in supporting agricultural crop production as high SAR values in clay and loam soils will reduce soil permeability, thereby concentrating salts near the surface and inhibiting plant growth. Sodium ion in small amount is good for plants. But excess sodium ions create problem for both plant and soil. Excess sodium ions contributes to salinity and it is toxic for some sensitive crops. SAR value 0-10 indicates low sodium water, 10-18 indicates medium sodium water, 18-26 indicates high sodium water and greater than 26 is very high sodium water.

98% of the area falls under low salinity-low sodium hazard & only 2% data lying in low salinity- high sodium hazard. Jaunpur and Unaao are the districts where SAR>10. Wilcox's diagram shows that water samples fall under excellent to good category, as per Permeability Index, the majority of water is moderate too good for irrigation purposes. Thus, groundwater can be used in irrigation in the study area except in areas of Jaunpur & Unnao. (*Locations samples shown in figure 5.57)*

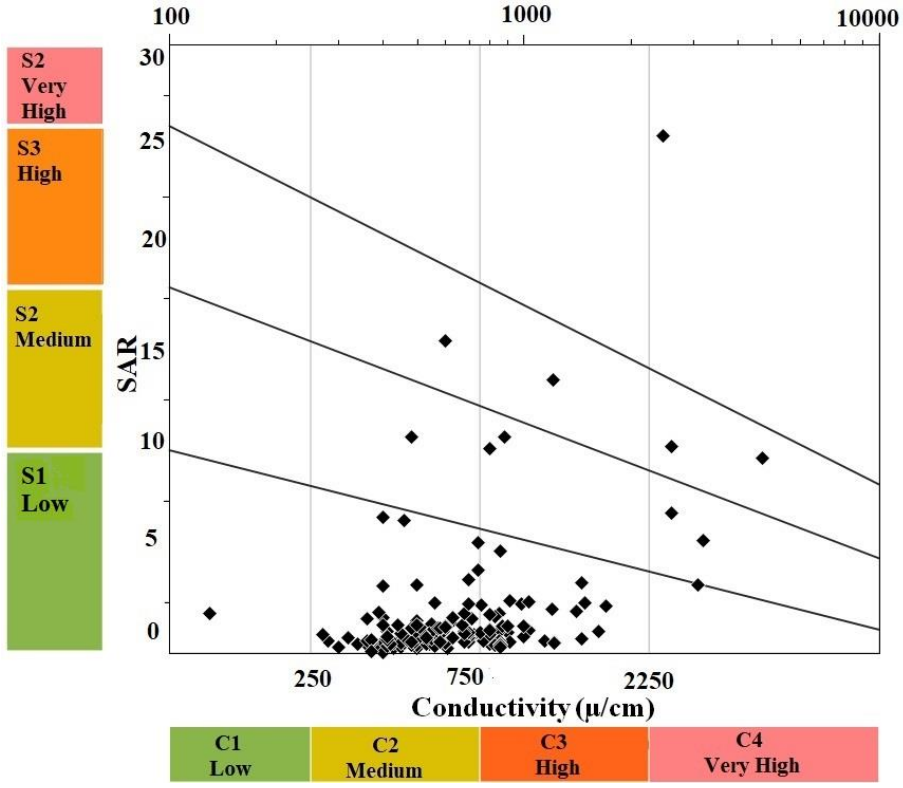

Fig. 8.17: Irrigation water quality. Sodium Absorption Ratio (SAR) vs EC

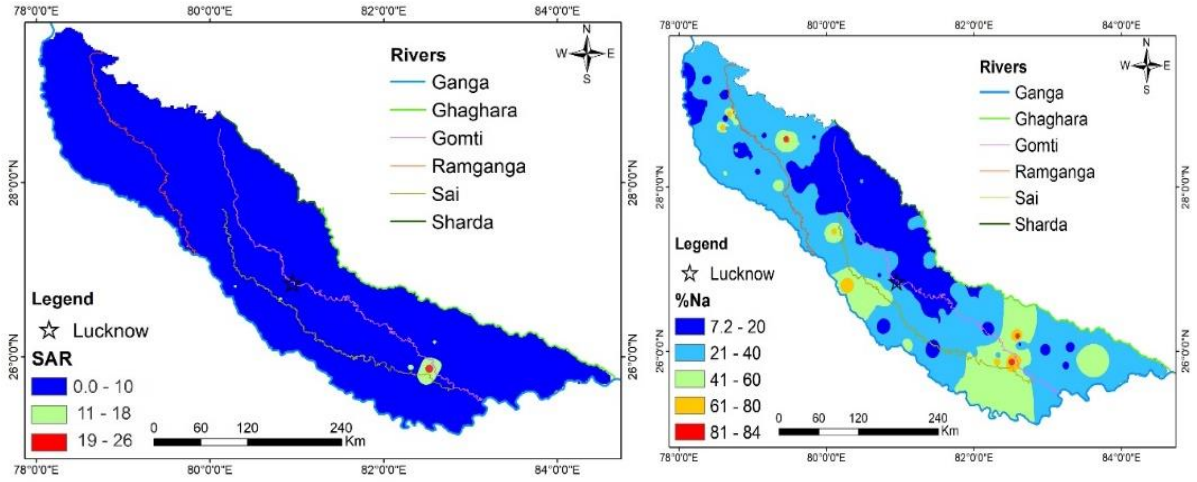

Fig 8.18: Spatial variation of (a) SAR and (b) %Na

Table 8.8: Water suitability for irrigation needs as per the assessed irrigation water quality indices

SAR Value	**Suitability of water for irrigation**	**% Of sample**	**%Na**	**Suitability of water for irrigation**	**% Of Sample**
0-10	Ideal	96.57	<20	Excellent	43.42
10-18	Good	3.40	20-40	Good	40.30
18-26	Doubtful	0.57	40-60	Permissible	8.00
>26	Unsuitable	0	60-80	Doubtful	3.42
			>80	Unsuitable	3.97

Permeability index(PI) (as a %)	**Suitability of water for irrigation**	**% Of Sample**	**KI (Kelly index)**	**Suitability of water for irrigtion**	**% Of Sample**
Class 1 (<75)	Suitable	20	Greater than or equal to 1	Not Recommended For Irrigation	11.428
Class 2 (25-75)	Good	73.71	< 1	Suitable for irrigation	88.57
Class 3 (<25)	Unsuitable	6.28			

Magnesium hazard (MH)	Suitability of water for irrigtion	% Of Sample	Potential salinity (PS)	Suitability of water for irrigtion	% Of Sample
Greater than 50	Not Recommended For Irrigation	27.428	Less than 3	Recommended For Irrigation	53.714

8.11 Isotopic Investigation

The isotopic composition of groundwater (at shallow and deep depths) has shown depletion in isotopic composition in the direction towards the Shiwalik hills similar to the expected trend in the isotopic composition of rainfall (depleting with increasing altitude). On this basis, it is inferred that local rainfall is the major source of the groundwater (shallow and deep depths) of this region. This trend reversed in the central region to southeast region. From the central zone (Lucknow district) to the south-eastern region isotopic depletion increases indicating recharge from the water source of depleted isotopic composition. This part of the region is covered by a dense network of canals that carry the water of depleted isotopic composition, and is probably the reason for the observed isotopic trend in this part of the study area. In this region, for example see the sample number 26 to 32 (fig xxx) the isotopic curves for the shallow and deep aquifer overlaps indicating presence of same water type in both the aquifers. It is further seen that the isotopic composition of the shallow aquifer, in general, showed more fluctuations than that of the deep aquifer. Such large fluctuations in the isotopic composition suggest that the shallow aquifer is getting recharged at multiple locations along its pathways by the water of different isotopic compositions arising from different water sources, such as highly depleted water (canal water), moderately enriched water (rainwater), and highly enriched water (municipal wastewater), etc.

This semiconfined condition of deep groundwater and semi-confined to the unconfined condition of shallow groundwater was further confirmed by the tritium dating of groundwater. The tritium-based age data distribution of groundwater, and the area percentage enclosed in four age range (<15years, 16-30 years, 31-45 years, and >45 years). The shallow groundwater shows its median age of ~ 23 years, and that for the deep aquifer, ~30 years. Through multi-technique investigations, it is concluded that from Shiwalik foot-hills to the central part of the study area (Lucknow district) rainfall is the major source of recharge to groundwater, and beyond this, canal water is the equally important contributing recharge source to the groundwater. The shallow groundwater is of the semi-confined to unconfined type and, hence, is getting recharged from different surface water sources along its pathway in addition to the rainfall as the major source. The deep groundwater is of the semiconfined type and is receiving recharge from the overlying aquifer in most of the study area.

4.12 Isotopic and chemical signatures for possible interaction zones-

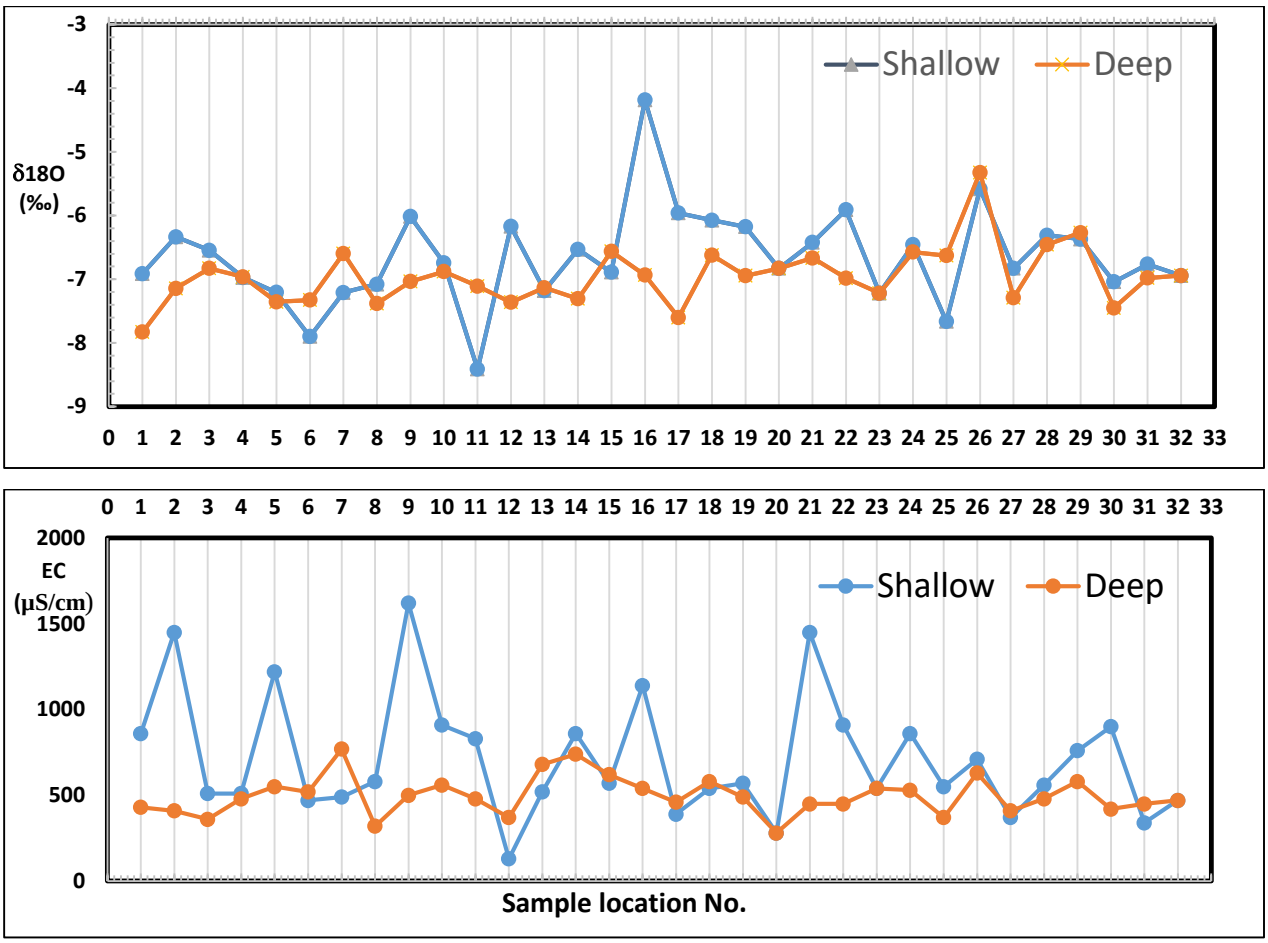

Fig. 8.19: Variation of (A) $\delta^{18}O$, and (B) EC with sample location

The younger groundwater is mostly located near the rivers. The quantity of tritium in the younger groundwater areas (2 years to 13 years) varies from 7 TU to 8 TU. In most areas, the groundwater age of shallow aquifers is between 0 years and 39 years while in the case of deep aquifers the age is between 25 years and 45 years.

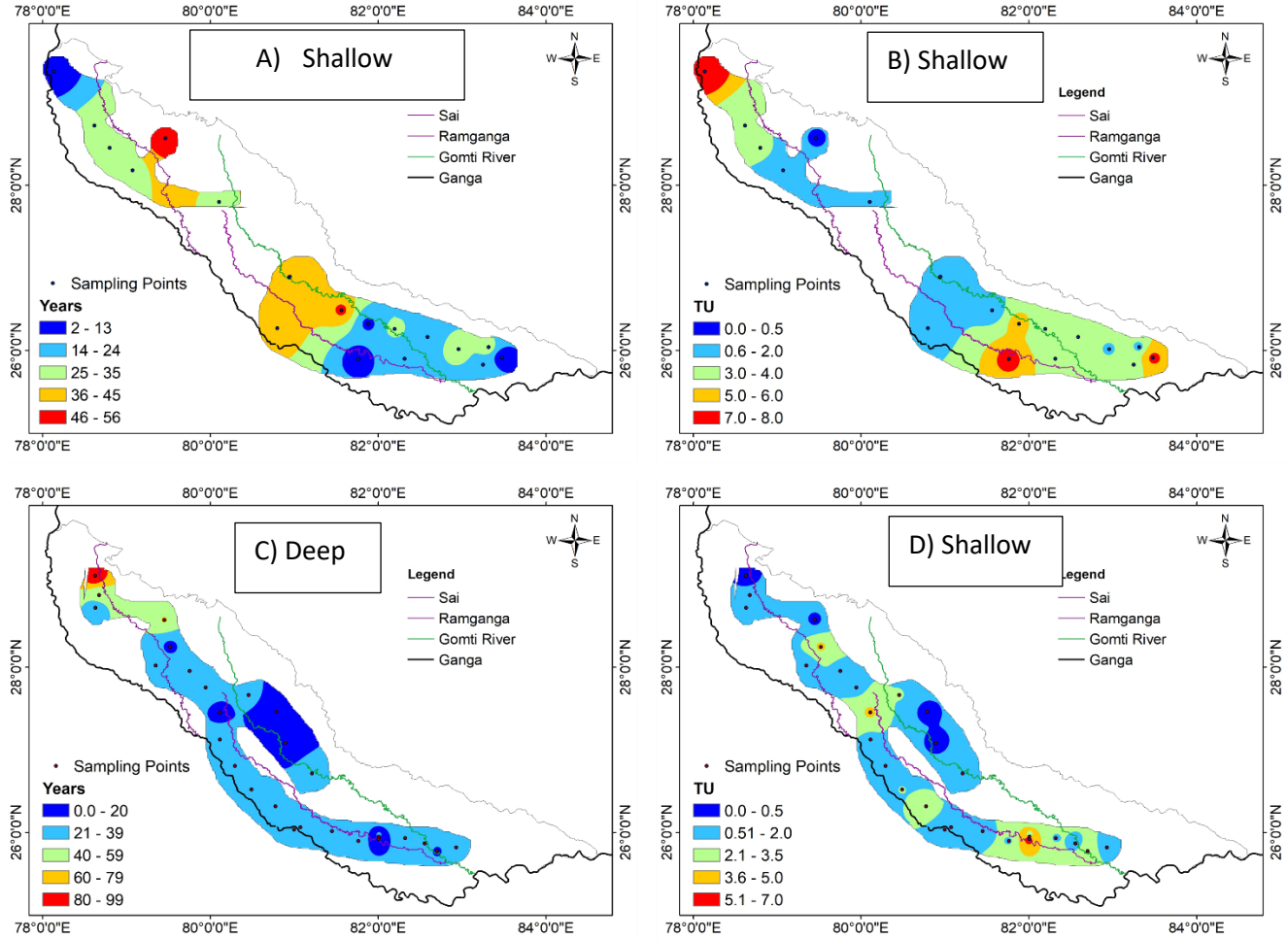

Fig. 8.20: Spatial variation of groundwater age. The deep aquifer groundwater age is shown in (A), the deep aquifer tritium levels (TU) are shown in (B), the shallow aquifer age is shown in (C), and the shallow aquifer tritium levels (TU) are shown in (D).

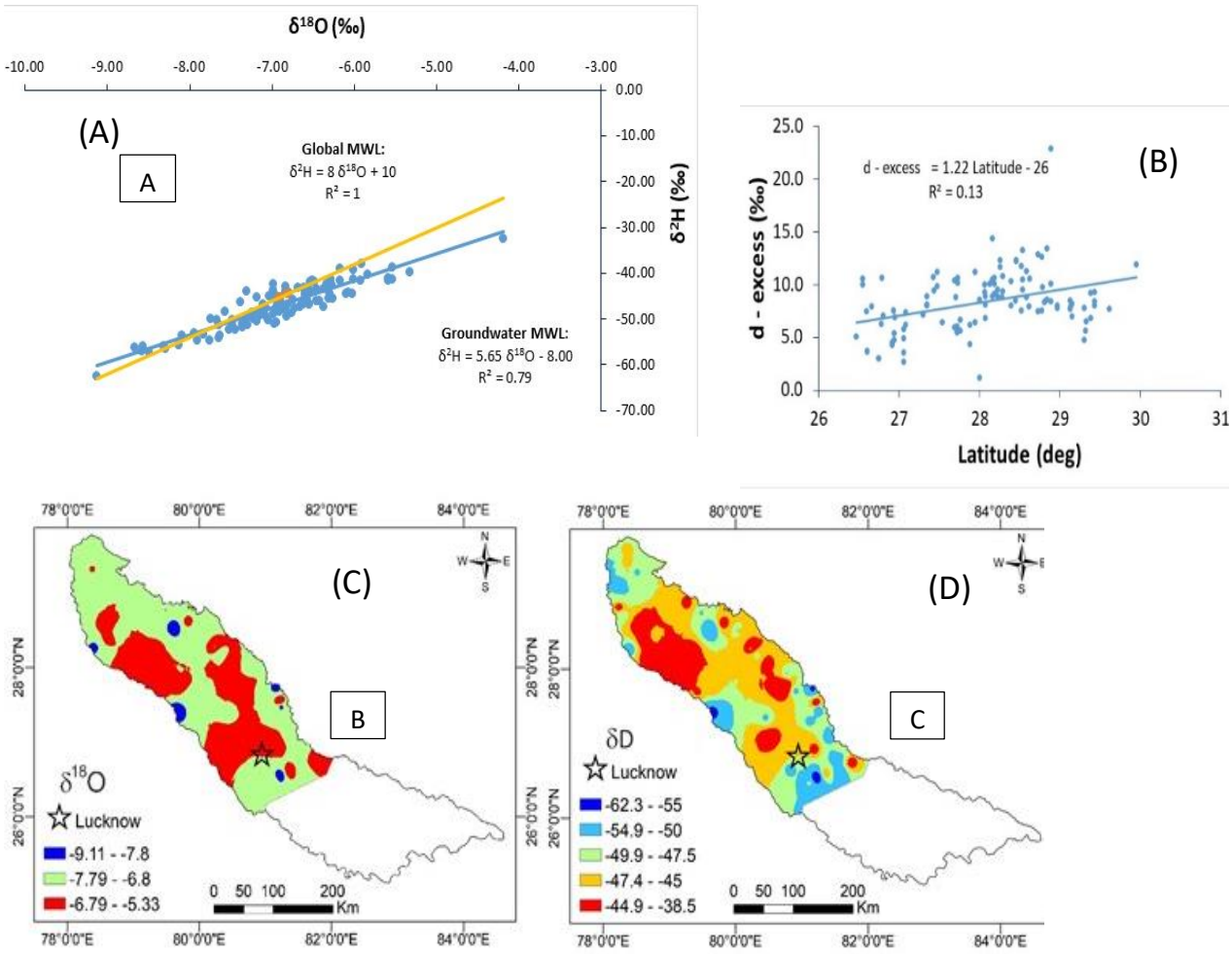

Fig. 8.21: Stable isotopic composition of groundwater. (A) Characteristic groundwater isotopic line. Also shown Meteoric Water Lines (MWL) for comparison; (B) Lattitudinal variation of isotopic composition (d-excess). (C) and (D): spatial variation of isotopic composition of groundwater in δ^2H, and $\delta^{18}O$ respectively

9. CONCLUSION

Groundwater Recharge Potential Zones (GWRPZ):

- **Thematic spatial maps were created for various parameters including decadal average rainfall pattern, geomorphology, slope, drainage density, lineament density, lithology, land use and land cover (LULC), groundwater fluctuation, and population density distribution.**
- **The resulting Grou**
-
- **ndwater Recharge Potential Zones (GWRPZ) map illustrates that 12% of the study area is categorized as having high GWRPZ, 30% as moderate GWRPZ, and 58% as low GWRPZ. A significant concentration of high potential zones is distributed in the foothill regions of Shiwalik range.**
- **A total of 92 sites were identified suitable for implementing artificial groundwater recharge measures to mitigate declining groundwater levels.**

Rainfall, temperature, and GWL trend:

- **Average annual rainfall observed to decrease systematically with distance from the Shiwalik hills. Spatial patterns of decadal average rainfall show non-uniform shifts in the wet and drought covered areas in the study area.**
- **The study area is categorized into four zones based on rainfall trends. Zones 1 and 3 exhibit decreasing rainfall trends at rates of 2.1 mm/year and 0.5 mm/year, respectively, while Zones 2 and 4 show increasing trends at rates of 0.5 mm/year and 0.4 mm/year.**
- **The decadal temperature pattern indicated that the nighttime temperatures have uniformly risen at an average rate of 0.018°C/yr.**
- **Groundwater level data spanning from 1998 to 2018 indicates a declining trend, with groundwater levels dropping at ~ 12 cm/year.**

Water quality analysis

- **Groundwater in the study area is moderately hard due to high concentrations of dissolved calcium and magnesium bicarbonate ions. Approximately 80% of samples**

exhibit a chemical composition dominated by Ca^{2+}, Mg^{2+}, and HCO_3^- ions. In 10% of the area, the composition is characterized by Na^+ and K^+ with HCO_3^-, while the remaining 10% shows a mixed ionic composition including enriched Cl^- concentrations. The hydro-chemical characteristics are influenced by rock-water interactions involving carbonate and silicate weathering, as well as reverse ion exchange reactions where Na^+ ions are replaced by Ca^{2+} and Mg^{2+}.

- **Drinking water quality is poor in 25% of the areas, whereas irrigation water quality is poor in 8% of the areas, notably concentrated in Jaunpur and Unnao districts.**
- **Heavy metal analysis indicates significant contamination of groundwater with Fe, Al, As, Cr, and Cu. Non-carcinogenic health risks associated with Fe and Al are observed in 5% of locations, while arsenic poses risks in 3% of locations. Carcinogenic health risks are identified for dissolved heavy metals such as Cu (80% of samples), As (70% of samples), and Cr (10% of samples).**

Isotopic Analyses:

- **Isotope analysis shows that shallow aquifers are predominantly unconfined to semi-confined, whereas deeper aquifers are semi-confined. The deeper aquifers receives rainfall from upper reaches (Shiwalik foothills) as well as from overlying aquifers in other parts. In the southwest region, significant recharge from canal water through overlying shallow aquifers is observed. Groundwater age ranges from less than 15 years to over 45 years, with shallow groundwater having a median age of approximately 23 years and deep aquifers around 30 years.**
- **Recharge sources vary across the study area: from the Shiwalik foothills to Lucknow district, rainfall is the primary source, while beyond this area, canal water also contributes significantly to groundwater recharge.**

End Use:

Implementing groundwater recharge measures at identified locations using suitable recharge sources can effectively mitigate the declining groundwater levels. These measures not only have the potential to dilute heavy metal contamination but also improve groundwater quality and enhance resilience against the impacts of climate change on groundwater resources.

Continuous monitoring of heavy metal pollution in identified contaminated groundwater locations is essential to safeguard water quality.

REFERENCES

1. Wada Yoshihide; Beek L.P.H.V; Kempen C.M.V; Reckman J.W.T.M; Vasak Slavek; and Bierkens M.F.P. Global depletion of groundwater resources. Geophysical research letters (2010). VOL.37, L20402.

(2) Bouwer.H. Artificial recharge of groundwater: hydrogeology and engineering © Springer-Verlag 2002.

(3) Dahar.W;Pistre.S;Kneppers .A;Bakalowicz.M;Najem.W. Karst and artificial recharge: Theoretical and practical problems. A preliminary approach to artificial recharge assessment. Journal of Hydrology 408 (2011) 189–202.

(4) Tang. Q; Gao. H; Lu.H and Lettenmaier D. P. Remote sensing: hydrology. Progress in Physical Geography 33(4) (2009) pp. 490–509

(5) Ali.R; McFarlane.D; Varma.S; Dawes.W; Emelyanova.I; Hodgson.G; Charles.S. Potential climate change impacts on groundwater resources of south-western Australia. Journal of Hydrology 475 (2012) 456–472.

(6) Clark.M.J. Putting water in its place: a perspective on GIS in hydrology and water management

Hydrological Processes. Hydrol. Process. 12, 823±834 (1998).

(7) McLeod.A.I. Kendall rank correlation and Mann-Kendall trend test.

(8) Hussain.Md.M and Mahmud.I pyMannKendall: a python package for non-parametric. Mann Kendall family of trend tests.

(9) Alhaji.U.U; Yusuf.A.S; Edet.C.O; Oche.C.O;and Agbo.E.P. Trend Analysis of Temperature in Gombe State Using Mann Kendall Trend Test Journal of Scientific Research & Reports 20(3): 1-9, 2018; Article no.JSRR.42029. ISSN: 2320-0227.

(10) Gocic.M; Trajkovic.S. Analysis of changes in meteorological variables using Mann-Kendall and Sen's slope estimator statistical tests in Serbia Global and Planetary Change 100 (2013) 172–182.

(11) Radhakrishnan.K; Sivaraman.I; Jena.S.K; Sarkar.S; Adhikari.S. A Climate Trend Analysis of Temperature and Rainfall in India Climate Change and Environmental Sustainability (October 2017) 5(2): 146-153.

(12) Mukherjee.A; Ramachandran. Prediction of GWL with the help of GRACE TWS for unevenly spaced time series data in India: Analysis of comparative performances of SVR, ANN, and LRM. Journal of Hydrology 558 (2018) 647–658.

(13) Sahoo.S;Swain.S;Goswami.A;Sharma.R;Pateriya.B. Assessment of trends and multi-decadal changes in groundwater level in parts of the Malwa region, Punjab, India. Groundwater for Sustainable Development 14 (2021) 100644.

(14) Feinerman.E; Knapp.K.C. Benefits from Groundwater Management: Magnitude, Sensitivity, and Distribution http://ajae.oxfordjournals.org.
(15) Jha.M.K; Chowdhury.A; Chowdary.V.M; Peiffer.S. Groundwater management and development by integrated remote sensing and geographic information systems: prospects and constraints. Water Resour Manage (2007) 21:427–467.

(16) Su.X; Yan.X and Tsai.C.L. Linear regression. Volume 4, May/June 2012 c 2012 Wiley Periodicals, Inc.

(17) Spane.F.A. Considering barometric pressure in groundwater flow investigations. WATER RESOURCES RESEARCH, VOL. 38, NO. 6, 1078, 10.1029/2001WR000701, 2002.

(18) Stuyfzand.P.J. Patterns in groundwater chemistry resulting from groundwater flow. Hydrogeology Journal (1999) 7:15–27.

(19) Winter.T.C. Relation of streams, lakes, and wetlands to groundwater flow systems. Hydrogeology Journal (1999) 7:28–45

(20) PRAKASH.S. R and MOHAN.R. Hydromorphogeological Mapping of Panwari Area, Hamirpur District, Uttar Pradesh Using Satellite Data. Journal of the Indian Society of Remote Sensing, Vol. 24, No. 2, 1996.
(21) Davisson. M. L; Smith D. K.; KenneallyJ; Rose.T.P. Isotope hydrology of southern Nevada groundwater: Stable isotopes and radiocarbon. WATER RESOURCES RESEARCH, VOL. 35, NO. 1, PAGES 279-294, JANUARY 1999.
(22) Gonfiantini.R; Fröhlich. K; Araguäs L.A.; Rozanski.K. Isotopes in Groundwater Hydrology. Isotope Tracers in Catchment Hydrology.

(23) Fontes, J.Ch. Environmental isotopes in groundwater hydrology. International Nuclear. Information System.
(24) Barbieri.M. Isotopes in Hydrology and Hydrogeology. Water 2019, 11, 291.

PLFS (2022-2023): Annual Report Periodic Labour Force Survey (PLFS) July 2022 – June 2023, Ministry of Statistics and Programme Implementation, Government of India.

UN (2022) World Population Prospects 2022: Summary of Results July 2022 www.un.org.development.desa.pd/files/undesa_pd_2022_wpp_key-messages.pdf

Sinha R. S. (2021) State of Groundwater in Uttar Pradesh -A Situation Analysis with Critical Overview and Sustainable Solutions, Water Aid, Groundwater Action Group, Lucknow, Uttar Pradesh, India

Gonçalves, Carlos M., Joaquim CG Esteves da Silva, and Maria F. Alpendurada. "Evaluation of the pesticide contamination of groundwater sampled over two years from a vulnerable zone in Portugal." *Journal of agricultural and food chemistry* 55.15 (2007): 6227-6235.

Li, P., Karunanidhi, D., Subramani, T., & Srinivasamoorthy, K. (2021). Sources and consequences of groundwater contamination. *Archives of environmental contamination and toxicology*, *80*, 1-10.

Benhamiche, N., Sahi, L., Tahar, S., Bir, H., Madani, K., & Laignel, B. (2016). Spatial and temporal variability of groundwater quality of an Algerian aquifer: the case of Soummam Wadi. *Hydrological Sciences Journal*, *61*(4), 775-792.

Passarella, G., & Caputo, M. C. (2006). A methodology for space-time classification of groundwater quality. *Environmental monitoring and assessment*, *115*, 95-117.

Sarkar, A., Shekhar, S., & Rai, S. P. (2017). Assessment of the spatial and temporal hydrochemical facies variation in the flood plains of North-West Delhi using integrated approach. *Environmental earth sciences*, *76*, 1-12.

Yuan, H., Yang, S., & Wang, B. (2022). Hydrochemistry characteristics of groundwater with the influence of spatial variability and water flow in Hetao Irrigation District, China. *Environmental Science and Pollution Research*, *29*(47), 71150-71164.

Machiwal, D., Cloutier, V., Güler, C., & Kazakis, N. (2018). A review of GIS-integrated statistical techniques for groundwater quality evaluation and protection. *Environmental Earth Sciences*, *77*(19), 681.

Stephanie Fraser (2021) Water Quality: Analysis and Interpretation. Syrawood Publishing House.

Hewitt C.N. (1992) Methods of Environmental Data Analysis. Springer Science +Business Media, B.V.

Appelo C.A.J. and Postma D. (2005) Geochemistry, Groundwater and Pollution, 2nd Edition, CRC Press.

Hem John D. (1985) Study and interpretation of the chemical characteristics of natural water, John D. Hem, Third Edition, USGS, Water-Supply Paper 2254

Mazor E (2003) Chemical and Isotopic Groundwater Hydrology: The Applied Approach. Third Edition, CRC Press

Freeze R.A. and J. A. Cherry (1979) Groundwater. Prentice-Hall Inc., New Jersey

Dutta V, D. Dubey, S. Kumar (2020) Cleaning the River Ganga: Impact of lockdown on water quality and future implications on river rejuvenation strategies. Sci Total Environ., 743: 140756. https://doi.org/10.1016/j.scitotenv.2020.140756

Chakraborti, Dipankar & Mukherjee, Subhash & Pati, Shyamapada & Sengupta, Mrinal & Rahman, Mohammad Mahmudur & Chowdhury, Uttam & Lodh, Dilip & Chanda, Chitta & Chakraborti, Anil & Gautam Kumar, Basu. (2003). Arsenic Groundwater Contamination in

Middle Ganga Plain, Bihar, India: A Future Danger?. Environmental health perspectives. 111. 1194-201. 10.1289/ehp.5966.

MoWR (2014) Ganga Basin, Ministry of Water Resources, Government of India (www.india-wris.nrsc.gov.in)

Bharati, L; Jayakody, P (2010) Hydrology of the upper Ganga river. Colombo, Sri Lanka: International Water Management Institute. http://publications.iwmi.org/pdf/H043412.pdf

Jha, V.C. and Bairagya, H.P (2011) Flood plain evaluation in the Ganga-Brahmaputra Delta: A tectonic review. Ethiopian Jrn of Environ. Stud. & Managem. **4** 12-24

MoWR (2022) Water Security. 21 MAR 2022 7:57PM by PIB Delhi

CGWB (2022) Groundwater Year Book Uttar Pradesh (2021 -2022), CGWB, MoWR,RD &GR, GoI

Mishra V., A Soka, K Vatta, U Lall (2018) Groundwater Depletion and Associated CO_2 Emissions in India. Earth's Future, **6**, 1672-1681

Benavides M. M., C. Eberle, L. Narvaez (2023) Water Depletion Technical Report, UN EHS

MoWR (2023) Union Minister For Jal Shakti Releases Dynamic Ground Water Resource Assessment Report For The Country For The Year 2023. PIB, 1st Dec 2023

S.K. Ambast, N.K. Tyagi, S.K. Raul (2006) Management of declining groundwater in the Trans Indo-Gangetic Plain (India): Some options. Agricultural Water Management, **82,** 279-296, https://doi.org/10.1016/j.agwat.2005.06.005.

Margat, Jean, and Jac Van der Gun (2013). Groundwater around the World: A Geographic Synopsis, 1st edition, Hoboken: CRC Press

Boulton, A. J., and P. J. Hancock (2006). Rivers as groundwater-dependent ecosystems: a review of degrees of dependency, riverine processes and management implications. Australian Journal of Botany, vol. 54, No. 2, pp. 133–44. DOI: 10.1071/BT05074

Rodella, Aude-Sophie, Esha Zaveri, and François Bertone (2023). The Hidden Wealth of Nations: The Economics of Groundwater in Times of Climate Change. Washington, DC: World Bank. Available at https://www.worldbank.org/en/topic/water/publication/the-hidden-wealth-ofnations-groundwater-in-times-of-climate-change.pdf

Susanne M., S. and D.O. Tréguer (2018) Beyond Crop per Drop Assessing Agricultural Water Productivity and Efficiency in a Maturing Water Economy. World Bank.

Panda DK, Ambast SK, Shamsudduha M (2021) Groundwater depletion in northern India: Impacts of the subregional anthropogenic land-use, socio-politics and changing climate. Hydrological Processes. 35:e14003. https://doi.org/10.1002/hyp.14003.

Mukherjee, A., Bhanja, S.N. & Wada, Y. (2018) Groundwater depletion causing reduction of baseflow triggering Ganges river summer drying. *Sci Rep* **8**, 12049. https://doi.org/10.1038/s41598-018-30246-7

Fistikoglu, Okan & Gunduz, Orhan & Simsek, Celalettin. (2016). The Correlation Between Statistically Downscaled Precipitation Data and Groundwater Level Records in North-Western Turkey. Water Resources Management. 30. 10.1007/s11269-016-1313-y.

Gunduz, Orhan & Simsek, Celalettin. (2011). Influence of Climate Change on Shallow Groundwater Resources: The Link Between Precipitation and Groundwater Levels in Alluvial Systems. 10.1007/978-94-007-1143-3_25. Chapter in NATO Security through Science Series C: Environmental Security

Hussin, Nur & Yusoff, Ismail & Raksmey, May. (2020). Comparison of Applications to Evaluate Groundwater Recharge at Lower Kelantan River Basin, Malaysia. Geosciences. 10. 289. 10.3390/geosciences10080289.

Fallahi, M.M., Shabanlou, S., Rajabi, A. *et al.* (2023) Effects of climate change on groundwater level variations affected by uncertainty (case study: Razan aquifer). *Appl Water Sci* **13**, 143. https://doi.org/10.1007/s13201-023-01949-8

Han Jiqin, Fikiru Temesgen Gelata, Samerawit Chaka Gemeda; Application of MK trend and test of Sen's slope estimator to measure impact of climate change on the adoption of conservation agriculture in Ethiopia. *Journal of Water and Climate Change* 1 March 2023; 14 (3): 977–988. doi: https://doi.org/10.2166/wcc.2023.508

Zaveri E, J Russ, R Damania (2020) Rainfall anomalies are a significant driver of cropland expansion. PNAS 117(19) 10225-10233 https://doi.org/10.1073/pnas.1910719117

Singh J, S. M. Das, A Kumar (2015) Forecasts of Rainfall (Departures from Normal) over India by Dynamical Model, Aquatic Procedia, 4, 764-771, https://doi.org/10.1016/j.aqpro.2015.02.159.

Zewdie, M.M., Kasie, L.A. & Bogale, S. (2024) Groundwater potential zones delineation using GIS and AHP techniques in upper parts of Chemoga watershed, Ethiopia. *Appl Water Sci* **14**, 85. https://doi.org/10.1007/s13201-024-02119-0

Dar, T., Rai, N., & Bhat, A. (2021). Delineation of potential groundwater recharge zones using analytical hierarchy process (AHP). *Geology, Ecology, and Landscapes*, *5*(4), 292-307.

Zeinalzadeh, K., & Rezaei, E. (2017). Determining spatial and temporal changes of surface water quality using principal component analysis. *Journal of Hydrology: Regional Studies*, *13*, 1-10.

Fatima, S. U., Khan, M. A., Siddiqui, F., Mahmood, N., Salman, N., Alamgir, A., & Shaukat, S. S. (2022). Geospatial assessment of water quality using principal components analysis (PCA) and water quality index (WQI) in Basho Valley, Gilgit Baltistan (Northern Areas of Pakistan). *Environmental Monitoring and Assessment*, *194*(3), 151.

Khan, Ramsha & Saxena, Abhishek & Shukla, Saurabh & Goel, Pooja & Bhattacharya, Prosun & Li, Peiyue & Ali, Esmat & Shaheen, Sabry. (2022). Appraisal of water quality and ecological sensitivity with reference to riverfront development along the River Gomti, India. Applied Water Science. 12. 10.1007/s13201-021-01560-9.

Rosu, Cristina & Pistea, Ioana & Roba, Carmen & Nes, Monica & Ozunu, Alexandru (2014). Groundwater quality and its suitability for dinking and agriculture use in rural area from Cluj County (Floresti Village) Scientific Papers Series : Management, Economic Engineering in Agriculture and Rural Development. 14.

Hailu, Birhane & Mehari, Hagos. (2021). Impacts of Soil Salinity/Sodicity on Soil-Water Relations and Plant Growth in Dry Land Areas: A Review. Journal of Natural Sciences Research. 12. 1-10.

Lu C, Li L, Xu J, Zhao H, Chen M. (2024) Research on the Critical Value of Sand Permeability Particle Size and Its Permeability Law after Mixing. *Water*. 16(3):393. https://doi.org/10.3390/w16030393

Chakraborty, M., Tejankar, A., Coppola, G. *et al. (2022)* Assessment of groundwater quality using statistical methods: a case study. *Arab J Geosci* **15**, 1136 https://doi.org/10.1007/s12517-022-10276-2

Alexakis, D. E. (2021). Water quality indices: Current and future trends in evaluating contamination of groundwater resources. *Water*, *13*(4), 401.

Horton, R.K. (1965) An Index Number System for Rating Water Quality. Journal of the Water Pollution Control Federation, 37, 300-306.

Liebman, H. (1969). Atlas of water quality methods and practical conditions. Munich: R. Oldenburg.

Soltan, M. E. (1999). Evaluation of groundwater quality in Dakhla Oasis (Egyptian Western Desert). Environmental Monitoring and Assessment, 57(2), 157–168. doi:10.1023/A:1005948930316.

Stigter, T. Y., Ribeiro, L., & Carvalho Dill, A. M. M. (2006). Application of a groundwater quality index as an assessment and communication tool in agroenvironmental policies–Two Portuguese case studies. Journal of Hydrology (Amsterdam), 327, 578–591

Sharma K, N. J Raju, N Singh, S. Sreekesh (2022) Heavy metal pollution in groundwater of urban Delhi environs: Pollution indices and health risk assessment, Urban Climate, **45**, 101233, https://doi.org/10.1016/j.uclim.2022.101233.

Elumalai V, Brindha K, Lakshmanan E. (2017) Human Exposure Risk Assessment Due to Heavy Metals in Groundwater by Pollution Index and Multivariate Statistical Methods: A Case Study from South Africa. *Water*.; 9(4):234. https://doi.org/10.3390/w9040234

Joshi S. K., S. P.Rai, R.Sinha, S. Gupta, A. L. Densmore, Y. S Rawat, S. Shekhar (2018) Tracing groundwater recharge sources in the northwestern Indian alluvial aquifer using water isotopes (δ18O, δ2H and 3H), Journal of Hydrology, **559,** 835-847, https://doi.org/10.1016/j.jhydrol.2018.02.056.

Schoeller H (1965) Qualitative evaluation of groundwater resources. In: methods and techniques of groundwater investigations and development. In: Proceedings of the UNESCO, pp 54–83

Schoeller H (1967) Geochemistry of groundwater. An international guide for research and practice UNESCO, chap 15, pp 1–18

Datta, P.S., Tyagi, S.K. (1996) Major ion chemistry of groundwater in Delhi area: Chemical weathering processes and groundwater flow regime. Jour.Geol. Soc. India v.47, pp.179-188.

Nasher, N M & Ahmed, Md. (2021). Groundwater geochemistry and hydrogeochemical processes in the Lower Ganges-Brahmaputra-Meghna River Basin areas, Bangladesh. Journal of Asian Earth Sciences: X. 6. 100062. 10.1016/j.jaesx.2021.100062.

Krishnaraj S, V Murugesan, Vijayaraghavan K, S. Chidambaram, A. Paluchamy, R. Manivannan (2011) Use of Hydrochemistry and Stable Isotopes as Tools for Groundwater Evolution and Contamination Investigations, *Geosciences*, Vol. 1 No. 1, 2011, pp. 16-25. doi: 10.5923/j.geo.20110101.02.